HU ISSN 2063-6997

GEOSCIENCES AND ENGINEERING

A Publication of the University of Miskolc

Volume 10, Number 15 (2022)

Miskolc, University Press

GEOSCIENCES AND ENGINEERING
A Publication of the University of Miskolc
Volume 10, Number 15
Miskolc, University Press
UNIVERSITY OF MISKOLC
FACULTY OF EARTH SCIENCE & ENGINEERING
HU ISSN 2063-6997

TABLE OF CONTENTS

Geosciences and Engineering, Vol. 10, No. 15 (2022), pp. 5–21.
https://doi.org/10.33030/geosciences.2022.15.005

WATER QUALITY CHANGE DUE TO THE MINE BACKFILLING AND ITS POSSIBLE RESPONSE TO TALC FLOTATION

ALAA I. H. ABBADI [1, *], VALÉRIA MÁDAI-ÜVEGES[2], LJUDMILLA BOKÁNYI[3]

Institute of Raw Material Preparation and Environmental Processing, University of Miskolc, Hungary
[1, *]*abbadi.alaa.imad@uni-miskolc.hu, https://orcid.gov/0009-0003-9533-7078*
[2]*valeria.uveges@uni-miskolc.hu, https://orcid.gov/0000-0003-4515-0697*
[3]*ljudmilla.bokanyi@uni-miskolc.hu, https://orcid.gov/0000-0003-2038-6556*

Abstract: A study was carried out in the framework of international R&D Project to determine the effect of water quality changes due to mine backfilling on talc flotation performance. The influence of two types of cemented paste backfill (Shotcrete and backfill) on flotation process water was investigated using the indoor soaking method, and the water quality was evaluated through water chemistry analysis, in addition to measuring pH, conductivity, and zeta potential as a function of soaking time. At the same time, talc batch flotation tests were performed using a KHD Humboldt Wedag lab cell for a period of 20 minutes. Soaking water at different soaking times was used as a process water for flotation, and tap water was also used to establish a reference response. Based upon the experimental results from the talc flotation and the several water quality parameters measured in the soaking water, conclusions were drawn.

Keywords: *paste-backfilling, water quality, flotation, zeta-potential, pH, conductivity*

1. INTRODUCTION

Mineral processing operations generate the so-called “mine tailings”, which are by-products in the form of fine gangue particles ranging from 1 to 600 μm in size and mixed with process water and potentially some chemical reagents. Tailings are characterized as being economically unfeasible to process since they contain low amounts of valuable minerals. The composition of tailings is dictated by the nature of the processed ores along with the separation techniques adopted. Traditionally, tailings are discharged in slurry form into tailings ponds for the purpose of solid separation from wastewater under gravity influence. The recirculation of solid-free wastewater for mineral processing operations leads to the accumulation of solids over time, and the management of such solids poses many challenges in terms of storage, stability, and safety, in addition to the negative environmental impacts [1].

Cemented paste backfill (CPB) is one of the various tailings management methods that have been increasingly used nowadays in order to limit finite resource consumption and prevent environmental pollution. The CPB method follows the trend of environmental protection and the current environmental regulations, and it

is described as being a safe storage, economical method to handle tailings. The CPB method is carried out according to the following steps: (I) It starts with storing the tailings underground, so no surface disturbance is generated. (II) The created paste has colloidal water-retention capabilities, which means that leachate generation is greatly reduced [2]. The main goal of using CPB is the formation of monoliths that serve as geotechnical supports for underground mine cavities. However, CBP can offer the prevention of air intrusion into tailings, which is important in the case of sulfide ores to limit their oxidation rate [3].

A survey by MEND [4] has reported that only a few studies have been carried out at that time to reveal the impact of using the cemented paste tailings on the surface and groundwater quality. The report also elaborated that the focus of the existing studies has been on the strength of the paste in addition to the type of additives used. It is unclear whether the paste technology has long-term effects on environmental stability from a geochemical standpoint, and whether it poses a risk of polluting underground water, which may endanger local people's water consumption or lead to process water variation for water-dependent enterprises such as flotation plants. What is clearly known is that there is an upward trend in the site-specific evaluation of paste characteristics of newly proposed mines in recent years, which is attributed to the increase in awareness of the backfill potential to generate contaminant plumes in the long term and the possibility of affecting ground and/or surface water.

A more recent study by [5] has reported that geochemical tests of cemented paste tailings have shown that the use of 3% binder as an additive to oxidized tailings greatly reduced the mobility of all evaluated constituents. The study also concluded that the release of all metal ions tested was controlled by diffusion and that cemented paste used as backfill would have no adverse or measurable effect on water quality, although certain species migration may have taken place.

Talc is a phyllosilicate mineral that is made up of hydrated magnesium sheet-silicates and has the formula $Mg_3Si_4O_{10}(OH)_2$. It is made up of two layers of silica tetrahedral bound together by octahedral brucite in a two-dimensional sheet structure. The surface area of talc is divided into two parts: the basal cleavage faces and the margins. Because there is no charged group on the face surface, the talc faces are thought to be non-polar and hydrophobic, but the edges are hydrophilic due to the presence of charged ions (Mg^{2+} and OH^-) [6].

Paper, plastic, paints, polymers, rubber, fertilizers, pesticides, ceramics, and cosmetics are just a few of the sectors that employ talc. To eliminate contaminants from talc, flotation is the favored concentration method. Particle size, pH, collector dosage, depressant dosage, pulp density, and frother dosage, as well as ionic strength and type of available electrolyte in the process water, all influence talc flotation [6]. For most of the metallurgical processes, water is considered an essential medium, which may influence the efficiency of the mineral processing. A thorough understanding of the effects of process water on the various mineralogical processes is thus required. The flotation technology as a process for mineral beneficiation is greatly influenced by the quality of the process water. The precise reasons for these effects are not fully understood. It was reported that water pH, dissolved solids,

organic hydrocarbon reagents, and dissolved oxygen affect the natural hydrophilic qualities of the gangue materials present with the ore so that the gangue is activated and floats in the ore concentrate, which results in adverse effects on the flotation process selectivity [7].

2. EFFECTS OF PROCESS WATER QUALITY ON FLOTATION

The efficiency of the flotation process is directly affected by the quality of the process water, as it plays a significant role in flotation. Therefore, it is essential to recognize and monitor the quality of process water to avoid any adverse effects on mineral flotation processes [8]. It is of paramount importance to understand the influence of water quality, such as the effect of electrolyte levels, to ensure that the water quality and the chemistry of reagents are controlled to guarantee optimum mineral flotation performance.

2.1. The effect of electrolytes on flotation reagents

Reagents are used in flotation by adding them to the flotation pulp. They are added to carry out certain roles, such as manipulating the pulp chemistry and enhancing the differences in mineral surface hydrophobicity, to create suitable flotation performance. It has been proven that it is essential to evaluate the reagent's behavior as a whole and to assess its effects on both the pulp and froth phases [9].

Polymer adsorption on the surface of talc mineral and the consequent depression of naturally floatable gangue are influenced by many factors. These factors include the type of the polymer, concentration, molecular weight, pH, ionic strength, and the degree of substitution. Many studies have been performed for the purpose of investigating the effects of ions present in the process water on the naturally floatable gangue. These investigations have shown that with the existence of Ca^{+2} and Mg^{+2} cations, the activity of a depressant such as carboxymethyl cellulose (CMC) on the talc is improved, pointing out that the solution ionic strength has a critical role in the adsorption of the CMC on the surface of talc. On the other hand, these ions have a damaging effect as they activate the unwanted gangue or depress the valuable mineral. For that, it is of paramount importance to comprehend the depressant behavior used for targeting the naturally floatable minerals in the case of using process water with high ionic strength to be able to optimize the pant performance [10].

[11] has reported that in the presence of Ca^{+2} and Mg^{+2} ions, maximum talc recovery has been obtained. It was suggested that these ions were enhancing the frother adsorption on talc surfaces, increasing the floatability.

2.2. The effect of solution pH on the flotation process

Depending on the water source, various amounts of dissolved solids exist, and thus the pH of the process water may vary. The slurry pH influences the surfactant hydrolysis, the mineral surface charge, and the degree of ionization in the solution. Eventually, the pH of the solution affects the flotation process and its selectivity by

enhancing or impeding the adsorption of the surfaceactive agent at the mineral-water interface [12].

If the pH of the solution is in the alkaline region, then metal ions tend to hydrolyze and precipitate in the form of hydrophilic metal hydroxides, carbonates, or sulphates. The precipitation takes place when their concentrations exceed their solubility limits, resulting in the formation of a hydrophilic barrier to collector adsorption on mineral surfaces [13]. In the literature, the most cited cations causing species precipitation are calcium, iron, and aluminum ions. These have detrimental effects on mineral recovery and grade. It has been reported that these multivalent ions result in depressing coal flotation in the pH region of metal hydroxide precipitation [14].

Generally, talc floatability is not affected by pH, but there is a negative correlation between talc suspension coagulation and pH. It should be noted that the surfaces of talc particles have a net-negative charge, and the zeta-potentials of the talc surface reduced as the pH increased. Talc has the lowest solubility at pH 9.4; by lowering pH, the negative charge of talc decreases, and its solubility enhances. As a result, pH may affect talc floatability. Talc floatability is diminished to varying degrees in acidic and alkaline solutions [6].

2.3. The effect of electrolytes on froth stability

The mineral recovery and grade achieved by the flotation process depend to a great extent on the froth phase stability and structure. The degree of froth stability depends on the type and concentration of the used frother along with the nature and amount of the suspended particles, in terms of size and floatability [15].

It has been reported that the froth phase stability tends to increase as the ion concentration in water increases, which is a consequence of the rise in the stability of the aqueous layer between air bubbles. Water recovery has been linked to the stability of the froth and it was concluded that as the froth stability increases, more water will be recovered in the flotation concentrate. Moreover, the increase in the ionic strength led to an increase in the solid and water recovery, which was linked to the increase in the froth stability [16].

The authors [16] also compared the effects of increasing the frother dosage along with increasing the ionic strength and reported that there is a possibility of varying the frother dosage and the ionic strength of the solution to achieve specific solids and water recoveries for a certain type of operation.

2.4. Electrolytes on the mineral-water interface and the electrical double layer

The chemical composition and the structure of the mineral surface, along with the nature of the electrical double layer, governs the ions' adsorption at the mineral-water interface. Adsorption can be of physical or chemical nature. Physical adsorption involves the counter ions in the double layer, while chemical adsorption is in the form of chemical reactions between the adsorption species and the ions comprising the mineral surface, which is termed chemisorption [17].

The metal ions present in the process water have the potential to change the particles' surface charge, which results in affecting the particles and waste gangue interactions or the interactions between particles and reagents. This leads to inefficient particle–bubble attachment and can affect the stability of the particle–bubble aggregates [18].

Zeta potential value changes due to the ion adsorption onto the mineral surface either by physical or chemical sorption. Moreover, the value of zeta potential can be lowered by changing the concentration of potential-determining ions or by increasing the ionic strength of the solution. If high electrolyte concentrations are present in a solution, the surface charge of particles may change due to the adsorption of cations onto the surface of these particles, which leads to a strong attraction between the particles [17]. This was demonstrated by [19], as it was reported that the adsorption of Ca^{+2} and other metal ions onto the surfaces of particles led to a decrease in their negative surface charge, which resulted in detrimental effects on the adsorption of xanthates onto galena, thus low recovery of galena by flotation.

This paper presents an experimental study conducted through water sampling, quality analysis, and batch flotation tests using talc, to reveal the potential for species migration from cemented paste backfilling specimens containing tailings towards the soak water and the possible influence of these species on the yield, grade, and recovery of talc flotation.

3. MATERIALS AND METHODS

3.1. Overview

The experimental test work was comprised of batch flotation tests using soaked water from two tubs containing two different types of cylindrical solid specimens representing the cemented paste (Shotcrete and Backfill) contained tailings and immersed in tap water. Moreover, the water quality of the soaked water was explored by taking samples and analyzing them for pH, zeta potential, and conductivity using a laser light-scattering BROOKHAVEN instrument (ZetaPALS), in addition to chemical analysis (Ca^{+2}, Mg^{+2}, K^{+} and Na^{+}) to reveal the water chemistry and species migration.

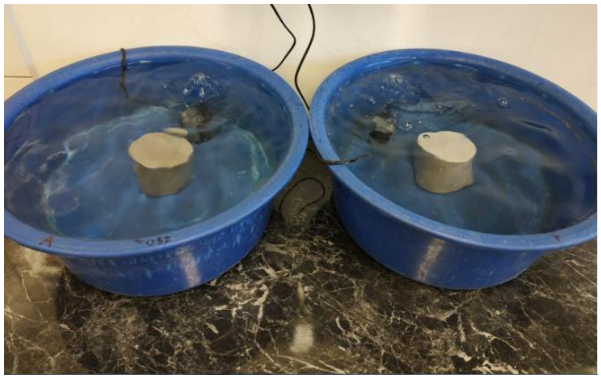

Figure 1
The cemented paste sample soak in tap water

The water tubs containing the cemented paste specimens were subjected to semi-dynamic conditions, being agitated for eight hours per day using submersible pumps to ensure water circulation and contact with the immersed specimen. *Figure1* shows the soak method, and *Table 1* presents the dimensions and the ingredients of the used specimens. The water samples for both quality measurements, and the flotation tests were taken based on different soaking times in the days following the immersion of the cemented paste specimens in the water tubs. Water samples for quality measurements, and for the flotation tests and their sampling times are shown in *Table 2.*

3.2. Sample Preparation

The sample used in the flotation tests, as well in zeta-potential measurements was talc ore from Talc Processing Plant in Gemerska Poloma, which was dry ground to ≤315μm during Bond-tests.

Table 1

Cemented paste specimens dimensions and the ingredients

	Shotcrete (S)	Backfill (B)
Dimensions:		
Diameter (cm)	10 cm	10 cm
Length (cm)	10 cm	10 cm
Ingredients:		
Cement		
Flotation tailings		
Aggregates [>10 mm]		
Technological water		
Additive MG504		
Additive HCA		

Table 2

Quality measurement and flotation tests water samples and their sampling time

Soaked Water Sample (Designation)	Soaking Time (Days)
S.W1, B.W1	Day 1
S.W2, B.W2	Day 2
S.W3, B.W3	Day 3
S.W4, B.W4	Day 4
S.W5, B.W5	Day 8
S.W6, B.W6	Day 9
S.W7, B.W7	Day 10
S.W8, B.W8	Day 11
S.W9, B.W9	Day 14
S.W10, B.W10	Day 15
S.W11, B.W11	Day 16
S.W12, B.W12	Day 17

3.3. Flotation Procedure

A 310 g sample of talc was put into a self-aerated KHD Humboldt Wedag AG flotation machine with a volume of 1 L, and the rotor of the cell was lowered into the cell. The air intake valve was closed, and the cell was filled with water up to the 1 L mark. The rotor (rotation speed = 1900 min^{-1}) was started to agitate the solids for 2 minutes to achieve good conditioning of the pulp and to eliminate any possible air pockets. Afterwards, 4.65 ml of frother (Aerofroth 70, diluted to 1 g/L) was added and conditioned for 2 minutes. The flotation was started by opening the air, which was controlled through the air admission valve, and this was timed using the stopwatch. An additional frother of 4.65 ml was added twice to the rougher stage after 4 and 10 minutes from the start of the test. The froth was collected into the concentrate pan at 15-second intervals for a total of 20 minutes. *Figure 2* illustrates the flotation process flowsheet. After flotation, the concentrates and the tailings were put in the oven at 105 ºC.

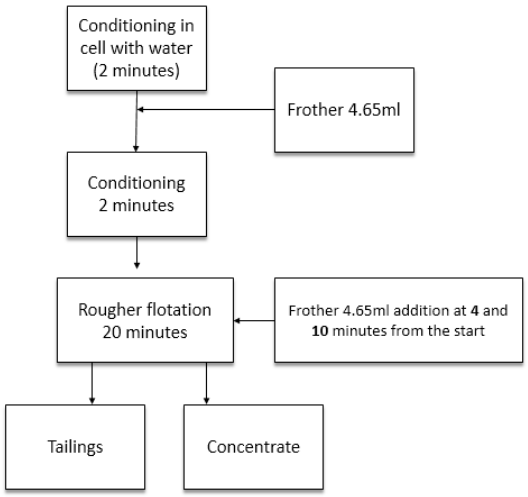

Figure 2
Flotation process flowsheet

3.4. Post Flotation Sample Preparation

The dry samples were removed from the pans, taking special care to avoid loss and contamination of the fine material. The concentrates and tails were placed into small plastic bags. The bags were weighed for dry mass determination and marked for chemical analysis.

4. RESULTS AND DISCUSSION

The results from the chemical composition analysis of the used specimens (Shotcrete, Backfill) can be seen in *Figure 3*, and it reveals that silicon dioxide (SiO2) makes up the largest percentage of the composition (>30%) followed by magnesium oxide

(MgO) and calcium oxide (CaO) in both specimens. In addition to that, there were minor traces of sodium and potassium oxides.

Based on the results from the chemical composition analysis of the cemented paste specimens, it was assumed that the species migration from the immersed specimens towards the soak water would be to a great extent composed of the above-mentioned compounds. The dissolution of these compounds would contribute to an increase in the concentration of the following ions: Ca^{+2}, Mg^{+2}, Na^{+}, K^{+}. Therefore, the water chemistry of the soaked water was analyzed to reveal the behavior of these specific ions.

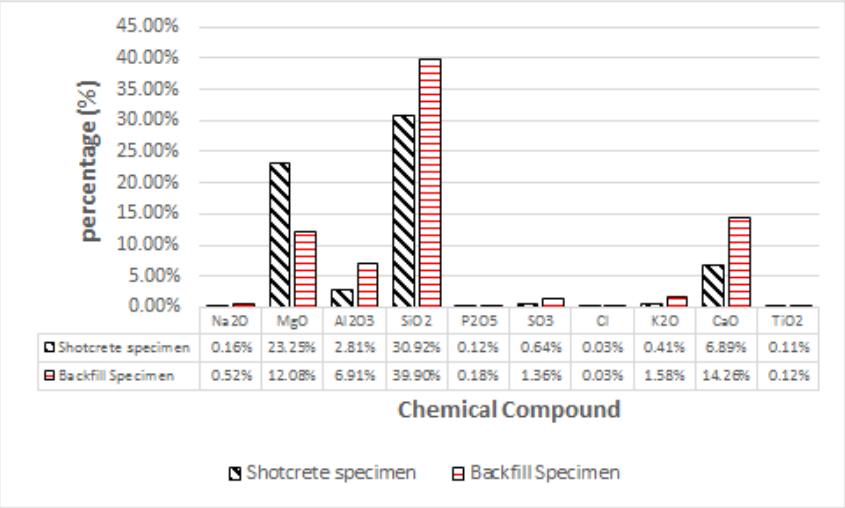

Figure 3
Chemical composition of Shotcrete and Backfill specimens

The test results from the chemical analysis of soak water in *Figure 4*, show that the concentration of calcium ions in the water samples *[Figure 4(a)]* has decreased sharply below that of tap water and continued to decline slightly as a function of soaking time. Magnesium ions *[Figure 4(b)]*, showed little to no change in concentration as the value didn't deviate from that of the tap water at 3.3 mg/L. The concentrations of Na^{+} and K^{+} [*Figure 4(c)* and *(d)*] varied erratically, but the common trend was that these ions were elevated moderately above the level in tap water. It can also be noticed from *Figure 4* that there is no significant difference in the behavior of the soak water from the shotcrete and the backfill specimens.

The initial assumption was that calcium and magnesium ion concentrations were expected to show an increasing trend as a function of soaking time, based on their high content in the immersed specimens. The actual results mentioned above disproved this claim, as the concentration of calcium was showing a decreasing trend as a function of sampling time, while the magnesium concentration showed no change in value. This may be due to favourable conditions for chemical reactions

leading to the consumption of these ions in the water, most likely chemical reactions and bonding between CO_2 and Ca^{+2} species.

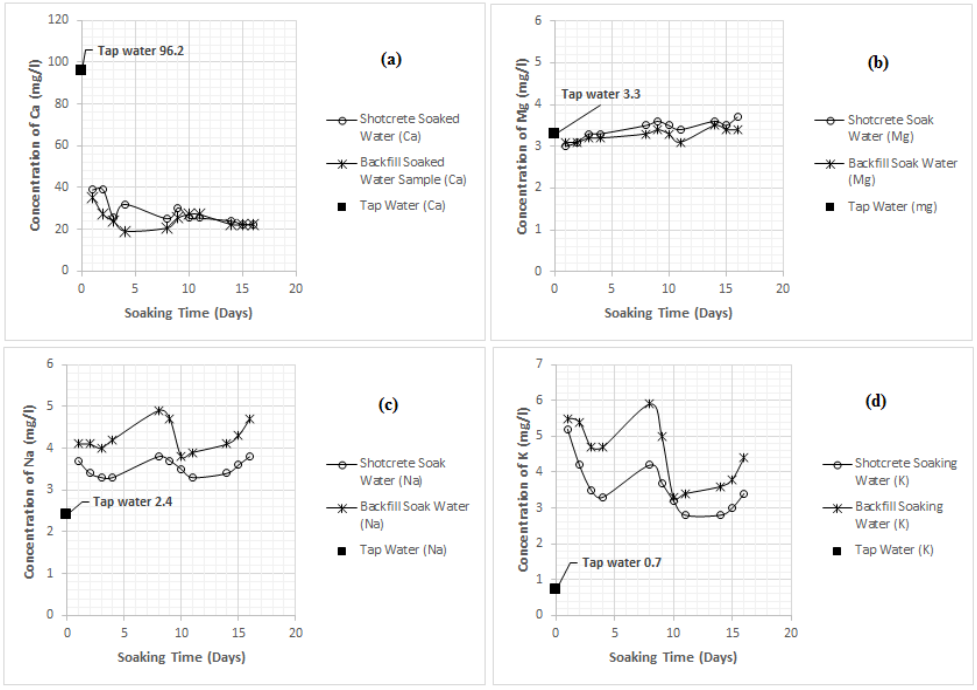

Figure 4
(a) *Concentration change of Ca^{+2};* ***(b)*** *Concentration change of Mg^{+2};*
(c) *Concentration change of Na^{+};* ***(d)*** *Concentration change of K^{+}*

Performing the rougher flotation stage for twenty minutes using the soak water from the two cemented paste specimens resulted in a complete recovery of the talc content in the feed. Therefore, the recovery values from the different flotation tests will not be used for further comparison of the soak waters' impact on talc flotation. The change in the concentrate grade as a function of the flotation mass pull is depicted in *Figure 5*.

Figure 5 shows that soaking water does have an adverse effect on flotation performance. From this, it is clear that the grade of the concentrate was decreasing with the increase of the concentrate yield. The grade of the concentrate was the highest (85%), corresponding to the lowest concentrate yield, with 50.92% obtained after using **B.W8** soak water. Furthermore, the highest concentrate yield (57.38%) using **S.W12** was associated with one of the lowest concentrate grades (74.10%). These results indicate that obtaining a higher concentrate yield had a negative effect on the final grade of the concentrate. Moreover, the soaking time does not appear to have a direct relationship with the yield obtained from the flotation test. However, a correlation of increasing grade with the increase in the soaking time of the cemented

paste specimens was observed. Also, it can be noticed that using shotcrete soak water resulted in a higher concentrate yield when compared to using backfill soak water, which is reflected in their lower concentrate grade.

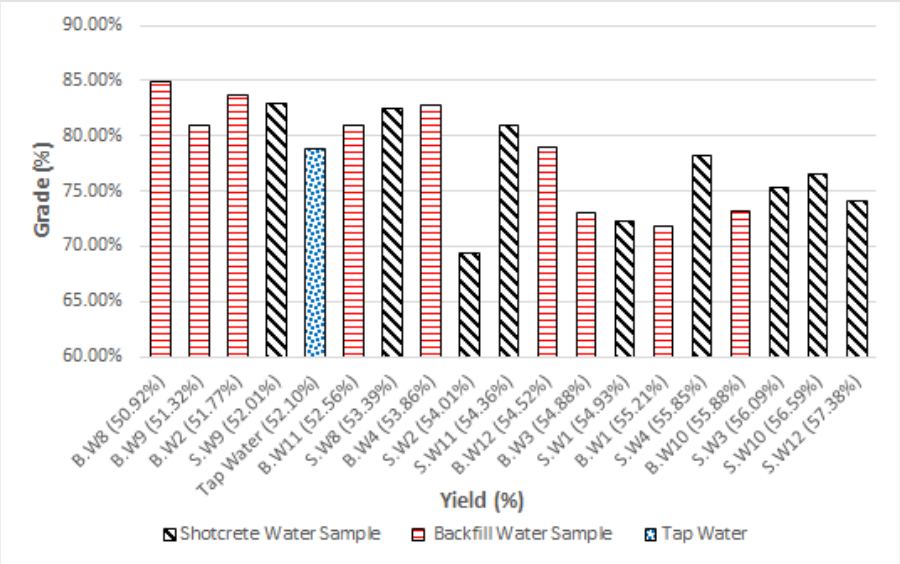

Figure 5
Flotation grade versus yield for different soak water

As initially expected, *Figure 6* shows that the pH of the soaking water has slightly increased over the pH of tap water, to be in the range of 7.8 to 8.15. The original assumption was that the pH increase would take place due to the increase in Ca^{+2} and Mg^{+2}, but based on the water analysis results, this assumption was proven to be invalid. This indicates that other species' migration and dissolution might be responsible for this increase in pH.

Figure 6 also shows that there is no link between the soaking time and pH, as the pH values, although higher than the original tap water, have changed randomly with different soaking times. Moreover, the shotcrete soaking water initially had higher pH values compared to that of the backfill, but as soaking time increased, this difference in pH values began to dissipate, and a less significant difference can be spotted.

In *Figure 7*, the talc flotation yield change as a function of pH is shown. In this plot, it can be seen the talc flotation yield increased with the increase of the pH value of the used process water. The increase was restricted to a pH value of 8.0, after which the talc flotation yield showed a decreasing trend.

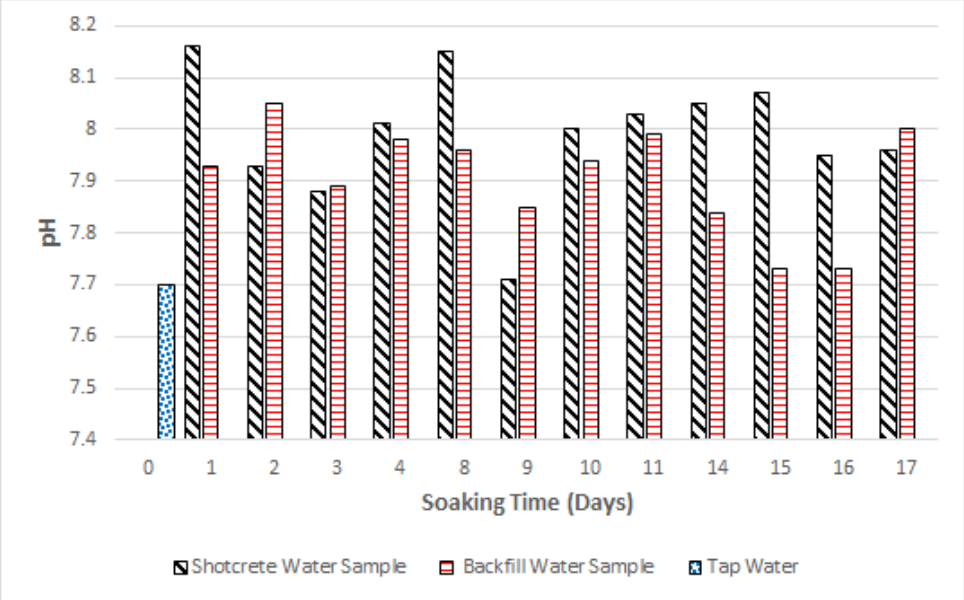

Figure 6
pH change with soaking time

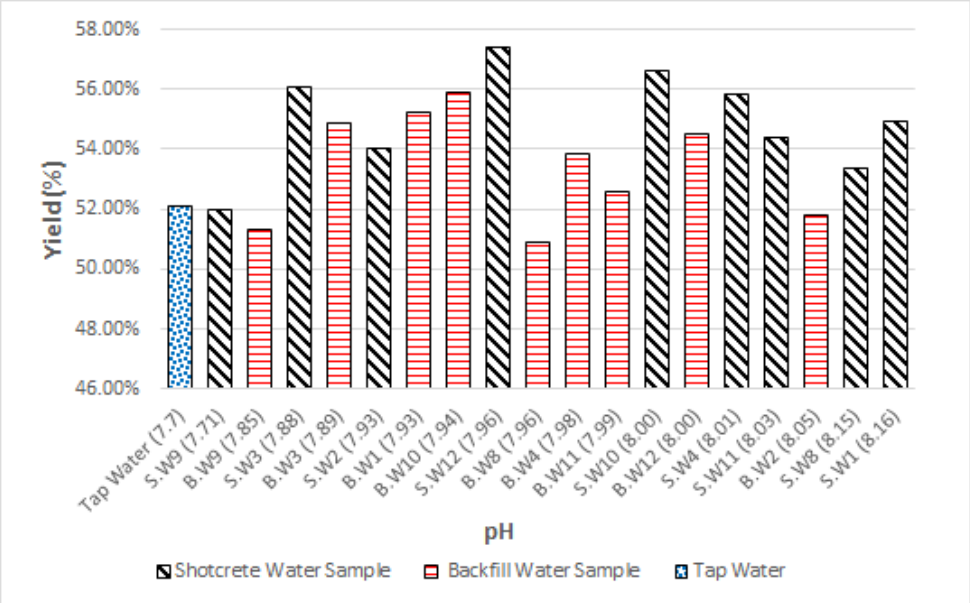

Figure 7
The plot of flotation yield versus pH

It can be seen from *Figure 7* that using shotcrete-soaked water generally results in a slightly higher talc flotation yield compared to using tap water or backfill soaked water. The yield while using shotcrete-soaked water showed a decreasing trend after pH of 7.96, and the yield using backfill soaked water declined after pH of 7.94. The highest flotation yield (57%) was achieved using shotcrete-soaked water after 17 days at a pH of 7.96, while the lowest (51%) was obtained by using the backfill soaked water sample after 11 days at a pH value of 7.96. These results are in agreement with [20], which, based on talc flotation tests, concluded that pH 8.0 was the optimum for talc's natural floatability.

The conductivity, as seen from *Figure 8*, is showing a gradual decrease as the soaking time progressed compared to the original conductivity value for the tap water (1208 µS). This trend in conductivity was completely unexpected since the original assumption was that the migration of species and their dissolution in water would result in higher conductivity values of the soaked water. These results indicate that the system has conditions favoring chemical reactions leading to the consumption of electrolytes in the soaked water. Finally, again, there was no significant difference in the behavior of shotcrete and backfill soaked water in terms of conductivity.

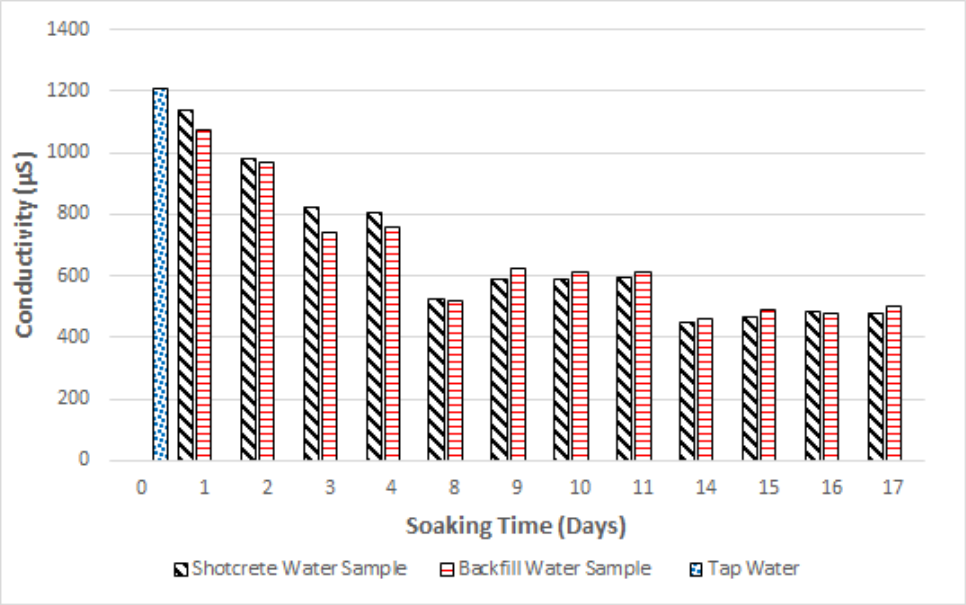

Figure 8
Conductivity change with soaking time

As observed in *Figure 9*, conductivity does influence talc flotation yield. The use of sample **S.W12**, with the lowest conductivity (477 µS) resulted in the highest flotation yield (57.38%).

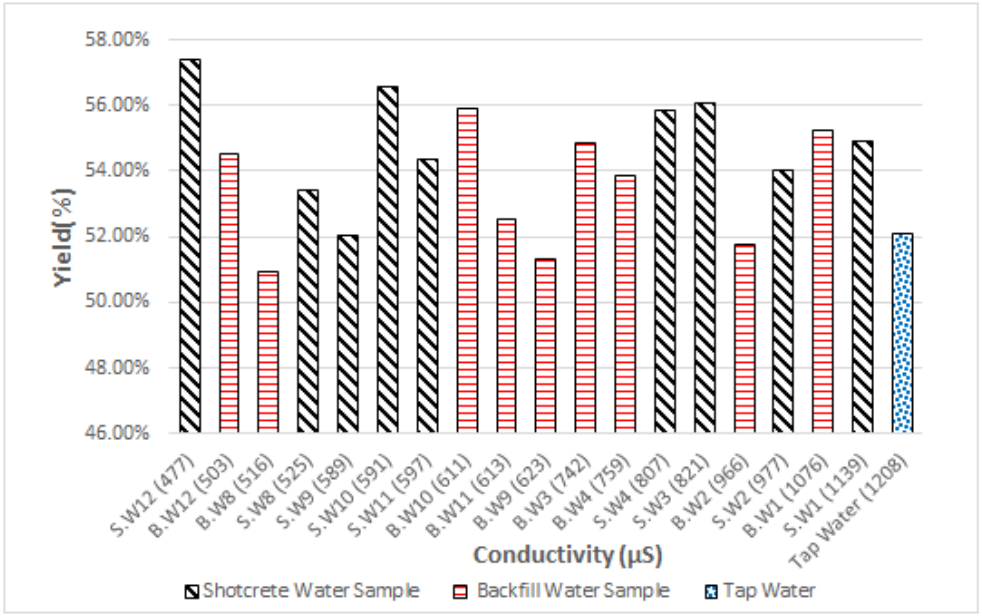

Figure 9
The plot of flotation yield versus conductivity

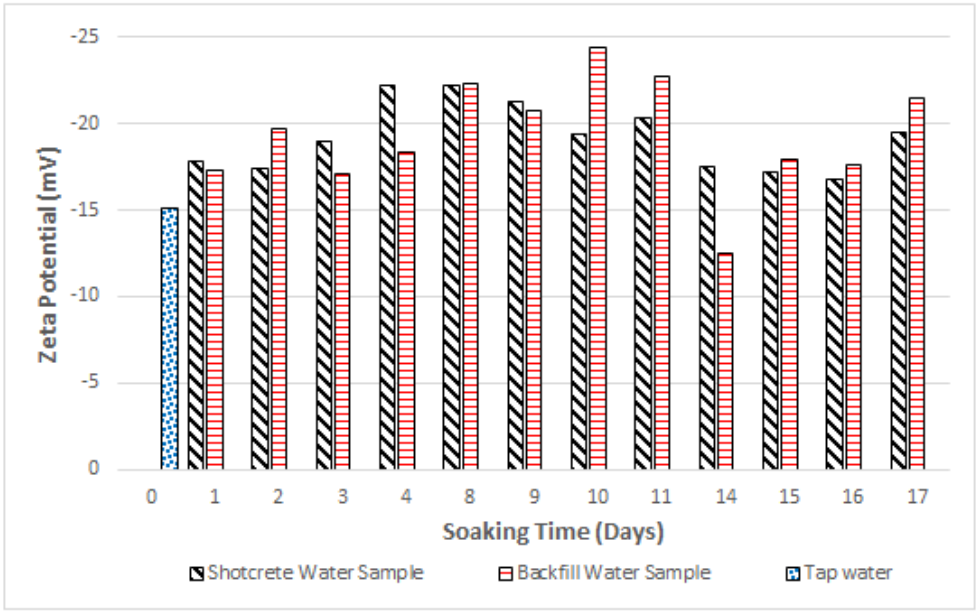

Figure 10
Zeta potential change with soaking time

Tap water with the highest

Tap water with the highest conductivity (1208 µS) produced one of the lowest flotation yield (52.1%) and according to [6] this can be attributed to the presence of high concentration of divalent cations such as Ca^{+2} (96.2 mg/l) which can decrease the natural floatability of talc resulting in a lower flotation yield.

The results from the zeta potential measurements revealed that there is indeed a migration of species from the cemented paste specimens towards the soaking water as the zeta potential values of talc have shown some changes as a function of soaking time. Although there is a lack of a certain trend in the zeta potential values of talc, as can be seen in *Figure 10*, it is observed that zeta potential values of talc increased slightly over the values obtained by using tap water, which indicates that there is some sort of species adsorbing onto the surface of talc particles. It can also be noticed that the behavior of talc zeta potential caused by shotcrete and backfill soaked water showed no significant difference.

From *Figure 11*, it can be seen the flotation yield has highly declined beyond the value of –19.5 mV, in particular with the backfill soaked water. However, this observation is not enough to generalize a legitimate link between zeta potential and talc flotation yield.

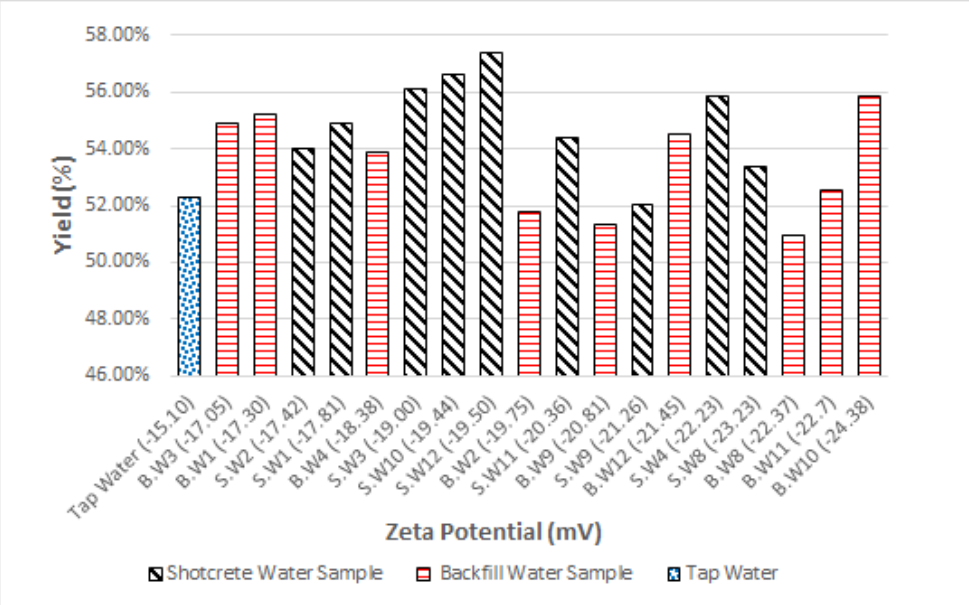

Figure 11
The plot of flotation yield versus talc zeta potential

5. CONCLUSIONS

Based upon laboratory analysis by measuring several water quality parameters (pH, conductivity, and zeta potential) for soaked water samples that resulted from the immersion of two cemented paste fillings at different soaking times, in addition to performing talc batch flotation tests using the soaked water samples, the following conclusions were drawn:

- The immersion of cemented paste fillings has proven to contribute to the migration of species towards the hosting water, and that was concluded based on changes taking place in the water chemistry of the soaked water, as well as due to the changes in the measured quality variables of pH and the conductivity of the soaked water along with the talc zeta potential.
- Although the initial assumption was that calcium and magnesium ion concentrations were expected to show an increase in the soaked water based on their high content in the used cemented paste filling specimens, the actual results disproved this assumption, as the concentration of calcium was showing a decreasing trend as a function of soaking time, potassium and sodium had minor increases, while the magnesium concentration showed no change in value.
- Shotcrete and the backfill specimens were different in composition as indicated in the preparation materials and chemical analysis, but both had similar effects on pH, conductance, and talc zeta potential.
- The results obtained in this study indicate that the soaking water has effect on flotation performance, in particular yield and grade, as a complete recovery was obtained from the 20-minute rougher flotation stage. Batch flotation results indicate that increased mass pull was associated with a lower concentrate grade. The mass pull was independent of the soaking time, while the grade showed some correlation with soaking time, since a better grade was achieved as more soaking time passed.
- Among the three measured variables, the conductance had a blatant tie with the flotation yield of talc since the yield decreased as the conductivity of the used soaked water increased, indicating that high conductivity had a negative effect on the flotation yield of talc mineral.

ACKNOWLEDGEMENTS

The research was carried out within the framework of 19007 – MineTALC. Backfill Mining Optimisation for Low- and Medium- Strength Deposits EIT RIS Project. The support of EIT is highly acknowledged. Special gratitude to Dipl.-Ing. Chrisoph Luckeneder and chemical laboratory staff in Gemerska Poloma.

REFERENCES

[1] Hefni, M., Ahmed, H., Omar, E., & Ali, M. (2021). The Potential Re-Use of Saudi Mine Tailings in Mine Backfill: A Path towards Sustainable Mining in Saudi Arabia. *Sustainability*, 13 (11), 6204. https://doi.org/10.3390/su13116204

[2] Jiao, H., Wu, A., Wang, H., Yang, S., Li, R., & Xiao, Y. (2011). The Influence of Cemented Paste Backfill on Groundwater Quality. *Procedia Earth and Planetary Science*, 2, 183–188, https://doi.org/10.1016/j.proeps.2011.09.030.

[3] Hamberg, R., Maurice, C., & Alakangas, L. (2017). Lowering the water saturation level in cemented paste backfill mixtures – Effect on the release of arsenic. *Minerals Engineering*, 112, 84–91. https://doi.org/10.1016/j.mineng.2017.05.005

[4] MEND. Mine Environment Neutral Drainage (2006). *Paste backfilling geochemistry- Environmental effects of leaching and weathering*. Available at http://www.mend- nedem.org.

[5] Schafer, William (2016). Geochemical Evaluation of Cemented Paste Tailings in a Flooded Underground Mine. In: Drebenstedt, C. & Paul, M.: *IMWA 2016 – Mining Meets Water – Conflicts and Solutions*. Freiberg/Germany (TU Bergakademie Freiberg), 714–724.

[6] Ann Bazar, J., Rahimi, M., Fathinia, S., Jafari, M., Chipakwe, V., & Chehreh Chelgani, S. (2021). Talc Flotation—An Overview. *Minerals*, 11 (7), 662. https://doi.org/10.3390/min11070662

[7] Muzenda, E. (2010). An investigation into the effect of water quality on flotation performance. *World Academy of Science, Engineering and Technology*. Retrieved 3 November 2021, from https://citeseerx.ist.psu.edu/viewdoc/download?doi=10.1.1.190.6757&rep=rep1&type=pdf.

[8] Slatter, K. A., Plin, T, N. D., Cole, M., De Vaux, D., Palm, N., Oostendorp, B. (2009). Water management in Anglo Platinum process operations: effects of water quality on process operations. *Int. Mine Water Conf*., Pretoria, South Africa, 19th–23rd Oct. 2009, Proc. ISBN Number 978-0-9802623-5-3 46–55.

[9] Bradshaw, D., Oostendorp, B., & Harris, P. (2005). Development of methodologies to improve the assessment of reagent behavior in flotation with particular reference to collectors and depressants. *Minerals Engineering*, 18 (2), 239–246, https://doi.org/10.1016/j.mineng.2004.09.012.

[10] Khraisheh, M., Holland, C., Creany, C., Harris, P., & Parolis, L. (2005). Effect of molecular weight and concentration on the adsorption of CMC onto talc at different ionic strengths. *International Journal of Mineral Processing*, 75 (3–4), 197–206, https://doi.org/10.1016/j.minpro.2004.08.012.

[11] Yehia, A., & Al-Wakeel, M. (2000). Talc separation from talc-carbonate ore to be suitable for different industrial applications. *Minerals Engineering*, 13 (1), 111–116, https://doi.org/10.1016/s0892-6875(99)00154-5.

[12] Deng, M., Liu, Q., & Xu, Z. (2012). *Impact of Total Dissolved Solids in Process Water on the Surface Properties of Silica and Sphalerite Minerals*. Society for Minining, Metallurgy, and Exploration, 225–236.

[13] Reyes-Bozo, L., Higueras, P., Godoy-Faúndez, A., Sobarzo, F., Sáez-Navarrete, C., Vásquez-Bestagno, J., & Herrera-Urbina, R. (2014). Assessment of the floatability of chalcopyrite, molybdenite and pyrite using biosolids and their main components as collectors for greening the froth flotation of copper sulphide ores. *Minerals Engineering*, 64, 38–43. https://doi.org/10.1016/j.mineng.2014.04.004

[14] Liu, W., Moran, C., & Vink, S. (2013). A review of the effect of water quality on flotation. *Minerals Engineering*, 53, 91–100. https://doi.org/10.1016/j.mineng.2013.07.011

[15] Wang, B., & Peng, Y. (2014). The effect of saline water on mineral flotation – A critical review. *Minerals Engineering*, 66–68, 13–24. https://doi.org/10.1016/j.mineng.2014.04.017

[16] Corin, K., & Wiese, J. (2014). Investigating froth stability: A comparative study of ionic strength and frother dosage. *Minerals Engineering*, 66–68, 130–134, https://doi.org/10.1016/j.mineng.2014.03.001.

[17] Manono, M., Corin, K., & Wiese, J. (2018). Perspectives from literature on the influence of inorganic electrolytes present in plant water on flotation performance. *Physicochemical Problems of Mineral Processing*, 54 (4), 1191–1214, https://doi.org/10.5277/ppmp18157.

[18] Ata, S. (2012). Phenomena in the froth phase of flotation — A review. *International Journal of Mineral Processing*, 102–103, 1–12. https://doi.org/10.1016/j.minpro.2011.09.008

[19] Ikumapayi, F., Makitalo, M., Johansson, B., & Rao, K. (2012). Recycling of process water in sulphide flotation: Effect of calcium and sulphate ions on flotation of galena. *Minerals Engineering*, 39, 77–88. https://doi.org/10.1016/j.mineng.2012.07.016

[20] Boulos, T., Ibrahim, S., & Yehia, A. (2016). The Art of Talc Flotation for Different Industrial Applications. *Journal of Minerals and Materials Characterization and Engineering*, 04 (03), 218–227. https://doi.org/10.4236/jmmce.2016.43020.

Geosciences and Engineering, Vol. 10, No. 15 (2022), pp. 22–36.
https://doi.org/10.33030/geosciences.2022.15.022

MINERAL COMPOSITION OF RARE ELEMENT ENRICHED ROCK BODIES FROM THE BÜKK MTS., NE HUNGARY

CSILLA BALASSA[1], FERENC KRISTÁLY[2], NORBERT NÉMETH[3]

[1, 2, 3]*Institute of Mineralogy and Geology, University of Miskolc*
[1]*balassacsillu@gmail.com, https://orcid.gov/0000-0001-6134-5262*
[2]*ferenc.kristaly@uni-miskolc.hu, https://orcid.gov/0000-0002-0075-5994*
norbert.nemeth1@uni-miskolc.hu, https://orcid.gov/0000-0002-4264-5136

Abstract: A rare earth (REE) and further rare element (Zr, Nb, Th, Ta) enrichment was found recently within the CriticEl project in 2016. Due to continuing studies, now we know about several enriched rock bodies from the SE and NE part of the Bükk Mts. The enrichment was caused by metasomatic processes, during which fluids penetrated through the rock bodies, causing chemical and mineralogical changes. The enriched rock bodies are Triassic metavolcanics and siliciclastic metasedimentary rocks. The protoliths consist of quartz, feldspars (albite and potassic feldspars), phyllosilicates (various micas and chlorites) and calcite, and in minor quantities Fe- and Ti-oxides, fluorapatite and titanite. The characteristic metasomatic minerals are monazite-(Ce), zircon and Nb-bearing Ti-oxide. Based on our data, micas and potassic feldspars were generated at least partly during the rare element mineralization process, while titanite, chlorite and albite were consumed. Apatite and Ti-oxides were decomposed and formed. The original mineral composition had a strong influence on the rate and mode of alteration.

Keywords: *Rare earth elements (REE), High Field Strength Elements (HFSE), metasomatism, alteration processes, phyllosilicates, feldspars, Bükk Mts.*

1. INTRODUCTION

As part of the CriticEl project and subsequent research programs, a previously unknown high field strength elements (HFSE)enrichment was found in the Bükk Mts [1]. The highest enrichment ratios compared to the upper crust average [2] reach 18 for Zr, 16 for Nb, 30 for Th, and 13 for Ce. The alteration was caused by metasomatic processes, which is proved by the presence of grain replacing aggregates, pseudomorphs and the small grain size (maximum a few tens of micrometers) of the HFSE-bearing minerals: monazite-(Ce), zircon, niobian Ti-oxides, and rare REE carbonates. In addition to the formation of new minerals, the process led to the alteration of the earlier rock-forming minerals. However, it was not the only alteration process to take place in the Bükk, so determining the exact origin of the minerals is often difficult.

Primary deposits of high field strength elements are rare and mainly connected to carbonatites and other alkaline bodies. High-field strength elements can be considered immobile in most geological environments. However, experience has shown that they can be transported by magmatic, metamorphic, and ocean-bottom

hydrothermal solutions. Their mobility is affected by the p-T conditions, pH, and the dissolved ions [3].

Fenitisation is a process which can be compared to what occurred in the Bükk Mts. This is a rock alteration associated with metasomatic enrichment of alkaline elements and HFSEs. The process takes place on a stable continental plate around carbonatites and other alkaline complexes [4]. During the process, the wallrock of the intrusion (which may also be sedimentary layer) is penetrated by volatile elements from an alkaline magma source [5]. According to IUGS, fenites are metasomatic rocks formed at high temperatures. The typical mineral association consist of potassic feldspar and albite, nepheline, alkaline pyroxenes, and amphiboles, as well as smaller amounts of biotite-phlogopite mica, magnetite, ilmenite, titanite and apatite, sometimes calcite [6]. The composition of the resulting fenitic rock depends on the original rock material and the composition of the source magmatic body. Minerals with HFSE content often form polycrystalline aggregates, sometimes with vesicular filling. The typical temperature range can vary from 450 to 700 °C, with a pressure range between 100 bar and 5 kbar. Areas affected by fenitisation can be found to a distance up to 4 km from the source intrusion [4]. In the Bükk Mts. we do not know the source body; probably, it is deeply buried and tectonically disconnected from the altered rocks.

2. GEOLOGICAL SETTING

The age of the outcropping rocks of the Bükk Mts. extends from late Carboniferous to Jurassic, covered with thick Cenozoic sediment. In the area of "Bükk Paraautochthonous" (i.e., Pre-Cenozoic Bükk without the Szarvaskő unit), the Permian-Triassic sedimentation is characterized by marine succession: continuous formation of carbonate platforms from the Late Permian to the Early Triassic, carbonate platforms in the Middle Triassic, and then basin facies sediment formation in the Late Triassic. After a sedimentary gap, they are over-lain by deep-sea siliciclastic-carbonate sediment formation in the Jurassic.

The Middle-Upper Triassic of Bükk is characterized by metamorphosed volcanics and deformed sedimentary layers. Metavolcanics are classified into three formations [7]. Major occurrences of Szentistvánhegy Metaandesite and Bagolyhegy Metarhyolite are located on the north side of the Great Plateau and to the east from it, separated from the small bodies of Szinva Metabasalt by a regional shear zone [1]. These small bodies are usually interbedded into carbonates and can even be peperitic.

In Cretaceous, the Paleozoic-Mesozoic rocks of the Bükk underwent dynamothermal anchizonal regional metamorphism. The degree of metamorphism is not uniform. [8]. Based on the different deformation styles three main tectofacies group can be specified: the North Eastern, Central, and South Eastern Units; among them the Central Unit is the most deformed. The units are divided from each other by fault zones which contain the HFSE-mineralized rock bodies. Mineralized bodies occur in two groups: at the boundary of the North Eastern and Central Units in Lillafüred,

NE Bükk Mts, and at the boundary of the Central and South Eastern Units in the SE Bükk Mts. Sampling localities are shown in *Figure 1*.

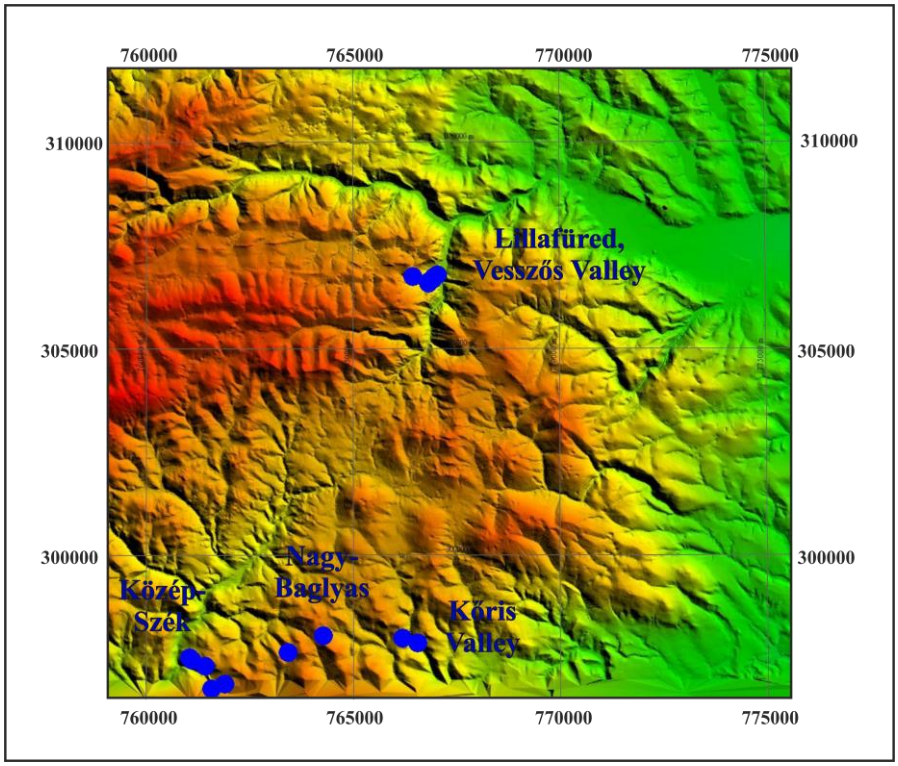

Figure 1
Schematic map showing the localities of the sampled rock bodies
(Digital Elevation Model created by Global Mapper)

3. APPLIED METHODS

The qualitative and quantitative mineral composition of the studied samples was determined by X-ray powder diffraction (XRD). For the measurement, a Bruker D8 Advance (40 kV, 40 mA Cu K-α radiation) machine with a Vantec-1 position sensitive detector was used. The instrument produces parallel beam geometry using a Göbel mirror. The qualitative evaluation was carried out using DiffracPlus EVA software, based on the ICDD PDF2 2005 database, while the quantitative evaluation was carried out with Diffrac.suite Topas software based on the Rietveld method.

Electron-microprobe studies were used to identify the chemical composition of the invidual grains (energy dispersive X-ray spectrometry, EDX point measurement) and to detect the presence of the different minerals on back scatter electron (BSE) images. This method has particular significance because no other method was suitable to detect the HFSE-bearing minerals due to their small grain size and low

amount. For the electron microprobe studies we used a SamX-controlled JEOL JXA 8600 Superprobe electron beam microprobe (15–20 kV accelerator voltage, 20 nA sample current), equipped with an SDD-EDX detector.

Because of the micrometric or submicrometric grain size of the alteration minerals, optical microscopy played a subordinate role, but rock-forming minerals and rock textures were thoroughly examined with it. Both examination methods described above were performed at the Institute of Mineralogy and Geology, University of Miskolc.

4. RESULTS

4.1. Mineral composition of the rock bodies, NE Bükk

In the NE Bükk enriched rock bodies were found at Vesszős Valley, Lillafüred. These rock bodies are siliciclastic sedimentary layers a few decimeters thick, embedded into carbonates of the Hegyestető Formation. Enriched and non-enriched beds with probably similar original composition and environment were also sampled. *Table 1* summarizes the mineral composition of the samples.

Table 1

Mineral composition of rock samples from NE Bükk, based on XRD analyses

	enriched metasedimentary rocks				**non-enriched metasedimentary rock**	**mineralized marly layers**		**wall rock limestone**		
Phase Name	**V18**	**KMA-1**	**KMA-2**	**KMA-3**	**V36**	**V181**	**V182**	**V183**	**V18Ma**	**V18Mb**
quartz	0.14	23.81	2.51	21.22	25.87	1.40	1.48	14.58	0.23	
microcline			1.50							
orthoclase				5.00						
albite					4.97		0.29	0.35		
talc										0.50
chlorite					3.43	2.11	1.08			
illite		9.13	14.06	17.45	10.64	4.39	4.20			
smectite					0.65					
biotite										2.02
muscovite	15.51	56.37	59.31	39.24	0	70.44	17.29	1.21	0.27	0
phengite	66.15	0	0	0	31.05	8.56	0.49	0	0	0
goethite	6.29				0.84		0.28			0.73
anatase					1.08	0.28	0.40			
rutile	0.55									
calcite			5.35		6.27		74.50	80.87	66.91	67.72
dolomite			0.67						26.53	16.50
amorphous	11.36	10.70	16.60	17.10	15.00	12.50		3.00	6.00	7.00

The main rock forming minerals are phengitic dioctahedral micas, but in some less enriched rocks the amount of quartz also can be significant (up to about 25 wt%). Calcite is also a rock forming component of marly beds. Feldspars are minor

components only. In only two samples was the feldspar content detectable with XRD: an enriched layer has about 5 wt% K-feldspar, while the non-enriched sample contains albite in the same amount. The most enriched sample consists almost completely of micas, with a significant amount of goethite (6 wt%) causing its reddish color. Based on the EDX measurements smectite is also an important phase in this rock.

In addition to siliciclastic sedimentary rocks, marly layers and wall rock limestones were also examined. The marly layers also have a slightly raised HFSE-content compared to the wall rocks. These layers contain lower amount of quartz or mica, and 1-2 wt% chlorite. The wall rock of the most enriched bed consists of calcite and dolomite (whereas the marly layers do not contain any dolomite). Other important minerals could be chlorites, phlogopite, and iron-oxides, and based on optical microscopy potassic feldspar is also present as vein and void filling phase.

Minor and accessory phases present in the Vesszős Valley samples are apatite, detrital zircon, and rare monazite, which can be distinguished from their metasomatic counterparts by their larger size (some tens of micrometers). Probably Ti-oxide minerals occurred also as detrital grains, replaced and transformed into niobian Ti-oxides and sometimes into REE-Nb-Ti oxides. The wall rock limestone also contains HFSE minerals.

4.2. Mineral composition of the rock bodies, SE Bükk

The studied rocks from SE Bükk are partly metavolcanics (Nagy-Baglyas, Kőris Valley), partly siliciclastic sedimentary beds (Közép-szék), although these latter beds may represent redeposited volcaniclastics as well. Mineralized metavolcanics most probably belong to the Szinva Metabasalt Formation, and could be divided into two groups, “pure” metavolcanics and peperites. Peperite is defined as tuff or breccia material, which is formed by pushing magma into wet sediment [9]. The mineral composition of the samples is summarized in *Table 2*. Metavolcanics usually contain micas and feldspars in similar quantities. Feldspars are albite and potassic feldspars (Ca-plagioclase is absent). In most of the cases chlorite is not detectable by XRD, only by electron-microprobe analyses. The quantity of quartz is highly variable, ranging from 5 to 40 wt%. The calcite is often significant as a peperitic constituent, but usually rock bodies with higher calcite content have lower HFSE values. Non-mineralized rocks from Szinva Metabasalt contain significantly more albite, chlorite and titanite, and only minor quartz.

The composition of the siliciclastic sediments from the area is variable, but most often they contain less feldspars than metavolcanics, and these feldspars are mainly albites. Dioctahedral micas and quartz are general constituents, but their quantity varies. Certain layers can contain calcite and/or chlorite.

In both rock types, iron- and titanium-oxides, apatite and dioctahedral micas are important minor constituents. The metasomatic mineral phases are niobian Ti-oxides, zircon, monazite, and in one sedimentary rock REE-carbonates.

Table 2

Mineral composition of rock samples from SE Bükk, based on XRD analyses

		mineralized metavolcanics		slightly affected metavolcanics	chert	peperitic metavolcanics				
Phase Name	**1167**	**HOR 12**	**HOR 31**	**HÓR 25**	**783/2**	**783/1**	**783/3**	**783/4**	**783/5**	**783/6**
quartz	34.0	14.6	12.8	19.51	36.41	30.62	41.32	18.85	23.20	6.23
tridymite								0.20		
microcline			13.2					6.62		3.61
albite	6.3	10.2	17.0	29.19	0.53	7.29	1.32	9.83	7.64	11.75
sanidine		25.1		0.91						
orthoclase	8.0	5.6			2.10	3.85	2.33	1.29	1.18	
kaolinite					2.14					
chlorite IIb			8.8	7.08						
smectite				0.85						
celadonite				13.73						
biotite 1M		0.5			6.25	1.54				
muscovite	1.9	5.7	26.2	7.69	7.01	3.61	4.1	1.51	1.36	1.9
illite	25.5	29.2	6.8	11.82	7.47	0	9.69	10.84	0	25.5
goethite					0.60	1.07	0.93	1.21		0.78
titanite			2.5							
anatase			1.0	2.22	0.52		0.29	0.09	0.16	0.32
rutile										0.13
calcite	17.0				18.09	23.05	17.47	19.93	19.05	28.10
calcite (Mg)					15.18	21.03	11.84	12.56	41.81	31.89
ankerite								0.48		
amorphous	7.3	9.1	8.4	7.00	3.70	7.95	10.70	16.60	5.60	17.20

	peperitic metavolcanics			wall rock carbonate	siliciclastic sedimentary rocks?				
Phase Name	**783/7**	**783/8**	**783/9**	**783/10**	**HOR 41**	**HOR 42**	**HOR 38**	**HOR 39**	**HOR 40**
quartz	5.55	7.92	6.62	14.63	7.71	15.4	52.09	24.20	63.96
microcline	2.01	2.30	3.37	0.66					
albite	10.51	8.26	11.85	10.47		14.1	5.85	0.69	0.26
sanidine					7.93	22.3			
orthoclase	2.29	3.24	4.56			4.9			
kaolinite			1.20						
chlorite							5.59	0.54	6.47
biotite		1.11	0.84			3.1	0.67	0.73	0.62
muscovite	0	0	0	0	1.56	0	20.78	50.63	17.38
illite	2.9	3.91	5.17	0	6.74	20.8	5.62	10.58	5.02
goethite	1.42	0.48	0.39	0.17		1.1			
titanite					0.72				
anatase	0.13	0.32	0.45	0.11		0.5	0.48	0.51	0.28
rutile	0.16	0.04	0.05	0.09					

	peperitic metavolcanics			wall rock carbonate	siliciclastic sedimentary rocks?				
calcite	28.82	33.58	29.15	36.19	26.57	13.5	3.90	0.12	
calcite (Mg)	39.41	30.83	28.44	30.39	43.81				
ankerite					1.96				
amorphous	6.80	8.00	7.90	7.30	3.00	4.2	5.00	12.00	6.00

4.3. Characteristics of the minerals

The identified mineral phases are partly inherited from the protolith, which itself is a metamorphic rock, or can be formed during metasomatism. Most of the mineral groups could be the product of different processes, e.g. micas could form during sericitization or other alteration processes, but sometimes original, deformed magmatic mica plates are observable as well. In the following we summarize the distinguishing characteristics of the most important mineral groups.

Feldspars

Except for some siliciclastic and marly layers from Vesszős Valley, all studied rock bodies contain alkaline feldspars. The higher the K-concentration in a rock body, the higher the rate of potassic feldspars to albite in general, but rocks with low feldspar and high mica content often have albite dominance. Potassic feldspars have the highest share of total feldspars in metasomatised metavolcanics, while other, non-mineralized metavolcanics from the Bükk Mts. usually contain albite. Based on our observations, metavolcanics with higher albite contents usually have lower HFSE-concentrations. There are albite phenocrysts which are relict and/or dissolved, and fine-grained albite occurs replacing other phenocrysts (with potassic feldspars, calcite and mica) and in the matrix. Potassic feldspars are either replacement phases or fine-grained matrix constituents, often associated with metasomatic monazite.

Micas

The micas in the rock bodies are predominantly dioctahedral with phengitic composition. According to XRD, they can have both illite and muscovite structure. The peperitic and carbonate samples with low HFSE concentrations contain very low amounts of mica. In other cases, micas dominate the oriented matrix, but also occur as replacement phases (in plagioclase and other pseudomorphs) and as vein fillings. The chemical composition measured by EDX are diverse *(Figure 22)*, with K-content ranges between 2.5–4.5 atomic%, Fe between 0.05–3 atomic%, Mg between 1–4 atomic%. These differences may indicate more than one generation of micas, but this could not be verified. Because of the small grain size of the mica in the matrix, neighbouring minerals often influence our measurements, or we measure a group of grains instead of an individual plate; therefore, chemistry data

based on EDX are not always absolutely accurate. Phengites from the most enriched layer usually lack Fe in their composition, and often have a low F-content (about 1 atomic %). Biotite may occur in metavolcanics as a rock forming mineral: these are mainly large, deformed plates, i.e., inherited crystals, which are clearly observed with an optical microscope. Sometimes secondary biotites could be present. They occur in vein filling and grain replacing position, in some cases together with metasomatic HFSE-minerals, like zircon. The wallrock carbonates from Vesszős Valley do not contain any dioctahedral micas, but the phlogopites are also iron-poor and have F-content up to 3.6 atomic %.

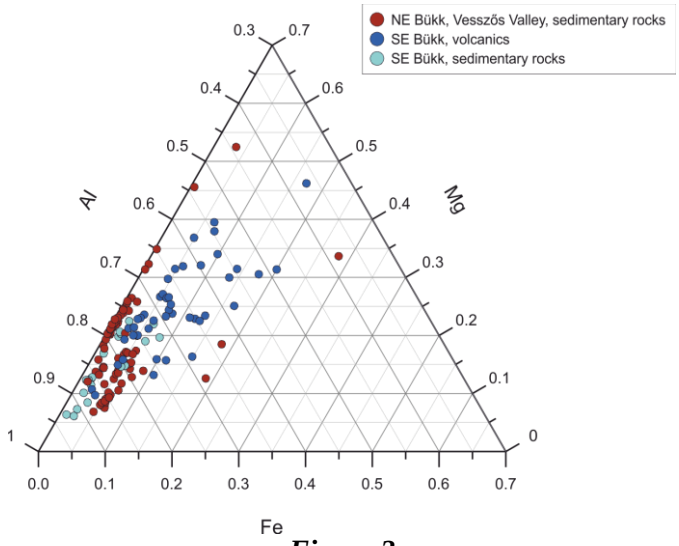

Figure 2

Crystal chemistry of dioctahedral micas, based on EDX data

Chlorites

Chlorite is a major rock forming mineral both in metavolcanics and shale formations of the Bükk Mts. In our sample set, it was detected with XRD in marly and carbonate samples and in non-mineralized rocks only, but it was often observed with electron microprobe at several points, mainly in less enriched samples. These are the samples that contain the most albites. Chlorite compositions might be diverse like in the case of micas, but some samples display specific compositions: the chlorites of the carbonate wall rock of the most enriched sample from Vesszős Valley do not contain any iron, similarly to the phlogopites of this layer.

Ti-oxides

Ti-oxides are common accessory minerals in all of the studied rock bodies. Based on XRD, Ti-oxide can be both rutile and anatase. Ti-oxides are very often present as decomposed, relict grains or as concretions on grain edges. Ti-oxides of the most

enriched rock body usually are disseminated micrometric, euhedral–rhombohedral grains, but in several cases, these form veinlets and nests associated with zircon of similar size. In other cases, Ti-oxides are associated with apatite, either in nests or on edges of relict grains. However, in samples from Szinva Metabasalt which are not affected by the alteration, electron microprobe studies showed that the characteristic Ti-containing accessory mineral is titanite [1]. Based on data in the literature, hydrothermal alteration of titanite can create titanium oxide [10].

Based on electron microprobe analysis, Ti-oxides of the mineralized rock bodies contain Nb. Typical Nb_2O_5 content ranges from 0.5% to 8% and can vary widely within a given sample. In the Vesszős Valley samples a REE-Nb-Ti-oxide mineral was also detected: according to its composition it is aeschynite or euxenite.

Other accessory minerals

Apatites can form small-grained assemblages associated with titanium-oxides, as nests of dissolved grains or with Ti-concretions on their boundary. Apatite phenocrysts are in several cases fragmented or zoned. Based on these types of appearance, it is possible that more than one generation is present. The occurring apatites are always F-apatites, with low Cl-content occasionally (0.1 to 0.2 atomic %). They could contain REEs, but according to EDX measurements always less than 1 atomic % (including Y). These grains occur next to HFSE minerals. Apatite grains with Ti-oxide on the edges rarely contain REEs.

Monazites of the studied samples are always Ce-dominant. Monazites are usually present as μm sized disseminated grains, but often form band-like concretions and linear arrays along grain boundaries or fractures. They could be associated to Fe-oxides. Sometimes monazites form 100 μm large aggregates, but it is a rare phenomenon. Although non-mineralised siliciclastic layer from Vesszős Valley also contains monazites, they are different in chemical composition and size from the others, which refers to their detrital origin.

Other REE minerals are rare, restricted to certain localities. HREE-bearing xenotimes were detected in two measuring points from siliciclastic sedimentary rock, SE Bükk only. REE carbonates (bastnäsite and parisite) were also found in metasediments of the SE Bükk.

Zircon is observed as idiomorphic phenocrysts or fragments in 100 μm magnitude, but also could be a metasomatic product. In this case it is micrometric, occurring in veinlets in the micaceous matrix or as replacement, associated with Nb-bearing Ti-oxides.

4.4. Possible alteration processes

Based on the results of chemical analyses HFSE-enriched rock bodies are usually characterized by an increased K-content compared to non-mineralized bodies. This suggests that fluids carried the HFSEs were originally K-rich, so the process that occurred was similar to the potassic case of fenitisation. This type is characteristic for shallower depths because K is more mobile than Na at low temperatures. The

potassic type fenite can contain up to 90% potassic feldspar and may include albite, apatite, pyroxene, and rutile. If Mg is added to the system, potassic feldspar may be transformed to phlogopite [11]. Although the typical mineral association is not totally the same as in the Bükk, here there are also signs that new potassic feldspars were generated, while the albites usually occur as partially transformed relict grains. In rare cases, slightly elevated HFSE-content without potassic metasomatism was also observed, but these anomalous samples belong to formations which had a relatively high HFSE content primarily. Based on the XRD data the potassic feldspars can be orthoclase, microcline and sanidine alike. Metavolcanics of the Bükk Mts. contain microcline and, in minor amount, orthoclase, but do not contain sanidine as a rock forming mineral in general, so sanidine also can be assumed to be the product of the metasomatism.

Metasomatized siliciclastic metasedimentary rocks with low total feldspar and high mica content often have more albite than K-feldspars, or albite is the only feldspar. The low rate of potassic feldspars does not mean the lack of K enrichment, but here micas incorporated the excess potassium. As chlorites occur in low abundance in the mineralized rocks, these were probably decomposed during the alteration process and altered to phengitic mica due to potassium gain. This is indicated by the similar Mg/(Mg+Fe) ratios of coexisting mica and chlorite phases, while an earlier generation of mica of the same rock has different ratios *(Figure 33)*. Mica and chlorite in these samples also display transitional compositions, and similar textural occurrence. Micas, both phengitic dioctahedral micas and biotite, are generally associated with HFSE-bearing minerals, which further supports their relationship with the mineralization. The differences in the chemical composition and appearance of the relict and metasomatic biotites are shown in *Figure 4*.

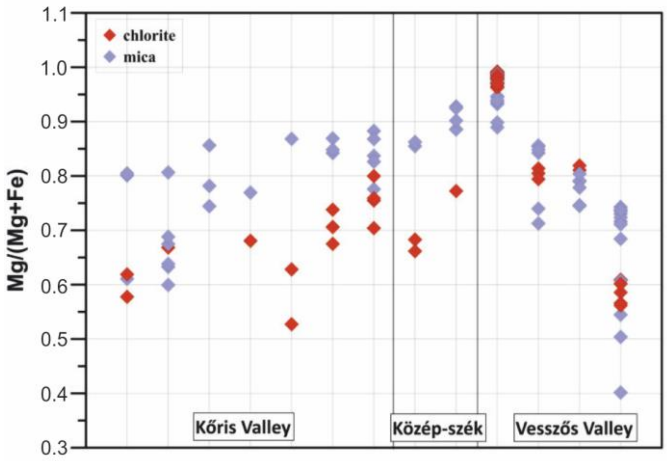

Figure 3
Crystal chemistry of micas and chlorites. Points below each other belong to the same samples.

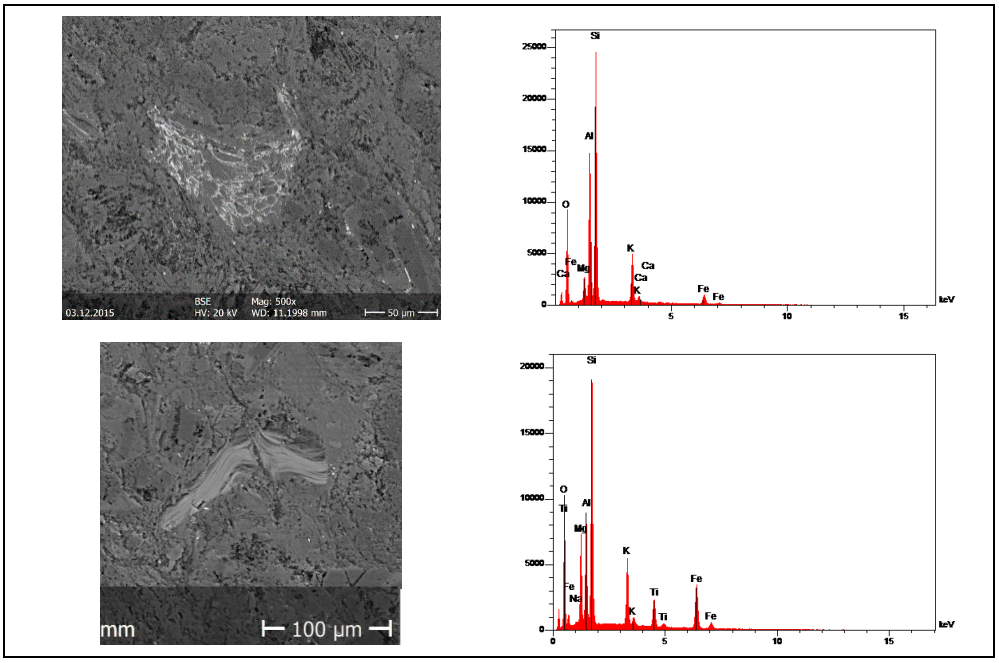

Figure 4

Newly formed biotite with zircon (upper image) and a bent, relict plate (lower image) (BSE images and EDX spectra). Ti is detected in the relict grain only.

The role of other rock-forming minerals during the mineralization is less clear. Some highly enriched rock bodies contain significant amount of quartz, while in others it is lacking almost completely. According to the classical definition of fenitisation, during the process the amount of quartz usually decreases, but depending on the initial composition the reverse situation also could occur [11–14]. Mineralized rocks in the Bükk Mts. also can display either a high abundance or a complete lack of quartz, although this may depend on the initial composition. The non-enriched, non-peperitic metavolcanics of the Szinva Metabasalt Formation usually have 1–3 wt% quartz, while the enriched ones 5–40 wt%, so it seems that here the enrichment causes quartz gain. However, it is not the most enriched samples that contain the most quartz, so the role of other circumstances should be considered. In the peperitic metavolcanics the amount of quartz of sedimentary origin is likely to be significant, just like in cherty limestone. In metasedimentary rocks there are enriched rocks without quartz (Vesszős Valley) or with quartz content up to 50 wt%. Here the initial composition was the main controlling factor. Examples from the literature prove that quartz could be consumed during the genesis of potassic feldspars [15]. Mica could be also generated from quartz and feldspars [16], while in other cases micas and quartz are the consuming phases and potassic feldspars are generated [15].

Accessory minerals also could play an important role during mineralization. Preexisting apatite can serve as a trap for REEs, or the P content may contribute to monazite formation [17,18]. Apatite may be the product of fenitisation[19] and we cannot exclude the possibility that newly formed apatites are also present. Based on our observations, apatite belongs to the group of consumed phases, as mineralized rocks are P-depleted. Several grains are remnants of partly dissolved phenocrysts. REE content is rarely detectable by EDX; therefore, it is not a significant host of the HFSE enrichment.

Ti is another depleted element in the mineralization, and titanite, an accessory phase of the precursor rocks, is lacking. Titanite, also a potential host of HFSE, can be replaced by aggregates of fine-grained minerals such as monazite, rutile, apatite, quartz, calcite, chlorite, due to hydrothermal processes [20]. Although no altered titanite was identified, similar alteration is also likely to occur in our case, producing fine-grained Ti-oxides and other minerals. Relict anatase grains are mostly replaced by fine-grained aggregates of Ti-oxides, zircon, and apatite. Ti-oxides can also be altered by a combined dissolution and deposition process, generating high-porosity trace-element-rich grains and newly formed Ti-oxide elsewhere at the same time [21]. In our case, the fine-grained assemblages on the grain edges, in veinlets and in replaced grains may be the newly formed phases. The most important role of Ti-oxides is to incorporate Nb into their structure, so the released Ti of preexisting minerals can serve as a significant contribution to the Nb enrichment. In the enriched Vesszős Valley rocks, the Nb-carrier phase is aeschynite, which probably also occurs as replacement of earlier Ti-oxides.

5. CONCLUSIONS

Metasomatic HFSE-enrichment in the rocks of the Bükk Mts. caused changes in the mineral composition, which depend highly on the preexisting mineral association. Silicate minerals – mainly feldspars and phyllosilicates – played the most important role in the alteration process. Consumed mineral phases are albite (mainly in feldspar-rich metavolcanics), chlorite, apatite and Ti minerals, but most probably the last two are also present as newly precipitated grains in decreased quantities. Minerals which are partly formed due to the alteration process are micas (mainly dioctahedral phengite-like micas, but also trioctahedral biotites), potassic feldspars, and HFSE-bearing minerals. The probable alterations are chlorite → mica, titanite → Ti-oxide and albite → potassic feldspars. If the quantity of feldspars is low in the original rock, micas incorporate the excess K. The alterations above correspond well with the general K-gain observed in HFSE-enriched rock bodies, although it is quite probable that other mineral phases (e.g., quartz, calcite) also took place in different reactions. The exact processes depend highly on the original composition of the protolith, so different parageneses were produced in rock bodies of different mineralogical composition.

ACKNOWLEDGEMENTS

The research was carried out at the University of Miskolc both as part of the project implemented in the framework of the Thematic Excellence Program funded by the Ministry of Innovation and Technology of Hungary, and the project supported by the Ministry of Innovation and Technology of Hungary from the National Research, Development and Innovation Fund in line with the Grant Contract issued by the National Research, Development and Innovation Office.

The authors would like to thank Délia Bulátkó-Debus for her help with the laboratory work.

REFERENCES

[1] Németh N., Baracza M. K., Kristály F., Móricz F., Pethő G., Zajzon N. (2016). Ritkaföldfém- és ritkaelem-dúsulás a Bükk hegység délkeleti részének vulkáni eredetű kőzettesteiben. *Földtani Közlöny*, 146 (1), pp. 11–26.

[2] Rudnick, R., Gao, S. (2013). Composition of the Continental Crust. *Treatise on Geochemistry*, 4, https://doi.org/10.1016/B978-0-08-095975-7.00301-6.

[3] Jiang, S.-Y., Wang, R.-C., Xu, X.-S., Zhao, K. (2005). Mobility of high field strength elements (HFSE) in magmatic-, metamorphic-, and submarine-hydrothermal systems. *Physics and Chemistry of the Earth Parts A/B/C*, pp. 1020–1029, https://doi.org/10.1016/j.pce.2004.11.004.

[4] Pirajno, F. (2013). *Effects of Metasomatism on Mineral Systems and Their Host Rocks: Alkali Metasomatism, Skarns, Greisens, Tourmalinites, Rodingites, Black-Wall Alteration and Listvenites*. https://doi.org/10.1007/978-3-642-28394-9_7

[5] Rock, N. M. S. (1976). Fenitisation around the Monchique alkaline complex, Portugal. *Lithos*, 9, pp. 263–279, https://doi.org/10.1016/0024-4937(76)90018-9.

[6] Zharikov, V. A., Pertsev, S. S., Rusinov, V. L., Callegari, E., Fettes, D. J. (2007). Metasomatism and metasomatic rocks. In *Recommendations by the IUGS Subcommision of the Systematics of Metamorphic Rocks*. British Geological Survey, https://silo.tips/download/9-metasomatism-and-metasomatic-rocksf.

[7] Less G., Kovács S., Pelikán P., Pentelényi L., Sásdi L. (2005). *A Bükk hegység földtana: Magyarázó a Bükk-hegység földtani térképéhez (1:50 000).* Magyar Állami Földtani Intézet, Budapest.

[8] Árkai, P. (1983). Very low- and low-grade Alpine regional metamorphism of the Paleozoic and Mesozoic formations of the Bukkium, NE-Hungary. *Acta Geologica Hungarica*, 26, pp. 83–101.

[9] Maitre, R., Streckeisen, A., Zanettin, B., Le Bas, M., Bonin, B., Bateman, P. (2004). Igneous Rocks: *A Classification and Glossary of Terms*. Cambridge, UK: Cambridge University Press.

[10] Morad, S., El-Ghali, M., Caja, M. Á., Sirat, M., Al-Ramadan, K., Mansurbeg, H. (2010). Hydrothermal alteration of plagioclase in granitic rocks from Proterozoic basement of SE Sweden. *Geological Journal*, 45, 105–116. https://doi.org/10.1002/gj.1178

[11] Elliott, H. A. L., Wall, F., Chakhmouradian, A. R., Siegfried, P. R., Dahlgren, S., Weatherley, S., Finch, A. A., Marks, M. a. W., Dowman, E., Deady, E. (2018). *Fenites associated with carbonatite complexes: A review*. https://doi.org/10.1016/j.oregeorev.2017.12.003

[12] Currie, K. L. (1971). A Study of Potash Fenitization around the Brent Crater, Ontario,—A Paleozoic Alkaline Complex. *Canadian Journal of Earth Sciences*, 8 (5), pp. 481–497, https://doi.org/10.1139/e71-052.

[13] Morogan, V., Woolley, A. R. (1988). Fenitization at the Alnö carbonatite complex, Sweden; distribution, mineralogy and genesis. *Contributions to Mineralogy and Petrology*, 100 (2), pp. 169–182. https://doi.org/10.1007/BF00373583

[14] Dowman, E., Wall, F., Treloar, P. J., Rankin, A. H. (2017). Rare-earth mobility as a result of multiple phases of fluid activity in fenite around the Chilwa Island Carbonatite, Malawi. Mineralogical Magazine, 81 (6), pp. 1367–1395, https://doi.org/10.1180/minmag.2017.081.007.

[15] Mian, I., Bas, M. J. L. (1987). The biotite-phlogopite series in fenites from the Loe Shilman carbonatite complex, NW Pakistan. *Mineralogical Magazine*, 51 (361), pp. 397–408. https://doi.org/10.1180/minmag.1987.051.361.06

[16] Ferguson, J., McIver, J. R., Danchin, R. V. (2010). Fenitisation associated with the alkaline-carbonatite complex of Epembe, South West Africa. *Trans. Geol. Soc. S. Afr*., 78, pp. 111–121.

[17] Chen, W., Honghui, H., Bai, T., Jiang, S. (2017). Geochemistry of Monazite within Carbonatite Related REE Deposits. Resources, 6 (4), p. 51. https://doi.org/10.3390/resources6040051

[18] Migdisov, A., Williams-Jones, A. E., Brugger, J., Caporuscio, F. A. (2016). Hydrothermal transport, deposition, and fractionation of the REE: Experimental data and thermodynamic calculations. *Chemical Geology*, 439(C), Article LA-UR-16-21989, https://doi.org/10.1016/j.chemgeo.2016.06.005.

[19] Dumanska-Slowik, M., Heflik, W., Kromska, A., Sikorska, M. (2015). Sodic fenites of the Oktiabrski Complex exposed in the Khlibodarivka quarry (East Azov, SE Ukraine): Reconstruction of their growth history. *Neues Jahrbuch für Geologie und Paläontologie – Abhandlung*en, 275. https://doi.org/10.1127/njgpa/2015/0471

[20] Pan, Y., Fleet, M. E., MacRae, N. D. (1993). Late alteration in titanite (CaTiSiO5): Redistribution and remobilization of rare earth elements and implications for U/Pb and Th/Pb geochronology and nuclear waste disposal. *Geochimica et Cosmochimica Acta*, 57 (2), pp. 355–367. https://doi.org/10.1016/0016-7037(93)90437-2

[21] Zeh, A., Cabral, A. R., Koglin, N., Decker, M. (2018). Rutile alteration and authigenic growth in metasandstones of the Moeda Formation, Minas Gerais, Brazil – A result of Transamazonian fluid–rock interaction. *Chemical Geology*, 483, pp. 397–409, https://doi.org/10.1016/j.chemgeo.2018.03.007.

Geosciences and Engineering, Vol. 10, No. 15 (2022), pp. 37–49.
https://doi.org/10.33030/geosciences.2022.15.037

INVESTIGATION OF THE POSSIBILITY OF EXTENDING SOIL MOISTURE SENSOR DATA

TAMÁS DEÁK, RÉKA DIÁNA BERTÓTI, ENDRE DOBOS

Institute of Geography and Geoinformatics, Faculty of Earth Science and Engineering, University of Miskolc

Abstract: Smart irrigation requires soil moisture (SM) data in order to determine the water needs of each point within the agricultural field. The aim of the study is to develop methodologies for testing different approaches and to present the provisional results. A complex methodology was applied to process and analyze the sensor data. First spatial variability was assessed using regression and geostatistical interpolation. A vertical distribution estimation was performed by extending the SM values of each sensor for all their depth levels. The latest results of this method show that the statistical correlations between the different depths can be used to characterize the soil types and their corresponding vertical SM distribution.

Keywords: *Soil science, soil moisture, statistics, Sentek, soil moisture sensor*

1. INTRODUCTION

In Hungary, drought periods are getting longer due to the deteriorating soil conditions caused by the agricultural sector since the first industrial revolution and as a result of the decreasing amount of rainfall [1]. More and more farmers are considering building their own irrigation systems in order to supply the water necessary for keeping their crops alive. Although Hungary has a great supply of water, the price over the years will increase and the question of "how much water do we need for the crop" will become more frequent and difficult to answer. Precision agriculture might have an answer. It uses spatially specific data to make decisions like where, when, why and how we should water the crops [2].

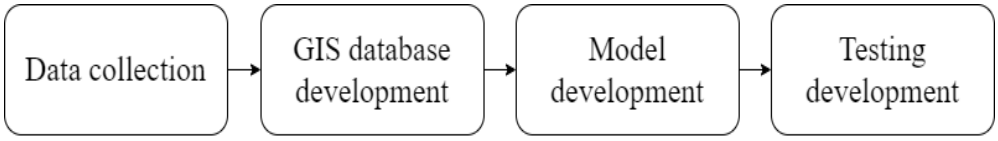

Figure 1
Soil moisture extension process

Our institute is involved in a new project for creating an automated irrigation system based on spatial data. To fulfill this, we need soil moisture data which can tell us the volume of the available water within the soil and also answer how much water the plants can take up with all their important nutrients. Many researchers have already used different methods regarding soil moisture mapping: Jackson used microwave radiometry [3], Paloscia used Sentinel-1 images [4], Wagner used an ERS scatterometer in western Africa [5] and also Kibirige and Dobos by integrating environmental data [6].
The soils of Hungary are very diverse [7]. Due to this, there can be a significant variability in soil moisture levels and the water storage capacity. This paper will discuss two types of methodologies to evaluate geostatistical interpolation.

2. GENERAL DESCRIPTION OF THE METHODOLOGY

2.1. Description of the physical geographical aspects of the study area

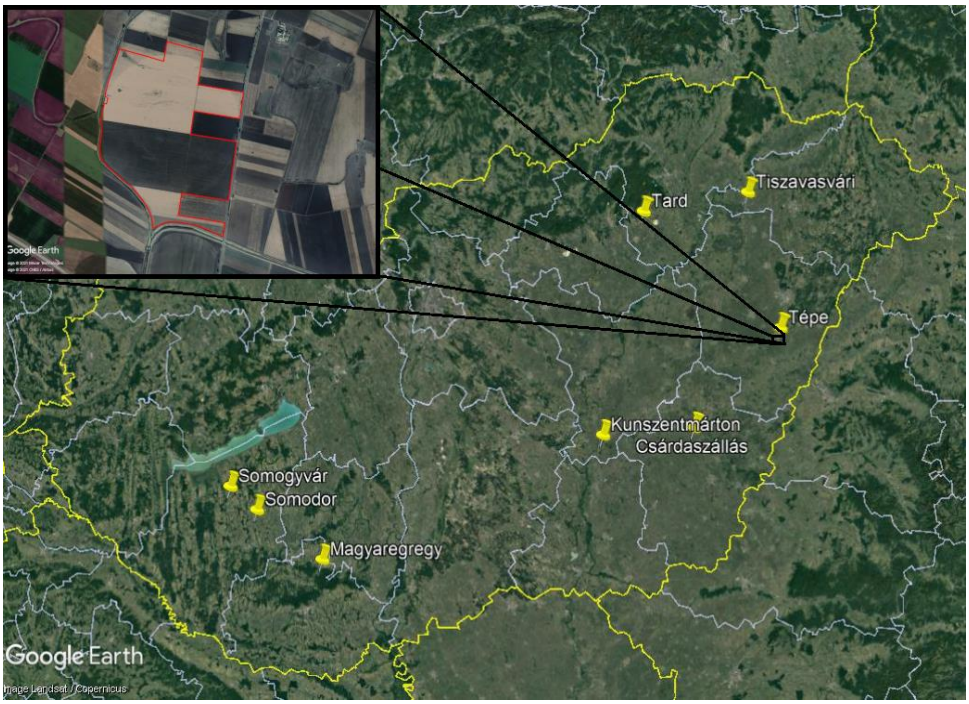

Figure 2
Locations of the Sentek EnviroSCAN sensors placed in Hungary; inset: the pilot area of the study

For this study, an agricultural field at Tépe has been selected as a pilot area, which is one of several locations where the SM data collecting sensors are placed. Tépe is a settlement in Hajdú-Bihar County, 26 km south of Debrecen *(Figure 2)*. It is located in the Berettyó–Kálló micro-region, which is part of the Berettyó–Körös

region. The elevation difference within the field is only a few meters [8] so at first glance, there should not be any significant differences as for geomorphological factors. However, due to the heavy agricultural use and the relative size of the pilot area, surface morphology is a significant factor, and finding the right parameters that will have the most correlation with the observed data is crucial in order to predict new SM values of the area.

Surface forms are mainly of a riverine origin, while the primary surface forming force is fluvial erosion, which brings all riverbed forms, reinforced by anthropomorphic impacts of agricultural use and surrounding channel networks. The geology of the micro-region is based on a 2.5 km deep, metamorphic bedrock formation. Three-quarters of the area is a Holocene floodplain with marsh mud and clay [8] where an increasing refinement of sand material can be observed in the East-West direction.

As for climate, the area has moderately hot and dry summers. During the vegetation season the average temperature is 17 °C, while the annual average temperature is around 10 °C. Annual average rainfall is 550 mm, with 320 mm of this in the vegetation season. The main wind directions are eastern and southern winds (just like throughout the whole Eastern Hungarian region) [8]. The flat surface allows wind to go unobstructed, thus the area is vulnerable to wind erosion. When checking the national averages for the amount of rainfall, the area does not belong to the driest nor to the wettest. Due to this, and as mentioned previously, canal and river networks are very common, e.g. the Eastern main canal, Berettyó and other smaller channels are surrounding the area.

Groundwater levels move between 2–4 meters. Stratified water is rare so there are a number of artesian wells in the area that can go down to 200 meters. The surface is formed mainly by river water, which results in various soil conditions at a micro-relief level. There are three typical main soil types to be mentioned here: chernozems on loess, gleysols and salt effected soils on lower lying, more clayey surfaces with groundwater impact [8].

2.2. Sentek data collection

The institute has been collecting SM data over three years now, nationwide. For this, we are using Sentek EnviroSCAN sensors [9]. These units are stand-alone, real time, soil moisture monitoring devices. Originally, they were used for general research purposes, but over the time they became critical units of irrigation systems for monitoring SM [10]. The equipment is not a single module but can be customized with many setups, at different depth levels. All of our units are calibrated to collect SM data at 10, 20, 30, 40, 60 and at 100 cm depths. The sensors use the dielectric constant values of the soil, water, and air to calculate soil moisture *(Figure 3)* [11]. Each sensor is placed in a different soil type that has its own electric capacity values and physical attributes; therefore, it is mandatory to calibrate each of the sensors properly before starting the data collection.

Figure 3
Overview of the Sentek EnviroSCAN sensor unit
(Source: sentekusa.com)

There are a total of 21 Sentek EnviroSCAN sensors scattered throughout the country, placed on agricultural areas of 8 settlements, each with different SM values, geomorphological features, soil types and cultivation methods currently used on the fields. For this present case, we have chosen Tépe as the study area of our analysis *(Figure 5)*. It is worth mentioning that each sensor position has its own corresponding soil, containing a number of new variables such as physical variability, chemical composition, etc. that can be useful for finding correlations between the sensor and soil data.

2.3. Development of the GIS database

Several environmental parameters were gathered to explain the soil moisture variability. This starts with the construction of the digital elevation model (DEM), which is created from a set of points, captured by RTK corrected GPS equipped machinery, containing many spatial variables like elevation, fuel consumption, etc. For this present case, elevation values were used to create an interpolated raster image with 5 m spatial resolution *(Figure 4)*. All of the geomorphological parameters – slope, aspect, flow accumulation and relative relief – are derived from this DEM using ArcGIS. Other dynamic raster datasets are also collected for the area, such as

Sentinel-1B backscattering images, preprocessed with VV polarization that has also been converted from linear to dB values using ESA SNAP [12].

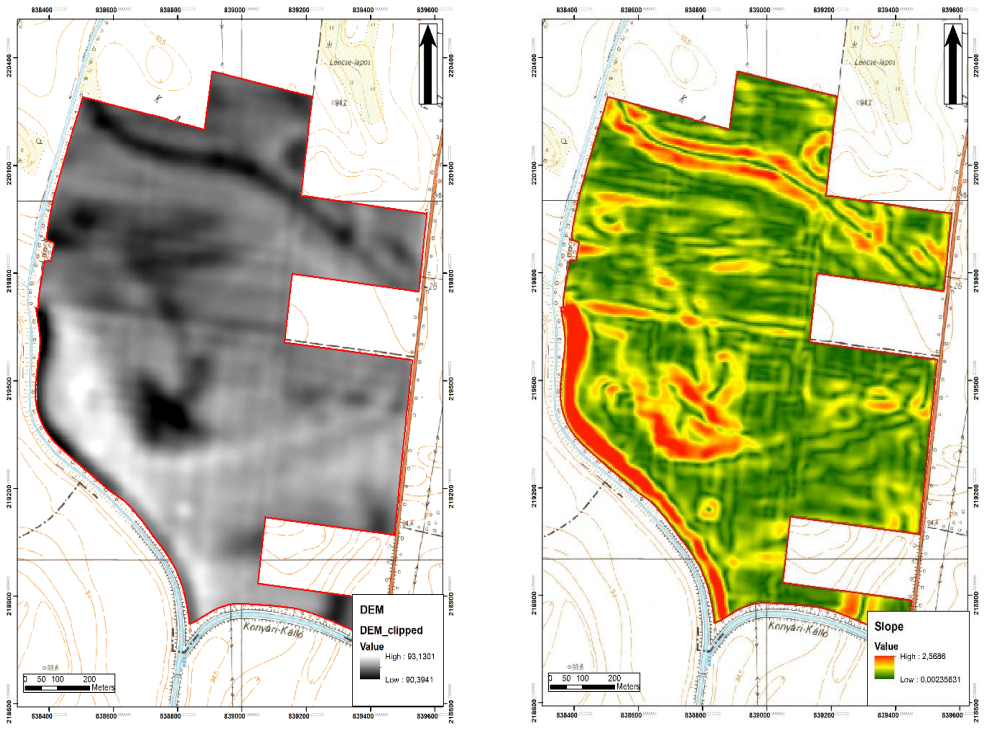

Figure 4

Digital elevation model (meters above sea level, left) and slope (degrees, right) geomorphologic parameters of the study area

Normalized difference vegetation indexes (NDVI) are also used from the Sentinel-2B bands. The satellite images were collected from the Copernicus Open Access Hub, made available by the European Space Agency.

The Hungarian vegetation season – between March and September – has been chosen as the timeline of the study, and the satellite images were selected to be as close as possible to the examined period of SM values. Based on all this, May 3rd, June 17th, July 4th and August 30th were picked as the sample dates.

2.4. Methodology to describe the spatial soil moisture distribution

The aim of the collected observed SM, static and dynamic spatial data was to estimate SM values for the entire field. The research methodology of Daniel Kibirige and Endre Dobos dealt with processing and analyzing low-cost, soil moisture sensor data in order to reach the same goal [13]. In their study, they used linear regression, the Ordinary Least Square method and cokriging, based on the observed SM data.

The model itself needs at least one or more independent variables, along with a dependent – observed – one.

The residual values were created by using the Ordinary Least Square (OLS) tool inside ArcGIS's Geostatistical Analysis toolbox. The "Square Root" and "Root Mean Square Error" were also calculated to measure the difference between the predicted model and observed data.

Ordinary kriging is a geostatistical interpolation method based on spatially dependent variance, which gives unbiased estimates of variable values at target location in space, using the known sampling values at surrounding locations [14]. One of the biggest advantages of cokriging compared to ordinary kriging is that it can use more than one variable. Like in the OLS model, slope was the independent variable and the observed SM data was the dependent variable for the cokriging model.

2.5. Methodology to describe the vertical soil moisture distribution

After reviewing how well the spatial distribution worked, the conclusion was that the available observed sensor data – in terms of the number of spatial samples – were not enough to do any kind of advanced spatial analysis, which has been confirmed by both the linear regression and cokriging results. Due to the high cost of the equipment, they had to be placed in low density, mainly to represent the different soil units within the area. This makes spatial extension difficult, because the points do not represent the same continuity. To overcome this limitation, we decided to characterize the vertical distribution of soil moisture within the upper meter, in order to make the different locations correlatable and interpolatable. At this point, spatial expansion was not possible, therefore a new methodology was needed, and the main goal had to be renewed as well. Examining the sensor data again proved that data usability lies in the vertical analysis, where each SM sensor needs to be analyzed with all of its depth levels.

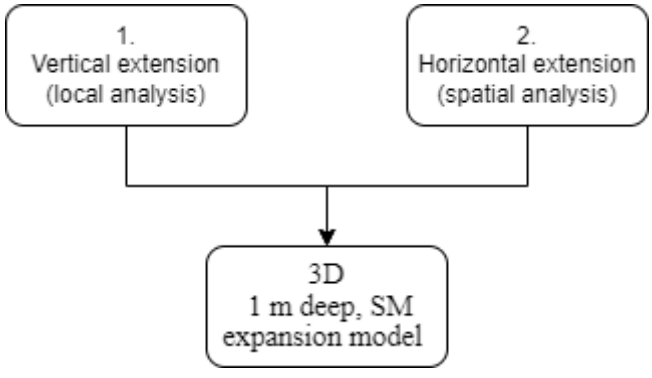

Figure 5
Flowchart of the vertical distribution process

A new goal has been set: creating a 3D, 1 m deep SM model *(Figure 5)*. Two steps need to be made in order to reach this: First, every sensor needs to be analyzed individually to find out the correlation between the different depths, and identify the soil type related relationships (1 in *Figure 4*). The analytical aspect needs to be changed into a vertical direction by doing descriptive statistics first. A Spline function was applied to to estimate the SM values for the entire profile [15] (2 in Figure).

3. THE RESULTS

3.1. Statistical correlation study to select the appropriate variable

The real problem of adapting the methodology of Kibirige and Dobos [13]for this case was the small sample size – 5 points, which is a huge disadvantage throughout the whole study and allows one independent variable for the model. A Pearson correlation analysis was done [16] to find out which static or dynamic variable would correlate best with the observed SM data. The results show that the slope variable had the best correlation *(Table 1)*.

Table 1

Pearson correlation matrix with the observed SM values

	aspect	**slope**	**rela_ref**	**DEM**	**flow_acc**	**SigmaVVdB**	**NDVI**
10 cm	0.310	0.586	–0.605	–0.379	–0.049	–0.214	–0.451
20 cm	–0.174	0.599	–0.58	–0.469	–0.469	–0.121	–0.364
30 cm	–0.252	0.398	–0.377	–0.286	–0.503	–0.164	–0.366
40 cm	0.247	0.656	–0.651	–0.352	–0.117	–0.178	–0.397
60 cm	0.259	0.917	–0.924	–0.772	–0.073	–0.078	–0.292
100 cm	0.236	0.96	–0.947	–0.644	–0.188	0.052	–0.217
MEAN	0.104	0.686	–0.681	–0.484	–0.233	–0.117	–0.348

3.2. Spatial soil moisture distribution

The error statistics for the OLS model are listed in *Figure 6*. Each sensor showed the largest difference at depths of 10–40 cm and 60+ cm, while it became zero between 40–60 cm. This applies to the upper (10–40 cm) and lower (60+ cm) water supply layers, which are completely separated by an impermeable clay layer, originating from agricultural cultivation as a result of mixing the upper soil depths. This assumption was validated with soil excavation, where the characteristic soil layers were referring to the residual values.

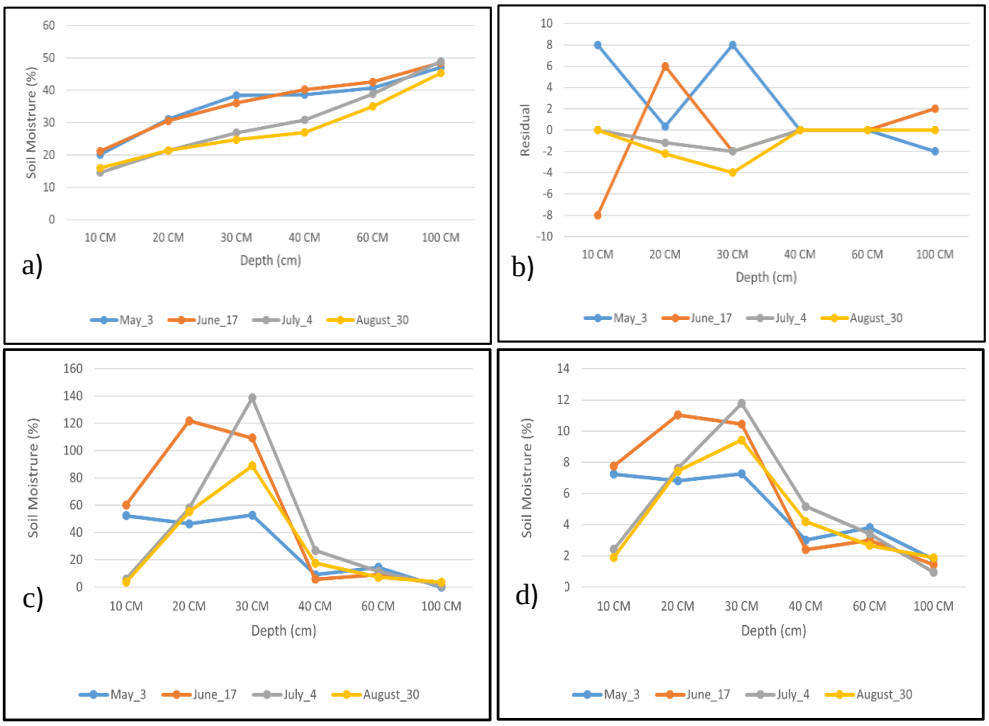

Figure 6

Ordinary Least Square model results: Observed SM values (a), residual for OLS predicted SM values (b), root square (c), and root mean square error (d)

Cokriging showed weak interpolations due to the small number of sample points. Each examined dataset with all depths showed mixed results, but in general, the 10 cm values had the best range of values, and it also shows the "least worse" results *(Figure 7)*. Nevertheless, there are still some correlations to be seen from these images. They show increasing SM values to the North-Northwestern direction, which indicates a mild inclining feature for the whole landscape. This has been validated by checking the topology maps showing the inclination, based on the contour line values *(Figure 7)*.

3.3. Vertical soil moisture distribution

Descriptive statistical analysis for all sensor locations at Tépe have been completed to show a general overview of the data *(Table 2)*. Correlation matrices were created to characterize the vertical moisture movements between the different depths *(Table 3)* and boxplots to identify the outlier values *(Figure 8)*.

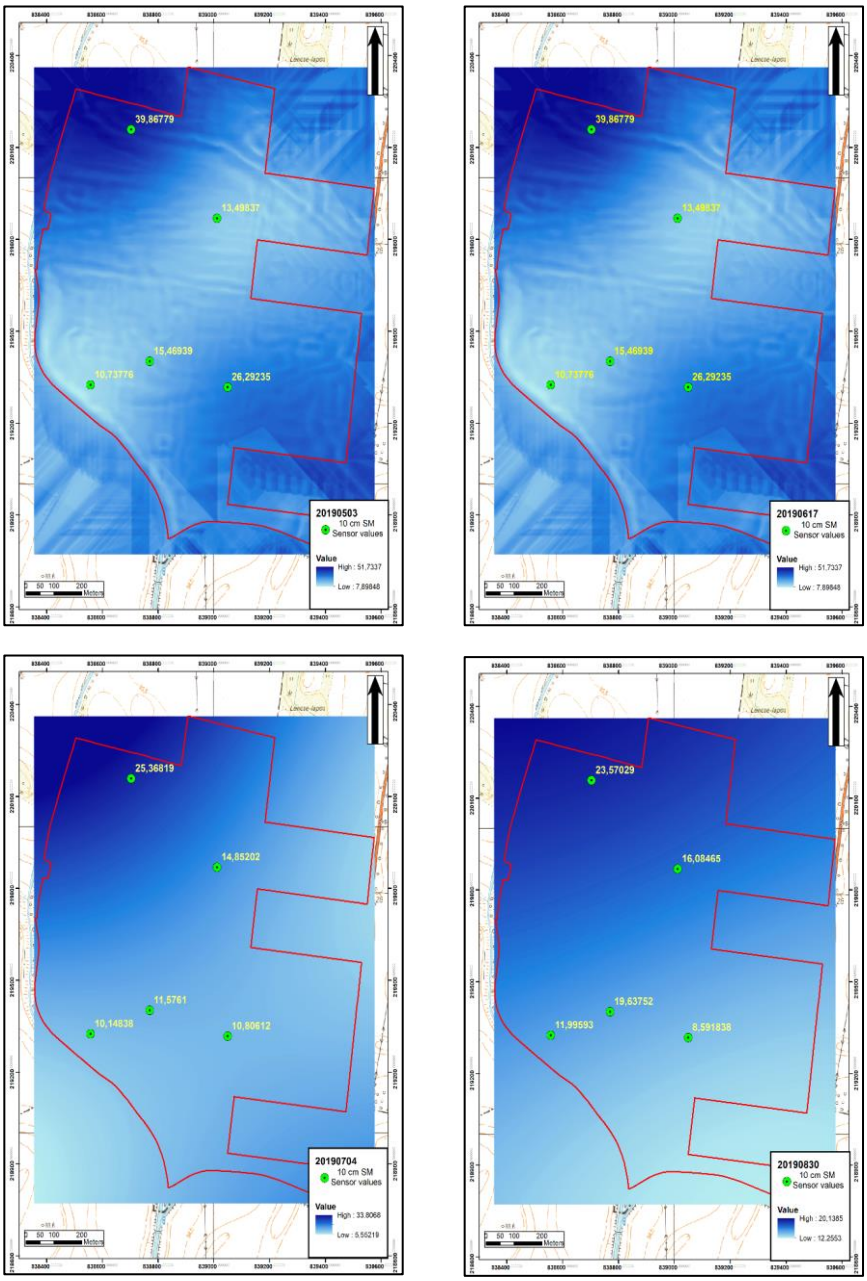

Figure 7

Predicted SM values with cokriging at 10 cm depth: 2019 May 3 (a), 2019 June 17 (b), July 4 (c), August 30 (d)

Table 2

Descriptive statistics of one of the SM sensors (ID 6, summer season)

	N	Range	Minimum	Maximum	Mean	Std. Deviation	Variance
10 cm	2208	32.064	11.873	43.937	20.586	6.370	40.582
20 cm	2207	28.586	5.753	34.339	12.764	8.001	64.022
30 cm	2208	39.309	4.997	44.306	15.777	12.537	157.167
40 cm	2206	26.845	17.340	44.185	31.112	10.346	107.032
60 cm	2208	13.015	27.082	40.097	33.453	4.577	20.950
100 cm	2208	6.101	38.382	44.483	41.956	2.169	4.706

Table 3

Correlation matrix of one of the SM sensors (ID 6, summer season)

	10 cm	20 cm	30 cm	40 cm	60 cm	100 cm
10 cm	1	0.413	0.215	0.464	0.314	0.031
20 cm	0.413	1	0.948	0.765	0.764	0.476
30 cm	0.215	0.948	1	0.811	0.823	0.525
40 cm	0.464	0.765	0.811	1	0.940	0.606
60 cm	0.314	0.764	0.823	0.940	1	0.786
100 cm	0.031	0.476	0.525	0.606	0.786	1

The correlation table indicates that the uppermost 10 cm do not correlate well with the deeper horizons. this is the layer most exposed to the surface weather, and it shows large fluctuations which do not necessarily appear in the deeper horizons. The same is true for the 1 m depth, whch is quite different from all overlying layers. It also shows the expected correlation trend, namely the decreasing correlation toward the surface. The strongest correlations were found between the 20–30 cm and the 40–60 cm depths. It is also logical, because the 20–30 cm depths belong to the middle and deep part of the plough layer, insulated from the atmosphere by the upper 10 cm. 40 cm is the plough pan, which is compacted and has a low infiltration rate, causing a stagnic water body to form above it. This layer also separates the plough layer and the deeper horizons, namely the 40–60 cm depths, which represents a slightly separated water body. These results are common in all soil profiles. *Figure 8* explains these features from another aspect. The upper 30 cm always has a much higher range, with often hectic data distribution, meaning that this plough layer is more exposed to the surface and top the vegetative use of SM. The depths of 40, 60 and 100 cm are more stable with far fewer hectic features and outliers.

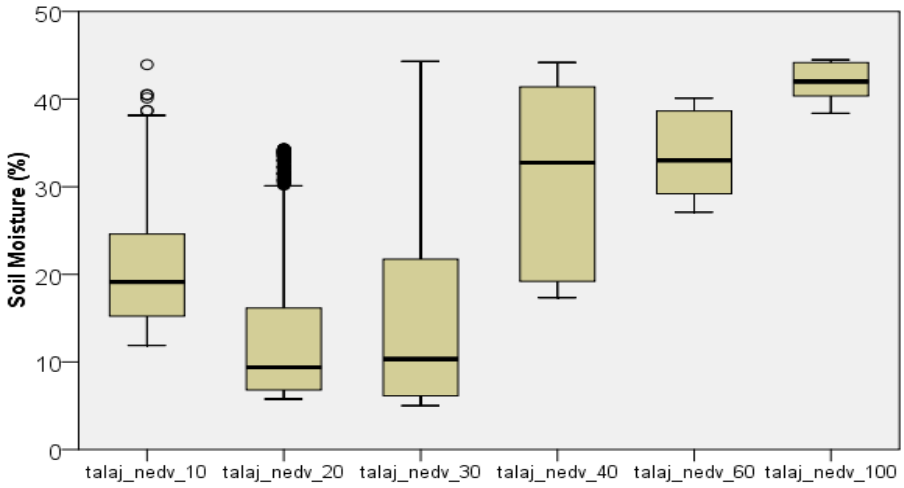

Figure 8
Boxplot of one of the SM sensors (ID 6, summer season)

4. SUMMARY AND CONCLUSION

Five soil sensors with six different depths of SM data were available for processing when examining the sample field at Tépe. The regression analysis had higher than acceptable error values, shown by the root square and root mean square error, which made this methodology irrelevant *(Figure 6)*. The geostatistical interpolation also gave weak results due to the limited amount of points inside the field (only five), resulting in maps with lower spatial resolution *(Figure 7)*.These are only preliminary results; a complete characterization of the methodology requires more sampling points and environmental covariances to better describe the spatial variability of the soil moisture. However, the data have great potential as separate, individual units, where the distribution and vertical extension could be done between the depths. We believe the latest methodology will bring more results in the future and will also answer the question of finding specific correlation levels between every soil type regarding variables and the observed SM depth values. This should allow associated soil types to be placed into water management type groups for the upcoming irrigation system.

REFERENCES

[1] Alsafadi, K., Mohammed, S. A., Ayugi, B. et al. (2020). Spatial–Temporal Evolution of Drought Characteristics Over Hungary Between 1961 and 2010. *Pure and Applied Geophysics*, Vol. 177, pp. 3961–3978. https://doi.org/10.1007/s00024-020-02449-5

[2] Shannon, D. K., Clay, D. E., Kitchen, N. R. (2018). *Precision Agriculture Basics.* American Society of Agronomy Crop Science, Society of America Soil Science, Society of America, https://doi.org/10.2134/precisionagbasics.

[3] Jackson, T. J., Le Vine, D. M., Hsu, A. Y., Oldak, A., Starks, P. J., Swift, C. T., Isham, J. D., Haken, M. (1999). *Soil moisture mapping at regional scales using microwave radiometry: the Southern Great Plains Hydrology Experiment*. *IEEE Transactions on Geoscience and Remote Sensing*, Vol. 37 (5), pp. 2136–2151, https://doi.org/10.1109/36.789610.

[4] Paloscia, S., Pettinato, S., Santi, E., Notarnicola, C., Pasolli, L., Reppucci, A. (2013). Soil moisture mapping using Sentinel-1 images: Algorithm and preliminary validation. *Remote Sensing of Environment*, Vol. 134, pp. 234–248. https://doi.org/10.1016/j.rse.2013.02.027

[5] Wagner, W., Scipal, K. (2000). *Large-scale soil moisture mapping in western Africa using the ERS scatterometer*. *IEEE Transactions on Geoscience and Remote Sensing*, Vol. 38 (4), pp. 1777–1782, https://doi.org/10.1109/36.851761.

[6] Kibirge, D., Dobos, E. (2021). *Estimation of surface soil moisture by integrating environmental data and remote-sensing satellites*. *Multidiszciplináris Tudományok*, Vol. 11, pp. 22–37, https://doi.org/10.35925/j.multi.2021.1.3.

[7] Stefanovits, P., Filep, Gy., Füleky, Gy. (1996). *Talajtan*. 4th edition. Budapest, Mezőgazda Kiadó.

[8] Dövényi, Z., Marosi, S., Somogyi, S. (2010). *Magyarország kistájainak katasztere*. 2nd edition. Budapest, MTA Földrajztudományi Kutatóintézet.

[9] *Sentek EnviroSCAN Soil Data Probe* [Online] Available at: https://sentek technologies.com/product-range/soil-data-probes/enviroscan [Accessed 7 Dec 2021].

[10] Al-Ghobari, H., Marazky, M., Aboukarima, A., Minyawi, M. (2016). Calibration of Soil Water Content Data from EnviroSCAN System Using Artificial Neural Network. *American Journal of Experimental Agriculture*, Vol. 12 (5), pp. 1–11, https://doi.org/10.9734/ajea/2016/26237.

[11] Al-Ghobari, H. M., Said, M., El, A. (2013): Field evaluation of EnviroSCAN performance for monitoring soil water content compared with other soil moisture sensors under arid conditions. *Wulfenia Journal*, Vol. 20 (4), pp. 54–70.

[12] Filipponi F. (2019): *Sentinel-1 GRD Preprocessing Workflow*. *Proceedings*. 18 (1), Art. 11, https://doi.org/10.3390/ECRS-3-06201.

[13] Kibirge, D., Dobos, E. (2021). Soil Moisture Estimation Using Citizen Observatory Data, Microwave Satellite Imagery, and Environmental Covariates. *Water*, Vol. 13 (6), p. 837, https://doi.org/10.3390/w13060837.

[14] Adhikary, S. K., Muttil, N., Yilmaz, A. G. (2017). Cokriging for Enhanced Spatial Interpolation of Rainfall in Two Australian Catchments. *Hydrological Processes*, Vol. 31 (12), pp. 2143–2161, https://doi.org/10.1002/hyp.11163.

[15] Voltz, M., Webster, R. (1990). A comparison of kriging, cubic splines and classification for predicting soil properties from sample information. *Journal of Soil Science*, Vol. 41 pp. 473–490. https://doi.org/10.1111/j.1365-2389.1990.tb00080.x

[16] Benesty J., Chen J., Huang Y., Cohen I. (2009). Pearson Correlation Coefficient. In: *Noise Reduction in Speech Processing*. Springer Topics in Signal Processing, Vol 2, Springer, Berlin, Heidelberg. https://doi.org/10.1007/978-3-642-00296-0_5

Geosciences and Engineering, Vol. 10, No. 15 (2022), pp. 50–62.
https://doi.org/10.33030/geosciences.2022.15.050

INVESTIGATION OF LANDFILL SATURATION BASED ON PERIODIC AERIAL PHOTOGRAMMETRIC MEASUREMENTS

ZOLTÁN EKE[1, 2], ISTVÁN HAVASI[2]

[1] *System Design Department, Bay Zoltán Applied Research Public Benefit Nonprofit Ltd., Zoltan.Eke@bayzoltan.hu*
[2] *Department of Geodesy and Mine Surveying, Institute of Geophysics and Geo-Information Science (IGGIS), University of Miskolc, gbmhi@uni-miskolc.hu*

Abstract: The actuality of the study of saturation in Hungarian landfills is indisputable; its research is definitely justified. In our paper, we undertake this task based on the periodic drone geodetic surveys of the landfill of a medium-population city in Hungary. After evaluating the results of each survey, the expected date of landfill saturation is determined by us, and possibilities for its further specification are also examined.

Keywords: *landfill saturation, periodic surveys with a drone, 3D models, volume computation*

1. INTRODUCTION

Nowadays, it is becoming more and more urgent to find a solution to reduce the amount of the generated waste. Although not the most significant in terms of quantity, municipal solid waste is of paramount importance in terms of its complexity and difficulties in its management. The basic goal is to preserve and improve the condition of both our narrow and wide environment, to ensure long-term living conditions so that not only local interests but also global ones prevail.

The amount of the generated waste needs to be reduced both on the generation side (production, manufacturing, packaging, transport, storage) and by increasing the rate of recycling (e.g. as a secondary raw material). The increasing use of secondary raw materials is also required by the finite amount of raw materials found in nature. Ultimately, the declining rate of landfilling should be a measure of system efficiency. Of course, the landfill takes place under controlled conditions, which are also designed to ensure that the utilization of the landfill is as high as possible. There are several ways to achieve this, such as compaction with heavy vehicles, keeping the moisture content of the waste mixture at an optimal level, and reducing the size of the waste components. Geodetic surveys make it possible to determine the degree of saturation. This is done by calculating the volume of the landfill area surfaces constructed from the results of these periodic measurements (ground or aerial) determined by the base plane or the plane of the previous

measurement result and the sidewall provides the desired result. The application of drone surveys to various volume computation tasks is described for example in [1], [2], and [3].

2. THE LEGISLATION OF THIS SPECIAL FIELD

First, let us briefly introduce the legislation governing waste management; the number of these laws also supports the importance of the problem [4], [5], [6]:

Laws:

- Act LIII of 1995 on the General Rules for the Protection of the Environment;
- Act CXL of 2004 on the General Rules of Administrative Authority Procedure and Service;
- Act CLXXXV of 2010 on Waste;
- and approximately
- 19 government decrees;
- 17 ministerial decrees.

Directive 2018/851 of the European Parliament and the European Council (30 May 2018) amending Directive 2008/98/EC on waste contains specific targets whose fulfilment can be partly confirmed by the degree of landfill saturation. Target values are linked to dates as follows:

- by 2025, the amount of municipal waste prepared for re-use and recycled should be increased to a minimum of 55% by weight;
- by 2030, the amount of municipal waste prepared for re-use and recycled shall be increased to a minimum of 60% by weight; and
- by 2035, the amount of municipal waste prepared for re-use and recycled should be increased to a minimum of 65% by weight.

In order to achieve the target values, it is necessary to reduce the amount of the landfilled waste, especially as we are currently far from this goal in Hungary. The National Waste Management Public Service Plan for 2021, based on 2019, states the following values: 3,203,000 tons of municipal solid waste were generated in 2019, of which 2,455,000 tons were landfilled (energy recovery was approximately 600,000 tons). Thus, the weight percentage of the landfilled quantity is 76.6%. The amount of waste which has not been landfilled has not reached 25%, i.e. half of the target value for 2025, while the time available is not enough. The legislation provides for the possibility of postponing dates of achievement, but it is not a solution.

The following is a list of legislation for aeronautical photogrammetric drones [7] in both the European Union and Hungary:

- Commission Implementing Regulation (EU) No. 2019/947 (24 May 2019) on rules and procedures for the operation of unmanned aircraft;

- Commission Regulation (EU) No. 2019/945 (12 March 2019) on unmanned aircraft systems and third country operators of unmanned aircraft systems;
- Act XCVII of 1995 on Aviation law;
- Government Decree 4/1998. (I. 16.) on the use of Hungarian airspace;
- Government Decree 39/2001. (III. 5.) on compulsory aviation liability insurance;
- Decree 26/2007. (III. 1.), on the designation of Hungarian airspace for the purpose of aviation, a GKM-HM-KvVM joint decree; and
- ITM Regulation 6/2021. (II. 5.) on the designation of organizations for the training and examination of remote pilots and on the detailed rules for the training and examination of remote pilots.

Additional relevant legislation in the case of flight (measurement) for remote sensing purposes [8] is Government Decree 399/2012. (XII. 20.) on the procedure for the authorization of aerial remote sensing and the use of remote sensing data.

3. DESCRIPTION OF DRONE SURVEYS

In the following our periodic airborne surveys of a landfill in a city of 40,000 inhabitants will be described. Based on these measurements, we made a 3D model of the final state of the saturated landfill, determined the expected date of saturation in the case that the amount of landfilled waste remained constant, and then checked the degree of saturation with further measurements.

Parameters of the surveying device:

drone:	DJI Phantom4 RTK,
camera model:	DJI FC6310R,
number of images:	590,
flight height:	92 m,
terrain resolution:	0.0270 m,
resolution:	5472 × 3648,
focus distance:	8.8 mm,
sensor size:	13.2 × 8.8 mm,
pixel size:	2.412 μm,
ortofoto size:	387.825 m × 418.275 m,
pixel resolution:	0.025 m.

The drone has an RTK (Real-Time Kinematic) GPS unit and is capable of receiving real-time correction. In order to minimize the uncertainty in the position resulting from the velocity during the flight, Ground Control Points (GCPs) were used for each survey, which were measured by us with a ground RTK GPS device (*Table 1* and *Figure 1*).

A network RTK service was used by us with VRS concept. According to the VRS concept, the mobile receiver first sends the approximate coordinates of its geographical position to the control panel (GGA message), the control panel

generates localized measurement results or corrections to this location, and then transmits these fictitious data about the virtual point to the mobile receiver. During the establishment of the control points, the level differences of the area and the shape characteristics of the landfill were taken into account *(Figure 2)*. When choosing the flight speed and altitude (102.8 m), we kept in mind the optimal terrain resolution as well as the maximum terrain level deviation in the area *(Table 2*). The *Table 3* contains various errors related to camera positions.

Table 1

Ground Control Points

Point numbers	Coordinates			Errors [m]				Number of projections
	X	Y	Z	X	Y	Z	3D	
2002	495832.026	121461.284	207.193	0.004	–0.005	0.006	0.008	57
2004	495849.217	21289.1681	200.617	–0.002	0.005	0.011	0.012	57
2006	495996.141	121247.290	186.133	–0.011	0.000	0.000	0.011	91
2008	496126.561	121305.340	186.014	–0.004	0.011	0.004	0.012	103
2012	496054.287	121410.432	188.794	0.007	0.008	–0.012	0.016	89
2014	495912.306	121546.513	207.840	0.005	0.001	0.009	0.010	41
2016	495936.900	121430.386	221.660	–0.003	0.002	–0.007	0.008	53
2018	495879.463	121350.849	217.996	–0.002	–0.002	–0.021	0.021	36
2020	495898.852	121265.816	212.460	0.002	–0.005	0.007	0.009	56
2022	496052.826	121333.072	212.715	0.003	–0.010	0.033	0.034	61

Figure 1

The measured GCPs and their field locations

Table 2
Surveying data

Number of images:	571	**Registered number of images:**	568
Flight altitude:	102.8 m	**Number of the key points per each image / average:**	1167
Terrain resolution:	0.0302 m	**Georeference:**	Yes

Table 3
Camera positions

X error [m]	Y error[m]	XY error[m]	Z error [m]	Total error [m]
0.374	0.309	0.486	0.149	0.508

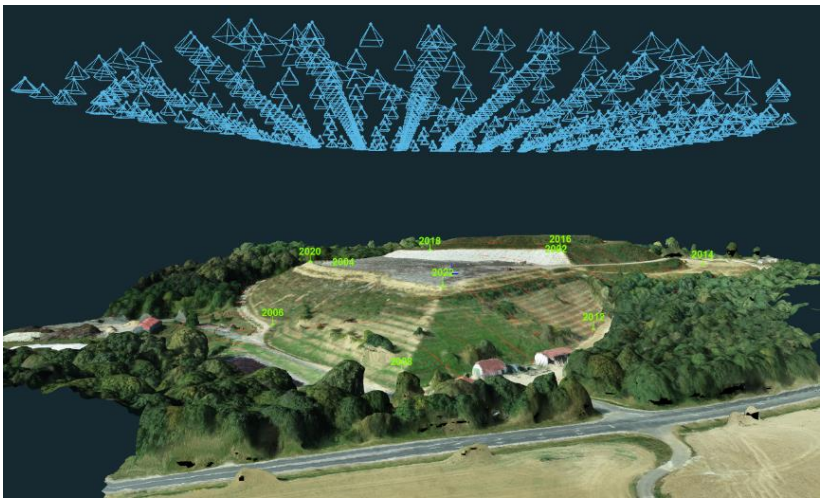

Figure 2
Landfill with control points and drone positions where photographs were taken during the survey

The measuring results were loaded into the 3D Survey processing software (photos, geocodes, telemetric data) together with the coordinates of the measured control points. The software corrected the above-mentioned uncertainty (considering the measured GCPs) in the process and created a digital surface model and a georeferenced orthophoto. We have chosen an optimized (global) processing method for the large amount of data available to us. The photogrammetric survey and processing were performed in a Unified National Projection System, for which we used a Vitel transformation.

Using the 3D survey, we determined the volume difference between each measuring state, which was checked with the Surfer program *(Figure 3)*.

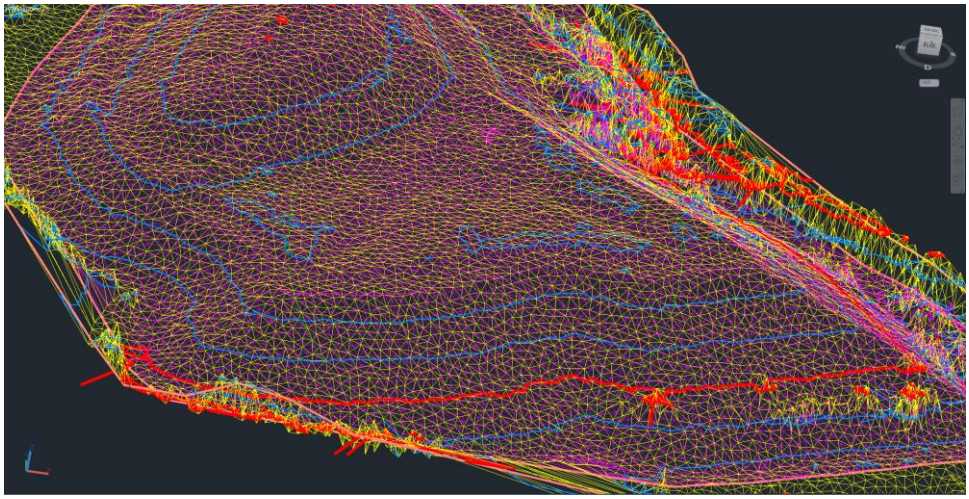

Figure 3
Triangulated Irregular Network (TIN) models made of two successive measurements (first measuring state: yellow, second one: purple) projected on top of each other

Surveying dates:

- first measurement – on September 22, 2020, for lack of a base plane, preparation of the reference surface;
- second measurement – on May 9, 2021, when the first volume computation and the final state model were produced as well as the saturation date calculation;
- third measurement – September 21, 2021, second volume computation.

The volume of the deposited quantity in the elapsed period was computed from the difference of the field levels prepared from the data of two consecutive measurements. The field level of the first (lower) measurement state was subtracted from the field level of the second measuring state, so that the space between the two measurements was obtained, determined by relative heights (level change [m]). The volume computation was not based on the total landfill area, but on the "active" landfill, where the actual disposal takes place. A negative value in some places in the landfill at a later date means that the level was lower than before. This is due to the accumulation of waste in the meantime on the basis of the landfill plan and the elimination of surface irregularities resulting from the compaction. The reason for the level changes appearing on the side of the landfill is the vegetation cover typical in different seasons, which is not included in the volume calculation as a result of narrowing. A triangular and grid model was produced from the point

cloud for volume computation, and the landfill was delimited with the help of the orthophoto.

In the following figures the cross-sections drawn from the TIN models of measurements 2 and 3 *(Figure 4)*, the terrain models of the first two measurements (*Figures 5* and *6*), the assumed end-state model after measurement 2 *(Figure 7)*, and the terrain model of measurement 3 *(Figure 8)* are illustrated.

Figure 4
Cross sections made of two TIN models

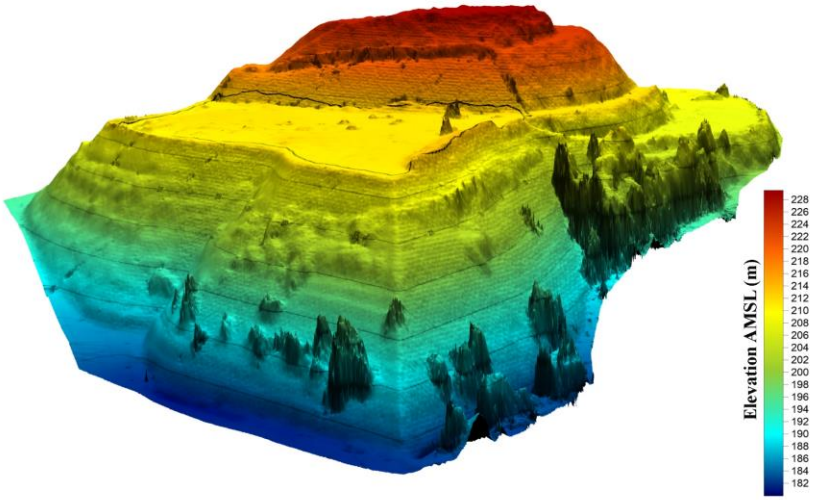

Figure 5
A terrain model of the 1st measurement

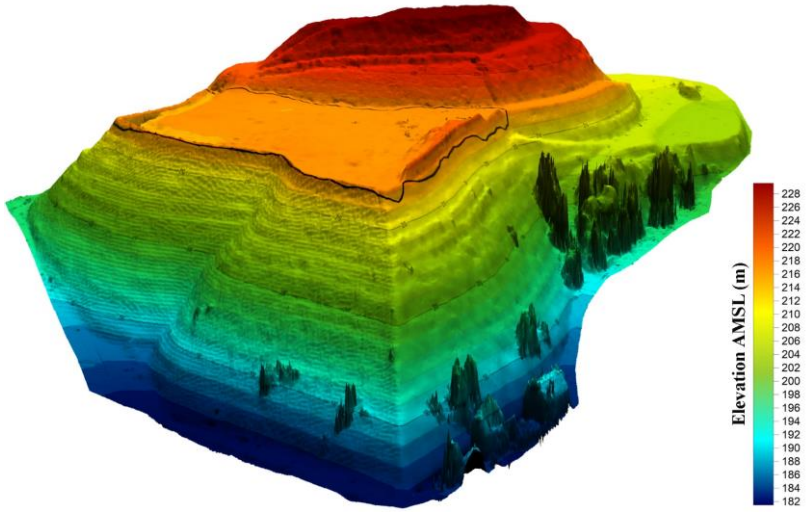

Figure 6
A terrain model of the 2nd measurement

Based on the first two sets of measurement data, a 3D model of the assumed final state of the landfill was created. The sealing level is the upper edge of the insulation on the hillside, with a maximum determined near 222 m (above Baltic Sea level). Subsequently, the difference between the two surfaces (between the second survey state and the assumed final one), i.e. the available free landfill volume, was calculated as before.

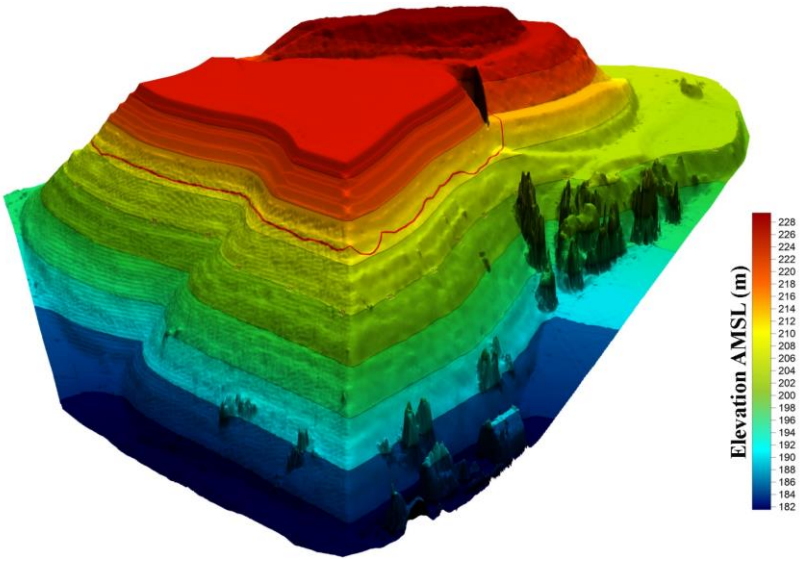

Figure 7
A 3D model of the assumed end state

It is important to note that the highlighted data in *Table 1* below are based on a hypothetical end-state model based on little information (the insulation on the side of the hill gives the final height of the landfill at 222 m Baltic Sea). This estimate includes both the landfilled waste and the landfill material. This should be taken into account when using the data. If more accurate information about the final state is available, the model can be refined, so we can obtain more reliable data.

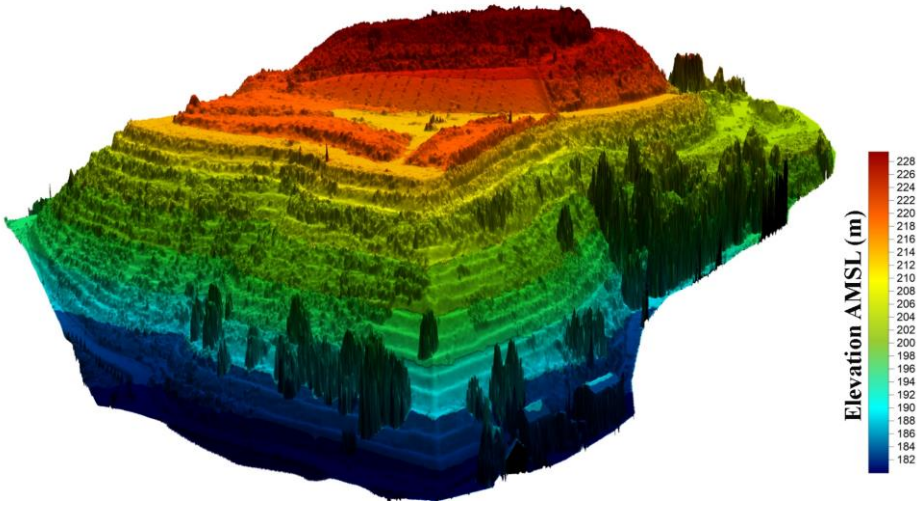

Figure 8
A terrain model of the 3rd measurement

4. DETERMINATION OF VOLUME CHANGES

In *Figures 9* and *11* the volume changes between each measurement time (1–2 and 2–3) and the free volume between the 2nd surveying occasion and the assumed final state can be seen *(Figure 10)*.

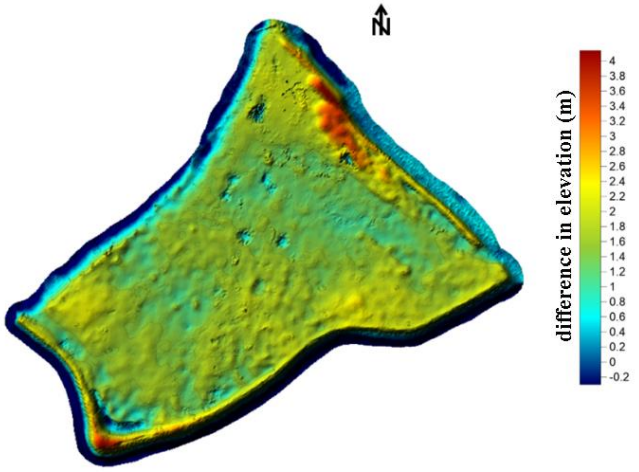

Figure 9
The computed volume (amount of filling) between the two measuring states (22/09/2020 and 09/05/2021): 23,070 m^3

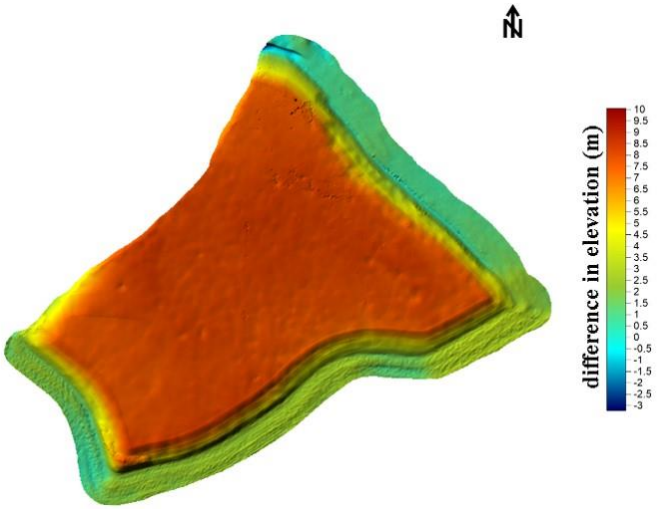

Figure 10
The computed free volume (101,650 m^3, 09/05/2021) available from the 2nd measuring state to the assumed final state level

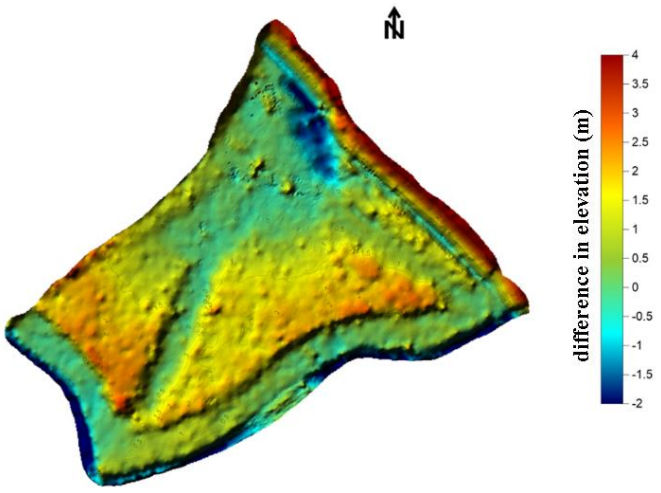

Figure 11
The computed volume (amount of filling) between the two measuring states (09/05/2021 and 21/09/2021): 13,040 m^3

The computer edited surface, as well as the expected saturation date calculated on the basis of the surveying results, calculated as the degree of saturation between the measurements, is given in *Table 4.*

Table 4
The evaluated data of landfill volume surveys (red – calculated values)

measurement 1	**measurement 2**	**volume changes [m^3]**	**number of days**	**m^3/day**
22. 09. 2020	09. 05. 2021	23070	227	101.6
measurement 2	**end state date**	**volume changes [m^3]**	**number of days**	**m^3/day**
09. 05. 2021	**30. 01. 2024**	**101650**	**997**	**102.0**
measurement 2	**measurement 3**	**volume changes [m^3]**	**number of days**	**m^3/day**
09. 05. 2021	21. 09. 2021	13040	128	101.8

The values marked in red in the table are calculated ones. From the first two measurements, a saturation rate for the period (101.6 m^3/day) was determined. The volume available up to the final state was divided by the degree of saturation (the value was rounded up to 102 m^3/day) to obtain the number of days (997) until saturation. This was added to the 2nd measurement date from which the saturation time was derived.

The change in volume between the second and third measurements was also divided by the elapsed number of days in the meantime to determine the degree of saturation for the new period. The value of 101.8 m^3/day is higher than before, which does not support the decreasing trend of the deposited volume. Of course, we measured different periods within a year, winter (heating) and a summer, which also show a difference in the composition of the waste, and the one-year period

studied can be considered short to draw this type of conclusion. We plan to continue the surveys if we have the opportunity. More reasonable conclusions can be drawn from comparing several periods within the same year.

However, based on what has been done so far, it appears that the landfill will be saturated before the date of the first EU target, creating a very difficult situation for the region's waste management sector.

5. CONCLUSIONS

In our study, after a short introductory part, we dealt with the Hungarian and EU legislation related to the research work, including the legal regulations related to the applied geodetic method (drone survey). Then we introduced the surveying device used for the measurements, we described each measurement and their processing. Then we gave the data characterizing the saturation of the landfill based on the specified volume change (especially its expected date) in tabular form. Finally, we examined the reliability of this important data and the need for further research for the sake of its refinement as well.

ACKNOWLEDGEMENTS

The authors express their gratitude for the support provided for the preparation of this study to the managers of Bay Zoltán Applied Research Public Benefit Nonprofit Ltd.

REFERENCES

[1] Raeva, P. L., Filipova, S. L., Filipov, D. G. (2016). Volume computation of a stockpile – a study case comparing GPS and UAV measurements in an open pit quarry. *The International Archives of the Photogrammetry, Remote Sensing and Spatial Information Sciences*, Volume XLI-B1, 2016, pp. 999–1004, XXIII ISPRS Congress, 12–19 July 2016, Prague, Czech Republic. https://doi.org/10.5194/isprsarchives-XLI-B1-999-2016

[2] Mantey, S., Aduah, M. S. (2021). Comparative Analysis of Stockpile Volume Estimation using UAV and GPS Techniques. *Ghana Mining Journal*, Vol. 21, No. 1, pp. 1–10, eISSN: 0855-210X. https://doi.org/10.4314/gm.v21i1.1

[3] Arango, C., Morales, C. A. (2015). Comparison between multicopter UAV and total station for estimating stockpile volumes. The International Archives of the Photogrammetry, Remote Sensing and Spatial Information Sciences, Volume XL-1/W4, 2015, pp 131–135, *International Conference on Unmanned Aerial Vehicles in Geomatics*, 30 Aug–02 Sep 2015, Toronto, Canada, https://doi.org/10.5194/isprsarchives-XL-1-W4-131-2015.

Waste management plans, legislation:

[4] *National Waste Management Plan (2021–2027)*, (Base year: 2018), 1704/2021(X. 6.) Government Decision, Ministry of Innovation and Technology, https://kormany.hu/dokumentumtar/orszagos-hulladekgazdalkokodasi-terv_2021_2027.

[5] NHKV National Waste Management Coordinating and Asset Management Private Limiting Company (NWMCAM PLC.). *National Waste Management Public Service Plan 2021*. https://nhkv.hu/wp-content/uploads/2020/09/OHKT_2021.pdf, https://nhkv.hu/vonatkozo-jogszabalyok/.

[6] *National Association of Waste Managers (NAWM), Hungary*. https://www.hosz.org/jogszabalyok/hazai-jogszabalyok

[7] *Drone regulation (Hungary).* https://mydronespace.hu/; https://www.hungarocontrol.hu/; https://legter.hu/

[8] *Hungarian Defence Forces Geoinformation Service (HDFGS).* https://honvedelem.hu/alakulat/mh-geoinformacios-szolgalat.html

Geosciences and Engineering, Vol. 10, No. 15 (2022), pp. 63–79.
https://doi.org/10.33030/geosciences.2022.15.063

PHASE SEGMENTATION OPTIMIZATION OF MICRO X-RAY COMPUTED TOMOGRAPHY RESERVOIR ROCK IMAGES USING MACHINE LEARNING TECHNIQUES

HASAN ATRASH, FELICITASZ VELLEDITS

Institute of Mineralogy and Geology, University of Miskolc
hasan.alatrash87@gmail.com

Abstract: We studied the performance and accuracy of some basic segmentation techniques in the analysis of the pore space and matrix voxels obtained from a 3D volume of X-ray tomographic (XCT) grayscale rock images. The segmentation and classification accuracy of unsupervised (K-means, modified Fuzzy c-means, Minimum cross-entropy, and Type-2 fuzzy entropy) and supervised Naïve Bayes methods were tested using an XCT tomogram of a carbonate reservoir rock. K-fold- cross-validation techniques were applied in the evaluation of the accuracy of the unsupervised and supervised machine learning classifiers. The average porosity obtained was 31 ±6%, in good agreement with the ground truth image obtained by manual segmentation. In general, the accuracy of segmentation results can be strongly affected by the feature vector selection scheme, since it is difficult to isolate a particular machine learning algorithm for the complex phase segmentation problem. Therefore, our study provides a segmentation scheme that can help in selecting the appropriate machine learning techniques for phase segmentation.

Keywords: *XCT imaging, porosity, image segmentation, machine learning*

1. INTRODUCTION

Micro X-ray computed tomography (XCT) images of a reservoir rock sample can help in the characterization of pore space and assist in modeling pore-network geometries. A 3D pore-network representation can improve the understanding of the evolution of permeability and porosity of a rock sample [1]. X-ray computed tomography images, also known as tomograms, consist of a cubic array of reconstructed linear X-ray attenuation coefficient values (also known as pixel values). Accurate image segmentation is the first step toward pore-network modeling and analysis [2]. Image segmentation is the process of classifying similar values of image gray intensity into distinct groups or classes using machine learning (unsupervised or supervised) segmentation algorithm. Porous materials such as carbonates contain areas of void, called the pore space, as well as a number of distinct mineral components, each with a comparatively uniform density and consequently a similar gray value. There are some difficulties in acquiring a clear distribution separating the pore phase from the mineral phase. These difficulties arise from low density pore inclusions (e.g., microporosity, clays) below the image resolution, which make it difficult to distinguish between solid phase and the pore phase.

There have been intensive studies to improve segmentation methods for better quantitative characterization of pore space feature. Iassonov et al. [3] broadly classified segmentation algorithms into globally and locally adaptive segmentation. The fundamental concept behind the global thresholding scheme is that a single gray value is selected as a threshold value separating one phase from the other. There are many subcategories under the scheme, and the most commonly used is the histogram shape (triangulation) [4]. In locally adaptive segmentation the segmentation decision is made for each pixel taking into consideration the neighboring pixels. Utilization of local information helps in reducing the effects of some image artifact. One repeatedly used method is the probabilistic fuzzy c-means [5], which belongs to the unsupervised segmentation category but requires high computational power. In other works, such as Cortina-Januchs et al. [6], a combination of different algorithms is used where they applied clustering and artificial neural network (ANN) to segment binary soil images. whereas Khan et al. [7] used the supervised technique least-squares support vector machine (LS-SVM) for segmentation of XCT rock images.

Machine learning and neural networks were developed to mimic human sight and were initially used for speech and image recognition [8], [9]. They were soon used for the resolution enhancement of, for example, satellite images [10] and medical images [11] like magnetic resonance imaging [12] and computed tomography (XCT) [13].

Unsupervised learning is a machine learning technique where there is no need to supervise the model. Instead, the model is allowed to work on its own to discover information. It mainly deals with unlabeled data.

Supervised learning uses collected data or produces a data output from previous experience. It helps to optimize performance criteria using experience. A supervised learning model uses training data to learn a link between the input and the outputs. This link is used to sort out information, similarly to the training data from an unknown data set. Several algorithms can be used in the supervised approaches (e.g. support vector machine, neural network, linear and logistics regression, random forest, and classification trees). The classification and interpretation tasks determine which of the many available segmentation routines should be used [14].

In this paper, two unsupervised and two supervised methods were used to segment the pixels in the tomographic image. The unsupervised approaches were the K-means and the Fast and Robust Fuzzy c-Means (FRFCM) [15] clustering techniques. The supervised algorithms were two different entropy techniques: the Minimum Cross-Entropy (MINCE), and Type-2 Fuzzy Entropy (T2FE) algorithms. To compare the results and measure the accuracy of the segmentation, we applied two machine learning algorithms. They were the naïve Bayes classification and the 10 k-fold cross-validation algorithms.

The aims were to identify the classification scheme that (1) is best at segmenting the pore space and (2) is the most accurate for determining the porosity. A schematic illustration of the applied workflow is shown in *Figure 1*.

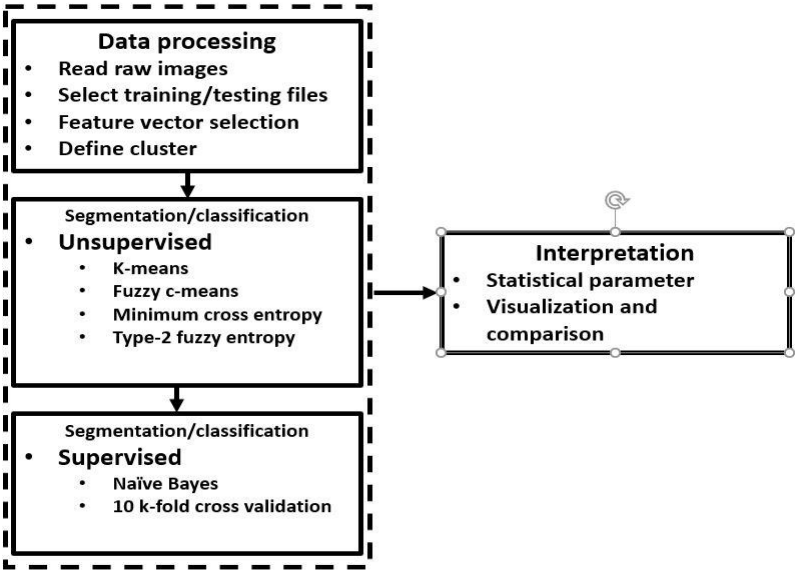

Figure 1
Flow chart describing the applied methodology

2. MATERIALS AND METHODS

2.1. Rock sample

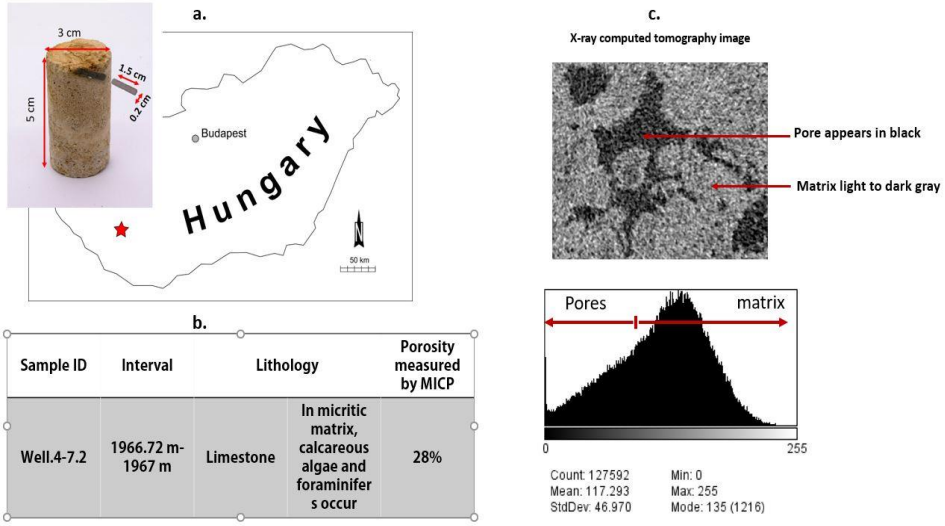

Sample ID	Interval	Lithology		Porosity measured by MICP
Well.4-7.2	1966.72 m-1967 m	Limestone	In micritic matrix, calcareous algae and foraminifers occur	28%

Figure 2
a. Are sample location and sample dimensions used for XCT scan,
b. sample depth lithology and measured porosity.
c. tomographic image used for this study and image histogram

For the analysis, a sample of shallow marine Sarmatian limestone [16] was used. The sample came from a cored section of a well drilled in the Mid-Hungarian Mega-Unit on the Northern part of the Somogy-Dráva basin, SW Hungary. The depth of the sample is 1967 m. The microscopic analysis showed a micritic matrix. Fossils such as foraminifers, algae, and other skeletal fragments were present in the sample [16]. The He porosity and Hg permeability were 28% and 55 mD, respectively. A cylindrical plug was taken from the main core with a diameter of 2 mm for μ-CT acquisition. The sample was scanned by micro CT. For the study, one tomogram was used. To avoid artifacts occurring on the edges of the scanned sample a subvolume was extracted for segmentation. The resolution of the extracted sub-volume lattice was 380 × 320 with a pixel size of 2 μm and pixel count of 127,592 *(Figure 2).*

2.2. Thresholding by entropy

2.2.1. Thresholding using minimum cross entropy

Entropy is a thermodynamic quantity used in physics; it was introduced by German physicist Rudolf Clausius in the second half of the 18th century. It measures the disorder of a system and the spontaneous dispersal of energy as a function of temperature. In physics, the notion of entropy is typically regarded as a measure of the degree of randomness and the tendency of physical systems to become less and less organized. In 1870, Willard Gibbs gave a general entropy expression for a thermodynamic system as:

$$S = \sum_j P_j log P_j \tag{1}$$

where Pj is the probability that the system is at state j. In 1877, Ludwig Boltzmann quantified entropy of an equilibrium thermodynamic system as:

$$S = K \cdot logW, \tag{2}$$

where S is entropy, K is the Boltzmann constant, and W is the number of states in the system.

In 1949, Claude Shannon redefined the entropy concept of Boltzmann/Gibbs as a measure of uncertainty regarding the information content of a system [17]. In information theory, entropy measures the amount of uncertainty of an unknown or random quantity [18].

Many entropy-based thresholding methods exist in the literature. These methods can be categorized into three groups: entropic thresholding, cross-entropic thresholding, and fuzzy entropic thresholding [18]. Cross-entropic thresholding formulates the thresholding as the minimization of an information-theoretic distance [19]. Entropy could be used also as "a measure of separation that separates the information into two regions, above and below an intensity threshold" [20]. Entropic thresholding considers "the image foreground and background as two different signal sources so that when the sum of the two-class entropies reaches its maximum, the image is said to be optimally thresholded" [19]. When the minimum cross-

entropy criterion is applied to threshold segmentation, it refers to searching for the threshold that can minimize the information content before and after segmentation.

The simplest and most direct scheme for threshold selection would be to iterate through all possible threshold values and to select th threshold that corresponds to the minimum of the cross-entropy.

2.2.2. Type-2 fuzzy entropy thresholding:

A classical set A can be defined as a collection of elements that can either belong to or not belong to set A. In contrast, a fuzzy set is a collection of objects without clear boundaries or well-defined characteristics. There are two types of fuzzy sets. A Type-I fuzzy set A, in a finite set, $X = \{x_1, x_2, \dots, x_n\}$ may be represented as in *Equation (3)*:

$$A = \{x, \mu_A(x) \mid x \in X, 0 \leq \mu_A(x) \leq 1\}, \tag{3}$$

where $0 \leq \mu_A(x) \leq 1$and $\mu_A(x)$ is called the membership function, which measures the closeness of x to A and which can only take a single value. In a Type-2 fuzzy set, a range of membership values is used instead of a single value. If A is a Type-2 fuzzy set, then:

$$A = \left\{x, \mu_A^{High}(x), \mu_A^{Low}(x) | x \in X, 0 \leq \mu_A^{High}(x), \mu_A^{Low}(x) \leq 1\right\}, \tag{4}$$

In the above definition, μ_A^{High} , and μ_A^{Low} are the upper and lower membership functions, respectively.

A digital image, $I_{Gr,}$ contains M × N pixels, where each pixel has a position defined by (m; n). The image has L intensity values that are stored in the pixels. In this context, the distribution of the intensity levels on the image can be represented by a histogram that can also be normalized as $H = \{h_0, h_1, \dots, h_{L-1}\}$. Each value, h_i, is computed using *Equation (5)*:

$$h_i = \frac{np_i}{(NP)}, \ \sum_{i=1}^{NP} h_i = 1, \tag{5}$$

where i is a level of intensity ($0 \leq i \leq L - 1$) and $NP = M \cdot N$ is the total number of pixels contained in the image. The term ultra-fuzziness can be used as a metric associated with a fuzzy set. It gives a 0 value when the membership values can be represented without any uncertainty. However, the value rises to 1 when membership values can be specified within an interval. For a digital image, the ultra-fuzziness for the i^{th} level of intensity is defined as

$$P_k = \sum_{i=0}^{L-1}(h_i * (\mu_k^{high}(i) - \mu_k^{low}(i))), K = \{1,2, \dots, nl\} \tag{6}$$

Fuzzy entropy measure is a concept used to assess the amount of vagueness within a fuzzy set. The type II fuzzy entropy for a k^{th} −threshold is therefore given as:

$$Fe_k = -\sum_{i=1}^{L-1}\left(\frac{(h_i*(\mu_k^{high}(i)-\mu_k^{low}(i))}{P_k}\right) * in\ \left(\frac{(h_i*(\mu_k^{high}(i)-\mu_k^{low}(i))}{P_k}\right), K = \{1,2, \dots, nl\}, \tag{7}$$

The sum of all the entropies for the $(nl + 1)$ levels is the total entropy defined as:

$$T_{Fe}(a_1, c_1, \dots, a_n, c_n) = \sum_{k=1}^{nt+1} Fe_i, \quad (8)$$

2.3. Image thresholding by clustering

2.3.1. K-means thresholding

Cluster analysis is a concept used to organize observed data into a meaningful structure by discovering the natural grouping(s) of a set of patterns, points, or objects, to gain further insight from them. In such a structure, the similarities between objects in the same group are high while the similarities between objects in different groups are low.

Hierarchical clustering is a method of cluster analysis where the algorithm builds a hierarchy of clusters either in agglomerative or divisive mode. In the cases of partitional clustering algorithms, the algorithms find all the clusters simultaneously, as a partition of the data, and do not impose a hierarchical structure. The most popular and simplest partitional algorithm is *K*-means clustering [21]. It is a simple unsupervised learning procedure. The calculation consists of two separate phases. The first phase is for the initializing *K* centroids. In the second phase, each data point is assigned to its closest centroid. The initial centroids are iteratively updated to the mean of the constituent data points. The algorithm finally converges when no further change occurs in the assignment of data points to the centroids. In this state, the points in any cluster have a minimum distance to the corresponding centroid. Several methods can be used to define the distance of the nearest centroid. Among them, Euclidean distance is one of the most frequently used approaches.

2.3.2. Fuzzy c-means clustering (FCM)

FCM is superior to hard clustering as it has more tolerance to ambiguity and retains more original image information [15]. The concept of characterizing an individual point's similarity to all the clusters was introduced by Zadeh (1965) [22]. The key to Zadeh's idea is to depict the similarity a point shares with each cluster by a membership function. Additionally, the sum of the memberships for each sample point must be unity. Each sample will have a membership in every cluster. Memberships close to unity signify a high degree of similarity between the sample and a cluster, while memberships close to zero imply little similarity between the sample and that cluster. The net effect of such a function for clustering is to produce fuzzy c-partitions of a given data set [22]. FCM value uses an iterative optimization of an objective function based on a membership function [23]. A local extremum of this objective function indicates an optimal clustering of the input data [24].

FCM has been used in image segmentation [25] [15], and it proved effective for images with simple texture and background [15]. Nonetheless, it fails to segment images with complex textures and background or images corrupted by noise because it only considers gray-level information without considering the spatial information

[15]. To resolve the problem, one popular idea is to incorporate the local spatial information in an objective function to improve the segmentation effect [15]. Lei et al. [15] proposed an improved FCM algorithm based on morphological reconstruction, and membership filtering (FRFCM). By introducing a morphological reconstruction operation, the algorithm manifests tolerance to the noise presented in the image. Consequently, image details are preserved. In the next step, the membership partition is replaced by membership filtering that depends only on the spatial neighbors of the membership partition [15].

The FRFCM algorithm can be summarized as follows:

Step 1: Set the cluster prototype value, fuzzification parameter, the size of the filtering window, and the minimal error threshold.

Step 2: Compute the new image and then compute the histogram of that image.

Step 3: Initialize randomly the membership partition matrix.

Step 4: Update the clustering centers.

Step 5: Update the membership partition matrix.

2.4. Supervised learning classifier

In supervised learning classifiers only labeled data (training patterns with known category labels) are involved. A supervised classifier is trained using a set of pre-defined features or classes (known as training data), where similar pixel values are sorted out from unknown data set (testing data) using supervised learning techniques. The performance of this classifier on the testing subset(s) indicates the stability of the clustering algorithm.

2.4.1. Naïve Bayes classifier

Treating image properties as random variables, and deriving a probabilistic model based on Bayesian decision theory [26] provides the foundation for Bayesian image segmentation. The motivation for the application of a stochastic framework is based on the assumption that the variation and interactions between image attributes can be described by probability distributions [27]. The naïve Bayes classifier is based on Bayes' theorem [28].

Bayes' theorem says that the probability that an event x belongs to a class k can be calculated by using the following equation:

$$P(c_k|x)=\frac{P(x|c_k)P(c_k)}{P(x)}, \tag{9}$$

In *Equation (9)*, $P(c_k|x)$ is a posterior probability, $P(x|c_k)$ is the probability of x occurring given evidence c_k has already occurred, $P(c_k)$ is the Probability of c_k occurring, $P(x)$ is the probability of x occurring. Based on the Bayesian decision we can decide the optimum class k for the event x by choosing the class with the highest probability among all possible classes. This choice can minimize the classification error [27]. For doing so, we need to estimate $P(x|c_k)$ providing that any particular value of vector x conditional on c_k is statistically independent of each dimension [27]:

$$P(x|c_k) = \prod_{i=0}^{n} P(x_i|c_k), \tag{10}$$

where x is a n-dimensional vector.
The naïve Bayes classifier can then be calculated as:

$$\mathrm{K} = \mathrm{argmax_k}\ \mathrm{p(c_k)} \prod_{\mathrm{i=0}}^{\mathrm{n}} \mathrm{P(x_i|c_k)}, \tag{11}$$

2.5. Model evaluation metrics and accuracy assessment

In classification problems there are several evaluation metrics to assist the classification accuracy. These metrics can be described as follows:

K-fold cross validation: The idea for cross-validation was first proposed by Larson (1931) [29]. Cross-validation is a statistical method of evaluating and comparing learning algorithms. It divides the data set into two subsets: one is used to learn or train a model and the other is used to validate the model. The problem with such a model is that it may demonstrate adequate prediction capability on the training data, but it might fail to predict future unseen data [1]. There are several approaches to estimate the accuracy of classifiers using different combinations of k-fold cross-validation techniques. Kohavi (1995) [30] and Dietterich (1998) [31] recommended 10-fold cross-validations as one of the best cross-validation techniques, as it mitigates biases despite variances in the size of training and testing datasets. At the onset of 10 k-fold cross-validations, the dataset is initially stratified and partitioned into 10 equal (or nearly equal) subsets or folds. Subsequently, 10 iterations of training and validation are performed such that, within each iteration, a different fold of the data is held out for validation, while the rest of the folds are used for learning. A schematic illustration of the workflow of 10 k-fold cross-validations in conjunction with naïve Bayes is shown in *Figure 3*.

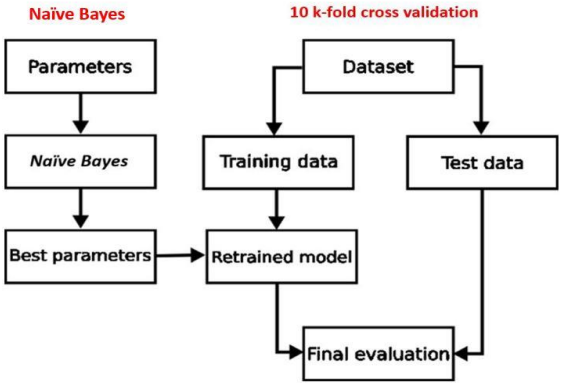

Figure 3

Schematic illustration of supervised machine learning algorithm using naïve Bayes and 10 k-fold cross validation. On the left side are the parameters resulting from the naïve Bayes classifier, and on the right side the data trained and tested, and the final evaluation is done using 10 k-fold cross validation

Precision is the proportion of positive cases that were correctly identified. The precision is the ratio tp / tp + tf, where tp is the number of true positives (positive cases that were correctly identified) and fp is the number of false positives (negative cases identified as positive). Recall is the proportion of actual positive cases which are correctly identified. F1 is the harmonic mean of precision and recall values for a classification problem. Area under ROC curve: the ROC (Receiver operating characteristic) curve is the plot between sensitivity and (1-specificity). (1-specificity) is also known as false positive rate and sensitivity is also known as the true positive rate. To bring this curve down to a single number, we find the area under this curve (AUC). Classification accuracy (CA) measures the number of correct predictions made divided by the total number of predictions made.

3. RESULTS

3.1. Image segmentation and segmentation accuracy

The classification process intends to categorize every pixel in a digital image. Each class of pixels is based on a specific feature. The categorized data could then be used to retrieve useful information. In this study, these classes were applied to compute porosity and assist in the calculation of pore size distribution.

One of the main challenges for the comparison of segmentation algorithms for X-ray CT images of porous materials is the lack of ground truth, i.e. the lack of knowledge of the optimal binarization result. Generally, two basic methods are applied to the objective evaluation of image segmentation: an analytical technique or an experimental technique [32].

The analytical technique evaluates an image segmentation algorithm by analyzing the principle of the algorithm. The experimental technique, which is widely used, interprets and compares experimental results of image segmentation algorithms to make an evaluation, and it can be subdivided into two distinct methods: superiority evaluation method and deviation evaluation method [33].

The superiority evaluation method evaluates an image segmentation algorithm by utilizing human visual traits [34]. In the deviation evaluation method, firstly a standard segmentation image is provided for comparison criteria. Then the disparity between actual segmentation and ideal one can be calculated to evaluate the image segmentation algorithm [35].

In the experimental technique, the different image segmentation algorithm is tested and compared in terms of four criteria: visual comparison, calculated pore size, pore volume, and pore count. Finally, the results are compared to a ground truth segmented image, where the latter is obtained by manual labeling of the pixels of the tested image based on the visual evaluation. It is worth mentioning that a ground truth image is not necessarily an optimal segmentation since the evaluation of the ground truth image is done visually. An additional datum assists in making the final decision.

For segmentation one XCT tomogram with the dimension of 320 × 380 was used. This tomogram was the best representation of the pore phase. The segmented images

were created by using k-means, fast and robust fuzzy c-means, minimum cross-entropy, type-2 fuzzy entropy, and the naïve Bayes classifier. In the letter case, all the available features were grouped into two groups. Each group had homogeneous features (in our case pores and matrix) and formed a feature vector. The whole dataset was used in the training the classifier. To test the classifier and to avoid data overfitting, a 10 k-fold cross-validation was implemented. In that process, the data was stratified and divided into 10 folds. One fold was held out for testing and validation, and the other nine were for the training. This process was repeated for each fold iteratively.

The naïve Bayes method classified the rock image into the pore phase and solid phase. This result was tested using each of the segmentation algorithms mentioned above. The classification accuracy resulting from each training was relatively high. This was reasonable since the unidentified threshold value was confined within a limited gray intensity range which was mainly represented by the transition zone lying in between the two phases.

Nevertheless, the set of misclassified pixels detected by the supervised machine learning algorithm for each training set varied. In fuzzy c-Means and type 2 fuzzy entropy, the number of the misclassified pixels was the highest. The reason for that could be attributed to the fact that in fuzzy classification, a single gray value could be a member of more than one group at the same time. In contrast, the naïve Bayes algorithm does not consider special location. Classification accuracy in the naïve Bayes classifier is listed in *Table 1*. The resulting binarized images for each segmentation method are shown in *Figure 4*.

Table 1

Comparison of classification accuracy on naïve Bayes classifier with different feature vectors

Classifier	AUC	CA	F1	Precession	Recall	Misclassified	Misclassified pixels gray range	Naïve Bayes Predicted Threshold value
K-means	0.965	0.877	0.871	0.897	0.877	15600	85-107	85
Fuzzy c-means	0.967	0.888	0.882	0.904	0.888	40310	85-104	85
Minimum cross entropy	0.974	0.946	0.944	0.95	0.946	6941	85-91	85
Fuzzy entropy	0.984	0.965	0.965	0.967	0.965	18064	85-112	103

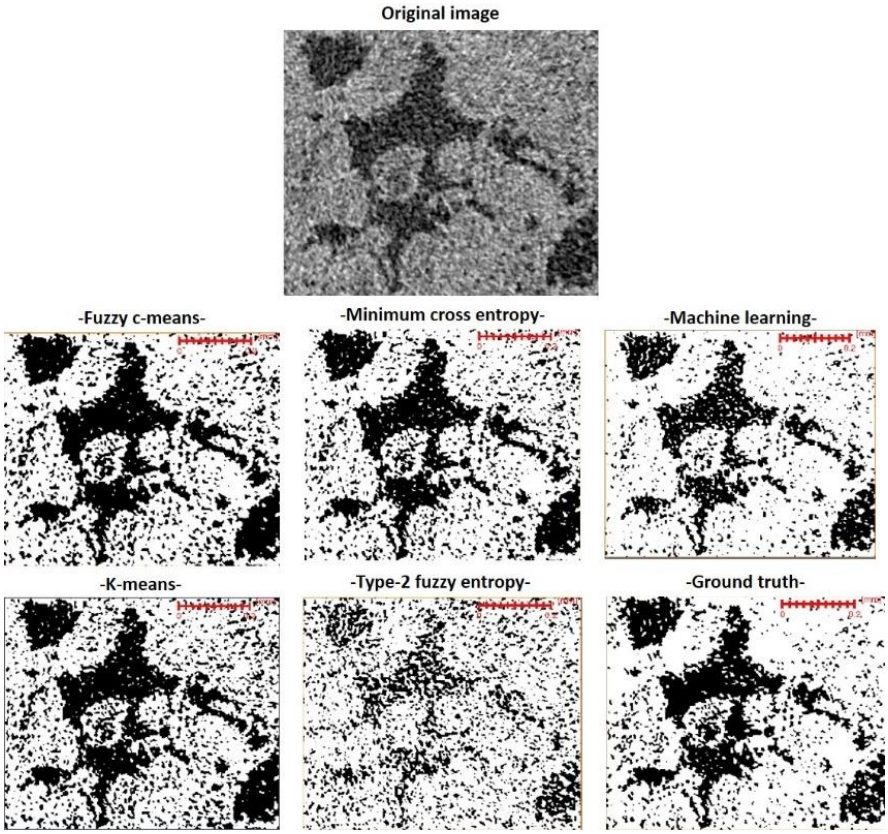

Figure 4

2-D segmented images and binarized using unsupervised and supervised segmentation where pores appear in black and matrix in white

3.2. Evaluation and comparison

The performances of the unsupervised and supervised classification methods are evaluated in terms of how well they classified the pore phase pixels in the XCT images. The volume fraction and pore counts are shown in *Figure 5*. The K-means and FRFCM clustering tend to over-segment the pore volume by 7% to 12% compared to other segmentation algorithms, where pore volume varies between 25% and 30%.

This variability in pore volume can be attributed to the presence of microcrystalline cement formed during diagenetic processes at the microstructural scale and deposited within the void space and on the pore edges, which cannot be resolved by the XCT. This situation leads to images having variable pixel intensities including the pore edges. These pixels of varying intensities would not have been segmented into the same classes by different machine learning algorithms. The aforementioned microcrystalline cement has been observed by microscopic examination of the thin sections taken from the same samples *(Figure 6)*. In *Figure 6*, we also compare

tomograms to thin sections and depicted similar attributes in both images in terms of complex pore shapes and pore distribution.
We used the calculated entropy to determine what fraction of the image needs to be carefully segmented. Image entropy is shown in *Figure 7*. The threshold window was determined by Gaussian curve fitting over the range between 82 and 138 *(Figure 7)*.

Column1	Label count	Pore volume
K-mean	845	38.02%
FRFCM	610	37.32%
MINCE	796	30.24%
FE	1423	24%
Naïve Bayes	680	25.80%
GT	564	29.30%

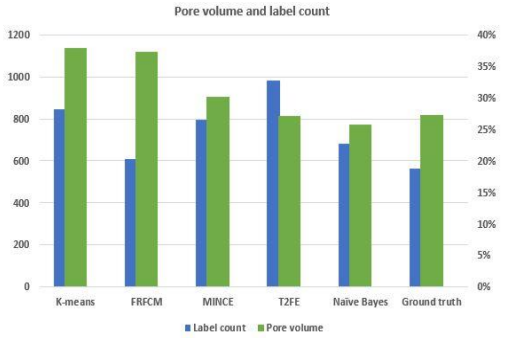

Figure 5
Porosity values and pore count obtained by using unsupervised and supervised classifiers

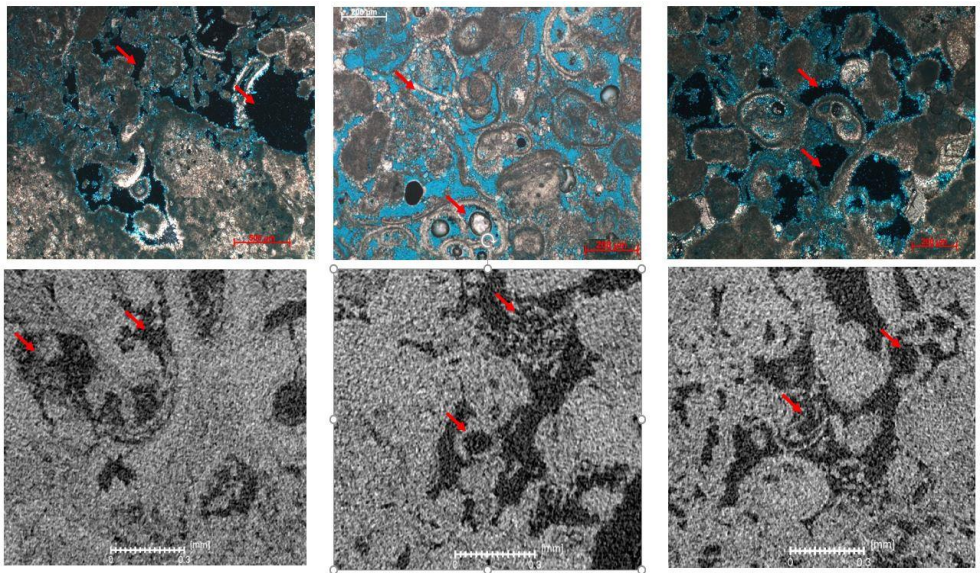

Figure 6
Visual inspection between thin sections (upper raw) and tomograms (lower raw). In the upper raw are microscopic images of thin sections taken from the sample. Grains appear in light whitish are microcrystalline cement, which also darkened in other places based on crystal orientations. The lower raw are XCT tomograms for the same sample. The arrows indicates to pore constituent in both images.

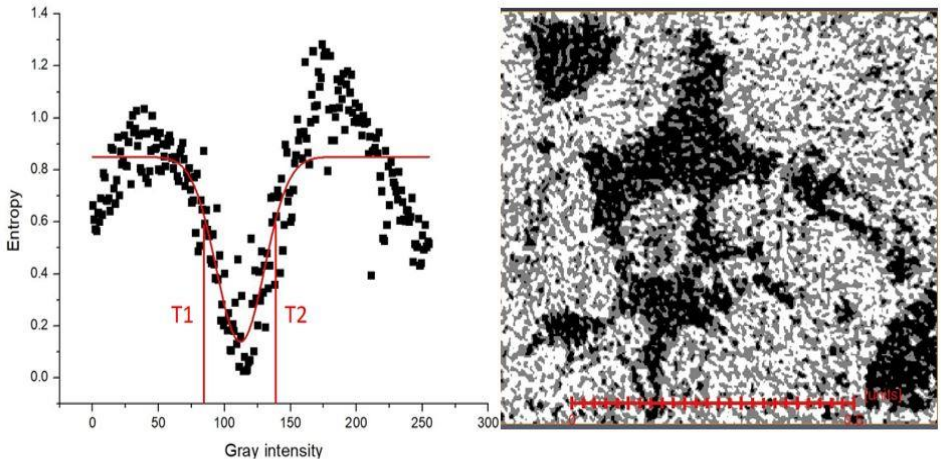

Figure 7

Studied image entropy measure where entropy appears in black and the red curve is Gaussian fit, T1 and T2 are the boundaries of the fuzzy interval determined by Gaussian at 82 and 138, respectively. The image to the right is an illustration for the fuzzy interval where the original image labeled where the pixels within 82 and 132 range appear in light gray, pores are in black and matrix in white.

The porosities were calculated using different segmentation algorithms *(Figure 5)*. In our case, the porosity was defined as the ratio between the pore phase voxels and the entire sample volume and expressed in percentage. The measured pore volume using unsupervised clustering techniques K-means and fuzzy c-means agree with each other, yet the pore counts were different. In type 2 fuzzy entropy small pores are more frequent compared to big pores, resulting in higher pore counts and lower pore volume compared to clustering and minimum cross entropy. In ground truth and the naïve Bayes classifier the measured pore volume and pore counts show approximately similar values.

The geometrical pore size distribution was calculated from the 8-bit segmented images using Avizo software. The pore sizes were determined by the morphological approach. This method fits spheres into the pores. The resulting pore size distributions coming from the different segmentation methods are shown in *Figure 8*. The calculations of P10, P50, and P90 values percentiles allowed the interpretation of geometrical pore size distribution in the terms of the micro- and macro-pore contributions to the total pore volume *(Table 2)*. *Figure 8* and *Table 2* show that segmentation by K-means clustering and MINCE the detected pores counts of the K-means clustering the MINCE methods are higher than those of the other methods. In the case of the T2FE, the small pores are more frequent than the big ones. However, in the case of FRFCM algorithm, the big pores are more dominant. The Ground truth and Naïve Bayes show similar pore size distribution.

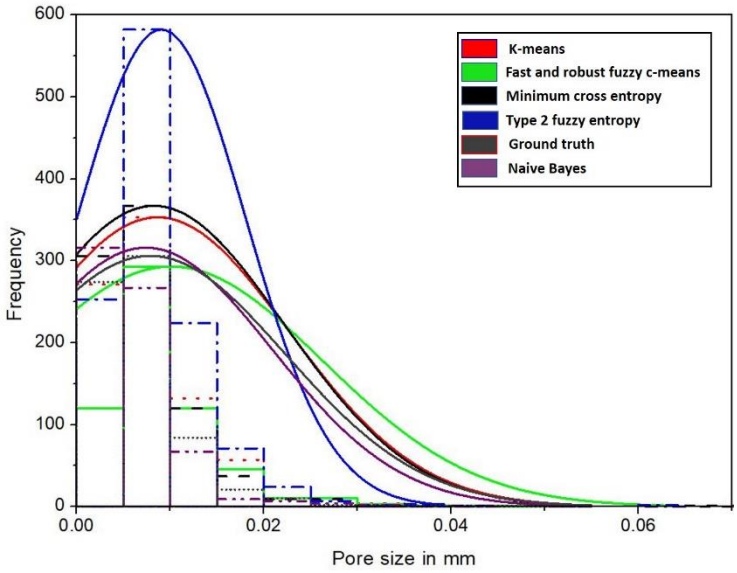

Figure 8
Histogram and normal curve for pore size distribution for each segmentation method

Table 2
Pore size diameter obtained for six segmentation algorithms

Classifier algorithm	D10 mm	D50 mm	D90 mm
K-means	0.00226	0.00638	0.01514
FRFCM	0.00391	0.00748	0.01596
MINCE	0.00226	0.00597	0.01373
T2FE	0.003909	0.007137	0.01497
Naïve Bayes	0.00226	0.00505	0.01131
Ground truth	0.00391	0.00677	0.01329

4. CONCLUSION

We have discussed some of the basic image segmentation algorithms. Also, we evaluated the quality of the image segmentation and the accuracy of the classifications. Our analyses showed that the K-means and MINCE algorithms performed well and gave good accuracy scores. The FRFCM and T2FE tended to over-segment the pore space. In the supervised machine learning method, the results were more realistic in comparison to other segmentation results and to the original image and ground truth image.

REFERENCES

[1] Chauhan, S., Rühaak, W., Anbergen, H., Kabdenov, A., Freise, M., Wille, T., Sass, I. (2016). Phase segmentation of X-ray computer tomography rock images using machine learning techniques: An accuracy and performance study. *Solid Earth*, 7 (4), pp. 1125–1139. https://doi.org/10.5194/se-7-1125-2016

[2] Gonzalez, R. C., Woods, R. E. (2008). *Digital Image Processing.* 3rd Edition. Upper Saddle River, NJ: Pearson, Prentice-Hall.

[3] Iassonov, P., Gebrenegus, T., Tuller, M. (2009). Segmentation of X-ray computed tomography images of porous materials: A crucial step for characterization and quantitative analysis of pore structures. *Water Resources*, Volume 45, pp. 1–12, https://doi.org/10.1029/2009WR008087.

[4] Zack, G.W., Rogers., W., Latt, S. (1977). Automatic measurement of sister chromatid exchange frequency. *J. Histochem. Cytochem*, 25, pp. 741–753. https://doi.org/10.1177/25.7.70454

[5] Pham, T. (2001). Image segmentation using probabilistic fuzzy c- means clustering. *Proc., 2001 IEEE International Conference on Image Processing*, Vol. 1, pp. 722–725, https://doi.org/10.1109/ICIP.2001.959147.

[6] Cortina-Januchs, M., Quintanilla-Dominguez, J., Vega-Corona, A., Tarquis, M., Andina, D. (2011). Detection of pore space in CT soil images using artificial neural networks. *Biogeosciences*, 8, pp. 279–288. https://doi.org/10.5194/bg-8-279-2011.

[7] Khan, F., Enzmann, F., Kersten, M. (2016). Multi-phase classification by a least-squares support vector machine approach in tomography images of geological samples. *Solid Earth*, 7, pp. 481–492. https://doi.org/10.5194/se-7-481-2016

[8] Fukushima, K. (1980). A self-organizing neural network model for a mechanism of pattern recognition unaffected by shift in position. *Biol. Cybermetics*, 36, pp. 193–202, https://doi.org/10.1007/BF00344251.

[9] [9] Lecun, Y., Bengio, Y., Hinton., G. (2015). Deep learning. *Nature*, 521, pp. 436–444, https://doi.org/10.1038/nature14539.

[10] Chang, Y., Luo, B. (2019). Bidirectional convolutional LSTM neural network for remote sensing image super-resolution. *Remote Sensing*, 11, pp. 1–18. https://doi.org/10.3390/rs11202333

[11] Kaji, S., Kida, S. (2019). Overview of image-to-image translation by use of deep neural networks: Denoising, super-resolution, modality conversion, and reconstruction in medical imaging. *Radiological Physics and Technology*, 12, pp. 235–248, https://doi.org/10.1007/s12194-019-00520-y.

[12] Pham, C., Tor-Díez, C., Meunier, H., Bednarek, N., Fablet, R., Passat, N., Rousseau, F. (2019). Multiscale brain MRI super-resolution using deep 3D convolutional networks. *Computerized Medical Imaging and Graphics*, 77, pp. 1–15, https://doi.org/10.1016/j.compmedimag.2019.101647.

[13] You, C., Li, G., Zhang, Y., Zhang, X., Shan, H., Li, M., Ju, S., Zhao, Z., Zhang, Z., Cong, W., et al. (2019). CT Super-resolution GAN Constrained by the Identical, Residual, and Cycle Learning Ensemble. *(GAN-CIRCLE). IEEE Trans. medical imaging*, 39, pp. 188–203. https://doi.org/10.1109/TMI.2019.2922960

[14] Chauhan, S., Rühaak, W., Khan, F., Enzmann, F., Mielke, P., Kersten, M., Sass, I. (2016). Processing of rock core microtomography images: Using seven different machine learning algorithms. *Computers and Geosciences*, 86, pp. 120–128, https://doi.org/10.1016/j.cageo.2015.10.013.

[15] Lei, T., Jia, X., Zhang, Y., He, L., Meng, H., Nandi, K. (2018). Significantly Fast and Robust Fuzzy C-Means Clustering Algorithm Based on Morphological Reconstruction and Membership Filtering. *IEEE Transactions on Fuzzy Systems*, 26 (5), pp. 3027–3041. https://doi.org/10.1109/TFUZZ.2018.2796074

[16] Mukhtar, T. (2020). *Sedimentological Control on the Productive and Dry Intervals in Four Investigated Wells*. Master Thesis, University of Miskolc.

[17] Sengur, A., Turkoglu, I., Ince, M. (2006). A Comparative Study On Entropic Thresholding Methods. *Journal of Electrical & Electronics Engineering*, 6 (2), pp. 183–188.

[18] Mahmoudi, L., El Zaart, A. (2012). A survey of entropy image thresholding techniques. *Proc., 2012 2nd International Conference on Advances in Computational Tools for Engineering Applications, ACTEA*, pp. 204–209. https://doi.org/10.1109/ICTEA.2012.6462867

[19] Sezgin, M., Sankur, B. (2004). Survey Over Image Thresholding Techniques And Quantitative Performance Evaluation. *Journal of Electronic Imaging*, 13 (1), pp. 146–165.

[20] Al-Attas, R., El-Zaart, A. (2006). Thresholding of Medical Images Using Minimum Cross Entropy, *Proc., Kuala Lumpur International Conference on Biomedical Engineering*, Kuala Lumpur, Malaysia, pp. 312–315.

[21] Jain A. (2010). Data clustering: 50 years beyond K-means. *Pattern Recognition Letters*, 31 (8), pp. 651–666.

[22] Zadeh, A. (1965). Fuzzy sets. *Information and Control*, 8 (3), pp. 338–353.

[23] Toz, G., Yücedağ, İ., Erdoğmuş, P. (2019). A fuzzy image clustering method based on an improved backtracking search optimization algorithm with an

inertia weight parameter *Journal of King Saud University - Computer and Information Sciences*, Vol. 31 (3), pp. 295–303.

[24] Nikhil, R., Sankar, K. (1993). A review on image segmentation techniques. *Pattern Recognition*, Vol. 26, pp. 1277–1294.

[25] Choudhry, M., Kapoor, R. (2016). Performance analysis of fuzzy c-means clustering methods for MRI image segmentation. *Procedia Computer Science*, Vol. 89, pp. 749–758

[26] Duda, R., Hart, P. (1973). *Pattern Recognition and Scene Analysis*. New York, Wiley-Interscience.

[27] Dong-Chul, P. (2016). Image Classification Using Naive Bayes Classfier. *International Journal of Computer Science and Electronics Engineering*, 4 (3), pp. 2320–4028.

[28] Jang, M., Park, D. (2016). Stochastic Classifier Integration Model. *International Journal of Applied Engineering Research*, 11 (2), pp. 809–814.

[29] Larson, C. (1931). The shrinkage of the coefficient of multiple correlation. *J. Educ. Psychol.*, Vol. 22, pp. 45–55, https://doi.org/10.1037/h0072400.

[30] Ron, K. (1995). A study of cross-validation and bootstrap for accuracy estimation and model selection. *Proc., The International Joint Conference on Artificial Intelligence (IJCAI)*, pp. 1137–1145.

[31] Dietterich, T. (1998). Approximate statistical tests for comparing supervised classification learning algorithms, *Neural Computation*, 10 (7), pp. 1895–1923.

[32] Sharon, E., Brandt, A., Basri, R. (2000). Fast multiscale image segmentation. *Proc., IEEE Conference on Computer Vision*, Vol. 1, pp. 70–77.

[33] Brink, D. (1992). Thresholding of digital images using of two-dimensional entropies. *Pattern Recognition*, 25 (8), pp. 803–808.

[34] Zhou, L., Gao, X. (2004). Image segmentation via fast fuzzy c- means clustering. *Computer Engineering and Application*, 40 (8), pp. 68–70.

[35] Wang, Q. (1998). One image segmentation technique based on wavelet analysis in the context of texture. *Data Collection and Processing*, 13 (1), pp. 12–16.

Geosciences and Engineering, Vol. 10, No. 15 (2022), pp. 80–95.
https://doi.org/10.33030/geosciences.2022.15.080

A REVIEW ON ROLE OF GEOSYNTHETIC CLAY LINERS IN CONTAMINATED SITE REMEDIATION

Hasan Eteraf[1], Tamás Madarász[2], Amir Mosallaei[3], Balázs Kovács[4], Viktória Mikita[5]

[1]*University of Miskolc, hghassan@uni-miskolc.hu, https://orcod.gov/0000-0001-5730-445X*
[2]*University of Miskolc, hgmt@uni-miskolc.hu, https://orcid.gov/0000-0002-3291-1605*
[3]*Budapest University of Technology and Economics, amir.mosallaei@epito.bme.hu https://orcid.gov/0000-0002-3291-1605*
[4]*University of Miskolc, kovacs.balazs@gama-geo.hu, https://orcid.gov/0000-0002-3594-7355*
[5]*University of Miskolc, gmv@uni-miskolc.hu, https://orcid.gov/0009-0006-9303-1368*

Abstract: Many environmental disasters occurred in the past due to site contamination caused by leakage of leachate to surround soil, surface water and ground water aquifer. The main concern is focused on the contamination potential due to migration of the leachate produced from the waste disposal or storage sites into the soil and underlying layers. Leachate quality, quantity and properties are directly relevant to waste management methods, environment conditions and waste characteristics, as well as the process of landfill processing, and the leachate may be the major source of various pollutants and emissions Problems associated with the cleanup sites have shown that remediation technologies need to be developed that are feasible, fast, and deployable in a wide range of physical settings. Using an effective landfill liner is a common way of preventing the movement of pollutants (with gas or leachate) from landfill sites or contaminated sites (e.g. brownfields, fuel stations, accidental spills, etc.). In this study different types of Geosynthetic clay liners were reviewed and they were compared in aspects of hydraulic conductivity, strength, material and chemical to improve GCL design to optimum.

Keywords: *GCL, Liner, leachate, Landfill, Hydraulic Conductivity*

1. INTRODUCTION

Many environmental disasters occurred in the past due to site contamination caused by leakage of leachate to surround soil, surface water and ground water aquifer. The main concern is focused on the contamination potential due to migration of the leachate produced from the waste disposal or storage sites into the soil and underlying layers. [1]

The characteristics of the leachate also depend on the pretreatment of the solid waste such as segregation of recyclable material like plastics, paper, metals, glass,

etc, shredding and/or bailing of the waste. the characteristics of landfill leachate vary over time and also they are different from one landfill to another. Many factors effect on the leachate compound such as types of wastes deposited, composition of wastes, moisture content, the particle size, the degree of compaction, the hydrology of the site and the climate. [1]

In response to spreading need to take environmental pollution into consideration, many remediation technologies have been developed to treat soil, leachate, wastewater, and groundwater contaminated by various pollutants. [2] The main goals of sustainable waste management are to protect human health and the environment and to reduce the number of natural resources consumed. [3] A particular contaminated site may require a combination of procedures to allow the optimum remediation for the prevailing conditions. Biological, physical, and chemical technologies may be used in conjunction with one another to reduce the contamination to a safe and acceptable level. [2]

There are numbers of soil remediation approaches such as: soil washing, soil vapor extraction, soil processing, soil flushing, solidification / stabilization, asphalt batching, vitrification, biopiles, phytoremediation, bioslurry systems, bioventing, encapsulation, aeration, thermal desorption. There are, on the other hand, various groundwater remediation methods such as: air sparging, groundwater injection and treatment technology, passive/reactive treatment walls, bioslurping, ultraviolet oxidation treatment, biosparging, groundwater drainage wells, horizontal well technology, natural attenuation. [2]

Problems associated with the cleanup sites have shown that remediation technologies need to be developed that are feasible, fast, and deployable in a wide range of physical settings. [2] Using an effective landfill liner is a common way of preventing the movement of pollutants (with gas or leachate) from landfill sites or contaminated sites (e.g. brownfields, fuel stations, accidental spills, etc.). 'Liner' is an identifier layers of materials performed before waste is collected to cover or line the surface of the waste disposal sites. [5]

2. LEACHATE

Throughout the waste disposal process, a managed disposal procedure is unavoidable, either for the disposal of actual waste or of materials remaining during the treatment phase or, if necessary, if the main phase cannot be carried out for a period of time due to failure, malfunction, remediation or other causes. Landfill is a main municipal solid waste disposal facility in most countries, some of which are still on the least developed category and face a linear rise in municipal solid waste and problems with waste management. [24]

The construction of an engineered sanitary landfill is certainly quite capital intensive. Having an overview of the performance of landfill sites demands experience and understanding of the characteristics of the landfill waste as well as the operating activities at the landfill site. [23]

Increased resource consumption results in large quantities of solid waste from different forms of manufacturing and domestic operations, which pose a major threat to human health and the environment. [25]

Leachate quality, quantity and properties are directly relevant to waste management methods, environment conditions and waste characteristics, as well as the process of landfill processing, and the leachate may be the major source of various pollutants and emissions. [26]

Chemical reactions such as biodegradation, adsorption, hydrolysis, dissolution, dilution, partitioning and precipitation are among the most important factors influencing the consistency of the leachate. [27]

The form and concentration of the pollutants in the leachate depends on the manner of disposal, along with the composition of the waste, and on the isolation of the waste prior to its final disposal. [28]

The lack of sufficient landfill infrastructure, such as liner, leachate storage and treatment systems, raises the risk for soil, groundwater and surface water pollution. [29]

In most situations, landfill leachate is composed of organic matter, inorganic chemicals and toxic substances. [31]

Hazardous substances in municipal solid waste (MSW) are identified in the form of paints, mercury-containing waste, batteries, vehicle maintenance materials and many other diffuse products. [30]

Solid waste disposal services, such as open dumps, landfills, sanitary landfills or incinerators, are a primary source of metals released into the environment. In addition, there is a greater risk of groundwater pollution in areas near landfill sites; this is due to the fact that most landfills and disposal facilities release a large amount of leachate into their surroundings. There are varying degrees of effects on human health and the environment depending on the form of landfill and its management. [22]

Principal leachate collection systems can have service lives that vary from less than a decade to more than a century, depending on design specifics, waste features and mode of operation. The use of liners is one of the most inexpensive ways to monitor and avoid contamination of the ground. Field tests and theoretical calculations indicate that composite liners are considerably stronger than single liners when it comes to preventing landfill leakage. Composite liners containing a geomembrane (GM) over a geosynthetic clay liner (GCL) resulted in considerably less leakage than those containing a compacted clay liner (CCL). High-density polyethylene (HDPE) GMs provide an excellent diffusive ion barrier. However, some organic compounds which are readily diffused through HDPE GMs and a combination of GM and a sufficient thickness of liner and attenuation layer are needed to regulate the effect at negligible rates. [11]

3. GCLs

During the last decade, structural engineers and environmental authorities have shown increasing interest in the use of geosynthetic clay liners (GCLs) as an alternative to compacted clays in over systems or, in some situations, bottom liners in waste containment facilities, as they also have very low hydraulic conductivity to water (kw < 10^{-10} m / s) and fairly low cost. In addition to environmental uses such as liner or solid waste storage systems, GCLs are also used as environmental barriers in transport facilities (road and rail) and geotechnical uses such as reducing contamination of subsurface layers from chemical leaks and drainage of road accidents. GCLs are also used as secondary liners for underground storage tanks of fuel to protect groundwater resources and are used as main liners for canals, reservoirs or surface impoundments. [6]

Containment measures can be classified as follows:
1. Bottom liners or barriers
2. Cover or cap liners
3. Vertical side barriers or cut-off walls

- The bottom liners are typically associated with the overlying drainage layer and the underlying low-permeable layer, often referred to as the geological barrier. A stable soil from a geotechnical point of view, ideal for base and building and not prone to subsidence, would be the geological barrier below and adjacent to the waste disposal site. Bottom barriers must sustain the mass of waste and should be almost impermeable in order to prevent leachate from spreading to the ecosystem. Most regulations therefore allow a low permeability of < 10^{-8}–10^{-9}/ s.
- Cover or cap liners shield waste or polluted land from rainwater penetration, gas emission and erosion. The main goals of the landfill cover are as follows:
  – minimizing water infiltration
  – preventing emission of mainly volatile pollutants
  – preventing erosion by water and wind
  – increasing the evaporation rate
  – re-cultivation and integration of the landfill into the regional landscape.
- Vertical side barriers or cut-off walls regulate lateral water flows (infiltration of groundwater or outflow of leachate) in landfills and contaminated areas. Material changes within the cut-off walls can be preceded by the same processes that affect the compacted clay liners: desiccation, freeze/thaw, chemical incompatibility, and excessive deformation.

Clay is most commonly used in containment systems to control the flow of water, leachate and gas to and from waste disposal sites. The compacted clay layer (CCL) can be used either individually or as a part of a lining system with an overlay of

synthetic high-density polyethylene (HDPE) membrane (geomembrane) and a drainage layer. The combination of a CCL with a geomembrane is often referred to as a composite liner. The CCL, usually with a thickness of 0.5–1.0 m or more, can be substituted by a manufactured geosynthetic clay liner (GCL), which is a thin layer of low permeable substance (e.g. clay, bentonite) covered by geotextiles and/or geomembranes that are held together by Needling, sewing and/or synthetic adhesives. [5, 12]

The types of geotextiles which are used with the various material, vary significantly in their manufacturing style (e.g. woven slit film, needle punched nonwoven, spun, heat bonded nonwovens, etc.) and in their mass per unit area [e.g. ranging from 85 g/m2 to 1000 g/m2]. The thickness of GCL is usually 4–6 mm. GCLs are shipped to the site at a moisture level ranging from 5 to 23 per cent based on the local humidity. [12]

Geosynthetic clay liners (GCLs) have gained popularity as a replacement for compacted clay liners in cover systems and composite bottom liners. These are also used as environmental barriers in transport facilities or reservoirs and as single liners for canals, ponds or surface impoundments. As a result, they are intensively studied, in particular with regard to their hydraulic and diffusion properties, chemical stability, mechanical behaviour, endurance and gas migration. [6]

Through this study GCL were reviewed from different point of view in different aspect. The priority was evaluation of hydraulic conductivity as it is the most important factor of GCL performance.

4. STRENGTH

In the refurbishment process for aged small earth dams, the sloping main zone is usually built as a water barrier on the upstream side of the bodies by using cohesion impermeable soil. However, these soils are not always accessible at dam sites and their supplying is also problematic. The installation of geosynthetic clay liners (GCLs) was suggested as one of the alternative approaches for the construction of a sloping core region. GCLs are commonly used in waste disposal facilities and are considered to be impermeable materials for small earth dams. Nevertheless, design criteria have not yet been formed as there are few studies on the mechanical characteristics of GCLs in small earth dams. Specifically, the shear strength parameters of the internal bentonite layer of GCLs during the earthquake must be studied. [7]

Ross & Fox presents the results of full-scale research to further investigate possible GCL damage factors in earth dam retrofit applications in seismically active areas. In particular, (a) investigate whether shear displacements may reduce the magnitude of GCL overlap during earthquakes; (b) explore the impact of gravel particles on GCL thickness at the localized point of contact; and (c) examine the implications of accidental exposure of exposed GCL to short-term precipitation in terms of moisture content and effects during subsequent compacting; The results of these experiments show that no changes were observed in the GCL panel even under

extreme shaking. Although gravel particles have been observed to reduce the thickness of the GCL to 2.2 millimetres locally, no plowing of the particle into the GCL has occurred due to a lack of shear displacement at the interface, resulting in no localized internal erosion through the barrier. In addition, hydration of GCL panels during construction due to surface wetting has been found to result in less hydration than post-construction. These findings show that while each of the three GCL damage factors cannot be ruled out to be relevant in operation, the performance of the GCL retrofitted earth dam tested was adequate under even extreme earthquake level 2 shaking and indicates that the retrofitting of small earth dams with GCLs is a promising strategy to optimize their static and seismic resistance. [13]

The design standard for small earth dams using GCLs is not known as there are few research on their mechanical features. Throughout Shigemoto's analysis, cyclic direct shear tests were performed on the internal bentonite layer of needle punched GCL in order to investigate the mechanical characteristics of GCLs laid in reservoirs during earthquakes. Tests were conducted under standard stress of 25 kPa, taking into account the low confining pressure in embankments and the shear displacement amplitude of 0.5, 1.0, 3.0 and 5.0 mm. The shear strength was observed to decrease with the amount of test cycles due to the fracturing of the needle-punching and the removal of the needle from the geotextiles. In addition, the results showed that the amount of decrease in shear strength expanded as the amplitude grew. [7]

There are few researches on the shear strength performance of the GCLs under dynamic loading. Lai et al. (1998) conducted stress regulated cyclic simple shear tests on the internal bentonite layer of GCL which is supported by geomembrane without needles-punching in hydrated and without moisture conditions. [7]

Tests show that small displacement amplitudes ($\Delta a \leq 10$ mm) had little to no impact on the post-cyclic static shear strength for GMX / GCL interface. Larger displacement amplitudes resulted in a decrease in post-cyclic static strength until a displacement amplitude of 20 mm was achieved, after which there was no further decrease in shear strength of the interface with increasing displacement amplitude. The mode of failure depended on the rate of cyclic shearing. Larger displacement amplitudes ($\Delta a = 30$ mm) needed faster shearing and led in interface failures for all normal stresses, whereas smaller amplitudes needed slower shearing and partial internal shearing to complete internal failures of the GCL. [13]

In another research, the post-cyclic static shear response of the GMX/GCL interface were examined. Each post-cyclic static test was carried out at a displacement rate of R = 1 mm/min. For $\Delta a < 15$ mm, the peak shear stress was not affected, and corresponded to the peak shear stress of the monotonic test completed with no previous cyclic testing. For $\Delta a \geq 15$ mm, the peak strength was greatly reduced. [21]

A waste containment facility liner or cover system must not only have a good hydraulic / gas barrier, but must also be structurally strong during all steps of the project (i.e. while construction, during and after waste storage). For this purpose, the determination of stability is a vital consideration for design engineering. [6]

Shan and Daniel (1991), Stark and Eid (1996), Gilbert et al. (1996), Eid and Stark (1997), and Fox et al. (1998a) provided a detailed collection of findings on the internal strength of unreinforced GCLs and reinforced GCLs. Peak shear strengths for non-reinforced GCL products were found to be similar to those for bentonite in aspect of having very low shear strength. This is the reason why it is not generally prescribed for slopes of more than 10H : 1V (Frobel, 1996; Richardson, 1997). At the other side, reinforced GCLs possess a higher internal peak strength due to the presence of fibers. Reinforced GCL strength behavior has also been shown to rely on fiber resistance and bentonite shear strength. When the fibers are pulled out and/or ripped at large displacements, bentonite can continue to absorb residual force. It should be noted that despite the internal failure of reinforced (needle punched) GCLs could happened in the laboratory, no known instances of slope failures can be attributed to internal shear failure of reinforced GCLs. [6]

A group of laboratory experiments were carried out to investigate the geomechanical and geoenvironmental properties of sepiolite alone, zeolite alone, sepiolite–zeolite soil mixtures as control content.

The rise in applied compaction energy greatly improved the unconfined compressive strengths (qu) of all soil mixtures. In comparison, all soil mixtures prepared at an optimum 5 per cent dry side and an optimum 5 per cent wet side got the highest and lowest qu values, respectively.

Sepiolite itself has yielded the highest qu values. Furthermore, the qu values were significantly risen with the addition of sepiolite to the zeolite soil. In addition, rising the sepiolite content, caused a significantly decrease in hydraulic conductivity value of soil mixtures due to high activity, high clay content, plasticity index and high specific surface area. [4]

5. MATERIAL

Landfill bottom liners are typically made of natural clay soils due to their high strength and low hydraulic conductivity characteristics. However, in recent years it has become increasingly difficult to find locally available clay soils that meet the essential engineering characteristics. [4]

Nevertheless, in previous years it has become more difficult to find locally accessible natural soil that satisfies the engineering properties described above. Scientists are now searching for alternate materials that can be used as liners in urban waste disposal sites. Recent studies have suggested replacing natural clay soils with soil likehood geomaterials such as sand-bentonite mixtures, foundry sand, fly ash, wood ash and tire rubber. [4]

Although these materials generally fulfilled the engineering properties required to be used in liner constructions, issues relating to their mechanical and environmental compatibility have been identified. [4]

Low hydraulic conductivity is typically met by CCL, which also includes smectites. Because wet clay content is often very difficult to handle and dry clay is very prone to cracking, sand and clay mixtures (often bentonite) are used as bottom

liners (Grantham and Robinson, 1988; Cancelli et al., 1994; Ebina et al., 2004). In this case, the hydraulic conductivity depends heavily on the content of the clay. A higher hydraulic conductivity was determined for Ca-type rather than Na-type clays. A combination of bentonite and zeolite also resulted in higher hydraulic conductivity in comparison to sand-bentonite mixtures (O¨ren et al., 2011). [5]

If expansive clays are mixed with fly ash-an industrial waste- the density of mixture increases that leads to a reduction in hydraulic conductivity. Fly ash-stabilized expansive clay may therefore also be suggested as an advanced clay liner material. It is therefore important to research the different physical and engineering characteristics of this new clay liner material. Liquid limit (LL) and free swell index are important factors to be reviewed for this clay liner material. The hydraulic conductivity of this new clay liner material refers to the amount of the fly ash in the mixture. Viana et al. presents experimental results gained on hydraulic conductivity (k) of fly ash stabilized expansive clay liner at varying levels of fly ash and solute concentration of transmit fluid. Tests were conducted with (DIW), $CaCl_2$, NaCl and KCl deionized water as permeating fluids. Fly ash content varied as 0, 10, 20 and 30 per cent by weight of expansive clay used in admixtures and the concentration of solute varied as 5 mM (milli molar), 10, 20, 50, 100 and 500. Rising amount of fly ash, solute concentration and kinematic viscosity, caused a decrease in Hydraulic conductivity (k). So it seems that Parameters such as solute concentration and kinematic viscosity of permeating fluids also affect the hydraulic conductivity of clay liners. [15]

For example, Edil et al. (1992) and Palmer et al. (2000) indicated that the use of fly ash in liner construction is practical. However, the field ash compaction process can be complicated and may result in higher hydraulic conductivity and lower stiffness (Palmer et al., 2000). In fact, fly ash itself contains a large amount of heavy metals, which is an unavoidable hazard for the environment. Sand – bentonite mixtures and foundry sand provided a reasonable level of stiffness and hydraulic conductivity with pure deoinized water influent solutions. Nevertheless, the hydraulic conductivity of these soils improved dramatically with the use of chemical influent solutions. [4]

Karunaratne et al. conducted laboratory research to explore the practical feasibility of combining alternative materials with bentonite to generate Modified low-cost GCLs. The alternative materials used were sand, clay and tire grain. Direct shear, consolidation and expansion tests were conducted on bentonite mixtures with differing percentages in the mass of the alternative material. Ramp tests and expansion tests were also performed on alternative GCLs produced with these types of mixtures. The findings obtained have shown that the presence of alternative materials in bentonite has improved the shear strength and permeability of the mixture and reduced its potential of expansion. Tests on bentonite-tire grain mixtures indicate that alternative GCLs developed with this form of mixture can be used in less critical barrier systems (especially under high stress levels) and as liner/protective layers below geomembranes, thus having better usage for waste tires in terms of environmental. Hydraulic conductivity and consolidation behavior of bentonite-

kaolinite mixtures have been analyzed. It was found that at least 30% bentonite was needed in the mixture to achieve the same decreasing coefficient of consolidation tendency with pressure as seen by pure bentonite. The 50 : 50 bentonite : kaolinite (50 : 50 B: K) ratio failed in approximately the same hydraulic conductivity, k, as pure bentonite; The hydraulic conductivity tests were performed using pure water, 0.25 M calcium chloride, 0.1 M hydrochloric acid, and 0.1 M sodium hydroxide. With the calcium chloride permeant, the hydraulic conductivity of the mixture was observed to be in the range of 10^{-10}m/s, while the hydrochloric acid and sodium hydroxide permeants yielded values of approximately 10^{-11}m/s. The idea of using a mixture of bentonite-kaolinite (B : K) instead of pure bentonite with a jute geo-textile as the foundation of a clay liner in a landfill is discussed exploring the potential use of kaolinite to replace the percentage of bentonite used in landfill and liner systems was the goal of one of performed research. [16]

Red mud is a waste material produced by the Bayer Process commonly used in the manufacturing of alumina from bauxite. Approximately 35% to 40% per ton of bauxite processed with the Bayer Procedure ends up as red mud waste. According to disposal issues, contamination has a detrimental effect on the environment. Exploring the various reuses of red mud waste is necessity to find a proper solution of this environmental issue. Tian et al.'s research evaluates the effects of red mud on unconfined compressive strength, hydraulic conductivity and swelling of compacted clay liners as a hydraulic barrier. The findings of the study indicate that compacted clay samples including red mud and cement-based mud additives had a high compressive strength and decreased the values of hydraulic conductivity and swelling in comparison to natural clay. It is therefore demonstrated that red mud and cement-red mud materials can be used successfully in geotechnical applications for the stabilization of clay liners. [17, 18]

6. CHEMICAL

Synthetic and natural municipal solid waste (MSW) leachate permeation affects the hydraulic conductivity and exchange complex of geosynthetic clay liners (GCLs). A number of laboratory experiments were carried out to analyze the geomechanical and geoenvironmental properties of sepiolite alone, zeolite alone, sepiolite–zeolite soil mixtures and Eskisehir clay as control material. Sepiolite did not have a noticeable effect on the pH of the effluent solutions even though it had approximately 23 per cent CaO material. On the other hand, the increase in sepiolite content lowered the electrical conductivity (EC) of sepiolite – zeolite soil mixture wastewater solutions. Column leaching experiments showed that sepiolite clay had a greater impact on adsorption ability of landfill liners. adsorption levels of Pb^{2+}, Cu^{2+}, and Zn^{2+} rose with the sepiolite material. On the other hand, temperature had a major effect on the adsorption of metals. for example, Steel adsorption at 35 °C was 375 times greater than steel adsorption at 5 ℃. [4]

The effect of temperature on the hydraulic conductivity values with bentonite swelling is elucidated using the NaCl solutions, not deionized water used in previous

studies, because the swelling capacity of bentonite in deionized water is so large that changes in hydraulic conductivity are negligible even at an elevated temperature. The free swell in the 60 °C NaCl solution is larger than that in the 20 °C NaCl solution. Although previous studies have suggested that the intrinsic permeability is smaller for the 60 °C NaCl permeation than for the 20 °C NaCl permeation, the measured intrinsic permeability values of GCLs are $5.9 * 10^{-18}$ m^2 for the 20 °C NaCl permeation and $2.5 * 10^{-17}$m2 for the 60 °C NaCl permeation. Consequently, the intrinsic permeability increases with temperature, and the relationships between the free swell and the hydraulic conductivity reported in previous studies are not applicable to the elevated temperature condition. [8]

The problem of cation exchange-induced changes in hydraulic conductivity for sodium bentonite GCLs has received considerable attention recently (Dobras and Elzeas, 1993; James et al., 1997; Melchior, 1997; Lin and Benson, 2000). This focus is due to the fact that an increase in GCL hydraulic conductivity (one to two orders of magnitude) has been observed in contact with calcium-rich soils or calcium solutions. Such findings refer to GCLs which are subjected to low compressive pressures (<20 kPa) as usual of landfill cover systems. It is expected that at high compressive pressures such as those found in the bottom liners of the landfills, no adverse impact will be found. (Daniel, 2000). [6]

Results of confined swell, consolidation, and hydraulic conductivity tests on the needle-punched geosynthetic clay liner (GCL) are stated. Effects of permeant [purified water, aqueous single-salt solutions with concentrations between 0.01 and 2.0 M NaCl and industrial municipal solid waste (MSW) leachate], static confining tension, hydrating medium and degree of bentonite hydration at the time of applying confined stress are tested. Increases in permeant salt concentration and declines in the severity of the container tension induced an increase in hydraulic conductivity. High concentrations of salt in hydrating fluids have been shown to increase hydraulic conductivity. GCLs with 0.6 M and 2.0 M NaCl solutions were more permeable than GCLs hydrated with water at first. The impact of bentonite hydration degree at the time of application of the confining stress was demonstrating the hydraulic advantages of maximizing overloaded stress prior to GCL hydration. Tests conducted using synthetic MSW leachate produced findings equivalent to those obtained with aqueous salt solutions between 0.2 and 0.8 M NaCl. [10]

Bentonite is a natural clay mineral commonly used in the mining and solid waste disposal industry, e.g. as a soil mixture for the installation of seepage barriers or as a part of geosynthetic clay liners (GCLs) to have low hydraulic conductivity. However, the deterioration of bentonites usually happens when permeated with acidic solutions, such as those used in mining applications, which may affect the physical characteristics and, in general, the hydraulic performance of geosynthetic clay liners. In Petrov et al. research, properties such as Atterberg limits, free swell index, and fluid loss of three specimens of bentonites with various concentrations of sulphuric acid solutions were calculated. Such features were shown to deteriorate even with low (0.015 M) sulfuric acid solutions; higher concentrations (up to 1 M)

resulted in greater degradation. X-ray diffraction and infrared spectroscopy have been used to track shifts in bentonites after interactions with acid solutions. Acid leachate typically results in the overall deterioration of the hydraulic utilization of geosynthetic clay liners and, potentially, of any bentonite-soil mixture. [9]

Eight commercially available geosynthetic clay liners (GCLs) permeated with a leachate characteristic of low-level radioactive waste (LLW) disposal facilities managed by the U.S. Department of Energy (DOE) were tested for hydraulic conductivity. Two GCLs (CS and GS) contained conventional sodium bentonite (Na-B). The rest formed a combination of bentonite – polymer (CPL, CPH, GPL1, GPL2 and GPH) or bentonite – polymer composite (BPC). All GCLs (except GPL2 and GPH) were specifically permeated with two synthetic LLW leachates that were essentially equal, except that one had no radionuclides (non-radioactive synthetic leachate or NSL) and the other had radionuclides (radioactive synthetic leachate or RSL). The hydraulic conductivity of RSL and NSL were equivalent. In the case of CS and GS GCLs, the hydraulic conductivity steadily rose by 5–25 because the divalent cations in the leachate substituted the original sodium cations bound to bentonite. CPL, GPL1, and GPL2 GCLs with low polymer loading (1.2–3.3 per cent) had hydraulic conductivity comparable to conventional GCLs. At the other side, hydraulic conductivity of CPH, GPH and BPC GCLs with high polymer loading (≥5 per cent) to RSL or NSL was equal or lower than hydraulic conductivity to deionized water. Leachate permeation reduced the bentonite swell index in all GCLs. [19]

Bradshaw et al. assessed the usage index properties such as liquid limit, sedimentation volume and swell index of bentonite hydrated with chemical solutions as a substitute measurement to see the influence of chemical solutions on the hydraulic conductivity of two GCLs. One GCL included higher quality bentonite HQB and the other one has lower quality bentonite LQB. Calcium chloride $CaCl_2$ solutions have been used for the research system as such solutions are known to improve the hydraulic conductivity of GCLs. In general, a rise in the concentration of $CaCl_2$ resulted in a reduction in the liquid limit LL, sedimentation volume SV, or swell index SI, and a rise in the hydraulic conductivity k of the GCL. Little to no change in an index property, however, did not automatically mean there was no change in k, and major changes in an index property appeared without significant changes in k. [20]

In Xaypanya et al. study, the effect of synthetic salt solutions on the consistency and compressibility behaviours of compacted clay at various concentrations was evaluated. Two forms of inorganic salts $MnSO_4$ and $FeCl_3$ are used at various concentrations of 2 percent, 5 percent and 10 percent. The Clay used was CL-clay (kaolinite). The result indicates that the consistency limits increased while the concentration of salts increased. although the compression index (Cc) decreased by rising the concentration from 2% to 5%, after that the Cc became almost unchanged. The swelling index (Cs) continues to increase steadily as the concentration of MnSO4 rises but it tends to decrease with risen in concentration of $FeCl_3$. [22]

7. CONCLUSION

In this study, GCLs performance were evaluated as a liner in landfill in aspect of Hydraulic conductivity, strength, swell index, etc. also the influence of leachate characteristic on hydraulic conductivity of GCL were reviewed. There is often a lack of clay supply at the site and a need for improved hydraulic conductivity in some projects, and cost efficiency may be the project's goal. Depends on the type of project, using an alternative material as a substitution can be a good solution in all the cases listed. Discussion and comparison of previous studies on this topic has the following outcome:

- Most regulations require GCLs to have low permeability of less than $10^{-9}\ \frac{m}{s}$
- Although Using fly ash as an additive cause decrease in hydraulic conductivity, it contains heavy metals which can be dangerous for environment.
- Sand–bentonite mixtures and foundry sand are a good choice because of their low hydraulic conductivity as barrier material in GCL. But their hydraulic conductivity would be increased in the situation of using chemical permeant (not pure water), so it does not make sense to use it.
- Red mud addition increases GCL efficiency by reducing hydraulic conductivity. It also causes increase in strength.
- The mixture of bentonite with tire grain has low hydraulic conductivity and is a suitable substitution material in GCl.
- Hydraulic conductivity depends on content of the clay deeply. Clay including Ca has higher hydraulic conductivity than Na-type clay. Bentonite-zeolite combination also has higher hydraulic conductivity than sand bentonite combination.
- Using sepiolite and zeolite in GCL will increase its shear strength. However, the presence of these two materials, especially sepiolite, has a major effect on the reduction of hydraulic conductivity.
- Hydraulic conductivity also relies on permeant fluid pH. Increasing pH can contribute to hydraulic conductivity increase.
- hydraulic conductivity depends on solute concentration and kinematic viscosity of permeating fluids
- Hydraulic conductivity of GCL against of salt solution is more than pure water. the diverge of acid fluid permeant ($8 * 10^{-11}$) with pure water ($3.14 * 10^{-11}$) is more than alkaline fluid permeant ($2.5 * 10^{-11}$) with pure water. So, the hydraulic conductivity of salt solution is more than pure water, like as acidic one.
- The presence of radioactive content in permeated fluid does not impact hydraulic conductivity of GCL. Significant raise in polymer amount of GCLs leads to increase in hydraulic conductivity.
- Non-reinforced GCL is not suggested for high-rate slopes due to their low shear strength.

- Although reinforced GCLs' failure is possible due to theoretical science, but it has never occurred in reality up to now.
- Needle-punch in GCL play a significant role in strength of it. fracturing of the needle-punching and the removal of the needle from the geo-textile during earthquake occurred result in decrease of shear strength.
- In both low and high normal stresses, small displacement amplitudes ($\Delta a \leq 10$ mm) has a neglectable effect on shear strength. whereas, larger displacements cause more decrease in shear strength.
- A further advantage of GCL is the adsorption of heavy metals. It is noteworthy to bear in mind that the temperature produced as a result of chemical and biological landfill processes has a major influence on heavy metal adsorption. By increasing in temperature, more heavy metals will be adsorbed.
- Several parameters affect GCL efficiency that their impact are not predictable because of dissimilar influence in different condition, For example The effect of leachate characteristics on swell index of liner and also Effect of temperature on hydraulic conductivity of GCL are not predictable.

After all, Using GCL as a liner in waste disposal is one of the best ways if not the best way to prevent leachate migration into environment and also they are a wise choice to use in case that resistance of liner is required. Choosing the type of GCL and its material depends on intent of the project and its applicability but having low hydraulic conductivity should be considered anyway. using a substitute material in GCL can improve its performance, however the optimoum amount of substitute material should be taken into consideration. Using more than optimum content can cause side effect. For example, the optimum amount of kaolinite is 50% In bentonite-kaolanite mixture and using more than 70% of it, cause increase in hydraulic conductivity.

ACKNOWLEDGEMENT

The described article/presentation/ study was carried out as part of the GINOP-2.3.2-15-2016- 00031 "Innovative solutions for sustainable groundwater resource management" project implemented in the framework of the Szechenyi 2020 program. The realization of this project is supported by the European Union, co-financed by the European Social Fund and the European Structural and Investment Funds.

REFERENCES

[1] Kumar, D. and Alappat, B.J. (2005). Evaluating leachate contamination potential of landfill sites using leachate pollution index. *Clean Technologies and Envi-ronmental Policy*, 7 (3), pp. 190–197. http://doi.org/10.1007/s10098-004-0269-4

[2] Khan, F.I., Husain, T. and Hejazi, R. (2004). An overview and analysis of site remediation technologies. *Journal of environmental management*, 71 (2), pp. 95–122, https://doi.org/10.1016/j.jenvman.2004.02.003.

[3] Allesch, A. and Brunner, P.H. (2014). Assessment methods for solid waste management: A literature review. *Waste Management & Research*, 32 (6), pp. 461–473, https://doi.org/10.1177%2F0734242X14535653.

[4] Guney, Y., Cetin, B., Aydilek, A. H., Tanyu, B. F. and Koparal, S. (2014). Utilization of sepiolite materials as a bottom liner material in solid waste landfills. *Waste management*, 34 (1), pp. 112–124. https://doi.org/10.1016/j.wasman.2013.10.008

[5] Wagner, J. F. (2013). Clay liners and waste disposal. In *Developments in Clay Science*, Vol. 5, Elsevier, pp. 663–676. https://doi.org/10.1016/B978-0-08-098259-5.00023-8

[6] Bouazza, A. (2002). Geosynthetic clay liners. *Geotextiles and Geomembranes*, 20 (1), pp. 3–17, https://doi.org/10.1016/S0266-1144(01)00025-5.

[7] Shigemoto, R., Sawada, Y., Maki, R. and Kawabata, T. (2018). Shear Strength Characteristics of Internal Bentonite Layer of Needle-Punched GCL Used in Small Earth Dams under Cyclic Loading. In *Geotechnical Earthquake Engineering and Soil Dynamics V: Slope Stability and Landslides, Laboratory Testing, and In Situ Testing*, pp. 365–372. VA: American Society of Civil Engineers, Reston, https://doi.org/10.1061/9780784481486.038.

[8] Ishimori, H. and Katsumi, T. (2012). Temperature effects on the swelling capacity and barrier performance of geosynthetic clay liners permeated with sodium chloride solutions. *Geotextiles and Geomembranes*, 33, pp. 25–33. https://doi.org/10.1016/j.geotexmem.2012.02.005

[9] Petrov, R. J. and Rowe, R. K. (1997). Geosynthetic clay liner (GCL)-chemical compatibility by hydraulic conductivity testing and factors impacting its performance. *Canadian Geotechnical Journal*, 34 (6), pp. 863–885. https://doi.org/10.1139/t97-055

[10] Rowe, R. K. (2005). Long-term performance of contaminant barrier systems. *Geotechnique*, 55 (9), pp. 631–678, https://doi.org/10.1680/geot.2005.55.9.631.

[11] Daniel, D. E. and Koerner, R. M. (1993). Quality assurance and quality control for waste containment facilities. Risk Reduction Engineering Laboratory, Office of Research and Development, US Environmental Protection Agency. https://nepis.epa.gov/

[12] Sawada, Y., Nakazawa, H., Take, W. A. and Kawabata, T. (2019). Full scale investigation of GCL damage mechanisms in small earth dam retrofit applications under earthquake loading. Geotextiles and Geomembranes, 47 (4), pp. 502–513, https://doi.org/10.1016/j.geotexmem.2019.03.001.

[13] Ross, J. D., Fox, P. J. and Olsta, J. T. (2011). Dynamic shear response of a geomembrane/geosynthetic clay liner interface. In *Geo-Frontiers 2011: Advances in Geotechnical Engineering*, pp. 2010–2020. https://doi.org/10.1061/41165(397)205

[14] Phanikumar, B. R. and Shankar, M. U. (2016). Studies on hydraulic conductivity of fly ash-stabilised expansive clay liners. *Geotechnical and Geological Engineering*, 34 (2), pp. 449–462, https://doi.org/10.1007/s10706-015-9956-7.

[15] Viana, P. M. F., Palmeira, E. M. and Viana, H. N. L. Evaluation on the Use of Alternative Materials in Geosynthetic Clay Liners. https://www.researchgate.net/publication/274080243_Evaluation_on_the_Use_of_Alternative_Materials_in_Geosynthetic_Clay_Liners.

[16] Karunaratne, G. P., Chew, S. H., Lee, S. L. and Sinha, A. N. (2001). Bentonite: kaolinite clay liner. *Geosynthetics International*, 8 (2), pp. 113–133. https://doi.org/10.1680/gein.8.0189

[17] Kalkan, E. (2006). Utilization of red mud as a stabilization material for the preparation of clay liners. Engineering geology, 87 (3–4), pp. 220–229. https://doi.org/10.1016/j.enggeo.2006.07.002

[18] Tian, K., Benson, C. H. and Likos, W. J. (2016). Hydraulic conductivity of geosynthetic clay liners to low-level radioactive waste leachate. *Journal of Geotechnical and Geoenvironmental Engineering*, 142 (8), p. 04016037. https://doi.org/10.1061/(ASCE)GT.1943-5606.0001495

[19] Lee, J. M., Shackelford, C. D., Benson, C. H., Jo, H. Y. and Edil, T. B. (2005). Correlating index properties and hydraulic conductivity of geosynthetic clay liners. *Journal of Geotechnical and Geoenvironmental Engineering*, 131 (11), pp. 1319–1329, https://doi.org/10.1061/(ASCE)1090-0241(2005)131:11(1319).

[20] Bradshaw, S. L. and Benson, C. H. (2014). Effect of municipal solid waste leachate on hydraulic conductivity and exchange complex of geosynthetic clay liners. Journal of Geotechnical and Geoenvironmental Engineering, 140 (4), p. 04013038, https://doi.org/10.1061/(ASCE)GT.1943-5606.0001050.

[21] Stern, A. N. (2009) 'Dynamic Shear Behavior of a Needle-Punched Geosynthetic Clay Liner/Geomembrane Interface at a High Normal Stress', p. 62. http://hdl.handle.net/1811/36959

[22] Xaypanya, P., Takemura, J., Chiemchaisri, C., Seingheng, H. and Tanchuling, M. A. N. (2018). Characterization of landfill leachates and sediments in major cities of Indochina Peninsular countries—Heavy metal partitioning in municipal solid waste leachate. Environments, 5 (6), p. 65. https://doi.org/10.3390/environments5060065

[23] Owusu-Nimo, F., Oduro-Kwarteng, S., Essandoh, H., Wayo, F. and Shamudeen, M. (2019). Characteristics and management of landfill solid waste in Kumasi, Ghana. Scientific African, p. e00052. https://doi.org/10.1016/j.sciaf.2019.e00052

[24] Pariatamby, A. and Tanaka, M. (2014). MSW Management in Asia and the Pacific Islands-Challenge and Strategic Solution. Environmental Science and Engineering, Springer: Singapore, https://doi.org/10.1007/978-981-4451-73-4.

[25] Ziadat, A. H. and Mott, H. (2005). Assessing solid waste recycling opportunities for closed campuses. *Management of Environmental Quality: An International Journal*, Vol. 16 No. 3, pp. 250–256. https://doi.org/10.1108/14777830510591679

[26] El-Fadel, M., Findikakis, A. N. and Leckie, J. O. (1997). Environmental impacts of solid waste landfilling. *Journal of environmental management*, 50 (1), pp. 1–25, https://doi.org/10.1006/jema.1995.0131.

[27] Kjeldsen, P., Barlaz, M. A., Rooker, A. P., Baun, A., Ledin, A. and Christensen, T. H. (2002). Present and long-term composition of MSW landfill leachate: a review. Critical reviews in environmental science and technology, 32 (4), pp. 297–336, https://doi.org/10.1080/10643380290813462.

[28] Ole, H., Lizzi, A. and Jette, B. H. (2000). *Leachate emission from landfill*. Final Report Swedish Environmental Protection Agency; Naturvårdsverket: Stockholm, Sweden. ISSN 1102-6944; TRN: SE0007199

[29] Kanmani, S. and Gandhimathi, R. (2013). Assessment of heavy metal contamination in soil due to leachate migration from an open dumping site. Applied Water Science, 3 (1), pp. 193–205, https://doi.org/10.1007/s13201-012-0072-z.

[30] Slack, R. J., Gronow, J. R. and Voulvoulis, N. (2005). Household hazardous waste in municipal landfills: contaminants in leachate. Science of the total environment, 337 (1–3), pp. 119–137. https://doi.org/10.1016/j.scitotenv.2004.07.002

[31] Umar, M., Aziz, H. A. and Yusoff, M. S. (2010). Variability of parameters involved in leachate pollution index and determination of LPI from four landfills in Malaysia. International Journal of Chemical Engineering, 2010. https://doi.org/10.1155/2010/747953

Geosciences and Engineering, Vol. 10, No. 15 (2022), pp. 96–109.
https://doi.org/10.33030/geosciences.2022.15.096

IMPROVEMENT OF SEISMIC SECTIONS AND WELL LOGS FOR JOINT GEOPHYSICAL INTERPRETATION

VIKTÓRIA KISS[1 *], NORBERT PÉTER SZABÓ[1], ERNŐ TAKÁCS[2]

[1]*Department of Geophysics, Faculty of Earth Science and Engineering, University of Miskolc*
[2]*Mining and Geological Survey of Hungary*
[*]*E-mail: kviktoria246@gmail.com*

Abstract: Seismic and well-logging data are useful for comparison and then integratation for a comprehensive geophysical interpretation. In the course of this work, seismic results were compared with well-logging geophysical data and profiles for more reliable evaluation of groundwater formations in the Tokaj region, north-east Hungary. The seismic results and profiles were obtained by the Common Reflection Surface (CRS) stacking technique. This is an advantageous stacking technique that is expected to greatly improve seismic profiles. In connection with this, we also examined some well-logging geophysical profiles so that we can improve later results. By comparing and examining the two types of sections together, we provide a basis for various method developments that improve the sections. Thus, the aim is to fill in the missing data, so that the well-logging and seismic sections can be examined together as accurately as possible in order to gain a more accurate picture of the subsurface formations. It is important to determine the lithology and petrophysical characteristics using well logs. The section replacement – the improvement of the units – is done using machine learning-based and inversion methods such as factor analysis or cluster analysis. An important outcome in the application of geophysical inversion methods is that the results of different methods can be jointly interpreted and this can significantly increase the reliability of the results. The application of these methods and their development is expected to reduce uncertainty and ambiguity and to increase the accuracy of the sections.

Keywords: *seismic, well-logging, hydrocarbon, inversion, factor analysis*

1. INTRODUCTION

In order to gain knowledge of the information obtained during seismic and well-logging geophysical measurements, data processing must be carried out, and thus sections must be created that are suitable for identifying the underground formations. In general, both seismic and well-logging geophysical sections are very rich in information but there is currently no machine learning-based or inversion procedure to improve the data obtained from the sections. This study aims to give an overview about some modern procedures to enhance the seismic and well-logging data before joint interpretation like machine learning and inversion methods. We focus on examples from the literature; however, we intend to implement the demonstrated procedures on real datasets in the very near future. Although seismic results have

been compared with well-logging geophysical data and profiles in terms of more reliable assessment of groundwater formations in North-Eastern Hungary, this paper shows that the common geophysical interpretation is very effective for hydrocarbon reservoirs and we want to highlight that fact.

Methods based on inversion and machine learning can improve sections obtained from structurally ambiguous formations such as complex hydrocarbon storage formations. In the case of these methods, in oilfield applications, it is important to properly interpret the in situ well-logging data, as they provide the basis for the hydrocarbon reserve calculations. In the case of hydrocarbon reservoirs, we usually speak of a complex geological environment [1]. We talk about complex hydrocarbon reservoirs when they consist of several minerals and multiple problems may occur during their exploration. One such problem is that in the case of such reservoirs, the measurements are usually noisier and the noise greatly degrades the quality of the sections. The petrological and petrophysical properties of the formations, such as porosity, may be more complex due to their mineral content, so there are different types of porosity and permeability [2].

There are several phases of research in hydrocarbon basins with diverse structural styles. The final phase is usually the investigation of hydrocarbon deposits accumulated in layer traps independent of structural elements. These are also called hidden traps. In industrial practice, the breakthrough was introduction of the AVO-based (Amplitude Versus Offset) Direct Hydrocarbon Indicators (DHI) and attribute tests for evaluating seismic data. A complex tectonic and hydrocarbon geological situation threatens these traps during re-investigation. The mapping of traps is also a problem in complex geological environments, as detecting them faces significant complications even with the now advanced seismic methods [3].

In hydrocarbon exploration, relatively expensive measurements are made to increase the likelihood of finding an economically valuable oil or gas field [4], so it is advisable to improve the seismic and well-logging sections in such a way that the layer traps or storage can be detected with the greatest possible efficiency and with the least possible risk.

Due to the constant demand for hydrocarbons that still exists today, many technologies and studies are being prepared for the distribution, accumulation, assessment and exploitation of resources. That is why nowadays the petroleum industry is not only trying to research conventional reservoirs. Non-conventional reservoirs are reservoirs that are generally provided by methods that go beyond the known conventional extraction of hydrocarbons; thus, their exploitation is a very difficult task. These non-average formations belong to oil and gas sources where industrial productivity is only possible by changing the permeability or fluidity of the rock [5].

2. SEISMIC SECTIONS AND WELL LOGS

The primary objective of this study is to improve the subsurface image of the layer of geophysical sections using combined seismic and well log data. These stratigraphic parameters are the correlated multi-well datasets, tied well-logging data for seismic

data, detailed seismic and well log facies interpretation, sediment identification delimitation of formations, their thickness and lateral changes, derivation of the deposition environments of the formations, and seismic characterization of the subsurface identification of lineaments between different combined applications data types. The main advantage of integrated data analysis is that it provides a more detailed subsurface analysis that intended to increases the reliability of geological inter-pretations [6].

There are several data processing methods available today, but not all of them give a sufficiently accurate picture of subsurface formations and strata boundaries. However, there is a relatively new method that improves profile images with great efficiency. This method is the common reflection surface (CRS) stacking procedure. Seismic sections obtained by CRS processing result in more coherent reflection signals due to increased coherence values. Since the method does not process a single point but an elementary, stacking surface, we can calculate all the reflection points on a given surface, even on curved surfaces. Lateral displacements occur during any processing, but this procedure works without losing lateral resolution [7]. Velocity analysis is very important in all seismic data processing methods, including the CRS method. It affects the quality of the accumulated data and can lead to an unacceptable image that is not very suitable for geological interpretation, so the method requires a more reliable velocity field that can be generated using the CRS method [8]. In contrast with the conventional seismic data processing method [Common Depth Point (CDP) method; *Figure 1*], in the case of the CRS method, the individual sections are very rich in information, so many conclusions can be drawn from them. With the CRS method, the sections and images have been improved in several aspects [8]. Higher signal-to-noise ratio is available, which is based on reflector continuity and noise reduction [9]. The images are clearer because of the better reflection events. This means the reflections are smooth and even, not confusing and fluctuating, the layers are easier to detect and separate. Thus, the seismic sections measured on the surface, the boundaries of the different types of rock bodies, and the traces of the faults and fractures are outlined [8]. The faults play a key role in trapping of hydrocarbons [10]. The CRS seismic method can produce a reliable image of a complex geological structure like complex hydrocarbon reservoirs or marine environments [7, 9]. The aim of hydrocarbon exploration is to identifyand delimit economically exploitable, accumulative structural and stratified traps. These traps can be very fine, complex, and therefore difficult to map accurately [11]. As shown in *Figure 2*, in the case of Miocene or substrate reservoir exploration, seismic mapping of complex structures can be refined by the CRS stacking technique, which facilitates the comparison of logs and seismic data.

Well log and seismic data are widely used in the petroleum industry and exploration to map the subsurface so it is important to improve the quality of these sections [11]. Because the multifocusing method is also suitable for mapping complex structures, it is also used with great efficiency in complex hydrocarbon research. The effectiveness of this method has been proven by Kiss and Takács [12], near to the town of Tokaj, among others.

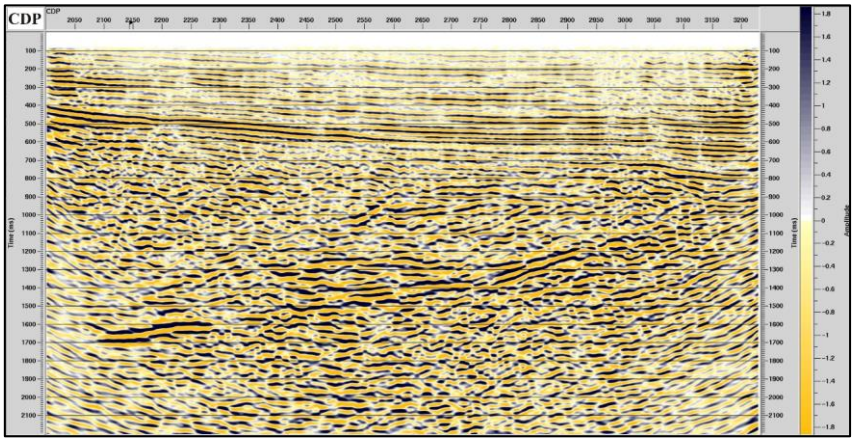

Figure 1

A migrated Common Depth Point stack in the Tokaj area: the x-axis shows the shot points in 50-meter increments, the y-axis shows the time in ms [12]

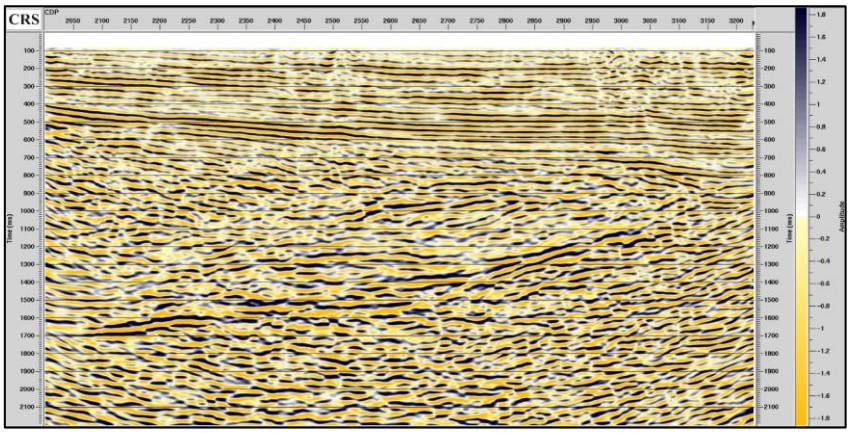

Figure 2

A migrated Common Reflection Surface stack in the Tokaj area: the x-axis shows the shot points in 50-meter increments, the y-axis shows the time in ms [12].

Seismic and well log data sources complemented each other [11]. The combined analysis of seismic and well-logging geophysical data also aids in geological-structural and petrophysical interpretation. To do this, the logs must be inserted into nearby seismic profiles [13]. Seismic profiles provide an almost continuous side view (lateral resolution) below the surface, while the well logs, which are measured with depth, provide a detailed vertical resolution of the geology of the surrounding formations in the vicinity of boreholes [11, 10, 14]. The resolution of well-logging geophysical sections *(Figure 3)* is usually 10-20 cm, much finer than that of seismic data, which is approximately 10-20 m [13].

Seismic profiles are surface seismic data measured in units of time, and can resolve structural and stratigraphic changes that vary beyond the locations of the wells from the arrival time and amplitudes of reflection events with high accuracy [11, 14]. The bandwidth of the seismic data limits the subsurface vertical resolution. High-frequency data are essential to delineate fine hydrocarbon traps. Well logs can be useful in both respects in interpreting seismic profiles. In contrast to seismic sections, they can clearly provide a high-resolution estimate of a number of relevant geological variables during drilling [11]. The number of applicable methods and rock physics parameters is much larger, consequently the mapping of rock layer properties is much more detailed, but well-logging geophysical measurements provide only local information about the studied rocks and raw material reserves, while seismic sections allow lateral extension [13]. The well-to-seismic tie may indicates that the hydrocarbon bearing reservoir is associated with direct hydrocarbon indicators on the seismic sections [11].

The interpretation procedure encompasses the integration of well logs with seismic data, seismic structural analysis, petrophysical analysis, and seismic attributes analysis [10]. For all these reasons, the integration of well logs and seismic data would provide a higher degree of reliability in the mapping of subsurface structural and stratigraphic objects, thus making subsurface understanding much clearer, and these play an important role in the modeling and development of an underground (hydrocarbon) reservoir [11, 14]. Thus, the integration process can also provide insight into the reservoir's hydrocarbon volume, which can be used in exploratory assessments and well planning [11].

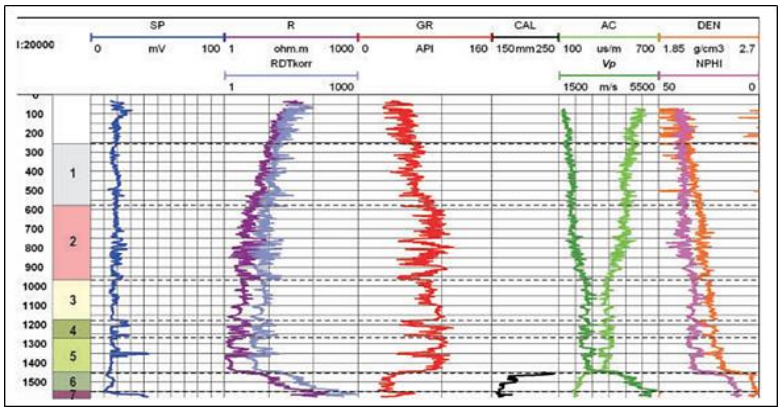

Figure 3

Geophysical well logs of the Magyardombegyház Domb. SW–6 well [15]
Legend: SP: spontaneous potential, R, RDT: electrical resistivity; GR: natural gamma-ray; CAL: caliper log; AC: acoustic profile; Vp: acoustic velocity; DEN: density; NPHI: neutronporosity log. Geological column: 1. Nagyalföld Fm (Upper Pannonian), 2. Zagyva and Újfalu Fm (Upper Pannonian), 3. Algyő Fm (Lower Pannonian), 4. Szolnok Fm (Lower Pannonian), 5. Endrőd Fm (LowerPannonian), 6. Endrőd Fm Tótkomlós Calcareous Marl Member (Lower Pannonian), 7. Variscan basement

3. THE INVERSION PROCEDURE

We need to apply method development to improve geophysical sections. It is generally accepted that the geophysical sections of the well log can be improved by inversion methods. Local inversion is one of the most commonly used techniques for the evaluation of borehole geophysical data [16]. The inverse problem, as its name suggests, is actually the inverse of the direct problem. The flow chart of the inversion procedure is described in *Figure 4*. We have some measured data and *a priori* knowledge and the first step is to define the parameters of the models – this is the direct task. We create the model and we predict the theoretical data from it. Then we compare the measured and calculated data; if the agreement is acceptable we accept the model parameters. If it is not, we have to refine the model until it is acceptable. Inversion methods rely on solving direct problems, so this gives the relationship between the calculated data and the model. It follows that the inverse problem is based on the assumption that there is a correlation between the calculated data and the parameters of the model, so that the model can be created based on this. During the inversion, it can be generally said that the number of measured data points and the number of model parameters do not match, and some norm of the differences between measured and calculated data is minimized [17].

There are both linear and nonlinear inverse problems. If an inverse problem is initially nonlinear, then the result is created by solving linear problems. Errors can be encountered in most geophysical interpretations. These can be either natural or artificial defects. Inversion procedures can be loaded with errors that are either data errors or model errors. Data errors result from measurement conditions, are proportional to the estimated model parameters, and are also errors. Modeling errors can also be encountered. For all these reasons, the precise development of inversion procedures is very important [17]. However, this method has some drawbacks. Measurement data can be noisy and in addition to this noise, the approximate choice of zone parameters also provides additional uncertainty in the result of inversion evaluation. It can also be said that the method is limited by the inversion evaluation per depth point, thus the number of identifiable unknowns is also limited [18]. Layer boundary or thin layer effects can skew the inversion results. At the same time, we can get a finer picture of the changes within the layer [13].

In addition to a number of disadvantages of the method, such as limiting the accuracy and reliability of the estimate, the method also has advantages such as high speed and good vertical resolution. Another disadvantage is that the local inversion method does not support the determination of formation thicknesses. For evaluation, it is advantageous to collect a complete dataset over a longer depth interval. A dataset also contains information on the boundaries of the formation that can be extracted by a particular inversion method, which is the so-called interval inversion method. This method allows the determination of layer boundary coordinates (or layer thicknesses) within the inversion procedure [16].

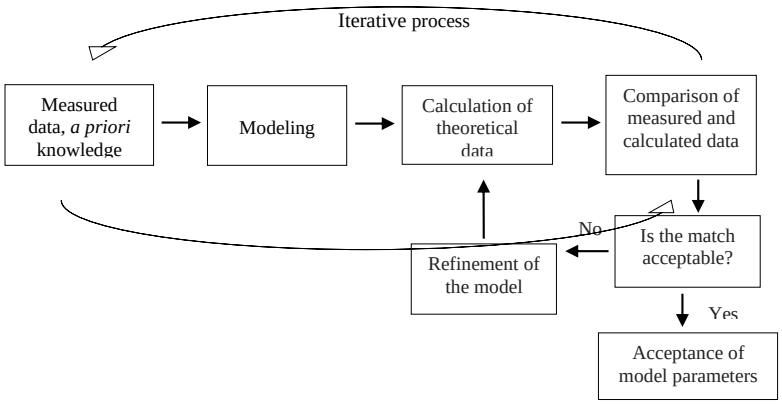

Figure 4
Simple flowchart of the inversion procedure

In well-logging geophysical exploration, we often encounter the problem of inversion. The quantities in the response functions of the probe can be divided into two groups. The first group includes the so-called zone parameters, which are either constant or change slowly over a longer depth. The second group consists of the layer parameters, which are almost constant in each layer. One of the positive features of the inversion technique is that it is also capable of joint inversion. In geophysical inversion, joint inversion means data measured by two or more different geophysical methods or by the same method, but in a substantially different measurement arrangement, by the same inversion method. The more frequently the parameters of the geological structure appear in the definition of the different datasets, the more successful the solution to the inverse problem can be [1].

As a next step, we would like to present a meta-algorithm-based inversion procedure that can simultaneously determine volume-specific petrophysical quantities and zonal parameters [18]. There may be local problems during the procedure. To avoid these, we can use a global optimization method, such as the Genetic Algorithm (GA), which looks for the absolute extreme point of the objective function and whose flowchart is shown in *Figure 5*. GA belongs to the class of evolutionary algorithms that solve optimization problems. Today, the most popular version is Float-Encoded GA, which improves the model population described by the model parameters in an iteration process [4]. In the first step of the method, an initial model is created and then the values of the zone parameters are determined by random search based on a real coded genetic algorithm (FGA). Then, with the fixed values of the newly obtained zone parameters, a series of depth-by-point inversion procedures is performed to calculate the volume-characteristic quantities [18].

The inversion strategy described above has a positive effect on solving the inverse problem. The method can be effectively used to determine the petrophysical proper-

ties of near-surface loose sediments. The application of the method ensures the best fit of the measured and calculated profile data [18]. An important indicator of the method is that each individual in the population has a fitness value that indicates its ability to survive. Those with a high fitness value will be the most suitable individuals in the genetic process and will reproduce more successfully in future generations than those who have low fitness values. To achieve the best solution, fitness function is maximized using genetic operations in a random optimum search procedure. For a well-logging inverse problem, a petrophysical model has a large misfit if there is little fit between the observed and calculated data. An appropriate combination of genetic operators, such as selection, crossing, mutation, and reproduction, is used to achieve the absolute maximum of fitness function [4].

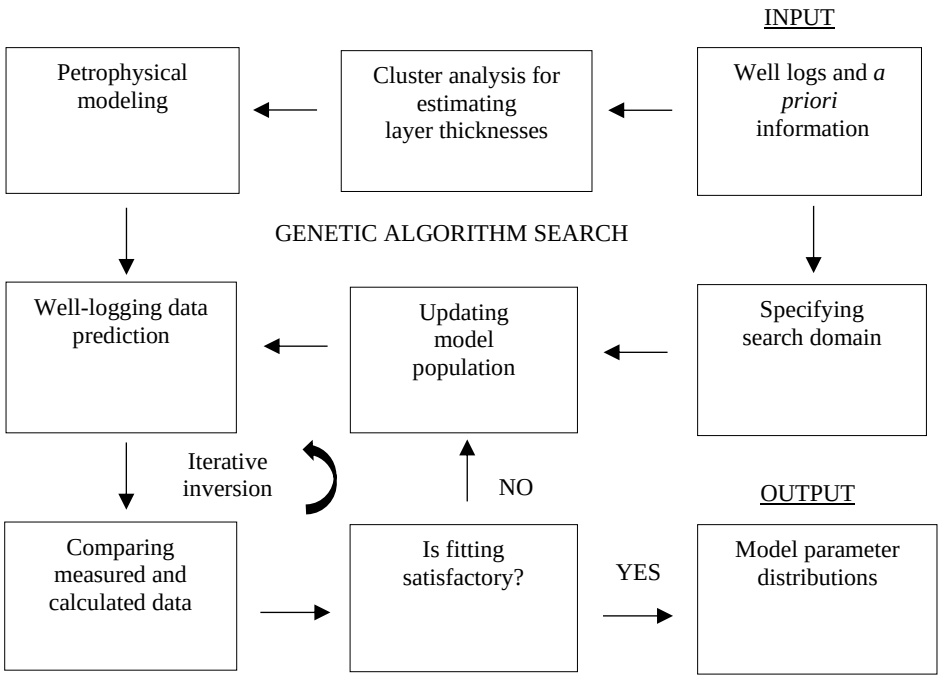

Figure 5
Workflow of the GA-based inversion procedure

As a next step, we present some artificial intelligence-based methods for improving geophysical profiles. The essence of machine learning is to create algorithms that can improve their own efficiency by utilizing the experience that they have gained during the process (for example in artificial intelligence networks). We can divide machine learning methods into three main groups. Without wishing to be exhaustive, the very first group, which is also the most commonly used, is based on supervised learning, including regression analysis and classifications. The second group is non-supervised learning, such as factor analysis and principal component analysis. The

last category of machine learning methods is the semi-supervised approach, a combination of the first two groups [19].

In this study, we found the method of factor analysis to be the most expedient to develop. Factor analysis is a multivariate statistical method that involves reducing a large dataset to a relatively smaller number of factors by finding a correlation between the observed variables. By reducing the dimension of variability, we are also able to explore the unobserved properties of the rock that are responsible for the log responses of the observed well [5]. One of the advantages of this method is that it processes all the data in the segmentation interval together and can be used in several dimensions. Petrophysical information from an independent source increases the overdetermination of the inverse problem, which means that it reduces the degree of estimation error and the possible ambiguity of the petrophysical parameters involved in the problem [20].

Factor analysis is also aided by methods of artificial intelligence, such as the differential genetics algorithm-based approach or iteratively re-weighted factor analysis for a more robust estimation of factors and related petrophysical parameters. The well logs extracted by this procedure correlate with the dataset variables. In this case, the extracted factors help to derive the shale volume of the formations [5]. Estimated shale volume values made by the above factor analysis closely fit the values calculated from the commonly used Larionov formula, which confirms the validity of the nonlinear approximation [21], as we seen in *Figure 6*.

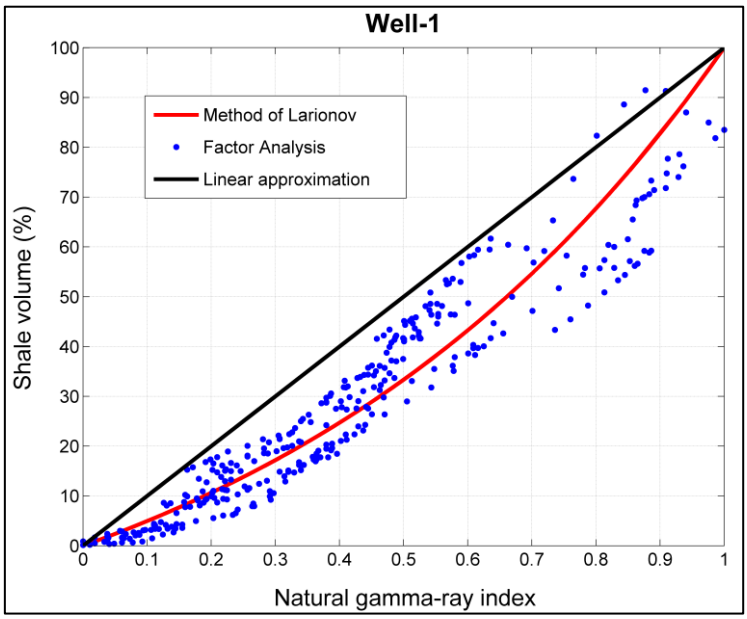

Figure 6

Representation of shale volume as a function of natural gamma-ray index in the Tokaj region [23]

The first factor profile formed from well-logging geophysical sections correlates strongly with the clay content of the reservoirs, so the first factor empirical relationship was established for the estimation of shale volume; from this, lithological units can be well distinguished [5, 20]. The first factor is a good shale indicator. Interpreting these together helps to quantify well logs [5]. The close relationship between the first factor and the clay content can also be well demonstrated in the water storage sections of hydrocarbon exploration wells [18]. Shale volume information given by factor analysis can also be used to reduce the number of unknowns of the well-logging inverse problem. Moreover, it can also be applied to resolve the ambiguity existing between parameters of the geophysical model [22].

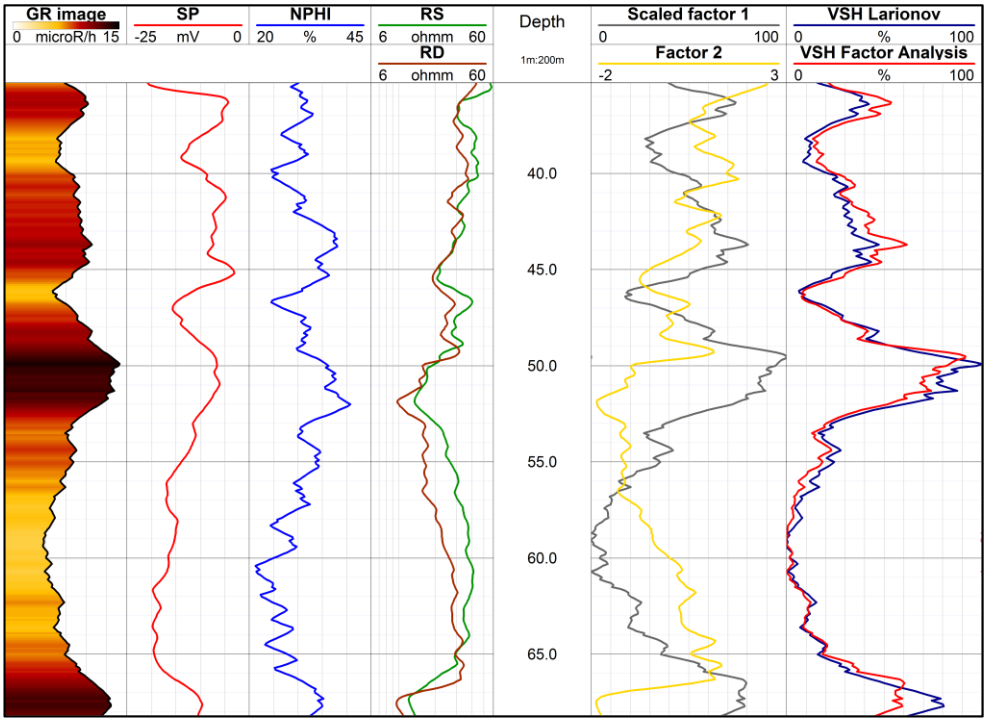

Figure 7

Results of factor analysis plotted on a well-logging section in the Tokaj region: GR – gamma ray, SP – spontaneous potential, NPHI – neutron porosity, RS – shallow resistivity, RD – deep resistivity

Not only seismic but also logging profiles were made in the Tokaj area from the data using factor analysis. An example of factor analysis of well logs can be seen in *Figure 7*. Thus, based on the two seismic sections, it can be said in general that the Tokaj region is a sediment collector. Several sedimentation cycles can be discovered

on the sections made in this area. Geologically, the area is 70–80% sand, which is interrupted by intermediate clays. The settlement of mud and silt can be observed in several layers. It can also be said in general that granular layers of quartz material are located below the cover layer. Rhyolite tuff can also be observed in the area, such as signs of andesite volcanism. Over time, a system of fractures has developed here, which has divided the mountain into blocks, thus creating a stepped structure of the bedrock. There was once a subsidence along these fractures. Then the wind-blowing of the sediments accumulated here, creating the loess cover typical of the area. Typically, a higher-resistance granular layer of quartz material is placed under the clay, with a low geoelectric resistance, followed again by a low-resistance bed or intermediate layer. The decrease in resistance in some places on the log sections corresponds to the clay layer that appears [23].

Fragmentation led to the formation of faults, which the seismic profiles (*Figure 1* and *2*) illustrate nicely. The seismic profile also indicates the pre-Cenozoic basement. The layers in the deepest position have a small amplitude, so sandy layers are unlikely to appear there. Both seismic and well-logging geophysical research has shown that the geological structure of the area begins with the Miocene and that the onset of volcanism can be traced back to this period. According to the interpretation of the seismic profile, the volcanism in the area was cyclical, just like in the case of sediment formation. Based on the two seismic profiles, the Upper Pannonian sedimentary assemblage settles on the Miocene sequence. Layer thicknesses can be determined on well-logging geophysical sections, and layer boundaries can be specified in combination with seismic sections. In well-log sections, the layer content can be determined with the help of core data, such as a clayey or sand layer, and in seismic sections, not only the vertical but also the lateral extent can be defined.

In the case of seismic exploration, the seismic waves return from different media at different times, so if we know the different layer contents from the well-logging data, it is easier to interpret them. Thus, from the point of view of geophysical models, it is very advantageous to investigate them together.

4. CONCLUSIONS

The aim of the study is to summarize the interpretation of seismic and well-logging geophysical sections. This can be achieved by developing different geophysical methods. The combined interpretation of well-logging data and seismic measurement results can effectively reduce the (short-term) geological risk of the exploration phase, so the geological model developed with their help can significantly contribute to the success of raw material production. The greatest uncertainty is the delimitation of the individual geological formations and the determination of their petrophysical state. Seismic measurements have a positive effect on reducing geological uncertainty [24]. Methods based on machine learning and inversion methods greatly improve the accuracy of the sum profiles and the combined interpretation of well-logged and seismic profiles. The growing demand of the oil industry for highly reliable petrophysical information requires advanced data processing techniques [4].

To achieve a good and unique solution, prior geological and geophysical information must be built-in by the user properly. Moreover, in case of the global optimization phase (GA), some experience is needed to set the combination and control parameters of genetic operators and to decide when it is possible to switch over to linear optimization. The optimal set of basis functions depends on the variation of lithology and pore fluids along a borehole. To increase the overdetermination of the inverse problem, it is important to search for parameters that can be fixed during the inversion procedure. This can reduce the uncertainty and ambiguity of inversion estimates [4]. With these procedures, seismic and well-logging sections can be improved in a number of ways.

Because of the joint interpretation of the seismic and well-logging profiles, geological formations can be better interpreted. In the examples shown, the coherency of the Pannonian sediments made possible a more precise mapping between the Mesozoic sedimentary and volcanic formations. The possible boundary and internal structure of the volcano can also be observed. The top of the pre-Cenozoic basement became more coherent due to the joint interpretation.

FURTHER OBJECTIVES

In addition to the development of machine learning methods on well logs, later plans include jointly interpreting borehole geophysical and seismic data using AVO analysis, which will allow for the spatial extension of information on possible strata content along the seismic profile.

ACKNOWLEDGMENTS

We would like to thank the Department of Geophysics of the University of Miskolc for the creation of the infrastructural background, the Mining and Geological Survey of Hungary for its support, and Háromkő Geological and Geophysical Research Bt. for the data.

REFERENCES

[1] Dobróka, M., Szabó, N. P. (2015). Well Log Analysis by Global Optimization-based Interval Inversion Method – In: C. Cranganu et al. (eds.). *Artificial Intelligent Approaches in Petroleum Geosciences*, Springer International Publishing Switzerland, pp. 245–268. https://doi.org/10.1007/978-3-319-16531-8_9

[2] Dobróka, M., Szabó, N. P., Turai, E. (2012). Interval inversion of borehole data for petrophysical characterization of complex reservoirs. *Acta Geodaetica et Geophysica Hungarica*, Vol. 47 (2), pp. 172–184. https://doi.org/10.1556/ageod.47.2012.2.6

[3] Lemberkovics, V., Kiss, K., Váry, M., Kiss, B., Kovács, G. (2020). A jó, a rossz és a csúf? – avagy a szénhidrogén-kutatás dicső múltja, (még) létező jelene és bizonytalan jövője a Pannon-medencében – Szemle. *Földtani Közlöny*, 150/4, pp. 571–610. https://doi.org/10.23928/foldt.kozl.2020.150.4.571

[4] Szabó, N. P., Dobróka, M., Kavanda, R. (2013). Cluster Analysis Assisted Float-Encoded Genetic Algorithm for a More Automated Characterization of Hydrocarbon Reservoirs. *Intelligent Control and Automation*, 4, pp. 362–370. http://dx.doi.org/10.4236/ica.2013.44043

[5] Szabó, N. P., Valadez-Vergara, R., Tapdigli, S., Ugochukwu, A., Szabó, I., Dobróka, M. (2021). Factor analysis of well logs for total organic carbon estimation in unconventional reservoirs. *Energies*, 14, art. no. 5978, p. 17. https://doi.org/10.3390/en14185978

[6] Isyaku, A. A., Rust, D., Teeuw, R., Whitworth, M. (2016). Integrated well log and 2-D seismic data interpretation to image the subsurface, stratigraphy and structure in north-eastern Bornu (Chad) Basin. *Journal of African Earth Sciences,* 121, pp. 1–15, https://doi.org/10.1016/j.jafrearsci.2016.05.018.

[7] Mann, J., Jäger, R., Müller, T., Höcht, G., Hubral, P. (1999). Common-reflection-surface stack — a real data example. *Journal of Applied Geophysics*, 42, pp. 301–318, https://doi.org/10.1016/S0926-9851(99)00042-7.

[8] Ahmed, K. A., Schwarz, B., Gajewski, D. (2015): Application of the 3D common-reflection-surface stack workflow in a crystalline rock environment. *Geophysical Prospecting*, 63 (4), pp. 990–998. https://doi.org/10.1111/1365-2478.12282

[9] Safitri, D., Nainggolan, T. B., Manik, H. M. (2020). Common reflection surface methods in low fold coverage seismic data of complex marine geological structures. *IOP Conf. Series: Earth and Environmental Science* 429 (2020) Art. no. 012032, 10 p., https://doi.org/10.1088/1755-1315/429/1/012032.

[10] Ologe, O., Bankole, A. S., Oke, A. S. (2014). Hydrocarbon prospecting over 'OK' field, Niger Delta using petrophysical and seismic attributes analysis. *Nigerian Journal of Technology* (NIJOTECH), 33(3), pp. 401 – 408. http://dx.doi.org/10.4314/njt.v33i3.19

[11] Emujakporue, G., Nwankwo, C., Nwosu, L. (2012). Integration of well logs and seismic data for prospects evaluation of an X field, onshore Niger Delta, Nigeria. *International Journal of Geosciences*, 3, pp. 872–877. http://dx.doi.org/10.4236/ijg.2012.324088

[12] Kiss, V., Takács, E. (2021). Vulkáni formáció szeizmikus leképezése egy Tokaj környéki kutatási területen CRS-összegzési eljárás alkalmazásával. *Magyar Geofizika*, 62 (1), pp. 61–72.

[13] Balázs, L. (2013). *Mélyfúrási Geofizika*. Budapest, Eötvös Loránd Tudományegyetem.

[14] Shelander, D., Smith, V., Leetaru, H., Will, R., Couëslan, M. (2014). The evolution and effect of the velocity model on various aspects of surface seismic data analysis. *Energy Procedia*, 63, pp. 4374–4384. https://doi.org/10.1016/j.egypro.2014.11.472

[15] Kovács, Zs. et al. (eds.) (2018). *Hydrocarbons in Hungary – Results and opportunities.* Budapest, Hungarian Energy and Public Utility Regulatory Authority, 332 p.

[16] Dobróka, M., Szabó, N. P. (2012). Interval inversion of well-logging data for automatic determination of formation boundaries by using a float-encoded genetic algorithm. *Journal of Petroleum Science and Engineering*, 86–87, pp. 144–152, https://doi.org/10.1016/j.petrol.2012.03.028.

[17] Kavanda, R. (2015). *Módszerfejlesztés a sorfejtéses inverzió területén lokálisan 1D előremodellezéssel*. Ph.D. dissertation, Univerity of Miskolc. https://doi.org/10.14750/ME.2016.031

[18] Szabó, N. P. (2018). *Fúrólyuk-geofizikai adatok értelmezése faktoranalí-zissel és inverziós eljárásokkal.* Thesis, Doctor of the Hungarian Academy of Sciences.

[19] Abordán, A., Szabó, N.P. (2021). Machine learning based approach for the interpretation of engineering geophysical sounding logs. *Acta Geodaetica et Geophysica*, 56, pp. 681–696, https://doi.org/10.1007/s40328-021-00354-4.

[20] Szabó, N. P., Kormos, K. (2012): Édesvíztároló Rétegek Agyagtartalmának Meghatározása Fúrólyukszelvények Faktoranalízise Alapján. *Magyar Geofizika*, 53 (2), pp. 80–90.

[21] Larionov, V. V. (1969) *Radiometry of Boreholes* (in Russian). Nedra, Moscow.

[22] Szabó, N. P., Dobróka, M., Turai, E., Szűcs, P. (2014): Factor analysis of borehole logs for evaluating formation shaliness: A hydrogeophysical application for groundwater studies. *Hydrogeology Journal*, 22 (3), pp. 511–526. https://doi.org/10.1007/s10040-013-1067-z

[23] Háromkő Geological and Geophysical Prospecting Company: *TOKAJ VÍZMŰ veszélyeztetett vízbázis diagnosztikai vizsgálata – Zárójelentés az elvégzett geofizikai munkákról.*

[24] Cserkész-Nagy, Á., Bauer, M., Takács, E., Csabafi, R., Gúthy, T., Kóborné Bujdosó, É., Török, I., Redlerné Tátrai, M., Szőts, G., Kovács, A. Cs., Hegedűs, E. (2020): A szeizmikus reflexiós módszerek szerepe a nem szénhidrogénipari kutatásokban magyarországon — Példák a magyar bányászati és földtani szolgálat és elődei tevékenységéből. *Földtani Közlöny,* 150 (1), pp. 151–168. https://doi.org/10.23928/foldt.kozl.2020.150.1.151

Geosciences and Engineering, Vol. 10, No. 15 (2022), pp. 110–124.
https://doi.org/10.33030/geosciences.2022.15.110

MATERIAL BED COMPRESSION EXPERIMENTS AND THE EXAMINATION OF THE BULK DENSITY OF THE PRODUCT

LÁSZLÓ TAMÁS[1], ÁDÁM RÁCZ[2]

[1]*Institute of Raw Material Preparation and Environmental Processing, University of Miskolc*
Refra-System Ltd, Újrónafő, Császárrét major 10.
laszlo.tamas@refra-system.hu
[2]*Institute of Raw Material Preparation and Environmental Processing, University of Miskolc, ejtracz@uni-miskolc.hu*

Abstract: Comminution of white fused alumina (WFA) and white fused mullite (WFM) is a challenging task, as these materials have very high hardness and compression strength and are also very abrasive. Selection of the best comminution process for each particle size range thus has great importance. For this, first we must understand the effects of different types of stresses and comminution methods used for the comminution of WFA and WFM. In this article a comparison of particle size distribution and bulk density of different fractions and the influence of the applied pressure is carried out on the product of material bed compression and traditional single particle compression by roller crusher. Comminution experiments were carried out in a laboratory scale piston press to achieve material bed compression like in HPGR technology, and in an industrial scale roller crusher. The results showed that the products of the two comminution methods have a significant difference on particle size distribution and the fraction's bulk density on both materials. The effective amount (<1 mm) of the fractured particles for WFA was 72% and 74% for WFM with material bed compression comminution and with single particle compression 30% for WFA and 28% for WFM. The highest growth in the bulk density compared to the roller crusher product was achieved by material bed compression by the piston press, with 12.3% on the 0.15–0.3 mm WFA fraction.

Keywords: *Comminution, WFA, WFM, Material bed compression, Piston press, Roller crusher*

1. INTRODUCTION

Due to the extraordinarily energy intensive processes of the raw material preparation industry, the conventional comminution and classification processes have been studied during the last few decades with the aim of decreasing the energy requirements, reducing the environmental impact, and saving money. To meet this request from the side of the manufacturing, the High-Pressure Grinding Roll technology has been studied and developed during the last 35 years [1]. The dry comminution process by HPGR first emerged in the 1980s in Germany and the basis of the technology was nearly defined by this time [2]. The main phenomenon of the HPGR comminution is

the breakage induced by particle-particle interaction. The particles of the disperse system are fed to the active comminution zone of the HPGR, where the material bed is stressed by two rotating rollers moving in opposite directions. The main difference from the conventional roller crusher is the horizontally applied high pressure, which causes highly energy efficient comminution, and the high yield of finer particles. In terms of energy utilization, the most efficient type of comminution is single particle breakage by compression loading, the second is loading the bed of particles by stress, followed by unconfined particle-bed comminution [3]. Single particle breakage can hardly be carried out continuously in operation process. Loading stress on a bed of particles can be achieved by HPGRs and unconfined particle-bed comminution by ball mills. The energetical approach of particle bed comminution was studied by German scientists. Several microprocesses take place in the particle bed during the whole comminution process, from the moment of compaction to the moments of new fragments, and their rearrangement in a new spatial distribution. Each of these processes has specific but not well-known and studied energy requirements (also with material dependence), such as energy loss due to the friction between the particles and their confinements, breakage energy, plastic deformation work, flow losses, energy loss caused by the wear of the confinements of the particle bed and energy loss due to thermoplastic effects, sound wave propagation and oscillation of elastically deformed fragments [4]. The effect of compressive stress velocity in confined particle bed comminution was studied on middle-hard limestone and hard quartz, showing that better comminution is available with the same energy absorption for the middle hard limestone. The increasing stress velocity resulted in higher energy absorption on the particle bed, but lower compression and comminution, also lower energy efficiency [5]. In another study, one of the microprocesses of comminution by stressed particle bed was examined, and that showed the flow losses of energy are only 0.1% of the total energy input in particle bed compression [6].

In an industrial environment, HPGRs were used primarily in the cement industry for the preparation of related raw materials and the dry comminution of the product, as the energy saving was a critical part of the production cost and the higher degree of energy utilization was an advantage for the low- and medium-added-value cement products [7]. Due to its successful application in the cement industry, the technology came to the attention of the mining industry and mineral raw material processing, such as diamond, copper, gold, and iron ore comminution [9–12]. Nonetheless for the HPGR applications, for ore comminution there was a difficult problem that had to be solved before these machines could be used widely: the common and severe wear on the rollers mantle by the abrasive ores. To avoid the negative consequences from comminution of more abrasive ores, the rollers mantle design was studied, and the mainly widespread and conventionally applied stud system was considered as an optimal option to reduce wear [13]. The active comminution zone of the rollers can be increased by the smaller studs, while the stress forces can be also increased, which can cause a finer product and a higher comminution ratio [13], but the higher friction due to the higher acting forces has remarkable wear too. Improved materials and casting

technology and the optimal stud system on the roller surface made it possible to build up a fine material bed, which led to lower wear due to the autogenous comminution on the rollers. In a comparison with ball mills, the major benefits of HPGRs are – for various types of minerals – better energy utilization, less selective crushing of coarse particles, and improved mineral liberalization from the ores [14–15].

Generally, it can be stated that the most widespread technology is hybrid comminution, to achieve the best energy utilization and particle size reduction ratio, because the HPGRs are more efficient at lower energy inputs, and the ball mill is more efficient at higher energy inputs. Systematic experiments were carried out to examine the energy efficiency of the comminution in a HPGR-Ball Mill system and the results showed a reduction ratio of 30, costing only 70% of the energy input compared to using only a single ball mill [8].

In this article, the particle size distribution and the bulk density of WFA and WFM materials are investigated for material bed compression induced comminution by piston press, and particle breakage by two rotating surfaces in the roller crusher. The effect of the pressure applied during material bed compression is also studied and discussed in this paper.

2. MATERIALS AND METHODS

White fused alumina (WFA) is an excellent high-tech advanced abrasive material with a high additional value for miscellaneous applications in industrial fields such as medical and dental technology, space and aerospace industry, optical industry, and laminate industry. White fused mullite (WFM) is also a very abrasive advanced material, with a lower Al_2O_3 content, which causes a lower value of mechanical strength. It has a brilliant white color, and the high purity makes it the perfect raw material for high-end ceramics and investment casting shell building.

After the melting of metallurgically pure alumina (chemical composition and properties are described in *Tables 1* and *2*) in an electric arc furnace at 2040 °C with a specific smelting work of 1.35 MWh/t, the melted WFA is casted into a mold and after solidification is over by the loss of heat, it is crushed by a jaw crusher to 0–100 mm fraction, then the roller crusher comminution results in a 0–3 mm fraction that is classified by sieves to the requested fraction. For the experiments, the pre-crushed 0–3 mm fraction was classified to 1–3 mm fraction with the particle size distribution defined in *Figure 1*; the fraction has a bulk density of 1.84 g/cm^3. Sample materials are from Refra-System Ltd.

Table 1

Typical chemical composition of metallurgical grade alumina by Alumina d.o.o. Zvornik [16]

Chemical comp.	Typical content [%]	Guaranteed limits [%]
Al_2O_3	98.8–99	min 98.7
SiO_2	0.005–0.010	max 0.015
Fe_2O_3	0.008–0.012	max 0.018

Chemical comp.	Typical content [%]	Guaranteed limits [%]
Na_2O_{total}	0.3–0.35	max 0.42
CaO	0.018–0.025	max 0.03
P_2O_5	0.0002–0.0005	max 0.0009
TiO_2	0.002–0.0027	max 0.003
ZnO	0.017–0.02	max 0.022

Table 2

Specification of the metallurgical grade alumina by Alumina d.o.o. Zvornik [16]

	Typical range	Guaranteed limits
Specific Surface Area BET	75–90 [m^2/g]	min 70 [m^2/g]
Bulk Density	1000–1050 [kg/m^3]	max 1070 [kg/m^3]
Loss of ignition (300 °C-1000 °C)	0.6–0.9 [%]	max 1 [%]
Angle of repose	32–34 [°]	max 35 [°]
+45 microns (wet sieve)	88–95 [%]	min 85 [%]
-20 microns (wet sieve)	1–2 [%]	max 2.5 [%]

The melting process of WFM also starts with the metallurgical grade alumina powder in an electrical arc furnace with 1.2 MWh/t specific smelting work at a temperature of 1850 °C. The chemical composition can be seen in *Table 3.*

Table 3

Typical chemical composition of WFM by Refra-System Ltd.

Chemical compound	Typical content [%]
Al_2O_3	76.00
SiO_2	23.50
Fe_2O_3	0.06
Na_2O_{total}	0.06
CaO	0.02
TiO_2	0.02

The production of the WFM and the mechanical preparation of the fused raw material is to the same process as for the WFA. The prepared 1–3 mm fraction for the tests has a bulk density of 1.35 g/cm^3 and the particle size distribution shown in *Figure 1.*

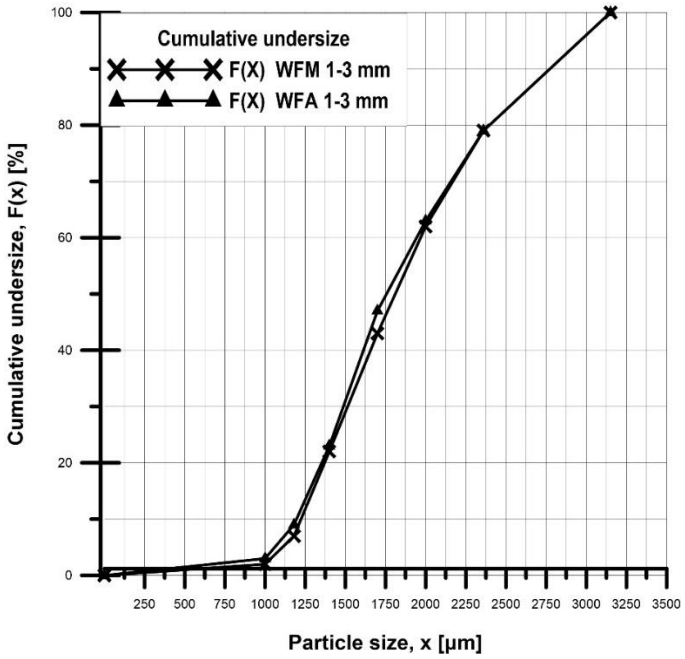

Figure 1

Particle size distribution functions of 1–3 mm WFA and WFM

The industrial scale roller crusher is a double-driven crusher by both cylinder shafts at the Refra-System Ltd. The two shafts are driven by different electrical. *Table 4* shows the geometrical and operating parameters of the roller crusher.

Table 4

Geometrical and operating parameters of the industrial scale roller crusher

Length of the cylinders	500 mm
Diameter of the cylinders	600 mm
Material of the cylinders	Unalloyed steel
Theoretical gap size	0.5 mm
Power of the motors	11 kW; 17 kW
Feed rate	2000 kg/h

The feed material fraction was 1–3 mm WFA and WFM defined with a particle size distribution of *Figure 1*. The product of the equipment was 0–3 mm, classified into different fractions to evaluate systematically, and the roller crusher and piston press

products were compared to each other for the effectiveness of crushing and particle size reduction ratio and for the bulk densities of the different size fractions.

The laboratory hydraulic piston press was built by the Institute of Raw Material Preparation and Environmental Processing, University of Miskolc for briquetting. Two pistons are situated in the equipment, one for the pressing force transmission and one for the sample discharge. The hydraulic pressure can be adjusted to 2750 bar by the oil pressure of the piston as a maximum value. The pressing velocity can be also adjusted up to 34.5 mm/s. *Table 5* shows the technical data of the machine parameters during the measurements.

Table 5

Geometrical and operating parameters of the laboratory scale piston press

Diameter of the piston	25 mm
Piston velocity	34.5 mm/s
Pressure at Ø25 mm piston	2500–1250 bar
Material bed height	20 mm

The feed materials and their particle size distribution function were the same as specified in Figure 1, and the products were classified and measured with the same process to obtain comparable data from the two different type of comminution processes. In this measurement stage the effect of the pressure was examined with the values of 2500, 2250, 1750 and 1250 bars to the different fractions.

A TAP sieve shaker AS 200 model was used to separate the products into the required fractions developed by RETSCH. The analytical test sieve shaker is used in research and development for separation, fractioning and determination of the particle size distribution. The movement of the sieve in the equipment is a horizontal circular motion with taps. The rotational speed of the sieves was 280 min^{-1} while the number of taps was 150 min^{-1} during the measurements. The applied feed mass was 100 g in each case.

The bulk density of the product fractions was measured according to the MSZ 6506-84 patent standard.

3. RESULTS

In this section the particle size distribution of the WFA and WFM products from the feed fractions and the comparison of the bulk density of the classified fractions are presented. Also, the evaluated data from material bed comminution with different pressure levels are presented in this chapter.

Four particle size distributions can be seen in *Figure 2*, where the curves of the coarse feed are shown on the right, and on the left side the 0–3 mm product curves. Both test materials have sharply classified 1–3 mm feed fractions, with 3% and 2% of under particles for WFA and WFM.

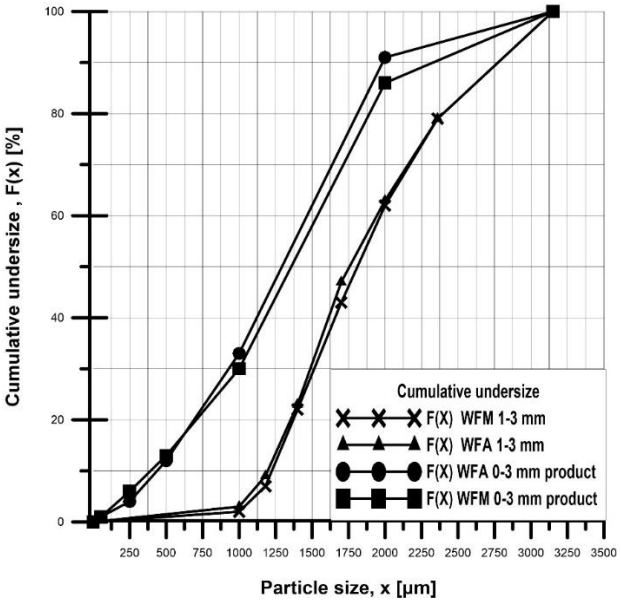

Figure 2

Cumulative undersize of 1–3 mm feed and the 0–3 mm products after roller crusher

After comminution in roller crusher, the mass ratios of the <1 mm particles were increased to 33% and 30%, respectively. This means that the effective mass of the ground particles <1 mm was 30% for WFA and 28% for WFM. Also, the size reduction can be seen at the fraction of >1 mm particles for both materials because of the horizontal shift of the cumulative undersize curves. The characteristics of the products are similar due to the similar feed fractions and stress conditions during the comminution process. The WFA product has x_{50} = 1.29 mm and x_{80} = 1.81 mm. The WFM product has x_{50} = 1.35 mm and x_{80} = 1.9 mm.

The characteristics of the piston press product were different from those of the roller crusher in for both materials Also, it can be stated that the material bed compression produced a finer product than the roller crusher. Heineckel et al. [1] stated that the particle size distribution (PSD) of HPGR products varies from a ball mill ground product. The PSD is not only shifted along the horizontal axis of the size distribution diagram but also twist towards more fines. Tavares [17] stated that high interparticle stresses result in a much greater proportion of fine particles in comparison to conventional crushing. The mass ratio of particles <1 mm was 72% and 74% in the product. The effectively generated 0–1 mm fraction of WFA is 69% and 72% in the WFM product. The WFA product has x_{50} = 0.5 mm and x_{80} = 1.35 mm. The WFM product has x_{50} = 0.47 mm and x_{80} = 1.28 mm.

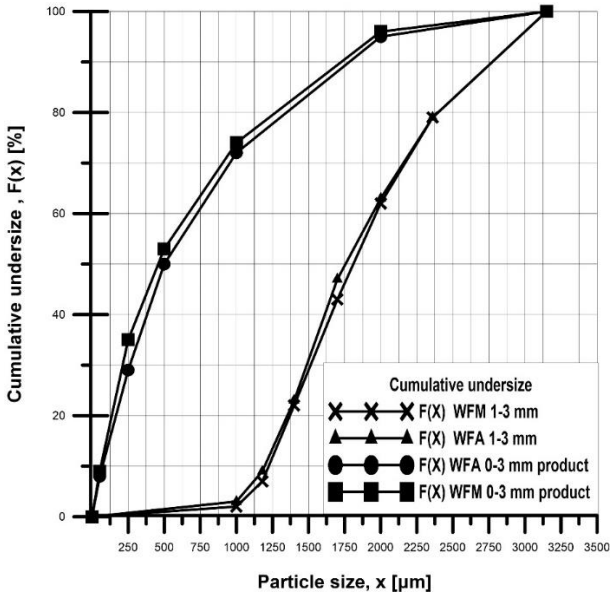

Figure 3

Cumulative undersize of 1–3 mm feed and the 0–3 mm products after material bed compression

The ratio of overground particles (<53 μm) produced by the piston press is higher by 7% for WFA and 8% for WFM than the ratio produced by roller crusher, as displayed in *Table 6*. The horizontal shift to the finer particle size ranges from the feed particle size distribution to the product distribution can be also seen in *Figure 3*.

Table 6

Amount of the produced overground particles by roller crusher and piston press

	<53 μm [%]
WFA Roller crusher	1
WFM Roller crusher	1
WFA Piston press	8
WFM Piston press	9

The bulk density of WFA fractions produced by roller crusher can be seen in Figure 4. The product of material bed compression and roller crushing was sieved to 0–150; 150–300; 300–500; 500–1000 and 1000–2000 μm fractions, and then the bulk density of each fraction was measured. The bulk density of the size fractions is an important parameter for the later application of the WFA and WFM products, so the comminution process should be selected according to this condition as well.

The bulk density values of the fractions of WFA roller crusher products increase with the increasing particle sizes. The minimal value of the bulk density (1.49 g/cm^3) can be seen in *Figure 4*, which occurred for the finest particle fraction 0–0.15 mm, and the highest bulk density (1.82 g/cm3) was measured for the 1–2 mm fraction.

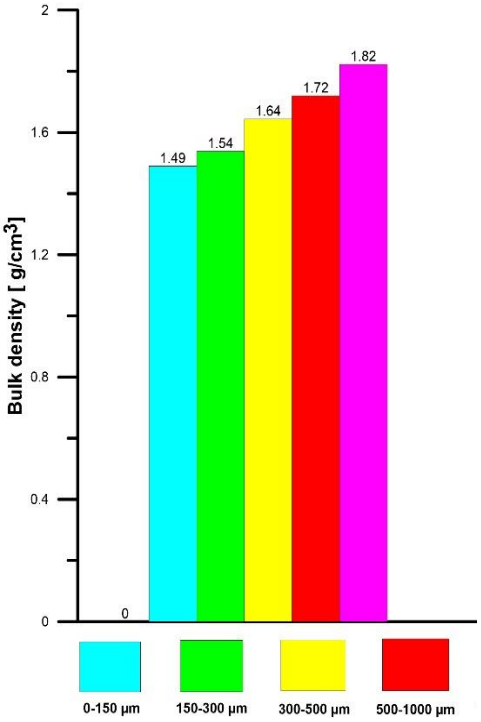

Figure 4

Bulk density of WFA fractions produced by roller crusher

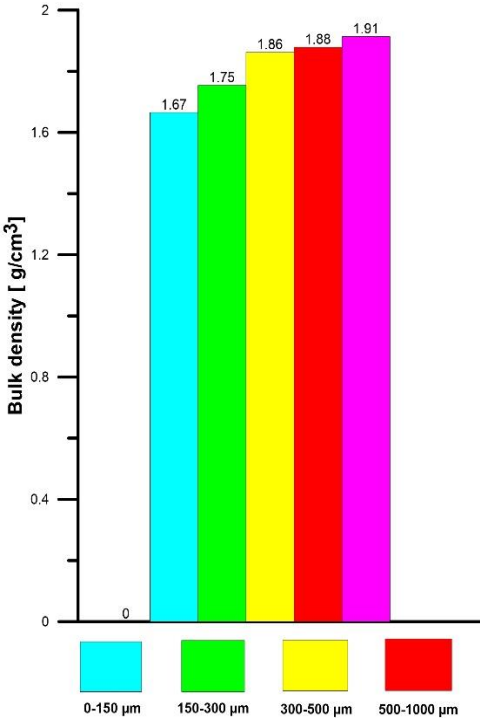

Figure 5

Bulk density of WFA fractions produced by material bed compression

An increasing tendency is also visible in the bulk density for the fractions of piston press product, with the increasing particle sizes, *(Figure 5)*. Also, the finest particle size class, the 0–0.15 mm fraction, has the lowest bulk density at 1.67 g/cm^3, and the 1–2 mm fraction has the highest value at 1.91 g/cm^3. At each particle fraction the material bed compression resulted in a higher bulk density.

It can be seen in *Figure 6*, that the tendency towards higher bulk density with a coarser particle size fraction is again detectable with WFM comminution by a roller crusher, where the minimum value is 1.21 g/cm^3, and the maximum is 1.33 g/cm^3.There is less increase in the bulk density for the coarser fraction in the case of WFM due to the lower particle density of WFM (3.15 g/cm^3).

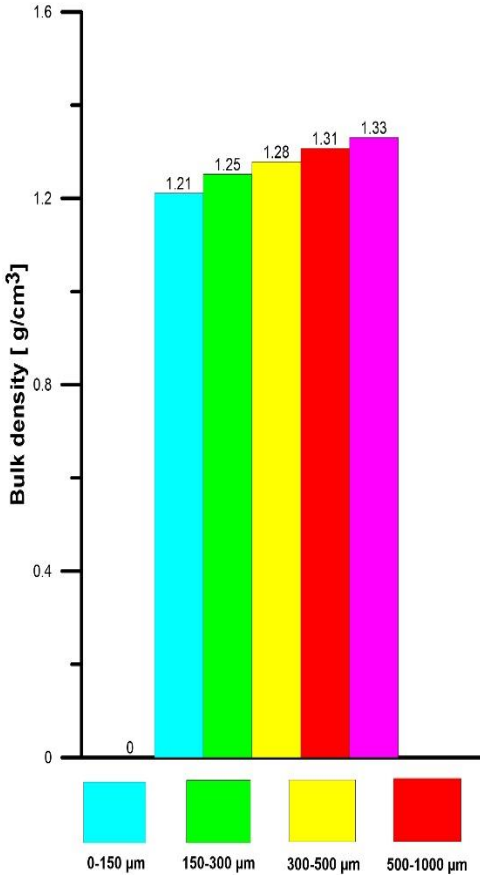

Figure 6

Bulk density of WFM fractions produced by roller crusher

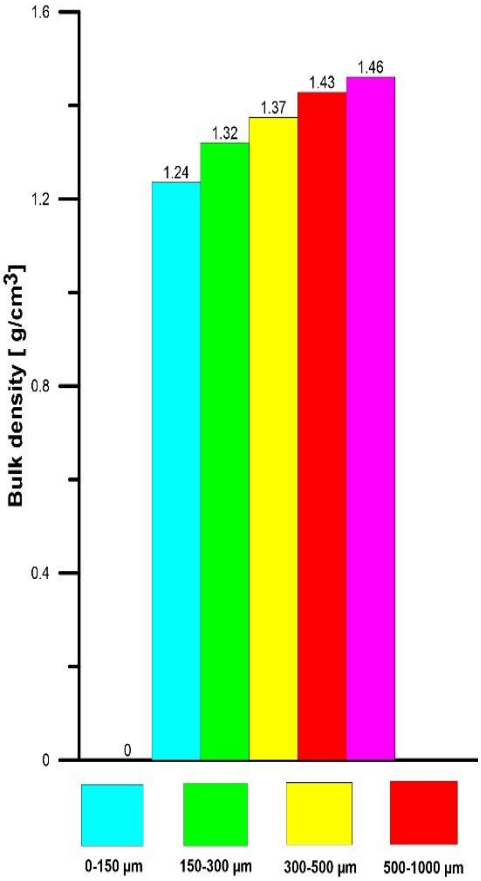

Figure 7

Bulk density of WFM fractions produced by piston press

The bulk density was higher at each particle fraction, and the tendency was also increasing with the coarser particle fraction in case of the material bed compression. In *Figure 7* it can be seen that the highest bulk density of WFM was achieved by the material bed compression of the 1–2 mm fraction, with 1.46 g/cm^3 value, and the lowest value was 1.24 g/cm^3 in case of the 0–0.15 mm WFM fraction.

The increase in the bulk density of the separated WFA fractions are displayed as a percentage from the roller crusher products in *Figure 8*. The bulk density of 0.15–0.3 mm fraction has the highest increase (12.3%) in the case of the piston press product compared to application of the roller crusher.

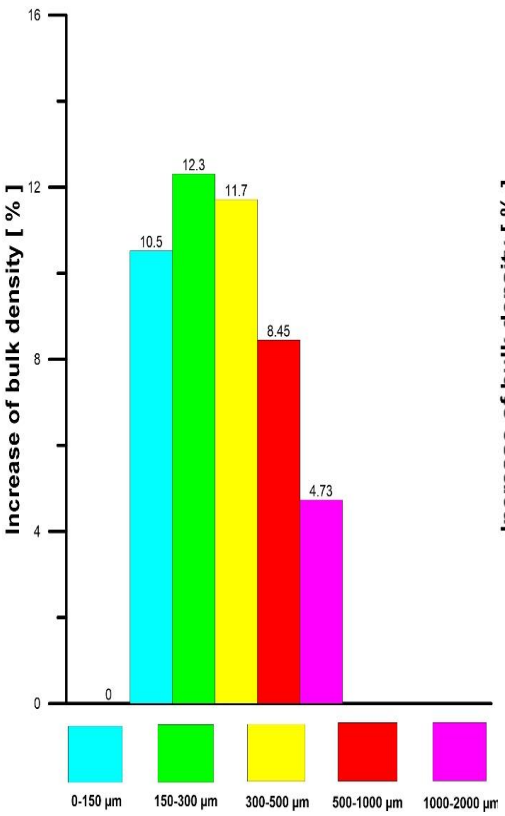

Figure 8

Bulk density of WFA fractions produced by piston press
(Basic value; Roller crusher)

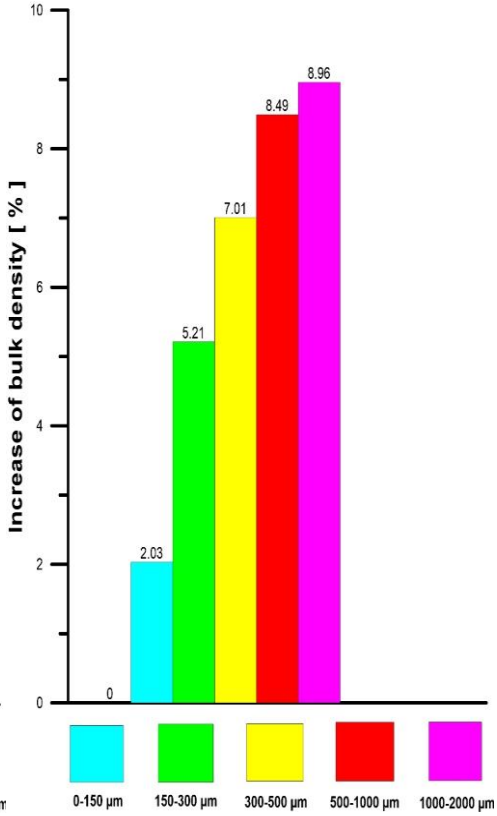

Figure 9

Bulk density of WFM fractions produced by piston press
(Basic value; Roller crusher)

The peak value is for the 0.15–0.3 mm fraction, then the increase in the bulk density becomes less prominent with the coarser fractions. The maximum growth (12.3%) was achieved with WFA according to the higher maximal specific gravity (4.1 g/cm^3).

The increased bulk density values for the material bed compression at the piston press are represented with the same methodology as for WFM. *Figure 9* shows that with a coarser fraction, the growth in the bulk density becomes higher, and the maximum value is 8.96% on the 1–2 mm fraction, while the lowest growth is 2.03% on the 0–0.15 mm fraction.

Figure 10 shows the effect of the reduced pressures on the material bed of WFA, i.e., how the fines of the products changes. The overground particles <53 µm, from 8% with the applied pressure of 2500 bar started to decrease with the lower applied pressure. With half of the pressure the overground particles fraction reached only

3.9%, while the reduction ratio is still good because the 0–1 mm fraction in the product is 63%. That also means with the reduced applied pressure from 2500 to 1250 bar, produced 51% less overgrounded particles, but at the same time the 0–1 mm fraction in the product from the feed 1–3 mm is still decreased by only 12.5%.

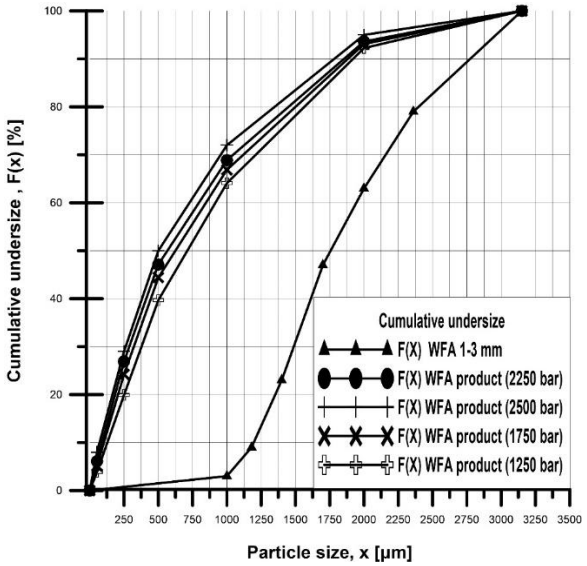

Figure 10

Effect of pressure on the material bed compression for WFA

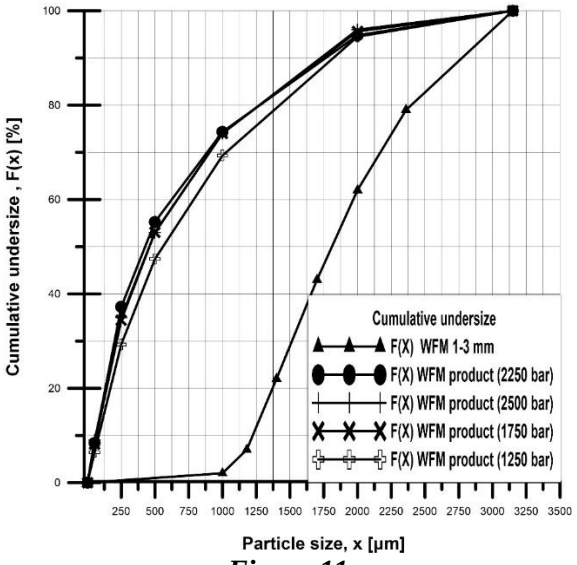

Figure 11

Effect of pressure on the material bed compression for WFM

The particle size distribution of the feed material and the products isshown in *Figure 11*. It can be seen that the amount of the overground particles decreased from 9% to 6.5% with half of the applied pressure of 2500 bar. The 0–1 mm fraction in the products changes from 72% to 69% with 2500 and 1250 bar pressure. This means only a 5% decrease in the 0–1 mm fraction production while the amount of the overground particles is less by 28%.

4. CONCLUSIONS

In the present study, the comminution of WFA and WFM by compression in roller crusher and material bed compression using a piston press was investigated. The particle size distribution and bulk density of the products were determined and compared. The effectiveness of comminution by material bed compression has already been proven by several authors [7, 9–12] and is also supported by the present measurement results. Comminution with the piston press by material bed compression produced 72% (WFA) and 74% (WFM) 0–1 mm fraction from the 1–3 mm feed fraction, while that produced by the roller crusher contained only 30% (WFA) and 28% (WFM). That means 2.4 times more desired product particles in WFA and 2.6 times more in WFM product compared to material bed compression. The overground <53 μm particles were 8% in WFA and 9% in WFM products with material bed compression in the piston press with the applied pressure of 2500 bar. The roller crusher product contained only 1% <53 μm particle.

The coarser product fractions had higher bulk density values using the piston press and roller crusher for both materials. The results showed that each fraction of WFA and WFM produced by material bed compression had a higher bulk density. The stress environment in the material bed showed that the rigid WFA and WFM particles effectively transmit the energy. Applied pressure as an optional way to reduce the amount of overground <53 μm particles showed good results. Using 1250 bar instead of 2500 bar by the piston press resulted in 51% less overground particles for WFA, while the yield of the 0–1 mm fraction decreased only by 12.5%. WFM showed similar results for the analogical tests, with the amount of particles <53 μm was reduced by 28%, and only a 5% mass decrease of the 0–1 mm fraction recorded.

The measurement results proved that material bed compression is more effective than simple particle compression as a comminution method for 1–3 mm WFA and WFM products in order to create high density product fractions.

REFERENCES

[1] Heinicke, F., Günter, H., Lieberwirth, H. (2016). *Modelling of HPGR Edge recycling with progressive grinding data*. https://www.koeppern-international.com/fileadmin/user_upload/downloads/Comminution/Paper_HPGR_edge_recycling_02-2016.pdf.

[2] Schönert, K. (1966). *Einzelkorn-Druckzerkleinerung und Zerkleinerungskinetik. Untersuchungen an Kalkstein-, Quarz-, und Zementklinkerkörnern des Größenbereiches 0,1–0,3mm.* Dissertation. TH Karlsruhe, 1966

[3] Schönert, K. (1979). Energetische Aspekte des Zerkleinerns spröder Stoffe. *Zement-Kalk-Gips*. Int. 32, 1–9.

[4] Schubert, H. (1967). Zu einigen Fragen der Kollektivzerkleinerung. *Chem. Technol.*, 19, pp. 595–598.

[5] Mütze, T., Husemann, K. (2008). Compressive stress: Effect of stress velocity on confined particle bed comminution. *Chem. Eng. Res. Des.*, 86, pp. 379–383, https://doi.org/10.1016/j.cherd.2007.11.007.

[6] Mütze, T. (2015). Energy dissipation in particle bed comminution. *International Journal of Mineral Processing*, 136 pp. 15–19. http://dx.doi.org/10.1016/j.minpro.2014.10.004

[7] Camalan, M., Önal, M. A. R. (2016). Influence of high-pressure grinding rolls on physical properties and impact breakage behavior of coarsely sized cement clinker. *Part. Sci. Technol*., 34, pp. 278–288. https://doi.org/10.1080/02726351.2015.1075636

[8] Fuerstenau, D. W., Kapur, P. C., Schönert, K., Marktscheffel, M. (1990). Comparison of Energy Consumption in the Breakage of Single Particles in a Rigidly Mounted Roll Mill with Ball Mill Grinding. *Int. J. Miner. Process*., 28, pp. 109–125, https://doi.org/10.1016/0301-7516(90)90030-3.

[9] Abazarpoor, A., Halali, M., Hejazi, R., Saghaeian, M. (2018). HPGR effect on the particle size and shape of iron ore pellet feed using response surface methodology. Miner. Process. *Extr. Metall. Trans. Inst. Min. Metall*., 127, pp. 40–48, https://doi.org/10.1080/03719553.2017.1284414.

[10] Anticoi, H., Guasch, E., Hamid, S., Oliva, J., Alfonso, P., Garcia-Valles, M., Bascompta, M., Sanmiquel, L., Escobet, T., Argelaguet, R., Escobet, A., de Felipe, J.J., Parcerisa, D., Peña-Pitarch, E. (2018). Breakage Function for HPGR: Mineral and Mechanical Characterization of Tantalum and Tungsten Ores. *Minerals*, 8, p. 170, https://doi.org/10.3390/min8040170.

[11] Schönert, K. (1988). A first survey of grinding with high-compression roller mills. *Int. J. Miner. Process*., 22, pp. 401–412. https://doi.org/10.1016/0301-7516(88)90075-0.

[12] Yin, W., Tang, Y., Ma, Y., Zuo, W., Yao, J. (2017). Comparison of sample properties and leaching characteristics of gold ore from jaw crusher and HPGR. *Miner. Eng*., 111, pp. 140–147. https://doi.org/10.1016/j.mineng.2017.06.012.

[13] Nagataa Y, Tsunazawab Y, Tsukadac K, Yaguchid Y, Ebisue Y, Mitsuhashie K, Tokorof C. (2020). Effect of the roll stud diameter on the capacity of a high-pressure grinding roll using the discrete element method, *Miner. Eng*., 154, https://doi.org/10.1016/j.mineng.2020.106412

[14] Ballantyne, G. R., Hilden, M., van der Meer, F. P. (2018). Improved characterisation of ball milling energy requirements for HPGR products. *Miner. Eng*., 116, pp. 72–81, https://doi.org/10.1016/j.mineng.2017.06.005.

[15] Liu, L., Tan, Q., Liu, L., Li, W., Lv, L. (2017). Comparison of grinding characteristics in high-pressure grinding roller (HPGR) and cone crusher (CC). *Physicochem. Probl. Miner. Process*., 53, pp. 1009–1022. https://doi.org/10.5277/ppmp170226.

[16] https://www.aluminazv.ba/en/category-products/8; downloaded: 01. 07. 2021.

[17] Tavares, L. M. (2005). Particle weakening in high-pressure roll grinding. *Miner. Eng*., 18, pp. 651–657, https://doi.org/10.1016/j.mineng.2004.10.012.

Geosciences and Engineering, Vol. 10, No. 15 (2022), pp. 125–137.
https://doi.org/10.33030/geosciences.2022.15.125

INVESTIGATION OF THE PETROLOGICAL PROPERTIES OF ANDESITES FROM TÁLLYA QUARRY, HUNGARY AND THEIR INFLUENCE ON THE RESISTANCE TO WEAR AND FRAGMENTATION

IZABELLA REBEKA MÁRKUS[1], RÁCZ ÁDÁM[2]

[1, 2]*Institute of Raw Material Preparation and Environmental Processing*
[1]*ejtmir@uni-miskolc.huauthor, https://orcid.gov/0000-0002-4264-5136*
[2]*adam.racz@uni-miskolc.hu, https://orcid.gov/0000-0002-6561-2177*

Abstract: The two most common used mechanical test in the aggregate industry for quality control are the resistance to wear (micro-Deval) and resistance to fragmentation (Los Angeles) tests. The quality of aggregates strongly depends on the textural, structural, and mineralogical features of the crushed material. These rock properties were experimentally studied on andesite samples from Tállya quarry. The mineralogical and chemical composition of samples were determined, textural observations were made on thin sections. The alteration was quantified using the chemical composition and mineralogical data. Micro-Deval and Los Angeles tests were conducted on the samples. The micro-Deval indices and the Los Angeles values showed similar trends, although the different type of stresses. The results showed that the examined mechanical properties of the Tállya andesites are complexly influenced by the textural and structural features, mineralogical composition, and alteration, however alteration has one of the most significant effects.

Keyword: *Rock texture, mineralogical composition, weathering index, micro-Deval, Los Angeles*

1. INTRODUCTION

The quality standards for mining aggregates are constantly becoming stricter in the EU therefore it is very important for the processing plant to produce the best quality products with the highest possible yield. The quantity of the good quality resources is decreasing, while the sustainable raw material management requires the utilisation of the low-quality raw materials with the compliance to the quality requirements for the products. The quality requirements of aggregates can be achieved by crushing and screening technology, for which it is essential to explore the relationship between the feed quality and the crushing and screening process. This depends on a lot of factors, such as the textural, structural, and mineralogical features of the feed material and the operating conditions and machine parameters of the crushers. In this paper the term texture is referred to the mineralogical composition, distribution, grain, shape, size, mode of interlocking, while the term structure to the mineral grain orientation, cracks and any other voids, and visible sign of alteration.

The relationships between petrological and mechanical properties of rocks have been investigated by numerous authors [1, 2]. The mechanical properties are mainly influenced by the mineral association, their distribution, shape, size, orientation or in other words the texture and the degree of alteration, cracks, and porosity.

There are conflicting findings on the effect of primary minerals such as quartz and feldspar contents on the mechanical strength of rock aggregates [3]. Secondary minerals, such as clay minerals and micas contribute to a decrease of rock strength, along with the altered plagioclase. The effect of alteration and the type of alteration, beyond the fact that behaves as a plain of weakness, can be significant. For example, an alteration zone abundant in potassium feldspar will be much harder to crush than a phyllic alteration zone that is rich in sericite [4].

In the case of similar mineralogical composition, the effect of the rock texture is more significant than the mineralogy itself [5, 6]. Akseli and Leinonen [7] emphasizes that the resistance to wear depends more on mineralogical composition, while the resistance to fragmentation depends more on the changes of the texture. The decrease in grain size of the minerals results in the increase of its specific surface, which leads to an increase of bond strength and hardness. If a mineral occurs as larger aggregates composed of several smaller grains, these may interact as a larger grain and give properties that compare with a coarser-grained rock, phase contact may act as discontinuities having an influence on fragmentation [8]. The shape and roughness of mineral grains influences the contact surface between the grains. The grain boundary irregularity results in extent intergrowth and strong bond between minerals which has a great impact on crack formation and on the strength properties [9]–[11]

A significant part of the presented studies focuses on magmatic rocks and ores. The presented petrological features and their effect on mechanical properties of rocks are relevant in the case of rocks of magmatic origin. However, the systematic study of one rock type, for example andesite, with different textural and structural properties is scarce in the international literature. The scope of our study was to examine the petrological properties of andesites from the Tállya quarry (Hungary) and their effect on mechanical properties of aggregates.

2. MATERIAL AND METHODS

Samples were collected from three different operation levels within the Colas Északkő Ltd. operated Tállya quarry. The locations were selected based on the quality of quarried material, the sample Tállya_1 representing a good quality finely grained, dark grey coloured columnar andesite, without signs of alteration or cracks. The sample Tállya_2 constitutes of finely grained, light purplish-grey vesicular andesite, . The third sample Tállya_3 was consists of altered, poor quality andesite with visible signs of alteration and oxidation *(Figure 1)*.

Figure 1
The collected samples from the Tállya quarry, from the left to right: Tallya_1, Tallya_2 and Tállya_3

X-ray powder diffraction analysis were carried out at the Institute of Mineralogy and Geology on a Bruker D8 Discover instrument, with Cu-Kα radiation (40 kV, 40 mA generator settings).

Chemical analysis was carried out at the Institute of Mineralogy and Geology by X-ray fluorescence spectroscopy on Cereox cemented powder pellets by wavelength dispersive measurement (WD-XRF) on a Rigaku Supermini200 type instrument. The chemical composition was used for the quantification of the alteration of the samples. Weathering indices measure the degree of depletion of mobile components relative to immobile components caused by the weathering.

Nesbitt and Young [12] proposed the following equation for the quantification of weathering, which they named Chemical Index of Alteration (CIA):

$$CIA = \left[\frac{Al_2O_3}{Al_2O_3+CaO^*+Na_2O+K_2O}\right] * 100 \quad (1)$$

where CaO^* is the amount of CaO incorporated in the silicate fraction of the rock, a correction is made for the carbonate and apatite content. The resultant value is a measure of the proportion of Al_2O_3 versus the labile oxides in the analysed sample. Harnois [13] proposed the following modified Chemical Index of Weathering (CIW) equation:

$$CIW = \left[\frac{Al_2O_3}{Al_2O_3+CaO+Na_2O}\right] * 100 \quad (2)$$

During the weathering Si, Mg, Ca and Na are leached, Al and Ti remain essentially in the system, iron and potassium have more complicated behaviour. Both indices increase with the degree of alteration, the range of the values depends on the mineralogical composition of individual samples, thus it can range from 0 to 100.

The thin section used for the polarized optical microscopy observation was prepared in the laboratory of the Institute of Mineralogy and Geology. The polarized optical microscopy observation was made in the Optical Microscopy Laboratory of

the Institute of Mineralogy and Geology on a Zeiss Axio Imager A2m optical microscope equipped with AxioCam MRc 5 digital camera for image acquisition.

The resistance to wear was determined in accordance with the MSZ EN 1097-1:2012 standard Tests for mechanical and physical properties of aggregates- Part 1: Determination of the resistance to wear (micro-Deval) [14] in the laboratory of the Institute of Raw Material Preparation and Environmental Processing. The test consists of measuring the wear produced by friction between the aggregates and an abrasive ball charge in a rotating drum under defined conditions. The test is conducted in a typical micro-Deval apparatus which consists of a hollow drum and rotated on a horizontal axis. The test is carried out on aggregate with the particle size between 14 mm and 10 mm. 500 ±2 g sample is placed in the drum with 5000 ±5 g of steel balls and 2,5 ±0,05 l of water, and rotated at a speed of 100 ±5 min^{-1} for 12000 ±10 revolutions. After the required revolution number, the material is emptied and the quantity of material retained on the +1,6 mm sieve is dried at 110 ±5°C and the mass is determined. The micro-Deval coefficient is calculated with the following equation:

$$M_{DE} = \frac{500-m}{5} \quad (3)$$

where m is the mass of the oversize fraction retained on a 1,6 mm sieve in grams.

The resistance to fragmentation was determined in compliance with the MSZ EN 1097-2:2020 standard Tests for mechanical and physical properties of aggregates- Part 2: Methods for the determination of resistance to fragmentation[15]. The test is conducted in a Los Angeles test machine, which consists of a hollow drum made of steeland rotates on a horizontal axis. The ball load consists of 11 spherical steel balls, the total load weighting between 4690 g and 4860 g. The test is caried out on an aggregate with the particle size between 14 mm and 10 mm 5000 ±5 g of sample is placed in the drum with the ball load, then the drum is rotated for 500 revolutions at a constant speed between 31 min^{-1} and 33 min^{-1}. The material is emptied on a 1.6 mm sieve and carefully washed. After drying it at 110 ±5 °C the mass of the retained material is weighted. The Los Angeles coefficient is calculated with the following formula:

$$LA = \frac{5000-m}{50} \quad (4)$$

where m is the mass retained on the 1,6 mm sieve in grams.
Lower M_{DE} and LA values representing better quality rock, and higher resistance against the stress.

3. RESULTS

3.1. Mineralogical composition

The XRD results did not show major differences in the type of rock forming minerals, just in their amount *(Table 1)*. The primary rock constituent minerals are intermediate plagioclases, mainly the oligoclase variety. The ratio of oligoclase

shows no significant changes in the sample being between 27,8–22,1 %. The group of intermediate plagioclases, alongside the oligoclase comprises the andesine and labradorite. This varieties form a solid-solution series with different ratios of Na-Ca content, but with similar mineralogical properties, thus treating the group as one mineral is more practical from the point of view of our study. The K-feldspars, sanidine and microcline in the case of the studied samples, are the products of the auto metasomatism occurring during the cooling phase of the magma, a faster decrease in temperature near the surface results in a decrease in the amount of K-feldspars as it can be seen in the case of sample Tállya_3 compared to the other two samples. Similar to the plagioclase feldspars, the K-feldspars have almost identical composition and properties, which results in similar properties, thus treating them as one is practical in the case of our samples. The amorphous content shows an inverse relationship with the depth related to the surface. The sample Tállya_1 has the lowest quantity of amorphous material resulting from the slower solidification and cooling of magma, while the sample Tállya_3 has the highest amount of amorphous material being at the marginal region of the rock body, cooling down faster resulting in an increase of glassy phase.

Table 1

Quantitative mineralogical composition of the samples (weight percent, error +/–5 relative percent)

Sample	Andesine	Quartz	Sanidine Na0.35	Smectite	Diopside	Titano-magnetite	Oligoclase An25	Dolomite	Labradorite An65	Ilmenite	Microcline	Cristobalite	Enstatite	Siderite	amorphous
Tállya_1	8.1	4.2	14.4	1.4	4.1	0.3	27.8	0.6	13.2	1.2	2.6	5,8	3.4	3.2	9.7
Tállya_2	8.8	1	11.7	1.4	5	0.2	24.5	1.1	16.1	0.8	1,2	6.6	3.3	3.8	14.8
Tállya_3	33.3	0.6	0.1	5.7	1.1	0.5	22.1	0.5	8.4	0.5	0,4	1.2	4.9	0	20.7

3.2. Chemical composition and alteration indices

The major element composition from the XRF analysis is presented in *Table 2*. Similar to the mineralogical composition, the results show no significant differences between the samples, variations can be seen in their amount. The increase in SiO_2 and Al_2O_3 is in correlation with the increase in the amorphous material. The difference up to 100% of the total is mainly the loss on ignition resulting from dehydration (amorphous material, smectite) and carbonate decomposition (siderite, dolomite). The minor amount of S is indicative for presence of sulphides, observed as rare pyrite grains.

Table 2

Chemical composition of the samples (weight percent, error +/–1 relative percent)

Sample	SiO_2	Al_2O_3	MgO	CaO	Na_2O	K_2O	Fe_2O_3	MnO	TiO_2	P_2O_5	S	Σ
Tállya_1	58,0	16,0	1,63	6,15	3,13	2,05	6,86	0,15	1,13	0,28	0,18	95,5
Tállya_2	57,3	15,9	1,33	6,08	2,95	2,10	7,09	0,18	1,16	0,29	0,13	94,5
Tállya_3	59,1	17,2	0,96	5,23	2,24	2,35	5,79	0,07	1,26	0,28	0,01	94,5

A direct relationship between the chemical composition of the material and the mechanical features cannot be drawn based on the earlier literature review, but it can be used for quantifying the degree of the weathering of the samples [16]. There are several calculation modes applied in the literature as presented previously by *Equation (1)* and *(2).*

$$[12]CIA = \left[\frac{Al_2O_3}{Al_2O_3+CaO^*+Na_2O+K_2O}\right] * 100[14][14][14][14][14][14][14][14][14][14]CIW =$$

$$CIA = \left[\frac{Al_2O_3}{Al_2O_3 + CaO^* + Na_2O + K_2O}\right] * 100[14][14][14][14][14][14][14][14][14][14]CIW$$

$$= \left[\frac{Al_2O_3}{Al_2O_3 + CaO + Na_2O}\right] * 100\text{The}$$

$$CIW = \left[\frac{Al_2O_3}{Al_2O_3 + CaO + Na_2O}\right] * 100\text{The}$$

Table 3

Calculated alteration indices of the samples (dimensionless values)

Sample	CIW	CIA
Tállya_1	63,26	58,91
Tállya_2	63,72	59,50
Tállya_3	69,70	63,99

Based on the nature of our samples, the dolomite [$CaMg(CO_3)_2$] content which contributes to the amount of CaO, and the K content, we considered more appropriate the use of the CIA proposed by Nesbitt and Young for the quantification of alterations

3.3. Textural properties

Based on the polarized light microscopy observation made on the thin sections the three samples have slightly different texture. The sample Tállya_1 has the largest phenocrystals and the finest grained matrix *(Figure 2)*. The phenocrystals are mainly plagioclase, which are generally idiomorphic, without signs of alteration, the size of individual minerals ranging from 200 μm up to 1000 μm, frequently forming aggregates with pyroxene and amphiboles. Beside the plagioclase, pyroxenes phenocrystals and rarely amphiboles can be observed which are slightly resorbed and altered. The matrix consists of finely grained acicular plagioclase, amorphous

material, and opaque minerals, which based on the XRD results are probably titano-magnetite and ilmenite.

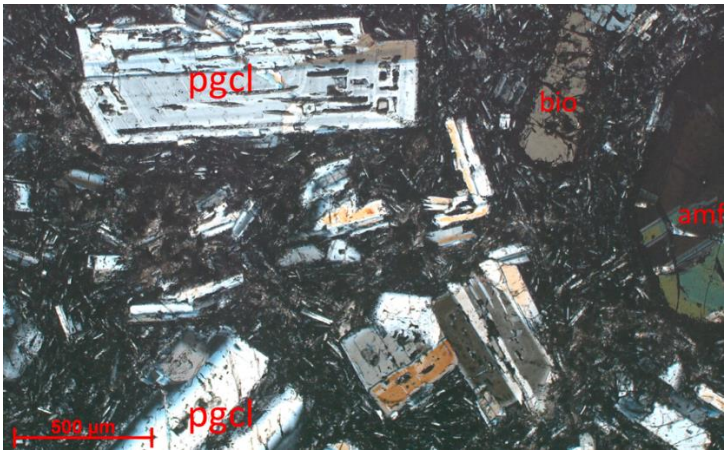

Figure 2

Polarized light optical microscopy image (+N) of the sample Tállya_1 (pgcl-plagioclase, amf- amphibole, bio- biotite)

In the sample Tállya_2 the size of the phenocrystals decreases, appearing mostly as anhedral to subhedral crystals with resorbed margins. The amount of amphibole and pyroxene phenocrystals decreases and they appear strongly fractured, altered. In the pores 150–500 µm radial siderite aggregates could be identified. The composition of matrix is similar to the previous sample but shows a significant increase in the grain size and extensive patches of carbonatization (dolomite based on the XRD results) could be identified *(Figure 3)*.

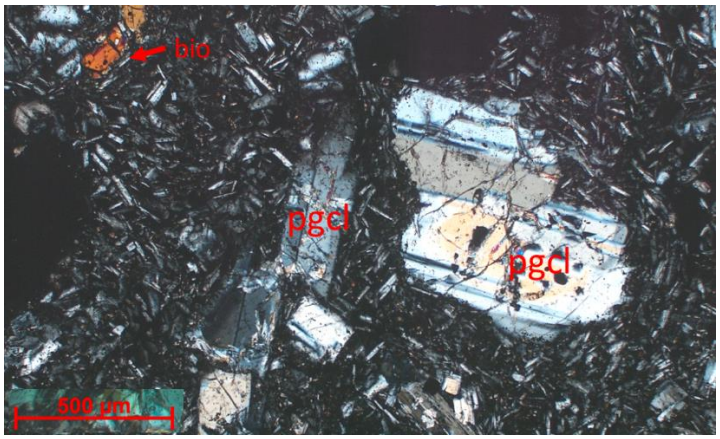

Figure 3

Polarized light optical microscopy image (+N) of the sample Tállya_2 (pgcl-plagioclase, bio- biotite)

The sample Tállya_3 is strongly altered which is in relationship with the increased amount a smectite detected by the XRD. The grain size of the phenocrystals and matrix is similar to the previously described Tállya_2 sample. The phenocrystals have a hypidiomorphic appearance, presenting strong signs of alteration. In the matrix the frequent presence of opaque and isotropic patches is related to the presence of amorphous materials, such as Fe-oxide-hydroxides and glass *(Figure 4)*.

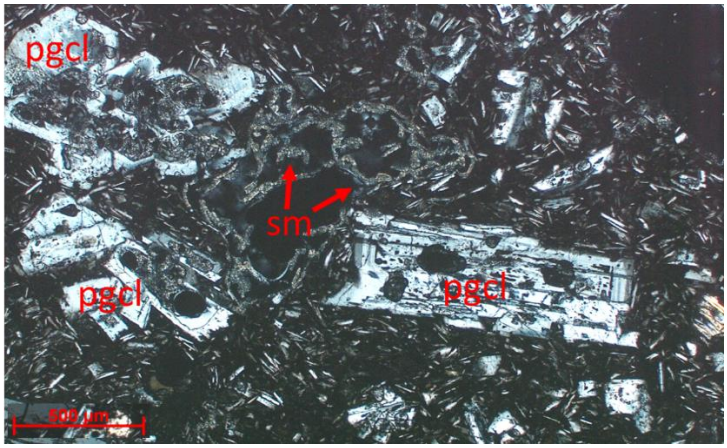

Figure 4

Polarized light optical microscopy image (+N) of the sample Tállya_3 (pgcl-plagioclase, bio- biotite, sm- smektite)

3.4. Resistance to wear

The resistance to wear was measured in the case of all three samples in accordance with the standard MSZ EN 1097-1:2012 and calculated with the formula given in *Equation (3)*. The samples showed an increase in the M_{DE} value, being least resistant to wear with the increasing degree of alteration *(Table 4)*. The M_{DE} values were plotted versus the alteration indices *(Figure 5)*. The change in the M_D values is not linear with the change in the alteration indices, which leads us to the conclusion that other petrological and mechanical factors have an effect, especially in the case of the difference between sample Tállya_1 and Tállya_2. The K-feldspar content has a negative correlation, while the amorphous material content has a positive correlation with the M_{DE} values *(Table 4)*.

Table 4

M_{DE} values of the samples and the K-feldspar and amorphous material content

Sample	M_{DE}	K-feldspar	amorphous
Tállya_1	3.94	17%	9.7%
Tállya_2	8.79	12.9%	14.8%
Tállya_3	20.66	0.5%	20.7%

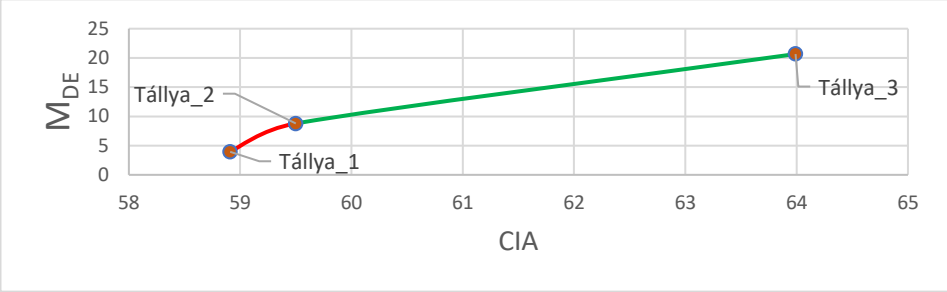

Figure 5
The relationship between M_{DE} indices and CIA

3.5. Resistance to fragmentation

Measuring of the resistance to fragmentation was carried out according to the standard MSZ EN 1097-2:2020 and *Equation (4)* presented before in the case of all three samples. The LA values showed similar trend to the M_{DE} values, the difference between the samples being even more significant *(Table 5)*. Plotting the LA values versus the CIA *(Figure 6)*, the change in the LA is not linear with the change in the CIA indices. Similar to the M_{DE} indices, the LA values show negative correlation with the K-feldspar and positive correlation with the amorphous material content.

Table 5
LA indices of the samples and the K-feldspar and amorphous material content (wt%)

Sample	LA	K-feldspar	amorphous
Tállya_1	14.85	17%	9.7%
Tállya_2	23.05	12.9%	14.8%
Tállya_3	37.2	0.5%	20.7%

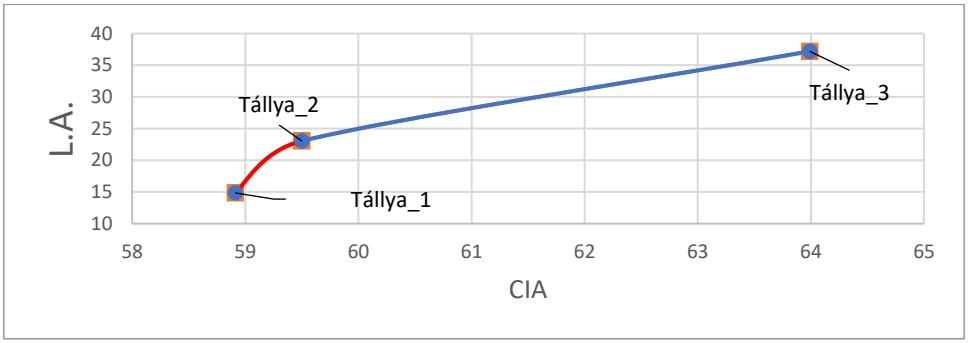

Figure 6
The relationship between LA values and CIA

4. DISCUSSION

In the present study, the relationship between mineral composition, texture, alteration and mechanical properties of andesites was investigated.

The mineralogical composition of the samples determined with XRD did not show significant difference in the case of rock forming minerals. The amount of K-feldspars showed an increase with the degree of alteration and a decrease with the decrease of the depth of the sample related to the surface and thus within the rock body. The amorphous content showed an inverse trend.

Based on the mineralogical results the positive influence of the quartz and the low quantity of amorphous material in the case of sample Tállya_1 is expected on the resistance to wear. The higher smectite content of the Tállya_3 sample has a negative influence on the mechanical properties of the sample. The increase of the K-feldspar and quartz content and decreasing smectite and amorphous content resulted in increasing resistance to the wear and LA values, thus the effect of the mineralogical composition is evident.

The optical microscopic observations revealed differences in the particle size and shape of phenocrystals. A decrease in the size of phenocrystal and the loss of their own shape could be observed with the increase of alteration, while an increase of the grain size of the matrix could be observed. The XRD and XRF result were used in the quantification of the alteration of the samples, complemented with the optical microscopic observation for the identification of the smectite type. The CIW and CIA are appropriate tools for quantifying the state of the alteration of samples, however we find the CIA to be more applicable in the case of our samples because of K content and Ca content in form of carbonates. The resistance to wear and fragmentation showed positive correlation with the alteration indices, but the change in the M_{DE} and LA values was not linear with the change in alteration indices. In the case of samples Tállya_1 and Tállya_2 the changes in the M_{DE} and LA values are also influenced by other petrological factors as the mineralogy and texture.

The grainsize of the matrix is the smallest in the Tállya_1 and the largest in the sample Tállya_3, which results decreasing cohesion between the grains [2], [9], as it is reflected in the results of the resistance to wear and fragmentation tests. The presumption that the irregular grain contact surface results in stronger intergranular bond [10], [11] was not supported by our results. Based on our optical microscopic observations the sample Tállya_2 should have resulted the highest M_{DE} and LA values. In the case of sample Tállya_3 the grain boundaries present greater irregularity then in the case of Tállya_2, but the alteration and the presence of smectite mineral plays a key role in the low resistance to wear and fragmentation.

The results showed that the examined mechanical properties of the Tállya andesites are complexly influenced by the textural and structural features, mineralogical composition, and alteration.

5. SUMMARY

The petrological properties of samples collected from Tállya quarry were determined. The XRD was used for the identification and quantification of mineralogical composition. The chemical composition was determined using XRF, from the results alteration indices were calculated for the quantification of the alteration. Polarised optical microscopy observations were made on thin section with the purpose of identifying main textural features and the type of alteration of the samples.

The resistance to wear was measured using the micro-Deval method recommended by the MSZ EN 1097-1 standard. The resistance to fragmentation was measured based on the MSZ EN 1097-2 standard using the Los Angeles method. The two methods apply different type of stresses, the Los Angeles test creates mainly impact stress, while the micro-Deval creates attrition. The two different stresses could result in different results, but the finding of our examination gave similar trends, the Tállya_1 sample representing the lowest M_{DE} and L.A. value, while the Tállya_3 the highest.

ACKNOWLEDGEMENT

Part of the project implemented in the framework of the Thematical Excellence Program funded by the Ministry of Innovation and Technology of Hungary (grant contract reg. nr.: NKFIH-846-8/2019) and the project supported by the Ministry of Innovation and Technology from the National Research, Development and Innovation Fund in line with the grant contract issued by the National Research, Development and Innovation Office (grant contract reg. nr.: TKP-17-1/PALY-2020)

REFERENCES

[1] Strzałkowski, P., Kaźmierczak, U. (2021). Wear and fragmentation resistance of mineral aggregates— a review of micro-deval and los angeles tests. *Materials*, Vol. 14, No. 18, MDPI, Sep. 01, 2021. https://doi.org/10.3390/ma14185456

[2] Abdelhaffez, G. S. (2020). Studying the effect of ore texture on the bond work index at the mahd ad dahab gold mine: A case study. *Rudarsko Geolosko Naftni Zbornik*, Vol. 35, No. 1, pp. 111–121, Feb. 2020. https://doi.org/10.17794/rgn.2020.1.9

[3] Adomako, S., Engelsen, C. J., Thorstensen, R. T., Barbieri, D. M. (2021). Review of the relationship between aggregates geology and Los Angeles and micro-Deval tests. *Bulletin of Engineering Geology and the Environment*, Vol. 80, pp. 1963–1980. https://doi.org/10.1007/s10064-020-02097-y/Published

[4] Bonnici, N. K. (2012). *The mineralogical and textural characteristics of copper-gold deposits related to mineral processing attributes*. Ph.D. thesis, University of Tasmania, p. 250.

[5] Oyarzún, M., Arevalo, A. (2011). Rock Texture and BWi Relationships, El Teniente Ore Deposit, Chile. In: *The First Ausim International Geometallurgy Conference*, 5–7 September 2011 Brisbane, Australia, pp. 181–186.

[6] Yuce, A. E. (2017). Grinding size estimation and beneficiation studies based on simple properties of ore components. *Physicochemical Problems of Mineral Processing*, Vol. 53, No. 1, pp. 541–552, 20. https://doi.org/10.5277/ppmp170142

[7] Akseli, T., Leinonen, S. (2015). Influence of Geological Characteristics on Mechanical Properties of Crushed Stone Aggregates Produced from Meta-Volcanic Rocks in Finland. In: *Engineering Geology for Society and Territory*, Volume 5. Manconi, A., Lollino G., Guzzetti F., Culshaw M., Bobrowsky P., and Luino F. (eds.). Cham: Springer International Publishing, 2015, pp. 111–114, https://doi.org/10.1007/978-3-319-09048-1_22.

[8] Tavares, L. M., das Neves, P. B. (2008). Microstructure of quarry rocks and relationships to particle breakage and crushing. *International Journal of Mineral Processing*, Vol. 87, No. 1–2, pp. 28–41, Apr. 2008. https://doi.org/10.1016/j.minpro.2008.01.007

[9] Popov, O., Talovina, I., Lieberwirth, H., Duriagina, A. (2020). Quantitative Microstructural Analysis and X-ray Computed Tomography of Ores and Rocks—Comparison of Results. *Minerals*, Vol. 10, No. 2, p. 129. https://doi.org/10.3390/min10020129

[10] Pérez-Barnuevo, L., Pirard, E., Castroviejo, R. (2013). Automated characterisation of intergrowth textures in mineral particles. A case study. *Minerals Engineering*, Vol. 52, pp. 136–142, Oct. 2013. https://doi.org/10.1016/j.mineng.2013.05.001

[11] Petruk, W. (2000). *Applied Mineralogy in the Mining Industry*. Elsevier. https://doi.org/10.1016/B978-0-444-50077-9.X5000-7

[12] Nesbitt, H. W., Young, G. M. (1982). Early Proterozoic climates and plate motions inferred from major element chemistry of lutites. *Nature*, Vol. 299, No. 5885, pp. 715–717, https://doi.org/10.1038/299715a0.

[13] Harnois, L. (1988). The CIW index: A new chemical index of weathering. *Sedimentary Geology*, Vol. 55, No. 3–4, pp. 319–322. https://doi.org/10.1016/0037-0738(88)90137-6

[14] MSZ EN 1097 -1:2012. *Standard Tests for mechanical and physical properties of aggregates*. Part 1: Determination of the resistance to wear (micro-Deval). Hungarian Standards Institution, pp. 0–45, 2012.

[15] MSZ EN 1097-2:2020. *Standard Tests for mechanical and physical properties of aggregates*. Part 2: Methods for the determination of resistance to fragmentation." Hungarian Standards Institution, pp. 0–14, 2020.

[16] Yıldırım, B. G. (2016). Development of a correlation between mineralogy, rock strength measures, and breakage of Copper Porphyries. Ph.D. thesis, Sustainable Minerals Institute, The University of Queensland, p. 293. https://doi.org/10.14264/uql.2017.34

Geosciences and Engineering, Vol. 10, No. 15 (2022), pp. 138–153.
https://doi.org/10.33030/geosciences.2022.15.138

PROBLEMS THREATENING SUSTAINABILITY IN SIWA OASIS AND RECOMMENDATIONS FOR UNDERSTANDING THE SOURCES OF WATER QUALITY DETERIORATION

MOHAMED HAMDY EID[*] [1, 2], PÉTER SZŰCS[1], ATTILA KOVÁCS[3]

[1]*Institute of Environmental Management, Faculty of Earth Science, University of Miskolc, 3515 Miskolc-Egyetemváros, Hungary*
mohamedhamdy@science.bsu.edu.eg, hgszucs@uni-miskolc.hu
[2]*Geology Department, Faculty of Science, Beni-Suef University Beni-Suef, 65211, Egypt, mohamedhamdy@science.bsu.edu.eg,*
[3]*MTA-ME Geoengineering Research Group, University of Miskolc 3515 Miskolc-Egyetemváros, Hungary, attila.geo.kovacs@gmail.com*
[*]*Corresponding author: Mohamed Hamdy Eid, mohamedhamdy@science.bsu.edu.eg*

Abstract: Siwa Oasis has been chosen as the location for the current investigations. Siwa Oasis is an isolated closed depression located in Egypt's Western desert. It is surrounded by the Mediterranean Sea to the north (about 330 km), to the west by the Libya-Egypt border (70 km) and Cairo to the east (560 km). There are three major activities in Siwa Oasis: that are represented by agriculture (palm tree, olive, fruits and vegetables), industry, (e.g. mineral water bottling and olive oil extraction), and tourism (medical treatment, safaris). The climate of the Western Desert, particularly in Siwa, is generally torrid and arid. The Siwa depression is occupied by Quaternary deposits (aeolian deposits and lakes), Middle Miocene, Upper Cretaceous (sandstone), and Precambrian (basement complex). The groundwater system in Siwa Oasis hastwo main productive aquifers: a Miocene aquifer (fractured limestone) and a Lower Cretaceous aquifer (Nubian Sandstone). Besides, the Quaternary (clay and sand) uppermost layer is water-bearing because of waterlogging. Siwa Oasis is suffering from waterlogging, increasing soil salinity, and deterioration of water quality in the aquifers. This review includes the problems in Siwa Oasis and recommendations for understanding hydrogeological situations and sources of water quality deterioration to avoid waterlogging and soil salinization through integration of flow modeling, geochemistry and isotopic tracers.

Keywords: *Siwa Oasis, groundwater aquifer system, soil salinity, waterlogging, water quality*

1. INTRODUCTION

In recent decades, much emphasis has been placed on the development of new settlements in Egyptian desert areas with significant groundwater potential in order to preserve the land in the Nile Delta and the Nile Valley. Efforts have been made in several integrated fields of study to achieve these goals. As Egypt is essentially a desert land (about 96 percent), much thought is given to the reclamation and use. Thus, many governmental institutions and private sectors have conducted studies in

the fields of geology, geophysics, hydrogeology, and for the selected desert in Egypt over the last two decades. These studies were carried out to ensure proper evaluation of new settlements. These areas include Siwa Oases, which is located in the Western Desert. The current study looks at how geological and hydrogeological techniques can be used to assess the potential of groundwater in the Siwa depression [1].

2. SITE DESCRIPTION

Siwa Oasis is an isolated closed depression located in the northwestern desert of Egypt. It is surrounded by the Mediterranean Sea to the north (about 330 km), to the west by the Libya-Egypt border (70 km) and by Cairo (560 km) from the east *(Figure 1)*. The depression is situated between latitude 29.12 N and longitude 25.43 E. There are three major activities in Siwa Oasis: agriculture (palm tree, olive, fruits and vegetables), industry, (including among others mineral water bottling and olive oil extraction), and tourism (medical treatment and safaris) [3].

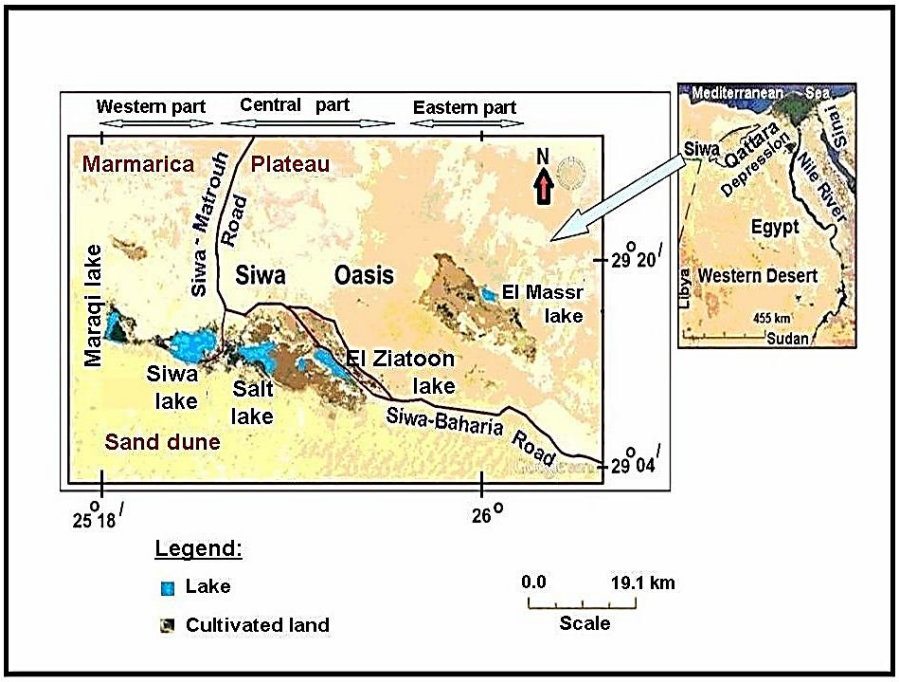

Figure 1
Siwa Oasis location map, Western Desert, Egypt [3]

The length of Siwa depression has elongated shape, which is about 82 km in E-W direction and its width ranges from 2 to 20 km. The total area of Siwa Oasis is approximately 1,050 km^2 (250,000 feddans). In 2010 the population in Siwa Oasis had reached about 23,546 residents [4].

3. GEOMORPHOLOGY OF SIWA OASIS

The topography of Siwa Oasis includes a terrain with an elevation range from 19 m below sea level to 154 m above sea level. The different geomorphological units in the area are mobile sand dunes, which are located along the southern part, a steep escarpment of limestone plateau situated in the northern part, and a flat depression that includes the agricultural land, salt lakes and playas in the center of Siwa Oasis [5, 6]. The major lakes in the flat depression are Maasir, Zeitoun, Aghourmy, Siwa, and Maraqi lakes, from west to east *(Figure 2)*. Water bodies of these salt lakes come from different sources such as drainage water from agricultural land, dug wells and springs [7].

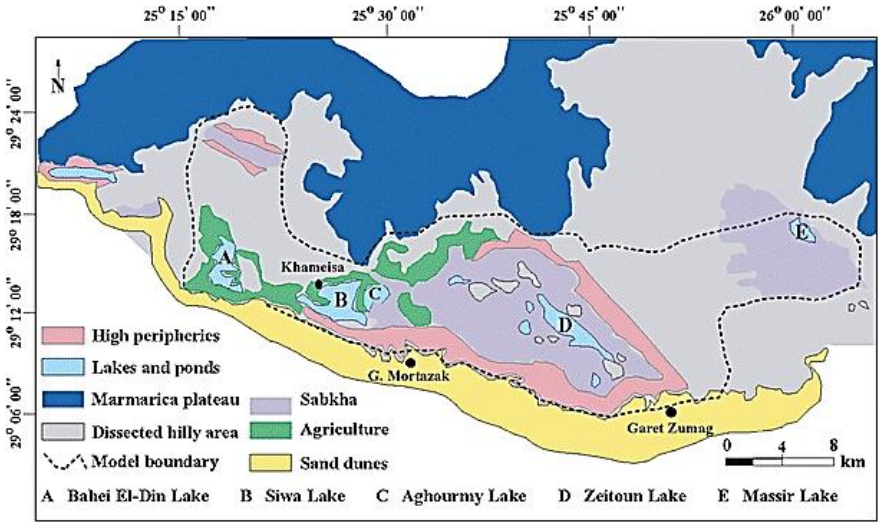

Figure 2
Geomorphological map of Siwa Oasis [7]

4. CLIMATE OF SIWA OASIS

Siwa Oasis is characterized by an extremely arid climate which is cold in winter and hot and dry in summer [8]. The different elements of climate in Siwa area are represented as follows:

4.1. Air temperature

Average air temperature ranges annually from low (14.12 °C) to high (29.32 °C) temperatures [8].

4.2. Soil temperature

The temperature of the soil at a depth of about 5 cm reaches a maximum value of 32.8 °C [9].

4.3. Wind direction

Wind in Siwa Oasis has three different directions: SE, NW and NE with different ratios (12.4%, 24.4% and 18.2%, respectively). The effect of wind from erosion and deflation becomes more obvious in April, when it carries salt particles and loose sand, transporting and depositing them in low land area through sequence in Siwa depression. The impermeable bed of soil is eroded, causing a decrease in the soil profile, hence the water table is raised [9].

4.4. Relative humidity and evaporation

The relative humidity in Siwa Oasis is about 45.3%. The rate of evaporation increases in Siwa due to high solar radiation and dryness of depression. Evaporation rate reaches 16.8 mm/d in summer, while in winter it attains about 5.4 mm/d [8]. High evaporation and evapotranspiration play an important role in salt weathering, leading to capillary rise of ground water to the surface sediments. For this reason, salt crystals are concentrated in surface soil and accelerate salt weathering [9].

4.5. Rainfall

Rainfall in the Siwa area is negligible, with annual precipitation about 10 mm [8].

5. GEOLOGY OF THE SIWA DEPRESSION

5.1. Surface geology

The stratigraphy of rocks that are exposed to the surface of Siwa Oasis is outlined as follows:

a) Quaternary deposits: these deposits include sand dunes in the southern part of Siwa depression and sabkhas (evaporite deposits of clay and silts) (see *Figure 9*),
b) Middle Eocene: these rocks consist of chalky limestone and neritic limestone intercalated with shale, which covers the southern area of the depression.

In the northern part of Siwa there are several drainage lines that are affected by a fracture system having two major directions (NE-SW and NW-SE).

5.2. Subsurface geology

The sequence of subsurface stratigraphy includes Palaeozoic, Mesozoic and Cainozoic strata. This sequence consists of two major cycles of deposition (clastic and carbonate deposition) *(Table 1, Figure 4)*.

The formation of Paleozoic and Mesozoic represent a clastic facies cycle (oldest sedimentary rocks). The cycle of carbonate facies consist of two formations (tertiary Eocene and Miocene). A Paleozoic, Mesozoic and Cainozoic stratigraphic sequence is located above basement rocks and affected by normal faults in different directions (N-S, E-W, NW-SE and NE-SW, *Figure 3*) [5, 10].

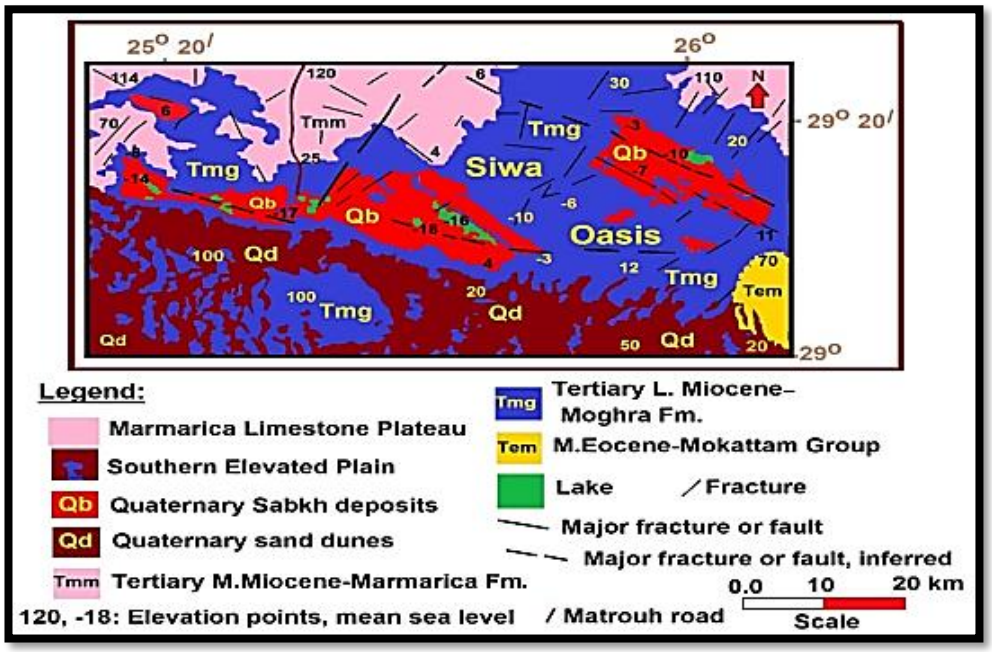

Figure 3
Surface geologic map of Siwa Oasis [11]

Table 1
Geologic formations of Siwa Oasis, Egypt [10–12, 13]

Era	Age	Log	Average Thickness	Lithic description	Depositional environment
Cenozoic	Tertiary – Miocene		250 m	Limestone with marl (Marmarica Fm.)	Shallow marine
				Sandstone, siltstone, shale (Moghra Fm.)	Fluvio-Marine
	Tertiary – Eocene		350 m	Limestone intercalated with shale, marl, evaporites beds (Mokattam Gr.)	Shallow marine
Mesozoic	Cretaceous		600 m	Sandstone with shale and carbonate intercalations (L. Cretaceous), overlain by impermeable layer of carbonaceous shale and argiliceous limestone (U. Cretaceos)	Shallow marine, near shore
Paleozoic	Carboniferous		912 m	Sandstone with shale and limestone	Near shore, Continental
	Devonian		347 m	Mudstone, siltstone, carbonaceous sandstone, limestone&dolomite	Fluviatile, Continental, Shallow marine
	Silurian		626 m	Mudstone and siltstone (Kohla Fm.)	Fluviatile, Marine
	Ordovician / Cambrian		315 m	Sandstone intercalated with shale and siltstone beds	Continental
Pre-Cambrian			?	Basement complex, Granite, Gneisses	

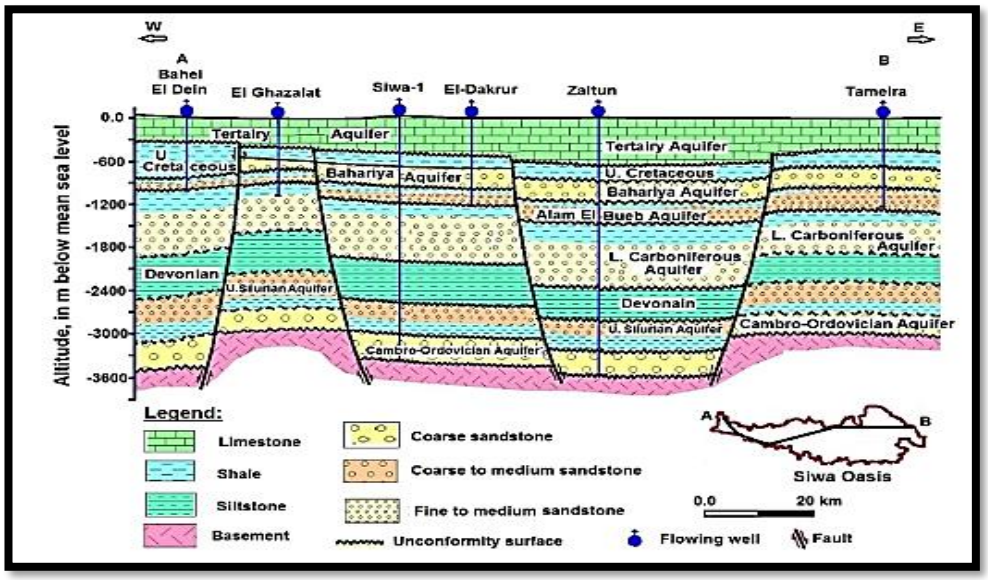

Figure 4
Cross section of hydrogeology in Siwa Oasis [14]

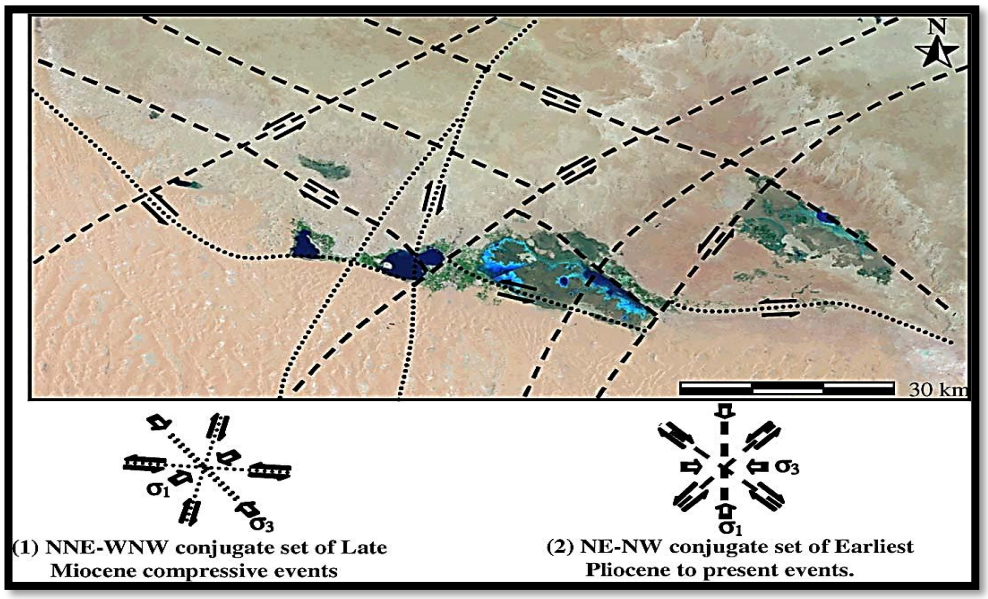

Figure 5
Major morphotectonic conjugate set of faults overlaying the Landsat742 RGB of 2003 image and proposed model of deformation in Siwa region [15]

6. TECTONIC ARCHITECTURE AND RELATIONSHIP TO THE HYDROGEOLOGICAL SETTING

Siwa depression is characterized by different tectonic architectures such as faults and fractures, but these features are poorly exposed because they are covered by sand dunes. However, these fracture zones on the earth's surface are important with respect to subsurface fluid flow. Siwa Oasis was formed by successive tectonic events and took its shape through topographic processes. The presence of surface linear features such as springs, lakes, and surface ponds gives an indication of vertical and near vertical fracture zones. The main controlling factor of connection between groundwater aquifers and lakes is fractures and faults. There are four main directions of vertical and near vertical fracture zones (NW-SE, NE-SW, WNW-ESE and NNE-SSW) in addition to, two sets of faults nearly perpendicular. The high conductivity between Siwa Lakes and groundwater is the result of the two sets of faults intersecting these lakes [15].

7. WATER RESOURCES

7.1. Surface water

The main reason for attracting Bedouin people to live in Siwa area was the presence of four water lakes before deterioration of the water quality of lakes by high salinity. The two major factors responsible for the increasing salinity of water lakes are the high evaporation rate and discharge from drainage of agricultural land.

Recently Siwa Oasis has begun to have serious problems with waterlogging. This problem derived from over-irrigation by flooding, where the excess water seeps downward to a shallow aquifer which is separated from the Miocene aquifer below; hence, the water table rises to or near to the ground surface. Drainage water from agricultural land contains a high concentration of anions and cations that causes increasing salinity of the shallow aquifer. Because of high salinity of water lakes, it is no longer suitable for domestic use, meaning that the demand for extraction of groundwater from the aquifer increased. More than 95% of water users in the Siwa area depend on groundwater [16].

7.2. Groundwater

Based on the hydrogeological setting of Siwa depression, there are five aquifers arranged from top to base:

1. Quaternary deposits (shallow aquifer),
2. Miocene,
3. Eocene,
4. Upper Cretaceous (carbonate aquifer),
5. Nubian sandstone aquifer (lower Cretaceous) [14, 17].

The most important aquifer is the Nubian aquifer, which is used for drinking, domestic use, and irrigation. It is characterized by high water quality of water according to WHO (1984).

7.2.1. Aquifer systems

There are five major aquifers in Siwa Oasis [6].

a) Shallow aquifer (Quaternary deposits)

People in Siwa do not use the Quaternary aquifer for irrigation or domestic use due to deterioration of water quality of the aquifer. This aquifer contains water with salinity (42,000 ppm) higher than the Miocene, Eocene and Nubian aquifers. The higher salinity comes from the downward seepage of water from agricultural land. The water table is found in shallow depths ranging from 0.25 m to 1.75 m below ground surface.

b) Miocene aquifer

This is the main aquifer in Siwa Oasis for irrigation purposes because of its low cost in drilling compared to the Nubian aquifer. This aquifer consists of fractured limestone which is located below the Quaternary aquifer. The water table depth in the Miocene aquifer ranges between 40 and 130 m below ground level. In some areas, the water quality of Miocene aquifer began to deteriorate, where salinity ranges from 2,000 to 4,000 ppm. The amount of water extracted from this aquifer reached about 100 million m^3 per year [19].

c) Eocene aquifer

This aquifer is not used for irrigation or drinking water as a result of the high salinity of its water, which ranges from 3,000 ppm to 16,000 ppm. The depth of the water table in the Eocene aquifer ranges between 220 m and 450 m.
The Eocene aquifer is composed of fractured limestone and dolomite and overly upper Cretaceous aquifer. Most of the springs in Siwa Oasis flow from this aquifer [19, 20].

Upper Cretaceous aquifer

This aquifer is a carbonate aquifer consisting mainly of fractured limestone intercalated with shale and overlain Nubian sandstone aquifer. There is not a large number of wells to extract groundwater from this aquifer owing to its salinit,y which ranges between 2,000 ppm and 8,000 ppm.
The water table is found at different depths between 395 m and 575m BGL. Most of the springs that flow naturally in the Siwa area feed from this aquifer and are used for medical purposes and tourism [19, 20].

d) Nubian sandstone aquifer (NSSA)

The NSSA is considered to be the main aquifer responsible for life in Siwa Oasis. It contains water with high quality which is suitable for both drinking and irrigation. Salinity of groundwater in the Nubian sandstone aquifer is the lowest

in Siwa, ranging from 500 ppm to 600 ppm. Farmers in Siwa find it difficult and expensive to drill wells in this aquifer due to its depth, ranging between 950 m and 1200 m [19]. About 95% of domestic, irrigation and drinking water comes from this lower Cretaceous aquifer (NSSA).

8. DESCRIBING THE HISTORICAL DEVELOPMENT OF THE STUDY AREA

In 1963, there were less than 200 springs of any use with depth about 12 m below the ground level [21]. From 1981 to 1996, farmers began to drill thousands of wells in the fractured limestone aquifer with poor design, which produced an excess of water and formed the lakes in the low land of the Siwa depression and led to the continuous deterioration of agricultural land. During this period, all wells were drilled in the shallow aquifers (carbonate aquifer) with no controlling valves and no casing. The total discharge from these wells reached to 400,000 m^3/d, where only 60% wasused for irrigation and excess water was discharged into lakes [22]. From 1996 to 2001, different actions occurred. One of them aimed at the rehabilitation of poorly designed wells (400 wells), while 665 wells were still with low priority. Continuous drilling of new wells made the problem worse with time.

9. GROUNDWATER DISCHARGE

The total amount of water that is discharged into different lakes is about 146 million m^3/year, *Table (2)* [22].

Table 2

Daily and annual flow from springs and wells

Catchment Area	Discharge rate (m^3/day)	Discharge rate (m^3/year)
El Maraqi	60,000	21,900,000
Siwa	140,000	51,100,000
Aghourmi	120,000	43,800,000
Zeitoun	80,000	29,200,000
	400,000	**146,000,000**

As a result of measured taken by the government from 1996 to 2001, the total amount of ground water discharge was reduced to 130 million m^3/year, *Table (3)*. The total amount of groundwater discharged into the lakes caused by poorly designed wells is 51 million m^3/year.

Table 3

Daily and annual flow from springs and wells [22].

Catchment Area	Total discharge rate (m^3/ y)	Cult. Area (Fed.)	Demand (m^3/y)	% Losses to the Lake related to total discharge
El Maraqi	25,820,940	1413	10,597,500	49 %
Siwa	65,208,600	5066	38,000,000	42 %
Aghurmy	26,417,820	2751	20,632,500	22 %
Zeitun	12,249,120	1283	9,622,500	22 %
Total	**129,696,480**	**10,513**	**78,847,500**	**39 %**

10. THE MAIN FACTOR CONTROLLING THE SUSTAINABLE DEVELOPMENT OF SIWA OASIS GROUNDWATER QUALITY

Water quality changes from the deeper aquifer (NSSA) to shallow aquifers (fractured limestone aquifers). Water in the Nubian sandstone aquifer is characterized by high quality, and water salinity ranges from 200 ppm in the upper zone (500 m thick) to 1500 ppm in the lower part of the aquifer. There is water quality deterioration for the fractured limestone aquifers through the leaching of salts during movement of water upward and interaction with the shale, clay and evaporite that are intercalated with the carbonate rocks [14].

11. THE MAIN PROBLEMS THROUGH PREVIOUS WORK IN SIWA OASIS

Waterlogging is the most significant problem in Siwa Oasis, with a continuous rise in the water table. Furthermore, there is deterioration of fertile soil because of soil salinization. The water table rose by 1.33 cm per year in the period from 1962 to 1977 but this rate changed to 4.6 cm per year in the period from 1977 to 1990. The main factors behind this phenomenon are the expansion in agriculture, with poor management and over-irrigation by flooding with poor drainage systems [23].

There is a decrease in vegetation cover in Siwa Oasis and an increase in soil salinity due to over-irrigation, which resulted in the rising water table. This appeared between 1987 and 1999. The salinity index was increased to double over 12 years. The water table was elevated from 1.2 m below the ground surface in 1987 to 0.54 m in 1999 [24].

The Siwa depression contains different tectonic architectures such as faults and fracture systems that are poorly exposed to the ground surface as a result of sand dune cover. The main reason for the formation of springs, lakes and surface ponds is the presence of vertical or near vertical fracture zones. Moreover, the two sets of faults make a connection between groundwater and lakes. The fracture system took three main directions NW-SE, NE-SW, WNW-ESE and NNE-SSW [25].

After 2000, soil salinization increased in Siwa Oasis, which led to the death of plants and agricultural deterioration. The reason for increasing soil salinization is the lack of good drainage system, poor management of available water resources, over-irrigation by flooding, and a very small amount of precipitation [25].

The total area of salt flats surrounding the lakes in Siwa depression increased by 20.55 km^2 from the year 1933 to 2002. The activity of salt weathering changes from one place to another according to changes of acceleration process. In low land areas around saline lakes, the activity of salt weathering reaches its maximum value [9].

Agriculture is progressively deteriorating in Siwa Oasis as a result of desertification. The negative impact of desertification appears in decreasing vegetation cover from date palms and olive trees [27].

The salt lakes in Siwa depression could be converted to a basin through the construction of a wall around marshes and lakes. The high evaporation rate in the summer will reduce the water level of lakes and produce karshef, a material made up of fossilized salt that settles on the shores of Siwa lakes. It is collected, mixed

with mud and water, and used to construct low-rise buildings with thick walls and shallow foundations. Walls constructed of karshef can help make the land be suitable for agriculture again [28].

The soil in Siwa depression contains 34 elements (Ca^{2+}, Na^{+}, Al, Mg^{2+}, V, Mn, Ti, Cr, Fe, Zn, Br, Ni, As, Co, Sr, Br, Zr, Rb, Cs, Sb, Ba, I, Eu, Ce, Tb, Nd, Dy, Yb, U, Tm, Ta, Hf, Th). The origin of iodine and chloride are the Siwa lakes, while arsenic originated naturally in soil owing to the absence of industrial activity. The elements Hf, Sc, La, Zr and Th, which have low solubility, originated from sediments and continental rocks [29].

There is variation in the water quality in different locations within Siwa Oasis. Salinity hazards increased at a high rate and resulted in excessive deterioration of water quality and the water became not within the acceptable limits of irrigation. The poor water quality is due to unsafe abstraction from NSSA, where it reduces the vertical movement of fresh water from NSSA to shallow limestone aquifer. Toxic elements such as boron are presented in specific locations exceeding the permissible level of concentration [30].

The water resources in the western and central part of Siwa depression have different characteristics. NSSA contains fresh water with low TDS, pH > 7(alkaline), meteoric water, and less mineralized water. The concentration of heavy metals in NSSA is lower than in springs, lakes and TCAS. In the central part of Siwa Oasis there are increasing concentrations of radiochemical constituents such as TDS, heavy metals and major ions. The activity concentration of ^{40}K, ^{232}Th and ^{226}Ra reached maximum values of 25.6 ±5.9 Bq/l (TCAS), 6.7 ±1.6 Bq/l (TCAS) and 5.6 ±0.7 Bq/l (NSSA) respectively. TCAS contains brackish water with TDS ranges from 1903 mg/l to 10,125 mg/l, $p^H > 7$ and three genetic types of water, Cl-Ca, Cl-Mg and SO_4-Na. The first and second type of water refer to the interaction of water with evaporite and marine deposits while the third type indicates the recharge from NSSA. Most of the springs contain brackish water with pH > 7 and have two genetic types of water (Cl-Ca and Cl-Mg types) indicating marine origin. Water of the lakes contains brine water with pH < 7 (acidic) and two genetic types of water, SO_4-Na and Cl-Ca [3].

There is low diversity in the bacterial composition of the three lakes (Maraqi, Zeiton and Aghormy) in Siwa Oasis, which indicates a hypersaline environment. The three lakes contain Bacteriodetes-like phylotypes while Maraqi and Zeiton are also characterized by the presence of Alphaproteobacteria-like phylotypes [3].

Surface water in Siwa Oasis came from deeper aquifers passing through fracture system and fault plain. The two major fault lines in Siwa depression are ESE-WNW and ENE-WSW. Salts became concentrated in lakes because of evaporation [31].

The most serious problems associated with the groundwater in Siwa Oasis are the following: waterlogging phenomenon [32], rapid falling water level and groundwater depletion [33–34,35], salt water intrusion [36–37,38] and disturbance to the overall groundwater system [39–42,43], and contamination of high groundwater quality of the deep Nubian sandstone aquifer with radionuclides [44]. The situation becomes worse when high natural discharge of poor-quality groundwater through natural springs and/or uncontrolled dug wells is involved, which is observed in Siwa Oasis.

12. RECOMMENDATIONS AND REQUIRED ANALYSIS TO UNDERSTAND THE HYDROGEOLOGICAL SYSTEM OF SIWA OASIS FOR SUSTAINABLE MANAGEMENT

12.1. Goals

This proposal aims at groundwater management to maintain and improve the state of water resources in Siwa Oasis. The principal objectives of water resources management and plans are to grant the increasing water demands for different uses in the most environmentally effective, socially acceptable, and economically efficient manner. Additionally, it is necessary to evaluate factors in the deteriorating groundwater quality in Eocene, Miocene and Nubian sandstone aquifer using geochemical modeling and isotope traces.

12.2. Methodology

12.2.1. Sampling

Water samples should be collected from groundwater aquifer systems including Nubian sandstone, Eocene, Miocene and Quaternary aquifers as well as surface waters (lakes, springs and drains). The sampling plan should cover the entire Siwa Oasis.

12.2.2. Measurements and analyses

The required analyses are as follows:

a. ***Field parameters*** including water temperature, pH, TDS, TSS, dissolved oxygen, electrical conductivity and salinity.

b. ***Laboratory measurements*** including ammonia, nitrate, nitrite, ortho-phosphate, sulfate, chloride, total hardness, total alkalinity, calcium, magne-sium, sodium, potassium, and heavy metals.

c. **Isotope analysis** such as stable isotopes $\delta^{18}O$, $\delta^{2}H$, $^{87}Sr/^{86}Sr$, ^{11}B, uranium ^{235}U, thorium, radon Ra, chlorine isotopes ^{36}Cl and ^{37}Cl.

d. **Data analysis and modelling**

- Analysis of potentiometric data and depth-pressure profiles to understand hydrodynamic conditions.
- Groundwater modeling of Siwa Oasis and its environs to understand driving forces, hydrodynamic processes and to provide predictions and analyze groundwater extraction scenarios.
- Geochemical modeling of groundwater-rock interaction (NETPATH Geocehmical Model) to detemine groundwater origin and boundary conditions for solute transport models.

- Solute transport modeling using the calibrated groundwater model to simulate salinization processes and to provide predictions and a management plan for decision makers.
- Synthesis of results and reporting: In the final stage of the reserach, the results achieved should be analyzed and synthesized to provide a coherent hydrogeological-geochemical description of the Siwa Oasis system and to provide recommendations for sustainable groundwater management.

REFERENCES

[1] El-Deen, H. M. M. E. (2021). Ground Water Potentiality in Siwa and Baris Oases, Western Desert, Egypt. In: *Groundwater in Egypt's Deserts*. Springer, Cham, pp. 131–152, https://doi.org/10.1007/978-3-030-77622-0_6.

[2] El-Naggar, H. M. (2010). Environmental engineering interventions to control the expansion of salty lakes and marshes in Siwa Oasis. *The Journal of the Egyptian Public Health Association*, 85 (3–4), pp. 223–245.

[3] El-Sayed, S. A., Allam, K. A., Salama, M. H., El Begawy, H. (2017). Investigation of chemical and radiochemical fingerprints of water resources in Siwa Oasis, Western Desert, Egypt. *Arab Journal of Nuclear Science and Applications*, 50 (1), pp. 158–178.

[4] Siwa Information Center, 2009. *Statement Support Centre and decision-making.* Matrouh Governorate, p. 6.

[5] Said, R. (ed.) (1962) *The Geology of Egypt*. New York, Elsiever.

[6] Abou El-Magd, I., Faid, A. (2007). Hydrogeological and environmental studies on Siwa Oasis, Egypt Using GIS technique. *Egypt. J. Soil Sci*, 47, pp. 435–450.

[7] Abdulaziz, A. M., Faid, A. M. (2015). Evaluation of the groundwater resources potential of Siwa Oasis using three-dimensional multilayer groundwater flow model, Mersa Matruh Governorate, Egypt. *Arabian Journal of Geosciences*, 8 (2), pp. 659–675.

[8] Abdel-Mogheeth, S. M. (1996). Groundwater hazards in Siwa Oasis, Egypt. *Proceedings of the UNESCO/NWRC/ACSAD Workshops on Wadi Hydrology and Groundwater Protection*, Cairo, Egypt, 3–6 June, pp. 113–118.

[9] Abdallah, A. (2007). Assessment of salt weathering in Siwa Oasis (The Western Desert of Egypt). *Bull. De la Soc. De Geog. De Egypt*, 80, pp. 66–83.

[10] Afifi, A. H., 2005, *Assessment of the hydrogeological conditions of groundwater in Siwa Oasis, North Western Desert, Egypt*. Ph.D. Thesis, Minufiya University., Egypt.

[11] CONOCO (Conoco Coral) (1986). *Geologic map of Egypt, scale 1:500000*. Sheet No. NH 35 SW Siwa: The Egyptian General Petroleum Corporation, Cairo, Egypt.

[12] GPC (the Egyptian General Petroleum Corporation) (1992). *Western Desert, oil and gas fields* (A comprehensive Overview). New Maadi, Cairo, Egypt, EGPC.

[13] Ibrahim, S. A. (1991). *Studies on groundwater possibilities in the northern part of the Western Desert Egypt*. Ph.D. Thesis, Cairo University, Cairo, Egypt.

[14] El Hossary, M. F. (2013). Investigating the development challenges to Siwa Oasis, northwestern desert, Egypt. *New York Science Journal*, 6 (4), pp. 55–61.

[15] Masoud, A., Koike, K. (2006). Tectonic architecture through Landsat-7 ETM+/SRTM DEM-derived lineaments and relationship to the hydrogeologic setting in Siwa region, NW Egypt. *Journal of African Earth Sciences*, 45 (4–5), pp. 467–477.

[16] Abou El-Magd, I., Faid, A. (2007). Hydrogeological and environmental studies on Siwa Oasis, Egypt Using GIS technique. *Egypt. J. Soil Sci*, 47, pp. 435–450.

[17] Dahab, K. A. (2004). Impact of the present groundwater exploitation system on the Nubia sandstone aquifer in Siwa Oasis, Western Desert, Egypt. *Proc., onf. on Geochemistry*, Alexandria University, Egypt, pp. 319–337.

[18] World Health Organization (WHO) (1984). *International standards for drinking water*. 3rd Edition. Vol. 1, Geneva, Switzerland, 130.

[19] RIGW (2000). *Groundwater at the Northwestern Coast*. Report prepared for NWRP, RIGW, and Cairo, 2001.

[20] Aggour, T. A., Faid, A. M. (2006). Hydrogcology of Siwa Oasis and Landuse map. *Egypt Journal of Remote Sensing & Space Sciences*, 9, pp. 135–156.

[21] Misak, R. F., Baki, A. A., & El-Hakim, M. S. (1997). On the causes and control of the waterlogging phenomenon. Siwa Oasis, northern Western Desert, Egypt. *Journal of Arid Environments*, 37 (1), 23–32.

[22] RIGW (1996). *Well inventory in Siwa Oasis*. Res. Inst. Groundw. (RIGW), Natl. Water Res. Center, Minist. Water Resour. Irrig. Cairo, Egypt.

[23] Misak, R. F., Baki, A. A., El-Hakim, M. S. (1997). On the causes and control of the waterlogging phenomenon, Siwa Oasis, northern Western Desert, Egypt. *Journal of Arid Environments*, 37 (1), pp. 23–32.

[24] Madani, A. A. (2005). Soil salinity detection and monitoring using Landsat data: A case study from Siwa Oasis, Egypt. *GIScience & Remote Sensing*, 42 (2), pp. 171–181.

[25] Masoud, A. A., Koike, K. (2006). Arid land salinization detected by remotely-sensed landcover changes: A case study in the Siwa region, NW Egypt. *Journal of Arid Environments*, 66 (1), pp. 151–167.

[26] Ibrahim, H. A., Kamh, G. E. (2006). Geoenvironmental studies on conservation of archaeological sites at Siwa Oasis, Egypt. *Environmental Geology*, 49 (4), pp. 511–519.

[27] Samy, A. R. (2010). A desertification impact on Siwa Oasis: Present and future challenges. *Research Journal of Agriculture and Biological Sciences*, 6 (6), pp. 791–805.

[28] El-Naggar, H. M. (2010). Environmental engineering interventions to control the expansion of salty lakes and marshes in siwa Oasis. *The Journal of the Egyptian Public Health Association*, 85 (3–4), pp. 223–245.

[29] Badawy, W. M., Ali, K., El-Samman, H. M., Frontasyeva, M. V., Gundorina, S. F., Duliu, O. G. (2015). Instrumental neutron activation analysis of soil and sediment samples from Siwa Oasis, Egypt. *Physics of Particles and Nuclei Letters*, 12 (4), pp. 637–644.

[30] Aly, A. A., Kishk, F. M., Gaber, H. M., Al-Omran, A. M. (2016). Long-term detection and hydrochemistry of groundwater resources in Egypt: case study of Siwa Oasis. *Journal of the Saudi Society of Agricultural Sciences*, 15 (1), pp. 67–74.

[31] El Awad, M, A, M., Gad, A., Garamoon, H, K., El Malky, M, G. (2018). Geochemical assessment of the Quaternary soil in Siwa Oasis, Western Desert, Egypt. *Journal of Environmental Science*, 43 (2), pp. 25–45.

[32] Masoud, A., Koike, K. (2004, September). Soil salinity induced land cover change detection and analysis in Siwa region, NW Egypt. In: *Proc., International Symposium on Geoinformatics for spatial Infrastructure Development in Earth and Allied Sciences (GISIDEAS04)*, Hanoi, Vietnam, pp. 16–18.

[33] Venot, J. P., Molle, F. (2008). Groundwater depletion in the Jordan Highlands: can pricing policies regulate irrigation water use? *Water Resources Management*, 22 (12), pp. 1925–1941.

[34] Konikow, L. F., Kendy, E. (2005). Groundwater depletion: A global problem. *Hydrogeology Journal*, 13 (1), pp. 317–320.

[35] Nour, S. (1996). Groundwater potential for irrigation in the East Oweinat area, Western Desert Egypt. *Environmental Geology*, 27 (3), pp. 143–154.

[36] Kashef, A. A. I. (1983). Salt-Water Intrusion in the Nile Delta. *Groundwater*, 21 (2), pp. 160–167.

[37] Ebraheem, A., Riad, S., Wycisk, P., El-Nasr, A. S. (2002). Simulation of impact of present and future groundwater extraction from the non-replenished Nubian Sandstone Aquifer in southwest Egypt. *Environmental Geology, 43* (1–2), pp. 188–196.

[38] Werner, A. D., Simmons, C. T. (2009). Impact of sea-level rise on sea water intrusion in coastal aquifers. *Groundwater*, 47 (2), pp. 197–204.

[39] Vrba, J., Pêkný, V. (1991). Groundwater-quality monitoring—effective method of hydrogeological system pollution prevention. *Environmental Geology and Water Sciences*, 17 (1), pp. 9–16.

[40] Abdelaziz Ali Ismael, A. M. (2007). Applications of remote sensing, GIS, and groundwater flow modeling in evaluating groundwater resources: Two case studies; East Nile Delta, Egypt and Gold Valley, California, USA.

[41] Ahmed, M. A., Samie, S. A., Badawy, H. A. (2013). Factors controlling mechanisms of groundwater salinization and hydrogeochemical processes in the Quaternary aquifer of the Eastern Nile Delta, Egypt. *Environmental Earth Aciences*, 68 (2), pp. 369–394.

[42] Pahl-Wostl, C. (2007). Transitions towards adaptive management of water facing climate and global change. *Water Resources Management*, 21 (1), pp. 49–62, https://doi.org/10.1007/s11269-006-9040-4-4.

[43] Biswas, A. K. (2004). Integrated water resources management: a reassessment: a water forum contribution. *Water International*, 29 (2), pp. 248–256.

[44] Allam, K. A. (2019). Radiological Risk Estimation of Drinking and Irrigation Water from Siwa Oasis, Western Desert, Egypt. *Journal of Radiation and Nuclear Applications*, 4 (3), pp. 193–199.

Geosciences and Engineering, Vol. 10, No. 15 (2022), pp. 154–172.
https://doi.org/10.33030/geosciences.2022.15.154

CHARACTERIZATION OF SOIL MOISTURE REGIME IN THE KAIROUAN REGION, TUNISIA

MOHAMED RAJHI[1], ENDRE DOBOS[2]
[1]*m.rajhi.inat@gmail.com, https://orcid.gov/0009-0006-2842-6240*
[2]*ecodobos@uni-miskolc.hu, https://orcid.org/0000-0002-9798-6376*

Abstract: Soil moisture (SM) is a major factor in agricultural practices and earth surface processes. Remote sensing has been widely applied to estimate the soil moisture. However, it is still a challenge to describe the horizontal and vertical availability and the redistribution of soil moisture in time. Therefore, it is necessary to develop a soil hydrological model capable of estimating soil moisture variation with high accuracy, which is important in planning and efficient use of land resources. Many methods based on optical or radar satellite data have already been developed to estimate SM under various climatic conditions and geographical distribution.

In this study, the agricultural region of Kairouan in central Tunisia was chosen as a study area. To perform SM estimation, we analyzed the relation between the optical satellite data indices, such as the NDVI and the NDWI, and the radar data. In addition, we studied the correlation between the different backscatters (V, H), optical data, DEM and the environmental covariates in order to extract the highest correlation and the most informative data sources. These results will be the input of our model. The combination of remote sensing data, the environmental variables and the associate geospatial data can provide valuable information for soil moisture estimation; this has the potential to support decision making to optimize the land use structure and the water resources management, and for use in precision agricultural applications.

Keywords: *Soil moisture, digital soil mapping, Remote sensing, Radar, Optical, Kairouan plain*

1. INTRODUCTION

Today, the world faces many challenges, such as food security, scarcity of water resources, climate change, and degradation and contamination of soils by salts, the so-called soil salinization. The social-economic reality of farmers in the center of Tunisia is very critical, because agriculture is the only means of making a living, but soil degradation and the uncontrollable variation in soil moisture threatens the lives of the inhabitants of these regions and the disruption of the demographic, economic and environmental ecosystem.

Soil moisture is described as the water available in the unsaturated soil surface derived from rainfall, snowmelt, or capillary attraction from groundwater [1]. The intricate connection between rainfall and soil moisture is of utmost importance in the field of land surface hydrology [2]. Therefore, there is a crucial need for an in-depth

study of the soil's characteristics and spatiotemporal distribution of the soil moisture in order to set up a monitoring system to aid in decision-making.

2. STUDY AREA

The governorate of Kairouan, located in the central region of the country *(Figure 1)*, occupies a strategic position at the regional and the national level. It extends over 658,000 ha and is in the form of a wide corridor of plains, which are limited to the west by mountainous areas and to the east by depressions made up of sebkhas. This natural environment is a made up of quite contrasting physical units (plains, hills, and mountains) offering climatic nuances and different resources, which necessarily generate specific uses and modes of occupation [3].

The study area, corresponding to the Merguellil basin, is included in the Kairouan plain. It is one of the three largest river basins on the southern flank of the Tunisian ridge, flowing into the Kairouan plain [4]. It is a relatively large homogeneous valley, but is also very sensitive to erosion [5]. The basin consists of two geographically dissimilar parts. The upstream section, which corresponds to the El Haouareb Dam's watershed, is mountainous. The Kairouan alluvial plain encompasses the downstream part [6].

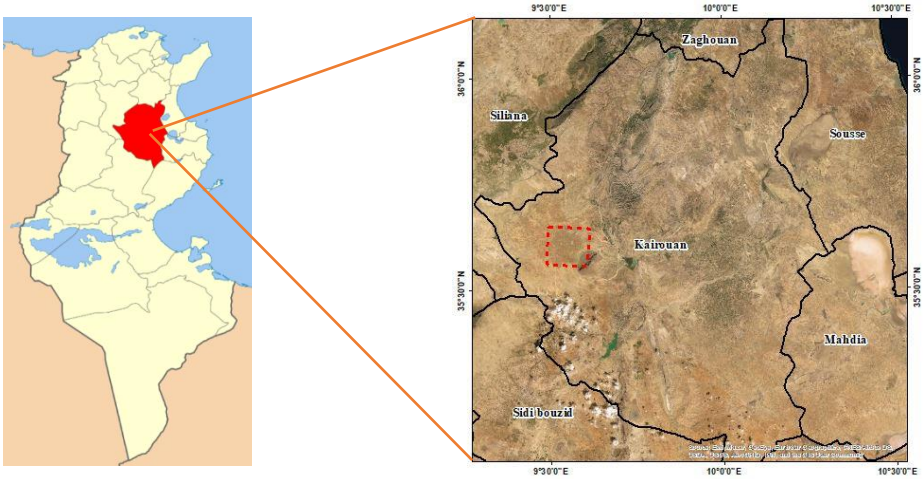

Figure 1
Study area – Merguellil downstream basin of the Kairouan plain [7]

The Merguellil upstream catchment (1200 km²) has a hilly topography (altitudes ranging from 200 to 1200 m, with a median elevation of 500 m) and diverse geology, morphology, vegetation, and land-use conditions. The Merguellil downstream watershed is part of the very large and flat Kairouan alluvial plain, which extends over about 3000 km² and with the altitude decreasing very gradually from 200 m to 80 m. [8] Our study area, the downstream part of the watershed, covered an area of 87 km² close to the dam, west of Kairouan city.

2.1. Geology

The upstream basin of Merguellil is composed of limestone, calcareous marl and marly sedimentary formations of the Cretaceous and Eocene *(Figure 2)*. The oldest formation dates from the Triassic. Our study area, the Merguellil downstream basin of the Kairouan plain, corresponds to a collapsed basin, where the Plio-Quaternary continental detrital filling can exceed 700 m in thickness. A small Cretaceous limestone structure outcrops at the western part of the basin located in the El Haouareb mountain [9].

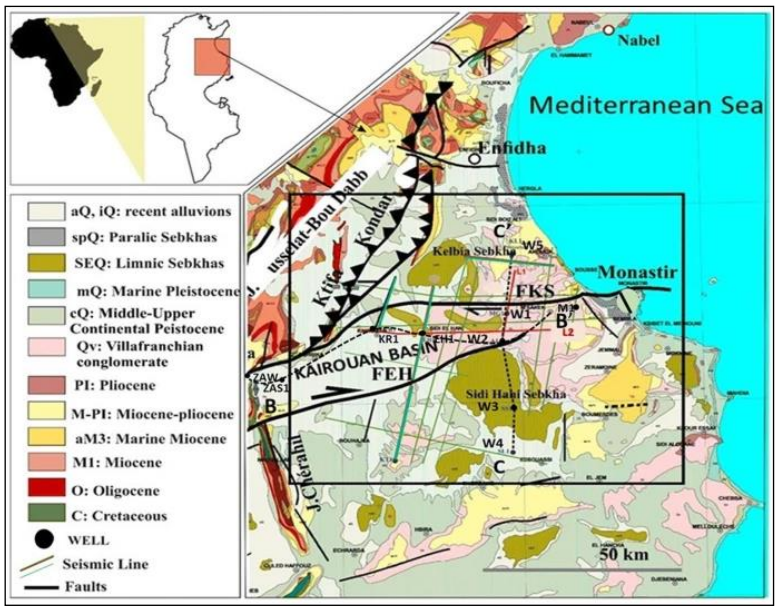

Figure 2
The geological map of the Kairouan Basin based on the 1/50,000 geologic map of Ben Hadj Ali et al. (1985) and the tectonic map of Khomsi et al. (2004) [10]

2.2. Climate of the Kairouan Region

The climate of central Tunisia, particularly in the Kairouan region, is distinguished by significant year-to-year and intra-year variations in rainfall. This fluctuation, along with water scarcity and drought periods, has a nagative impact on rain-fed agricultural productivity, resulting in unpredictable yields [11].

The study of several parameters, namely precipitation and temperature, serve to characterize the climate of the study area and to assess its degree of aridity. Indeed, these parameters have a significant impact on water availability [3].

The amount of precipitation varies a lot from year to year. The annual precipitation rate is less than 402 mm, with significant temporal and spatial variability. The daily mean temperature ranges from 9 °C in the winter to 34 °C in

the summer, with the hottest months being July and August *(Figure 3)*. The annual potential evapotranspiration rate is estimated to be around 1460 mm. [12]

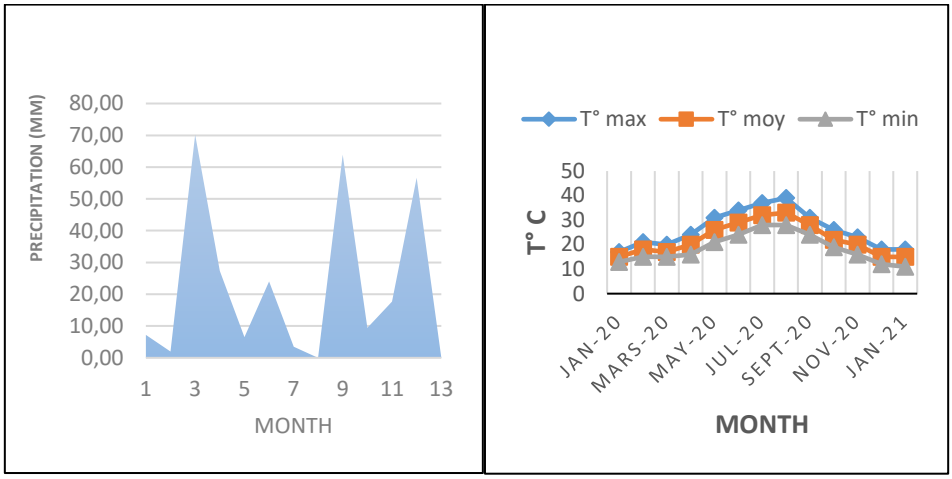

Monthly rainfall - Sidi Saad Station [13]

Monthly minimum, average and maximum temperature curve in Kairouan [14]

Figure 3
Precipitation and temperature in the study area [13–14]

3. MATERIALS AND METHODS

3.1. Materials

3.1.1. Sentinel 1 Imagery

SENTINEL-1 is an imaging radar mission providing continuous all weather, day-and-night imagery at C-band *(Table 1)*. The Sentinel-1 mission offers a range of distinct imaging modes, each with its own resolution, ranging from as low as 5 meters, and coverage extending up to 400 kilometers. It encompasses double polarization capability, rapid revisit times, and expedited product delivery. Additionally, precise spacecraft position and attitude measurements accompany every observation [15]. Sentinel-1B satellite imagery was used to characterize soil moisture in this study. The Sentinel-1B data used in the study has the following specifications:

Table 1
Specifications of the Sentinel-1B data used in the study [16]

Specifications	**Sentinel-1B**
Polarization	VV-VH
Imaging frequency	C-Band (5.4 GHz)
Resolution mode	5 meters
Acquisition times	January 2018–June 2020

3.1.2. Sentinel 2 Imagery

SENTINEL-2 is a European multi-spectral imaging mission with a wide and a high-resolution swath. The twin satellites, which are in the same orbit but phased at 180°, are designed to have a high revisit frequency of 5 days at the Equator. SENTINEL-2 is equipped with an optical payload that samples 13 spectral bands: four at 10 m, six at 20 m, and three at 60 m spatial resolution. The orbital swath is 290 kilometers wide [17].

During this research, the Sentinel 2 image will be used to calculate the values of the Normalized Difference Vegetation Index (NDVI) and Normalized Difference Water Index (NDWI).

3.1.3. Digital elevation data

Digital Elevation Models (DEMs) are used in geographic information systems to create relief maps by mapping terrain elevation. Since 2019, the Copernicus program has had a global and consistent high-resolution DEM available to all of its users for a wide range of applications. DEMs are classified into two types: digital surface models (DSM) and digital terrain models (DTM). DSM represents the Earth's surface envelope, including vegetation and man-made things like buildings and other forms of infrastructure, whereas DTM represents ground elevation. [18].

The Copernicus DEM is a Digital Surface Model (DSM) that depicts the Earth's surface, including structures, infrastructure, and vegetation. GLO-30 Public and GLO-90 are two Copernicus DEM instances provided by ESA *(Figure 4)*. At 90 meters, GLO-90 provides global coverage.

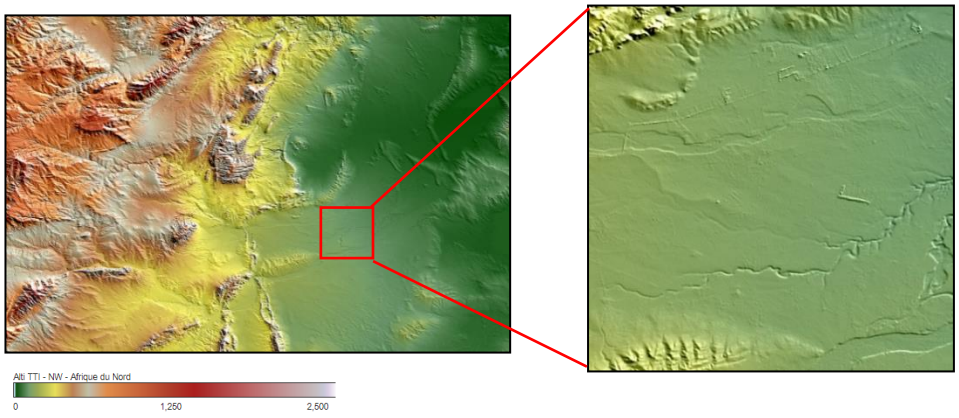

Figure 4
The DEM of the study area using Copernicus DEM GLO-30 m

The elevation shows that our study area is at the limit of the mountain's range, it is mainly consolidated materials, colluvial and alluvial materials coming from the mountain. This is what fills up our study area.

The geography of this study site is primarily defined by geology, with the plain dominating and the presence of mountains such as Jebel Trozza from the north-south direction. Clayey and clayey-sandy textures may be observed in the agricultural areas. As a result, topography is the main factor affecting soil formation in the study area.

3.2. Methods

My research strategy consists of collecting data from three sources: radar-sentinel 1, optical-sentinel 2, and Eras5-Global Precipitation Measurement (GPM). The first source will provide information about the Backscatter coefficient, while the second will provide information about the NDVI and NDWI, and the third will provide information about environmental factors such as temperature and rainfall. The obtained information will be processed at the advanced level in order to get the trained model, which will be calibrated using in-situ data. Furthermore, the model will enter the cycle of three phases, which are development, validation (with the support of in-situ data), and optimization, as seen in *Figure 5*.

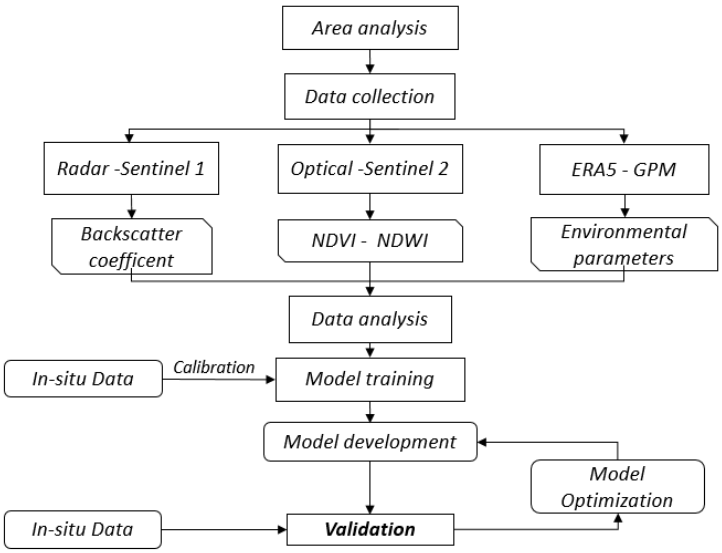

Figure 5
Methodological diagram of the model development

3.2.1. Data collection

The environmental covariates, Sentinel-1 (Backscatter coefficient), Sentinel-2 (NDVI and NDWI) and Digital terrain data were chosen as target explanatory variables to integrate. NDI is calculated as the difference between reflectance values in two bands divided by the sum of those values [19].

3.2.2. Extraction of Covariates

A combination of literature and statistical processing was used to select certain factors. According to the literature, covariates had to follow three criteria: first, they had to represent soil-forming elements; second, they had to have a direct link with SM; and third, they had to be readily available [20].

On the basis of these specifications, three kinds of data were chosen as environmental covariates: Sentinel-1 C-band, terrain data derived from DEM, and Sentinel-2 data to explain the biomass/vegetation influence on the SM [21].

3.2.3. Statistical Methods

In this paper, the statistical method used to describe and analyze soil moisture is the linear correlation. In a data-poor environment, linear regression produces more realistic spatial patterns over the landscape [22].

3.2.4. Characterization of Soil Moisture

Many researchers have developed models to characterize the soil moisture, and these models showed that soil moisture and backscattering coefficient have a fundamental relationship, e.g. [22]. The backscatter coefficient and Sentinel-2 data are considered main parameters that can help to characterize the soil moisture.

4. RESULTS AND DISCUSSION

4.1. Radar remote sensing

An optical image and a Sentinel-1 radar image are shown in *Figure 6* to visually analyze the area. The radar image (polarizations) is colored with an RGB composite: red = VH, green = VV, and blue = NDI, where NDI refers to the Normalized Difference Index of the VH and VV polarizations.

We can immediately distinguish the dominance of the bluish color, the greenish color and the presence of a reddish color at the level of the study area's south.

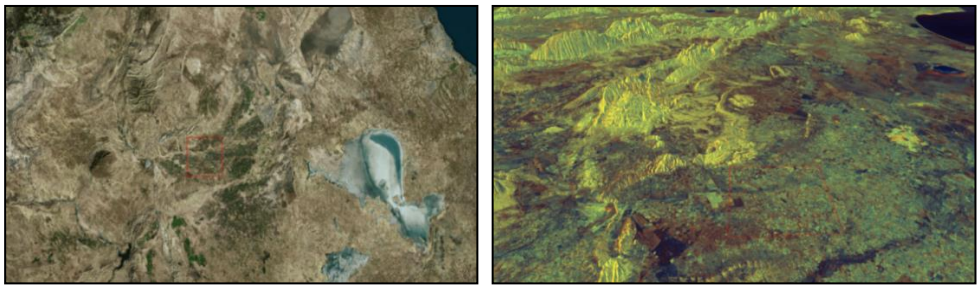

Figure 6

Optical image from the Bing Map and Sentinel-1B imagery of the study area

First of all, we did the visualization exercise with the RGB composite. A more detailed analysis on different polarizations *(Figure 7)* was made as follows:

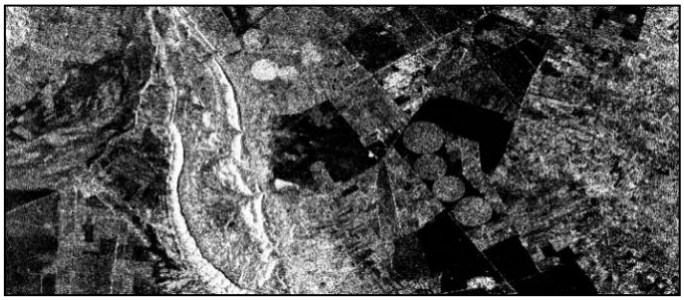

(a) Polarization VV

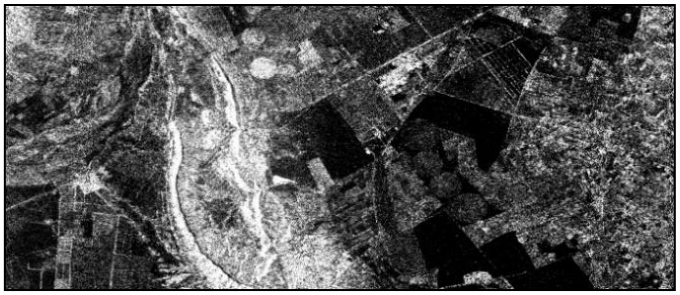

(b) Polarization VH

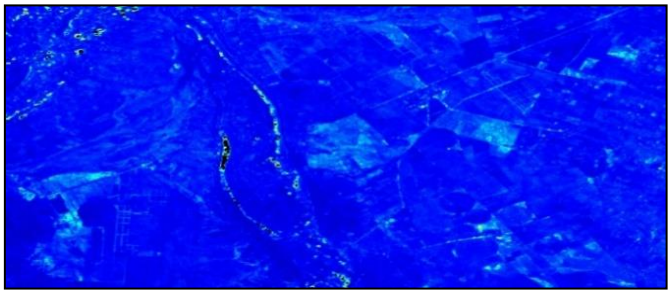

(c) Elevation

(d) Optical Image

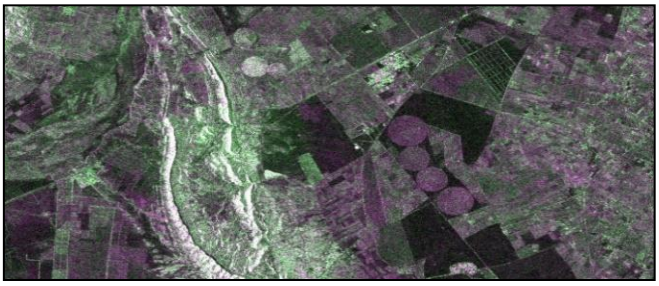

(e) RGB (VV, VH, VV)

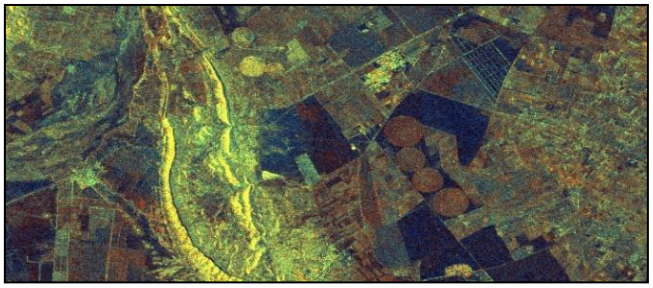

(f) RGB (VH, VV, NDI)

Figure 7

(a) *Polarization VV;* ***(b)*** *Polarization VH;* ***(c)*** *Elevation;* ***(d)*** *Optical Image;* ***(e)*** *RGB (VV, VH, VV);* ***(f)*** *RGB (VH, VV, NDI)*

Because SAR signals are prone to multiple scattering at various layers of vegetation, as well as at the subsurface or terrain level, interpreting vegetated parts of a SAR image demands the high level of understanding. The intensity of such scattering is heterogeneous in nature, varying from one SAR image to another, due to the changing nature of plant structures and closures.

The VH polarization produces comparable results to VV polarization, with the exception of greater separation of water masses and more precise information about the water region in the generated image [23]. The VV polarization is more informative for land use and for the vegetal cover analysis.

The wide histogram of the VV and the VH polarization image helps for a better discrimination of thematic classes including possible differentiation of identifying the open water, Irrigated area, soil roughness and the urban area. Although the RGB exercise of like-polarized and cross-polarized data can be considerably more informative.

Figure 7e and *7f* are a false-color composite of the Merguellil watershed's downstream. These images were acquired by the Sentinel-1 radar satellite. To aid the visual interpretation, the multiple channels of polarimetric data can be used to present the data in a colored image, in which certain image features are recognizable. As a simple example, a color image can be made using a VV = Red, VH = Green and VV = Blue channel assignment *(Figure 7e)*. This tends to "look realistic", as soil

water content reflections have a higher VH component than VV, and vegetation has a higher average than VH backscatter.

We use the Sentinel-1 SAR image in VV and HV polarization modes *(Figure 7f)* by presenting the VH/VV/NDI in RGB mode. Changes in the intensity of each color are related to surface conditions and covers; such as variations in surface roughness, biomasses, plant density, soil wetness, and soil types. Higher radar reflectance represented in VH/VV (yellow) is found in semi-consolidated and consolidated rocky material; lower backscatter in NDI polarization (dark blue) and VV/NDI (reddish) appears where erosional deposits and material related to fluvial erosion are abundant. Brighter colors are dominant where distinct bedrock layering can be observed. The units in bright yellow are typically caused by strong backscatter and VH polarization modes with VV represented as blue approaches zero.

The reddish areas in the image are the ploughed terrain. The yellow-greenish areas are cultivated areas with high soil moisture. The green areas are due to the relative high intensity of the VV channel, which is strongly correlated with the amount of biomass. The C-band VV and VH channels show the biomass variations over the entire region.

We can distinguish three major units in dark violet, brighter violet, and green colors using the Sentinel 1 SAR image in VV and HV polarization modes *(Figure 7e)* representing VH/VV/VV as RGB. Higher VV/VV (violet) radar reflectance is seen on plowed terrain with high roughness, but lower backscatter in VV polarization (dark violet) appears when uncultivated soils are abundant. We can distinct bedrock layering in the mountain by brighter colors predominant. Units in bright yellow are usually caused by high backscatter of VH polarization modes with VV, while the blue approaches zero. This can also indicate high soil moisture and a cultivated area.

4.2. Optical remote sensing

4.2.1. Characterization of the vegetation cover using NDVI

Figure 8 shows two images of the normalized difference vegetation index (NDVI) of the study area.

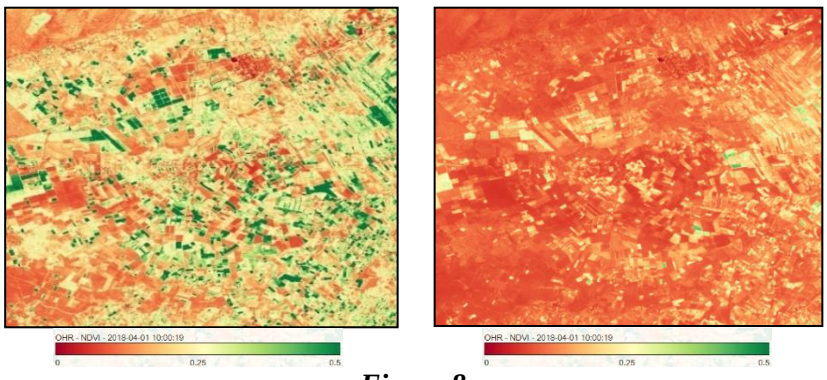

Figure 8

Normalized difference vegetation index (NDVI) of the study area

The image from January 2018 depicts wet conditions, while the one from July 2019 shows dry conditions. We can see a difference in vegetation cover between the two seasons; the first image displays a relatively dense vegetation cover, while the second image reveals sparse vegetation cover.

Figure 9a shows the variation of the normalized difference vegetation index (NDVI) of the study area. We can see the maximum and the minimum as well as the mean of the NDVI from January 2018 until December 2020. We see a big difference between the maximum and the maximum. This is explained by the difference between cultivated and non-cultivated areas, as well as plant life cycle differences. *Figure 9b* shows the variation of the NDVI between 2018 and 2020. We see the same trend of the three curves explained by the plant life cycles and the cultivation practices of farmers in the region.

$$\textbf{NDVI of the AOI} = \sum \textbf{Pixel value} / \textbf{N}$$

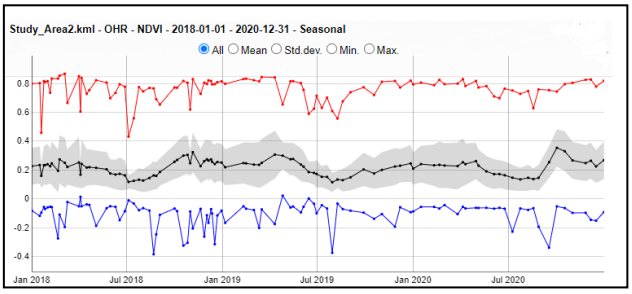

(a)

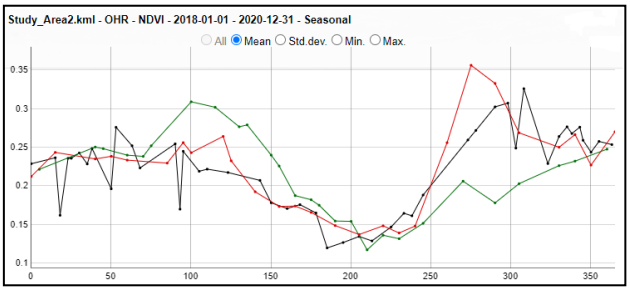

(b)

Figure 9

(a) *The maximum and the minimum of the NDVI value of the study area,*
(b) *variation of the NDVI value as a function of time*

4.2.2. Characterization of soil moisture using the water index

Figure 10 shows two images of the Normalized Difference Water Index (NDWI) of the study region. The image for June 2018 shows the dry time, but the image of October 2018 marks the beginning of the wet season. The first image shows various moist fields, which we can explain by the irrigated area, and the second image shows

land conditions following the rain, from which we can estimate that it had rained less than 48 hours before the date of the image.

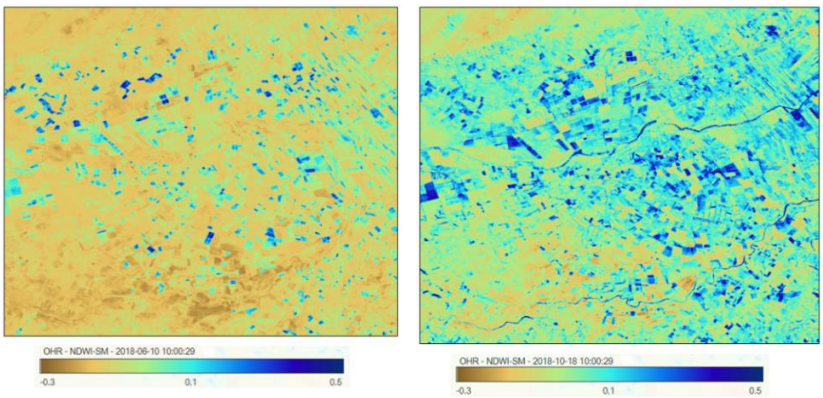

Figure 10
Normalized difference water index (NDWI) of the study area

The variation of the water index (NDWI) of the study area is depicted in *Figure 11a*, where we can observe the maximum, the minimum, and the mean of the NDWI from January 2018 to December 2020. In addition, we can notice a large gap between the maximum and the minimum, which demonstrates a large amount of land use, plant cover, and soil variability, indicating that soil moisture is determined more by land use and soil variability than by climate. *Figure 11b* shows the change in the NDWI from 2018 to 2020, and we can notice the similar pattern of the three curves described by the plant life cycles and the weather in the region.

The NDVI and NDWI results show that the study area is classified into several basic categories, which represent variations in land use/land cover and different crops. In our study area, conventional irrigation is dominant. The results show that vegetable crops such as tomatoes, peppers and plots of olive trees are the dominant crops in the study area.

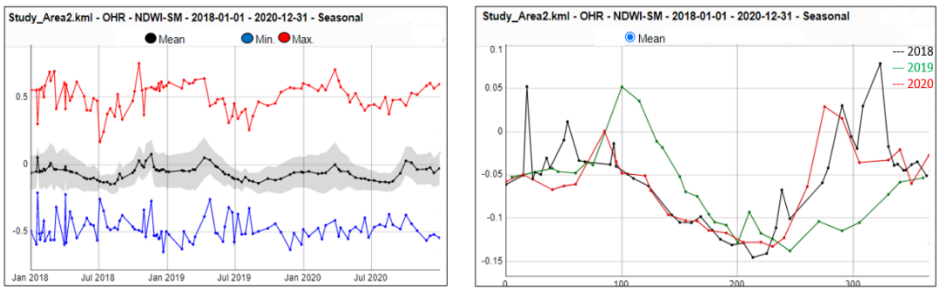

(a) (b)

Figure 11
(a) *The maximum and the minimum of the NDWI value of the study area,*
(b) *variation of the NDWI value as a function of time*

Pilot Area – Sub-pilot areas

To better understand the soil moisture regime and the impact of the environment parameters, we will focus our study on one parcel. On this parcel we will select two sub-pilot areas which are exposed to the same conditions and the same environment. We can visually observe the difference between the two sub-pilots; the plant cover of Pilot 1 seems less developed and less dense than Pilot 2.

A study was conducted on NDVI and NDWI on the two sub-pilots *(Figure 12)* for a period of three years between 2018 and 2020.

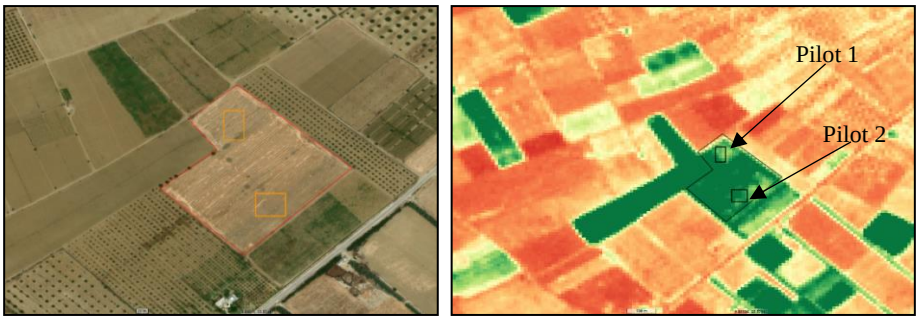

Figure 12
Normalized difference vegetation index (NDVI) of Pilots 1 and 2

During the rainy season, the NDVI of Pilot 1 is lower than that of Pilot 2 *(Figure 13)*, while it is higher during the dry seasons.

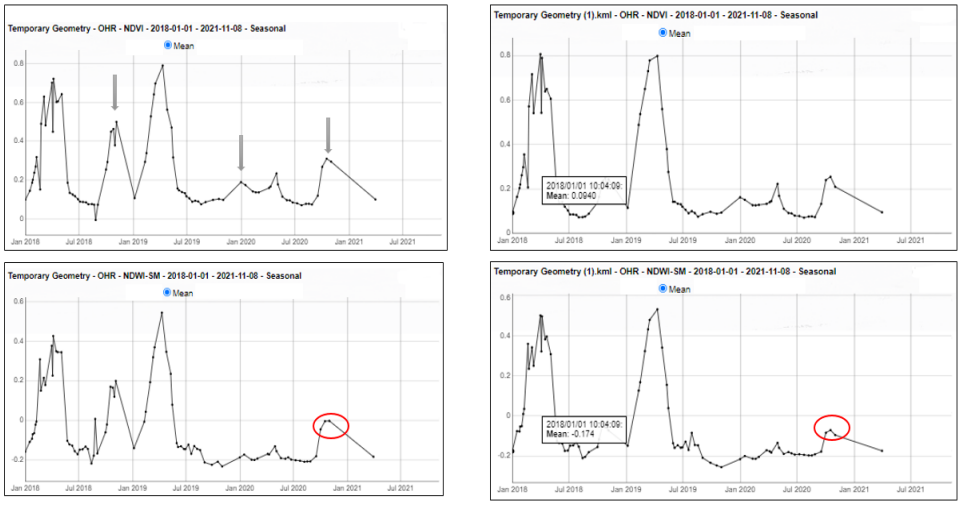

Pilot 1 Pilot 2

Figure 13
Comparison between the NDVI (top) and the NDWI (bottom)of sub-pilot areas

The NDWI of Pilot 1 is higher than that of Pilot 2 during both the dry and rainy seasons. Here, we can interpret that the type of soil in Pilot 1 and Pilot 2 is different, and that the soil of Pilot 1 has a higher water retention capacity than the soil of the pilot 2. We can also explain why the value of NDVI is lower for pilot 1 than pilot 2, despite a higher water retention capacity, by the soil of pilot 1 being close to reaching water saturation, which is not favorable to the development of vegetation.

4.2.3. Correlation between the NDVI and the NDWI

A statistical analysis was made between the NDVI and NDWI values of the study area between 2018 and 2020. *Figure 14* shows the results of the linear correlation between the two indices NDVI and NDWI. We see a strong correlation between the two parameters, with R = 0.79 and R^2 = 0.64.

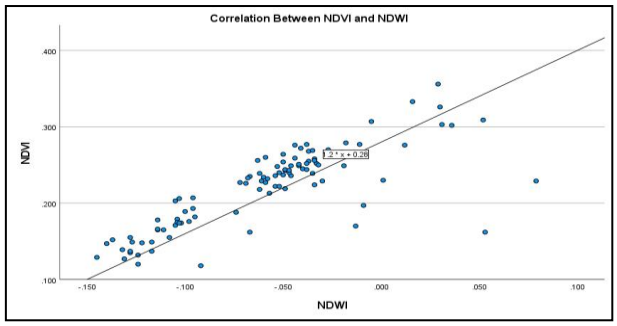

Figure 14
Correlation between NDVI and NDWI

This result is explained by the strong correlation between the water and the biomass in the nature and also technically the two parameters are based on the near-infrared as one of the major points.

We noticed some points a little away from the line of the correlation curve that raised questions, which is why we investigated further to check the reasons. As shown below, a measure of the correlation coefficient was performed between the means of NDWI-NDVI, the maximums of NDWI-NDVI and the minimums of NDWI-NDVI.

(a) Pilot 3 (b) Pilot 4 (c) Pilot 5

Figure 15
Delimitation of Pilot 3, Pilot 4 and Pilot 2

The results reveal that maximums and means have a higher correlation, whereas minimums have a lower correlation. Furthermore, a small pilot area (Figure 15a) is used for validation; its correlation coefficients are calculated as shown in the pilot curves below *(Figure 17)*, and this pilot reveals strong correlations between maximums, means, and minimums. The weak correlation between the minimums in the study area *(Figure 16)* can be explained by the presence of free water or by the presence of certain urban areas. In addition, the out-of-range points could be explained by a technical error while the output results are symbolic of the same date, this error could be considered as noise.

To be sure of this assumption, we worked on two other small pilots (4 and 5) who have the same occupation. Olive trees occupy Pilot 4, while Pilot 5 is covered by horticulture. The results show a strong correlation between the means of NDWI-NDVI and the maximum of NDWI-NDVI; on the other hand the minimum of NDWI-NDVI shows a correlation coefficient lower than the average and the maximum and is also unpredictable. We can explain the weak and unpredictable results of the minimum NDWI-NDVI by the presence of different land cover, which can be wet without vegetation, and we can say that the minimum is not representative.

Pilots 4 and 5 (*Figure 18* and *Figure 19*) shows the same out rang points as the first and the second analysis. That is why we can consider the out rang points as noise.

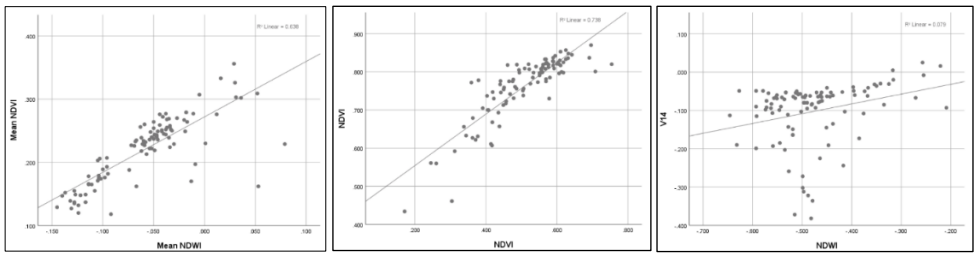

R = 0.79 R^2 = 0.64 R = 0.859 R^2 = 0.638 R = 0.28 R^2 = 0.079

Figure 16

Correlation between the NDWI and NDVI of the study area

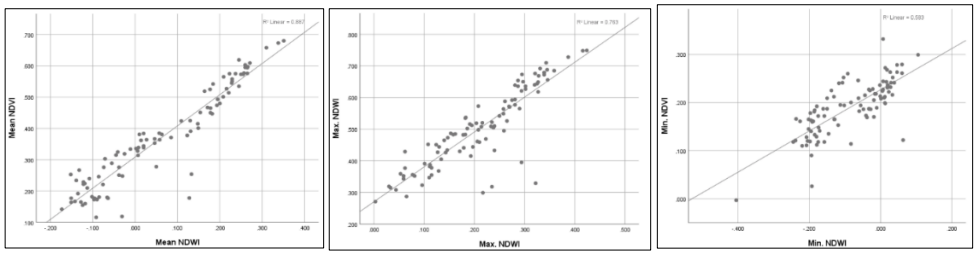

R = 0.87 R^2 = 0.89 R = 0.94 R^2 = 0.76 R = 0.764 R^2 = 0.58

Figure 17

Correlation between the NDWI and NDVI of Pilot 3

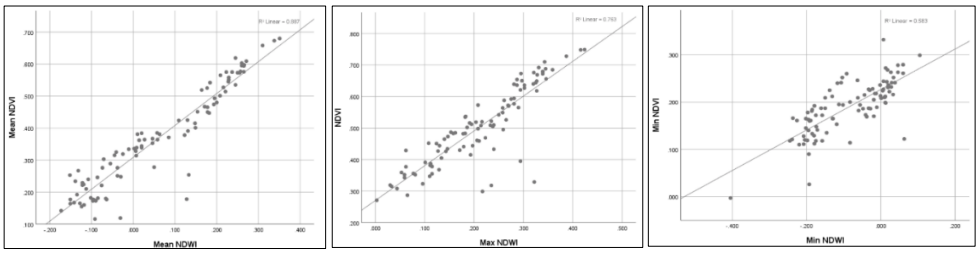

R = 0.94 R² = 0.89 R = 0.87 R² = 0.76 R = 0.76 R² = 0.58

Figure 18

Correlation between the NDWI and NDVI of Pilot 4

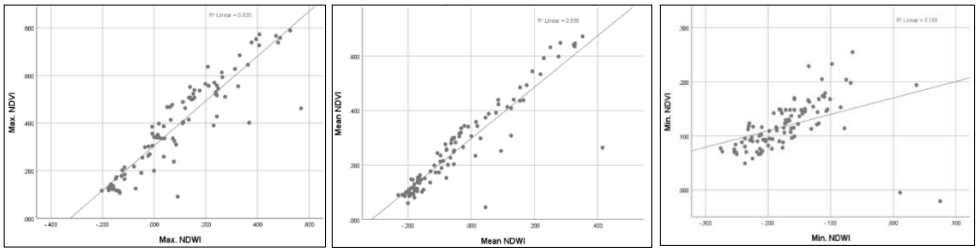

R = 0.91 R² = 0.84 R = 0.91 R² = 0.84 R = 0.41 R² = 0.17

Figure 19

Correlation between the NDWI and NDVI of Pilot 5

5. CONCLUSIONS

In this study, the correlation method was used to characterize the soil moisture regime using Sentinel-1B C-band SAR satellite data, the Normalized difference vegetation index (NDVI), and the Normalized difference water index (NDWI). Five pilots in the study area were chosen and analyzed to identify the relation between the optical and radar satellite data and the soil moisture. In order to extract the highest correlation and most informative data sources, we evaluated at the correlation between different backscatters (V, H), optical data, DEM, and environmental variables. The Normalized difference vegetation index (NDVI), the Normalized difference water index (NDWI), the Radar data (VV and VH polarization) and the soil types showed a strong correlation with the wetness and the vegetation conditions. The applied basic cognitive and statistical tools combined with local knowledge has demonstrated that these datasets have comparative potential in explaining the soil water regime and its relationship to the vegetation condition. The method is a promising and useful tool that may be used to characterize the soil moisture regime in the region. The environmental covariates should be statistically tested through the correlation methods to determine which covariates had the highest correlation with soil moisture.

REFERENCES

[1] Petropoulos, G. P., Griffiths, H. M., Dorigo, W., Xaver, A., Gruber, A. (2013). Surface Soil Moisture Estimation: Significance, Controls, and Conventional Measurement Techniques. In: Petropolous, G. (ed.). *Remote Sensing of Energy Fluxes and Soil Moisture Content*. CRC Press, Boca Raton, Louisiana, pp. 29–48.

[2] Sehler, R., Li, J., Reager, J. T., Ye, H. (2020). Investigating Relation-ship Between Soil Moisture and Precipitation Globally Using Remote Sensing Observations. *Journal of Contemporary Water Research & Education*. https://doi.org/10.1111/j.1936-704X.2019.03324.x

[3] Sarra Bel Haj Salem (2013). Utilisation des traceurs environnementaux pour l'étude des mode de recherche des eaux du bassin de Zéroud (Plaine de Kairouan). pp. 51, 2, pp. 272–284, doctoral dissertation, University ofSfax, Sfax, Tunisia..

[4] M, Zribi, A. C, and B. N. (2020). Editorial for the special issue Soil moisture retrieval using radar remote sensing sensors. *Remote Sens.*, Vol. 12, No. 7. https://doi.org/10.3390/rs12071100

[5] Le Goulven, Patrick & Leduc, Christian & Bachta, Mohammed & Poussin, Jean-Christophe. (2009). Sharing scarce resources in a Mediterranean River Basin: Wadi Merguellil in central Tunisia. International Water Management Institute Books, Reports H042452, International Water Management Institut.

[6] Taoufik Hermassi, Mohamed Amine Cherif, Hamadi Habaieb (2014). Solid Transport study at the Merguellil watershed, central Tunisia: case study of Ettiour and Rajela watersheds. *La Houille Blanche*, 100, 4, pp. 88–96. https://doi.org/10.1051/lhb/2014043

[7] Lacombe, G. (2007). Evolution and uses of water resources in a semi-arid managed watershed. The case of Merguellil in Central Tunisia. Doctoral dissertation at the Montpellier University, Science and Techniques of Languedoc.

[8] Chulli, B., Favreau, G., Jebnoun, N., Bédir, M. (2011). Impact of changing climate in the Kairouan Hydrological basin (central Tunisia). *Journal of Environmental Science and Engineering*, 5, pp. 682–688.

[9] Safouan Ben Ammar, Kamel, Zouari, Christian Leduc., Jemaiel, M'Barek. (2006). Isotopic characterization of the dam—aquifer water transfer in the Merguellil catchment (Kairouan Plain, central Tunisia). *Hydrological Sciences Journal*, 51, 2, pp. 272–284, https://doi.org/10.1623/hysj.51.2.272.

[10] Bédir, M., Soltani, A., Mohamed, A. B. et al. (2020). Cretaceous petroleum system modeling of Kairouan Basin in eastern Tunisia. *Arab. J. Geosci*., 13, 683, https://doi.org/10.1007/s12517-020-05550-0.

[11] Mougou, R., Mansour, M., Iglesias, A. et al. (2011). Climate change and agricultural vulnerability: a case study of rain-fed wheat in Kairouan, Central Tunisia. Reg Environ Change 11 (Suppl 1), pp. 137–142. https://doi.org/10.1007/s10113-010-0179-4

[12] Hamdi, Mohamed & Tarhouni, Jamila & Zagrarni, Mohamed & Laouini, Ghassen & Müller, Hans. (2017). Assessment of groundwater flow dynamic using GIS tools and 3D geological modeling: Case of Sisseb El Alem-Nadhour Saouaf basin, Northeastern Tunisia. 19. 2028-9324. *International Journal of Innovation and Applied Studies*, Vol. 19, No. 1, Jan. 2017, pp. 226–238, Innovative Space of Scientific Research Journals.

[13] Safouane Mouelhi , Saida Nemri , Sihem Jebari and Mohamed, Slimani (2016). Using the Markov Chain for the Generation of Monthly Rainfall Series in a Semi-Arid Zone. *Open Journal of Modern Hydrology*, 6, pp. 51–65. https://doi.org/10.4236/ojmh.2016.62006

[14] Fletcher, Karen (ed.) (2012). SENTINEL 1: ESA's Radar Observatory Mission for GMES Operational Services. European Space Agency. https://sentinel.esa.int/web/sentinel/user-guides/sentinel-1-sar/overview.

[15] Fletcher, Karen (ed.) (2012). SENTINEL 1: ESA's Radar Observatory Mission for GMES Operational Services. European Space Agency. https://sen tinels. copernicus.eu/web/sentinel/missions/sentinel-1/overview/mission-sum mary.

[16] Roland Meynart, Steven P. Neeck, Haruhisa Shimoda (2013). Sensors, Systems, and Next-Generation Satellites XVII. Proceedings of SPIE, Volume 8889, Article 88890K, https://doi.org/10.1117/12.2028755.

[17] Franks, Shannon, and Rajagopalan Rengarajan (2023). Evaluation of Copernicus DEM and Comparison to the DEM Used for Landsat Collection-2 Processing. *Remote Sensing*, 15, No. 10, p. 2509. https://doi.org/10.3390/rs15102509

[18] Chen, F., Van de Voorde, T., Roberts, D., Zhao, H., Chen, J. (2021). Detection of Ground Materials Using Normalized Difference Indices with a Threshold: Risk and Ways to Improve. *Remote Sens*., 13, p. 450. https://doi.org/10.3390/rs13030450

[19] Dobos, Endre, Daroussin, Joël, Montanarella, Luca (2010). A Quantitative Procedure for Building Physiographic Units Supporting a Global Soter Database. *Hungarian geographical bulletin*, 59, pp. 181–205.

[20] Dobos, E., Micheli, E., Baumgardner, M. F., Biehl, L., Helt, T. (2000). Use of combined digital elevation model and satellite radiometric data for regional soil mapping. *Geoderma*, Vol. 97, No. 3–4, pp. 367–391. https:doi.org/10.1016/S0016-7061(00)00046-X

[21] Kibirige, D., Dobos, E. (2020). Soil moisture estimation using citizen observatory data, microwave satellite imagery, and environmental covariates. *Water (Switzerland)*, Vol. 12, No. 8, https://doi.org/10.3390/W12082160.

[22] Qian Zhang, Xiangnan Liu, Meiling Liu, Xinyu Zou, Lihong Zhu and Xiaohao Ruan (2021). Comparative Analysis of Edge Information and Polarization on SAR-to-Optical Translation Based on Conditional Generative Adversarial Networks. *Remote Sens.*, 13, p. 128, https://doi.org/10.3390/rs13010128.

Geosciences and Engineering, Vol. 10, No. 15 (2022), pp. 173–184.
https://doi.org/10.33030/geosciences.2022.15.173

HYDROGEOLOGICAL INVESTIGATIONS IN BASEMENT TERRAINS USING GEOLOGICAL, GEOMORPHOLOGICAL AND GEOPHYSICAL METHODS, WESTERN HAMISSANA AREA, NE SUDAN

MUSAAB A. A. MOHAMMED[1, 2, 5], ABDALLA E. M. ELSHEIKH[4], NORBERT P. SZABÓ[1, 3 6], PÉTER SZŰCS[1, 3, 7]

[1]*Faculty of Earth Science and Engineering, University of Miskolc, Miskolc, Hungary*
[2]*Faculty of Petroleum Geology and Minerals, University of Bahri, Khartoum, Sudan*
[3]*MTA-ME Research Group of Geoengineering, University of Miskolc, Miskolc, Hungary*
[4]*Faculty of Petroleum and Minerals, Al Neelain University, Khartoum, Sudan*
Abdalla.elsheikh@gmail.com
[5]*musab20501@gmail.com, https://orcid.org/0000-0002-0097-0037*
[6]*norbert.szabo@uni-miskolc.hu, https://orcid.org/0000-0003-4331-5603*
[7]*peter.szucs@uni-miskolc.hu, https://orcid.org/000-0002-6061-2514*

Abstract: This study aims at identifying target zones for groundwater exploration in basement terrains using geological, geomorphological, and geoelectrical methods. The study area is located on the northwestern side of the Red Sea Hills in the western Hamissana area. It is part of the Arabian Nubian Shield (ANS), which dates to the Pan-African Era. The study area is covered by Precambrian basement rocks which are overlain by alluvial deposits. The climate in the region is arid. As a result, severe water shortage is experienced. The geological and geomorphological investigations were carried out to locate potential sites for groundwater prospecting. On this basis, three categories of groundwater potential zones were delineated as good, moderate, or poor. The electrical resistivity method using vertical electrical sounding (VES) technique was used to determine the vertical geological profile of the study area. The sequence was revealed to consist of four zones: a high-resistance unsaturated zone, an intermediate-resistance water-bearing formation, a low-resistance wet weathered basement, and high-resistance fresh basement rock. Catchment boundaries were delineated using digital elevation models, and potential locations for surface and subsurface dams were proposed to improve the groundwater recharge.

Keywords: *Groundwater exploration, Basement terrain, Geomorphology, Electrical method, VES, Hamissana, Red Sea hills, Catchments*

1. INTRODUCTION

Earlier, crystalline rocks – like other hard rocks – were not given due attention for groundwater development on account of their low permeability and difficulties in water-well drilling. However, in the last few decades, due to the need for safe drinking water for vast rural populations, especially in the developing countries, crystalline rocks are being investigated in detail for groundwater development [1–3]. Groundwater is scarce in hard rock terrains; it is essentially limited to fractured and weathered zones [4]. Groundwater investigation in basement terrains involves a

comprehensive study of the geology and geomorphology of the investigated area, which are influenced directly or indirectly by weathering grade, drainage pattern, landforms, and climate [5, 6].

The general geology and topography of the study area caused the observed water scarcity. The predominant rock type in the area is basement rocks. Surface topography has a significant impact on groundwater occurrences, since steep slopes increase flow and hence reduce potential recharging. Due to the scarcity of direct precipitation as a source of groundwater recharge, the natural hydrogeological conditions must be enhanced through artificial recharge [7].

The study area is situated on the northwest side of the Red Sea Hills in the Hamissana area, Red Sea State. The area is confined between latitudes (20. ° 00624-21°.0024°) N and longitudes (34. °4969°-35°.31254°) E. Hamissana area is defined by its arid environment and undulating topography landscape *(Figure 2)* which receives an average yearly rainfall of 20 to 25 millimeters *(Figure 1)*. The drainage pattern of the Red Sea Hills is fundamentally controlled by faults and folds that form rectangular drainage patterns. The main objective of this study is to use combined hydrogeological and electrical resistivity methods to detect the lithological and geological structures that control the water-bearing formations and furthermore comment on suitable methods for water resources management and development.

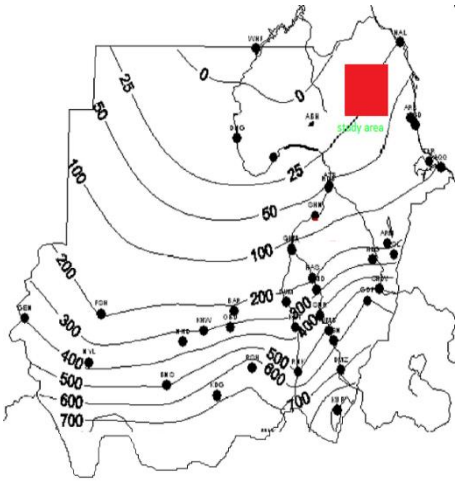

Figure 1
Average annual rainfall in the Sudan, 1971–2000, the study area shown in red box

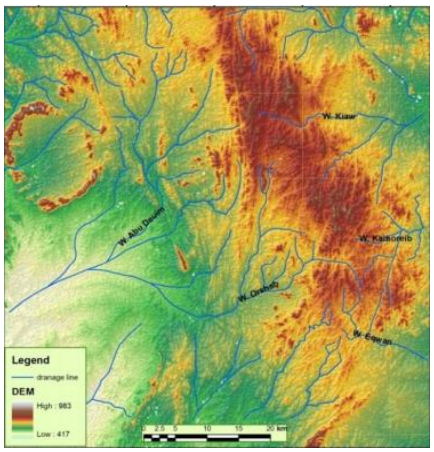

Figure 2
Digital Elevation Model of the study area

2. GEOLOGICAL SETTING

The study area lies geologically in Red Sea hills and structurally within the Hamissana shear zone. The Red Sea Hills region of NE Sudan is part of the Arabian-Nubian Shield of Proterozoic era. It lies in the central part of the Nubian segment. It

extends northwards through the eastern desert of Egypt and southwards across the Sudan-Eritrean border into the Ethiopian plateau. To the east it is bound by the Red Sea coastal plain and by the Nubian Desert to the west. Several geologists have described the geology of the Red Sea Hills of NE Sudan [8–10]. The general regional geology of the Red Sea hills can be divided into six major groups from younger to older: recent deposits, Quaternary sediments, Tertiary volcanic, Cenozoic sediments, Paleozoic sediments, and basement complex. The Hamissana shear zone (HSZ) is a massive deformation zone running north to south and is one of the greatest basement formations in NE Africa [11]. The region is dominated by metasedimentary, metavolcanic, and ophiolitic rocks, *(Figure 3)* which define an ancient boundary between the Gabeit and Gabgaba terrains [12].

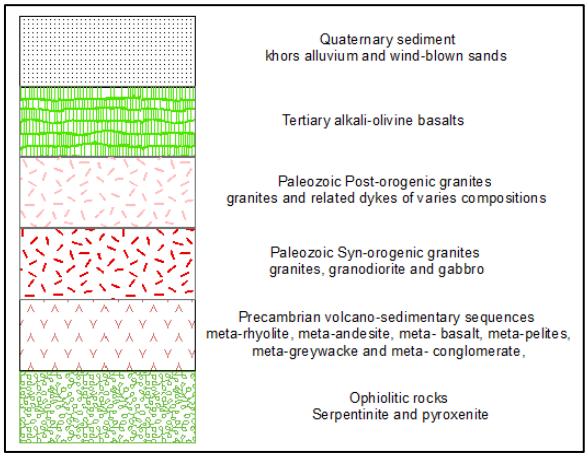

Figure 3
Geological column of study area

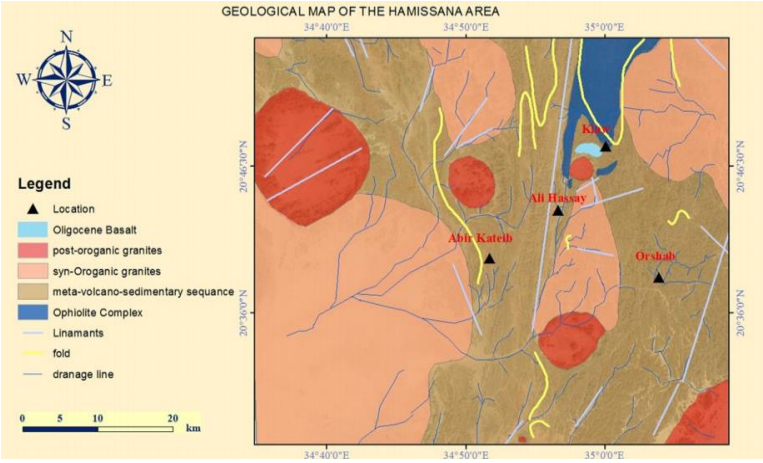

Figure 4
Geological map of the study area

These sequences are intruded by the syn- to late-orogenic and post-organic igneous intrusions. It represents important part of geology of the Red Sea Hills and comprises a very different type of rocks which are highly deformed *(Figure 3)*. The area under consideration is highly fractured with lineament concentration in the northern and southeastern parts. An earlier study [13] applied structural analysis in the study area to classify the lineament features from a hydrogeological point of view; the authors noted that the open potential fractures are commonly found in NW-SE and in NE-SW directions, while the closed shear fractures are oriented in N-S direction.

3. METHODOLOGY

The methods of the study were planned to achieve the objectives of the study. It began with the collection of available data such as meteorological, hydrogeological, and geophysical data. The hydrogeological investigation mainly focused on the study of the geological and geomorphological features that control the groundwater occurrence in the study area. Surface mapping of various lithological units, as well as their structural characteristics is part of geological studies, using satellite images as base maps. Geomorphological investigations include delineation and mapping of various landforms that make up the area and characterize the drainage systems running across the study area. The geophysical method used in this study is the electrical resistivity method using a vertical electrical sounding technique for the delineation of sub-surface layers. The vertical electrical sounding (VES) measurements were established using a Schlumberger array to acquire information about the vertical lithological variations and aquifer depths. The measurements were conducted using a portable (ABEM SAS1000) instrument. The interpretation of the resistivity data was accomplished with the assistance of IP2WIN software, assuming depth equals AB/4. This software is reliable to a good extent in determining the depth of the different boundaries and gives an automatic interpretation of the apparent resistivity.

4. RESULTS AND DISCUSSION

4.1. Geological and geomorphological investigation

Geological investigations include surface mapping of different lithological units and their structural and geomorphological features using satellite images as base maps *(Figure 4)*. Field mapping guided by remote sensing images and interpretation of geophysical data have yielded information about the thickness and composition of different rock units. The majority of the studied area is covered by a thick layer of weathered materials, which makes it a significant hydrological unit and potential ground water zone. Hydrogeologically, different rock types in the study area are grouped into three major categories *(Table 1)*:

Crystalline rocks: These include granite, granodiorite and gabbro, and the groundwater occurrence in these rocks is mainly associated with weathered horizon

and fractured media. These granitic rocks are considered to be good for groundwater prospecting.

Meta volcano-sedimentary rocks: These rocks are the dominant rocks in the study area, the groundwater occurrence in these rocks is generally dependent on the degree of fracturing. In terms of groundwater availability, these rocks are defined as poor potentiality rocks.

Clastic rocks: These include alluvium and wind-blown deposits, and in these rocks the groundwater occurs within the intergranular pore spaces. The hydrogeological characteristics of the clastic rocks is moderate.

Table 1

Hydrogeological classification of the rocks in the study area

Rock group	Rock types	Aquifer structure	Potential
Crystalline rocks	Granite, gabbro granodiorite, etc.	Weathered horizon and fractures	Good
Meta Volcano-sedimentary	Meta-rhyolite, -dacite, -andesite, etc.	Fractures	Poor
Clastic rocks	Wadi alluvium	Intergranular pore space	Moderate

Geomorphological investigations include delineation and mapping of various landforms and drainage characteristics [14]. These features significantly contribute to locating favorable sites for groundwater recharge and development potential. Geomorphological mapping is accomplished via remote sensing data derived from satellite images. The erosional landforms of the study area comprised of structural hills, erosional valleys, buried pediments and valley fills *(Table 2)*.

Structural hills: These are described as large-scale rock structures. They occupy vast areas in the northern, eastern and southern part of the study area. They act as run-off zones and the groundwater potential is very poor.

Erosional valleys: These occur as narrow valleys between two adjacent structural hills. The bedrock in the erosional valleys is often weathered and has a thin layer of unconsolidated material. The potential for groundwater occurrence is very limited.

Buried pediments: These areas are covered with a rather thick layer of weathered material ranging in thickness from 20 to 70 meters. In the study area, these features are located practically throughout the whole length of the main drainage systems. The groundwater potential is described as moderate to good in these regions.

Valley fills: These are described as the deposition of unconsolidated materials in an erosional environment in hard rock terrains. Valley fills are the key landforms for the development of groundwater in a crystalline rock environment. This was found

in the middle, western and southwestern parts of the study area. The groundwater prospect in this area is good.

Table 2
Landforms of the study area

Landform	Description	Lithology	Potential
Structural hill	Large-scale rock structures	Crystalline rocks	Poor
Buried pediments	Thick layer of weathered material	Crystalline with veneer of soil cover	Moderate
Erosional valley	Narrow valley between two adjacent structural hills	Weathered rocks	Very limited
Valley fills	Deposition of unconsolidated materials in erosional environment	Coarse sediments and in situ weathered materials	Good

The drainage system is one of the critical indications of hydrogeological characteristics in basement rock terrains. The stream pattern is a reflection of the rate that precipitation infiltrates compared with the surface runoff [15]. Surface drainage is the subdued replica of topography. It is controlled by the basement rocks. The drainage pattern is mostly controlled by the underlying geological structure that causes groundwater flow to coincide with surface drainage [16]. The drainage lines were extracted and then superimposed over the Landsat image to obtain the drainage length density map. The drainage length density (Dd) is a parameter to detect the potential of groundwater storage. It is defined by the ratio of cumulative length of streams to the size of the study area *Equation (1).*

$$Dd = \sum_{i=1}^{i=n} \frac{Si}{A} \qquad m^{-1} \tag{1}$$

where $\sum_{i=1}^{i=n} Si$ is the cumulative length of all streams or drainage and A is the area of the catchment (m^2).

The general slope of the area is from north to the south flanks, which represents the inconsiderable variation in elevation with the adjacent surrounding areas. In the study area, the dendritic and parallel types are the most common drainage patterns. Parallel types of drainage patterns are an indication of the presence of structures that act as conduits or barriers for groundwater systems. Generally, low drainage density is associated with areas of high resistance or permeable surface and low relief. High

drainage densities are found in areas with impermeable subsurface materials and mountainous relief, which have poor infiltration rates *(Figure 5).*

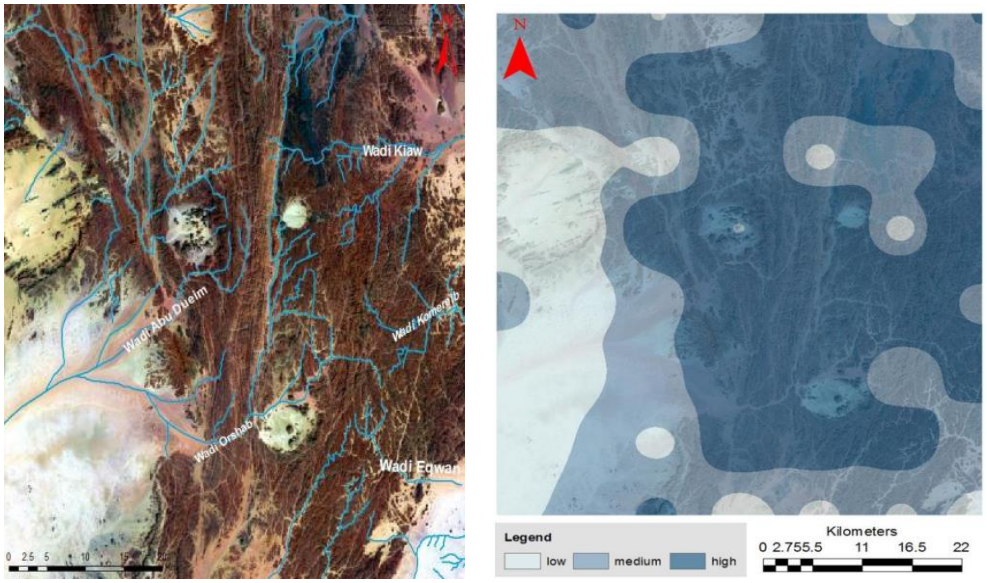

A *B*

Figure 5

(A) Drainage map and (B) drainage density map of the study area

4.2. Geophysical investigation

The use of geophysics for groundwater exploration has intensified during the last few years due to the rapid advancement in computer software and numerical solutions. Because of its simplicity, vertical electrical sounding (VES) has proven to be very popular in groundwater prospecting. The geophysical electrical resistivity method was applied to define the anomalies, thickness and lithological variation of the alluvial and basement aquifers. In this study a total number of 24 vertical electrical sounding points (VES) using Schlumberger configuration were carried out based on the geological and geomorphological investigations to identify the vertical lithological sequences *(Figure 6)*. VESs were conducted in the key micro-watersheds such as Wadi Orshab, Wadi Abu Deuim and Wadi Eqwan. The VES points are interpreted using IP2WIN software. Based on the interpreted data it was found that the resistivity of the basement complex rock ranges from high values of 6290 Ohm.m to infinity, with the higher values indicating hard basement rocks while lower values referred to weathered and cracked basement rocks. The surface deposits may be classified into two groups: dry topsoil (sands and gravels) with resistivities more than 700 Ohm.m, and wet clay and clayey sand with resistivities between 10 and 100 Ohm.m *(Figure 7)*.

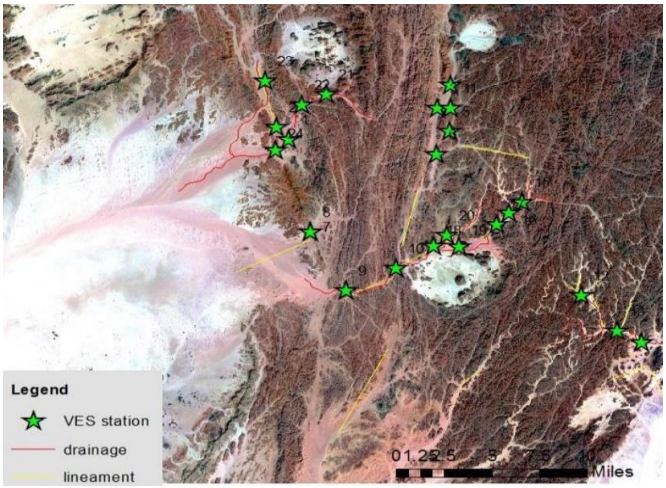

Figure 6
Locations of the VES stations in the study area

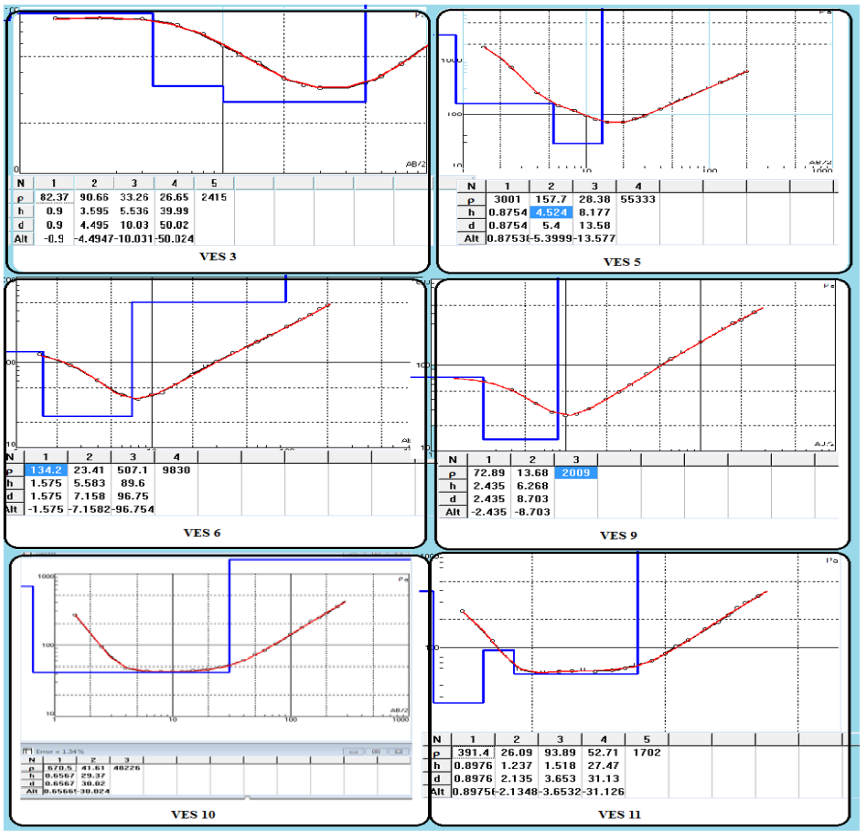

Figure 7
The VES curves in Wadi Orshab

Generally, the curves show that succession consist mainly of four layers from the surface: dry topsoil at 1–3 m, followed by alluvial deposits, and then weathered basement overlaying the fresh basement of higher resistivity values. The result of the geophysical investigations revealed that the succession consists of two aquifers: the shallow alluvial aquifers at depths ranging from 8 to 15 meters below the ground surface; and the deep weathered/fractured basement rocks aquifers that range in depth between 20 and 50 meters below the surface.

4.3. Aquifer Recharge Management

The term management of aquifer recharge (MAR) is now being increasingly used for artificial recharge to imply an additional input of water underground besides natural infiltration [17]. The improvement of the aquifer recharge is done through constructing surface and subsurface dams *(Figures 8–10)*. Surface dams are important in groundwater management scenarios as they provide natural storage for water for use during a dry period. The subsurface dams are implemented to prevent water from migrating beyond the expected catchment area toward a neighboring area. Subsurface dams are feasible in narrow and gently sloping valleys where the bedrock occurs at a shallow depth, overlain by a valley-fill deposit of 4–8 m thickness. The main aim of these dams is to increase the groundwater quantities and reduce the underground seepage, which finally leads to the enhancement of the hydrogeological condition in the area.

Watershed analysis

The annual rate of precipitation in the study area ranges between 25 and 50 mm, and the annual evapotranspiration is much greater than the annual precipitation. From the literature in similar areas in Sudan, about 85% of the precipitation during the rainy season is lost due to evaporation. Accordingly, the above-mentioned data was used in this study to calculate the total yield of each wadi *(Equations 2–4)*. The calculated watersheds are Wadi Orshab, Abu Deuim and Eqwan.

The course of Wadi Orshab runs parallel to the direction of the release fractures in NE-SW direction *(Figure 8a)*. It is one of the biggest and most important watersheds in the study area. The main rock type in Wadi Orshab is meta-volcano sedimentary intruded by synorogenic granite. The catchment area of Wadi Orshab is about 200×10^6 m^2 and the total yield of Wadi Orshab is:

$$Q = 200 \times 10^6 \text{ m}^2 \times 4.5 \times 10^{3-} \text{ m} = 1035 \times 10^3 \text{ m}^3 \quad (2)$$

Wadi abu Deuim watershed drains the northern part of area *(Figure 8b)*. The course of Wadi Abu Deuim runs parallel to the direction of the extension and tension fractures in NW-SE direction. The main rock type of Wadi Abu Deuim is synorogenic granite. The catchment area is about 490×10^6 m^2, the annual rainfall is the lowest value in the area, therefore the value of 25 mm/y was used for calculation

of the annual precipitation. The remaining water from the annual rainfall is about 3.75 mm on average; using the same remaining percent, then the total yield is:

$$Q = 490 \times 10^6\ m^2 \times 3.75 \times 10^{-3} m = \quad (3)$$

Wadi Eqwan watershed is calculated at about $215 \times 10^6\ m^2$ *(Figure 8c)*. The remaining 15% of the average annual precipitation (30 mm/y) is equal to about 4.5 mm, so the total yield of Wadi Eqwan is:

$$Q = 215 \times 10^6\ m^2 \times 4.5 \times 10^{-3}\ m^3 = 968 \times 10^3\ m^3 \quad (4)$$

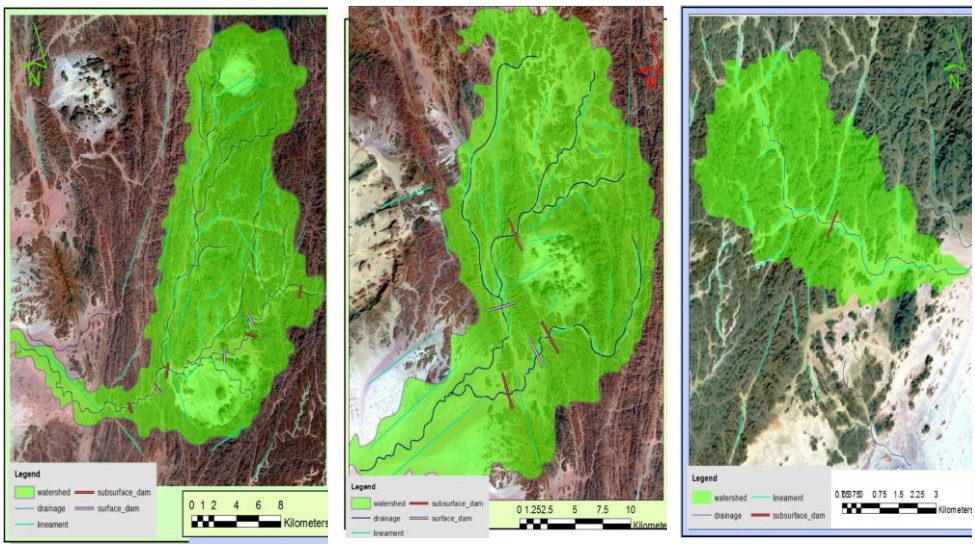

(a) *(b)* *(c)*

Figure 8

The watersheds of Wadi Orshab, Abu Duiem and Eqwan, including the suggested location of surface and subsurface dams

5. CONCLUSIONS

The aim of this study is to assess the groundwater resources in the Hamissan area by combining different exploration peckages including geological, geomorphological, and geophysical methods. The integration of these methods has proven to be efficient in identifying the groundwater potential zones. On the basis of the geological and geomorphological investigations, three classes of groundwater potential zones were revealed: poor, moderate and good. The electrical resistivity method using vertical electrical sounding technique was applied to detect the vertical lithological variation and the thickness of each unit. The result of the geophysical investigations revealed that the area contains two types of aquifers: shallow alluvial aquifers and the deep

weathered/fractured basement rocks aquifers. Due to scarce annual precipitation, high evaporation and steep slope in the study area, several locations of surface and underground dams have been proposed to improve groundwater recharge. To improve water supply in the study area, this study recommends application of electromagnetic and ground penetration radar to acquire more information about the thickness of the saturated weathered materials. Based on the investigation and interpretation of the data during this study, we also recommend construction of rainfall stations and runoff gauges to obtain more information about water balance in the study area.

REFERENCES

[1] Wright, E. P. (1992). The hydrogeology of crystalline basement aquifers in Africa. *Geological Society, London, Special Publications*, 66 (1), pp. 1–27. http://dx.doi.org/10.1144/GSL.SP.1992.066.01.01.

[2] Lloyd, J. W. (1999). *Water resources of hard rock aquifers: in arid and semi-arid zones* (No. 631.7 L5).

[3] Ahmed, S., Jayakumar, R., Salih, A. (eds.). (2008). *Groundwater Dynamics in Hard Rock Aquifers: Sustainable Management and Optimal Monitoring Network Design*. Springer Science & Business Media. https://doi.org/10.1007/978-1-4020-6540-8

[4] Prasad, R. K., Mondal, N. C., Banerjee, P., Nandakumar, M. V., & Singh, V. S. (2008). Deciphering potential groundwater zone in hard rock through the application of GIS. Environmental geology, 55, 467-475.

[5] Jaiswal, R. K., Mukherjee, S., Krishnamurthy, J., Saxena, R. (2003). Role of remote sensing and GIS techniques for generation of groundwater prospect zones towards rural development--an approach. *International Journal of Remote Sensing*, 24 (5), pp. 993–1008. http://doi.org/10.1080/01431160210144543

[6] Lokesha, N., Gopalakrishna, G. S., Mahesh, M. J. (2007). Hydrogeomorphological studies in Kallambella watershed, Tumkur district, Karnataka state, India using remote sensing and GIS. *Journal of the Indian Society of Remote Sensing*, 35 (1), pp. 107–115, http://doi.org/10.1007/BF02991839.

[7] Mohammed, M. A. A. (2020). The use of Landsat ETM+ in Hydrogeological Investigation in Basement Terrain, Hamissana Area, N-E Sudan, *Humanitarian and Natural Sciences Journal*, 1 (6), pp. 370–378.

[8] El-Nadi, A. H. (1984). *The geology of the late precambrian metavolcanics, Red Sea Hills, NE Sudan.* Doctoral dissertation, University of Nottingham.

[9] Vail, J. R. (1983). Pan-African crustal accretion in north-east Africa. *Journal of African Earth Sciences* 1 (3–4), pp. 285–294. http://dx.doi.org/10.1016/S0731-7247(83)80013-5

[10] Ahmed A. A. M. (1980) General outline of the geology and mineral occurrences of the Red Sea Hills. *Geol. Min. Res. Dept. Bul.*, 31, pp. 30–63.

[11] Stern, R. J., Kröner, A., Manton, W. I., Reischmann, T., Mansour, M., Hussein, I. M. (1989). Geochronology of the late Precambrian Hamisana shear zone, Red sea Hills, Sudan and Egypt. *Journal of the Geological Society*, 146 (6), pp. 1017–1029, http://dx.doi.org/10.1144/gsjgs.146.6.1017.

[12] Almond, D. C., Kheir, O. M., Poole, S. (1984). Alkaline basalt volcanism in northeastern Sudan: a comparison of the Bayuda and Gedaref areas. *Journal of African Earth Sciences*, 2 (3), pp. 233–245. https://doi.org/10.1016/S0731-7247(84)80018-X

[13] Elsheikh, Abdalla EM, Khalid A. Elsayed Zeinelabdein, and Sami OH El-Khidir (2014). The use of remote sensing and GIS techniques as a guide to other geological methods for groundwater investigations in Hamisana Basement Terrains, Red Sea Hills, NE Sudan. *International Journal of Geosciences and Geomatics*, 2 (2), pp. 40–46.

[14] Singhal, B. B. S., Gupta, R. P. (2010). *Applied Hydrogeology of Fractured Rocks*. Springer Science & Business Media. http://dx.doi.org/10.1007/978-90-481-8799-7

[15] Charon, J. E. (1974). Hydrogeological applications of ERTS satellite imagery. In *Proc. UN/FAO Regional Seminar on Remote Sensing of Earth Resources and Environment*. Commonwealth Science Council, Cairo, pp. 439–456.

[16] Balasubramanian, A. (2007). *Methods of Groundwater Exploration*. Centre for Advanced Studies in Earth Science, University of Mysore, Mysore—*6.*

[17] Dillon, P. (2005). Future management of aquifer recharge. *Hydrogeology Journal*, 13 (1), pp. 313–316, http://dx.doi.org/10.1007/s10040-004-0413-6.

Geosciences and Engineering, Vol. 10, No. 15 (2022), pp. 185–201.
https://doi.org/10.33030/geosciences.2022.15.185

APPLICATION OF NANOTECHNOLOGY IN ENHANCED OIL RECOVERY

SOBHAN ANVARI[1, 2], ZOLTÀN TURZO[1, 3]

[1]*Faculty of Erath Science and Engineering, Institute of Petroleum and Natural Gas, University of Miskolc, Hungry*
[2]*sobhan_anvari@yahoo.com, https://orcid.gov/0000-0002-0235-6890*
[3]*Turzo@uni-miskolc.hu, https://orcid.gov/0000-0002-7147-1163*

Abstract: Responding to the growing demand in the oil industry is possible in two ways: by finding new hydrocarbon resources or by increasing extraction from existing oil reservoirs. Increasing production efficiency by modifying EOR methods is quite obvious while the process of exploring new oil fields is declining and many oil fields are in the final stages of production; Because in many reservoirs of the world about two-thirds of the oil in situ cannot be extracted by conventional methods.

Recovery mechanisms in EOR operation can also be enhanced using nanotechnology. Nanotechnology-assisted EOR processes depend on several factors: mobility control using viscosity-increasing solutions, altering the rock wettability, reducing the interfacial tension (IFT), and lowering the oil viscosity using nanocatalysts. The efficiency depends on how the process behaves at both the macro and micro scales.

The microscopic efficiency considers the displacement of the fluids at a poral scale and measures how effective the displacing agent is in mobilizing oil and rocks to make contact. In this regard, the geometry of the pores, capillary pressure, viscous forces, rock wettability, and rheological behavior play a major role.

The macroscopic efficiency is the relationship between the connected reservoir volume being swept by the injected fluid and the volume of oil originally in the reservoir and parameters affecting this factor are: the rock heterogeneity and its anisotropy, the absolute permeability, the mobility ratio, and the gravitational segregation.

Downstream processes such as petroleum refining are employed to extract up to 40% more gasoline in catalytic cracking units than their predecessors. In upstream operations, the first application of nanotechnology was the development of nano-enhanced materials.

Nanotechnologically enhanced oil recovery processes involve (a) the addition of nanoparticles in the displacing agent enhancing its rheological properties, which are known as nanofluids; (b) the use of nanoparticles as stabilizing agents in the formation of nanoemulsions; and finally, (c) active nanoparticles working as nanocatalysts injected to perform in-situ upgrading operations in the porous medium before extraction.

Keywords: *Nanotechnology, EOR, Nanoparticles, Nanoemulsions, Nanofluids, Nanocatalysts*

1. INTRODUCTION

The growing demand in the oil and gas industry and responding to it has made the use of Enhanced Oil Recovery (EOR) methods from oil reservoirs an inevitable

necessity, given the development of nanotechnology and its significant share in the oil industry and various fields such as exploration, drilling, enhanced oil recovery, refining, and distribution.

Recently, nanotechnology with the improvement of reservoir geomechanics and surface tension modification along with the improvement of oil reservoirs has the potential to change and modify the usual EOR methods and has attracted the attention of many researchers on a laboratory and industrial scale. An industrial scale has been used to identify the effect of injecting fluids at high temperatures into heavy oil reservoirs or generating heat inside the reservoir by thermal on-site as well as non-thermal methods to increase extraction.

Conventional EOR methods from heavy oil reservoirs are divided into two general categories of thermal and non-thermal methods .Some of the methods that have been successful so far are:

a) Thermal EOR, which involves applying heat to a reservoir, such as injecting water vapor, to reduce the viscosity of heavy oil and improve its ability to flow through the reservoir.
b) Injection of gases such as natural gas, carbon dioxide, and nitrogen that expand in the reservoir and cause oil to move to the wellhead. Injecting other gases that dissolve in the oil and reduce its viscosity can also make it easier for the oil to move inside the reservoir.
c) Injections of chemicals, such as surfactants, are used to reduce surface tension and prevent oil droplets from forming as the oil passes through the reservoir.

However, each of these methods is abandoned due to high cost or in some cases poor performance and efficiency in reservoir extraction.

The operation of wells includes all activities that lead to its production, maintenance, and increase. Certainly, the use of nanotechnology can facilitate and accelerate operations and ultimately lead to increased production from reservoirs. (Pourali – Pirmoradi, 2010)

2. VARIOUS APPLICATIONS OF NANOTECHNOLOGY IN THE OIL AND GAS EXPLORATION AND PRODUCTION INDUSTRIES

2.1. Application of nanotechnology in the exploration process

One of the applications of nanotechnology in the exploration process is the use of small sensors made of fiber optics to measure pressure, temperature, oil flow, and sound waves in oil wells. Another application is to inject nanosensors into the tank and receive more detailed information about the structure of the reservoir and also use of nanosensors in seismic imaging.

2.2. Application of nanotechnology in drilling operations

It involves the addition of some nanomaterials to drilling cement, which results in a uniform distribution of the cement mixture and thus uniformity of cement properties. Adding calcium silicate nanoparticles to drilling cement improves the application of

cement at high temperatures (deep wells and geothermal wells), Addition of some nanomaterials causes, stability of cement quality, removal of excess water, having a suitable specific gravity, initial compressibility, and proper timing, stronger cement coating, lower permeability and permeability of cement, inhibition of gas migration, prevention of fluid waste and proper insulation of layers. Construction of more durable drilling equipment (especially drilling rigs) using nanocrystals as coating and improvement of thermal and compressive strength of drilling rigs, as well as the use of nanomaterials in better absorption of oil residues from drilling mud and the use of nanoparticles (zinc oxide, to absorb H_2S from drilling fluids and use compounds), nano-lubricant, and other applications of nanotechnology in drilling operations for oil and gas wells, are in drilling and lattice operations.

The combination of chemical EOR agents with different nanomaterials has shown increased recovery efficiencies in rock formations that had otherwise reached their operational limit (Asrilhan, 2005; Suslick et al., 2009).

However, the potential advantages of the application of nanomaterials in oil recovery should also be carefully considered from an environmental point of view. Some concerns have been raised since the same features that make nanotechnology so attractive to oil recovery processes might also harm the environment and human health. These include the potential long-term side effects associated with medical applications as well as with the biodegradability of nanomaterials being used(Raffa – Druetta, 2019; Holsapple et al., 2005; Balshaw et al., 2005; Tsuji et al., 2006; Borm et al., 2006; Powerset al., 2006).

Even though during the last years many nanomaterials have been inserted into the market, the amount of information over their impact on the environment is minimal. For instance, there is almost no information about the associated risks in the manufacturing, usage, and final disposal of nanomaterials (Hashemi et al, 2014). Focusing on EOR techniques, it has been shown that a percentage of the nanoparticles will remain underground and deposited in the rock formation, remaining for many years, and this could cause the contamination of groundwater sources. Thus, one of the desirable properties of these nanoparticles should be high durability and recyclability in a cost-effective process to decrease their impact on the environment (Hashemi et al., 2014)

2.3. Application of nanotechnology in equipment protection

The total cost of corrosion, which is imposed annually in the world of the oil and gas industry, is about millions of dollars that were spent on corrosion of surface plumbing and equipment, and also spent on in-well pipes. As one of the biggest concerns in the oil and gas industry, corrosion of equipment, coating, fabrication of parts using nanotechnology can increase the strength, stability of the equipment, and reduce their depreciation.

Nanomaterials can be used in many sectors of the oil and gas industry. By making several materials at the nanoscale, equipment that was lighter, more stable, and more powerful than conventional equipment (Taghavizadeh & Hashemizadeh, 2014). The

use of nanostructured materials in this area by using nanocomposites, nanocomposite coatings, nanoparticles, and nano-lubricants can be divided into the following will be mentioned. Nanocoatings have a higher coefficient of thermal expansion, hardness, and toughness compared to micrometer coatings. They are more resistant to corrosion, abrasion, and erosion (Taghavizadeh & Hashemizadeh, 2014)

2.4. EOR using nanosurfactants

Surfactants refer to substances that reduce surface tension. These materials can be divided into biosurfactants, nanosorfactants, and polymeric surfactants based on the structure and method of production. When these materials are dissolved in the solvent, they form structures with nanoscale to micrometer dimensions. These materials are often composed of a hydrophilic head and a hydrophobic tail, and depending on the nature of their tail into categories: non-ionic or uncharged, anionic or negatively charged, cationic or positively charged, and amphoteric, both positively charged and amphoteric. Has a negative charge, they are divided (Towler et al., 2017).

2.5. EOR using nanoparticles

Among the important applications of nanoparticles in this field is the use of nanomaterials to facilitate the separation of oil and gas inside of reservoir and nanosensors inside the reservoir rock. These nanoparticles when combined with rocks containing crude oil they drop their shipments and recycle crude oil.

According to studies, one of the main applications of nanoparticles is to change the wettability of reservoir rocks. The wettability of a reservoir rock fluid system is defined as the ability of a fluid to spread on the rock surface in the presence of another fluid. Wettability not only determines the initial distribution of fluid but is also a major factor in how fluid flows in the reservoir and plays an important role in oil and gas production. In general, hydrophilic reservoir rock is preferable to the oil-friendly reservoir rock. Because the reservoir rock is oil-friendly, the oil tends to stick to it and thus reduces production.

When the well is being operated, due to the damage to the formation, the reservoir rock may become oil-friendly, in which case the wettability of the reservoir rock can be well improved by using nanoparticles. For this purpose, the effect of nanofluids on the wettability of carbonate rock as one of the main factors in enhanced oil recovery has been investigated in studies, and ZnO_2, TiO_2, $CaCO_3$, and SiO_2 nanoparticles are used in this regard (Nazari Moghaddam et al., 2015).

2.6. Improvement in place of heavy oils with the help of nanocatalysts

Nanocatalysts are used to upgrade heavy oil in situ and convert them to lighter compounds to reduce the viscosity of the fluid inside the porous medium and its ease of movement towards production wells can be used as an effective method to increase the extraction of heavy oils (Hashemi et al., 2012; Hashemi et al., 2014). Hydrogen and colloidal catalyst can be injected simultaneously through a well; In

another method, the first hydrogen is injected and after a sufficient time for complete hydrogen penetration into different areas of the tank, the catalyst mixture is injected. After the injection operation, sufficient time is given for the injected mixture to contact the tank oil and to perform the necessary reactions to improve the heavy oil position through the hydrogenation process. By successive sampling of the oil produced by the well and according to the temperature, pressure, and porosity of the formation, the suitability of the viscosity of the produced oil for its economic production will be measured (Owen).

The time required for the injected mixture to come into contact with the tank oil, called the "catalytic wetting" time, varies from less than one day to hundreds of days, depending on the tank conditions and the properties of the heavy oil (Owen).

2.7. Use of nanoparticles in solvent flooding operations to increase chemical EOR

In reservoirs that for various reasons, including environmental and technical issues, the type of reservoir structure and the probability of sand production, high content Asphaltene and permeability, porosity, it is not possible to use thermal methods to increase oil extraction/(EOR), chemical improvement of oil recovery coefficient may be a suitable method. The main mechanisms for increasing the extraction/(EOR) of heavy oil in flooding operations with solvent-based emulsions include control of mobility, reduction of oil viscosity, and emulsification.

Fluid flow control is one of the most important factors in the extraction of hydrocarbon fluids. In this case, the front of the injected fluid must move as evenly as possible so that it can penetrate the formation properly. To improve this process, researchers have succeeded in producing nanoparticle-based surface and non-permeable agents that can improve the flow rate in extraction and production operations. In this case, nanoparticles are needed that:

1) Do not stick to the body of the formation matrix in any way.
2) It can be detected in very low concentrations.
3) Can cause the deformation of the fluid inside the cavity.
4) Can change the surface tension between hydrocarbons and saline water or between the fluid and the surface of the reservoir rock (Onyekonwuand Ogolo, 2010).

Researchers at MIT have also discovered that the addition of water-repellent magnetic nanoparticles, when mixed with oil and eventually using a strong magnet, can easily separate the oil-water mixture. The exploitation of oil reservoirs plays a very important role. This process must take place outside the oil recycling tanks to prevent contamination of the environment by nanoparticles. According to Zhan's research, this process, which uses ferrofluids fluids that contain magnetic nanoparticles has shown very positive results. In this process, a mixture of water and fluid is passed through the canal and outside the canal, a suitable magnet is placed to guide it to the desired location so that the separation operation can be done in a very suitable way.

2.8. Use of nanoparticles to improve polymer flooding operations

Some polymers have excellent properties and solubility to improve injection properties in oil reservoirs. Polymers are widely used in EOR operations. Such compounds act as modifiers of the rheological properties of the reservoir fluid to improve the continuous phase viscosity and thus the mobility ratio and flooding efficiency to ultimately increase the recovery rate and oil production rate. Polymer systems must be able to withstand the conditions in oil reservoirs.

In addition, the polymer used must be completely soluble, have high viscosity at low concentrations of the solution, and have low surface tension and good mobility control relative to the oil phase. The polymer used must also be economical. To solve the problems related to conventional polymer systems, the use of chemically bonded nanoparticles has recently attracted a lot of attention. Flooding with water is one of the most successful and common methods of secondary recycling. Improving the control of water movement and oil movement in low permeability areas is of great importance in this type of operation. For this purpose, cohesive particles are injected into the reservoir as a blocking agent, as a result of which high permeability areas are blocked and low permeability pathways are exposed to flood (Al-Manasir et al., 2009).

2.9. Effect on viscosity

Other applications of nanotechnology include changing the viscosity of injected fluids into the oil phase, including water, CO_2, or surfactant solutions in the form of intelligent fluids (Saidur et al., 2011). Viscosity remains largely intact, so researchers are always trying to reduce their viscosity by using enhanced oil recovery methods.

One of the effective factors in increasing the enhanced oil recovery is the viscosity of the fluid that is injected into the reservoir to move the oil, which is usually less than the viscosity of the oil. The addition of nanoparticles can adjust the viscosity of the injected fluid to the optimum level and improve the movement in the reservoir, thus increasing the oil extraction efficiency. The results of studies Shah Rusheet, (2009) showed that the viscosity of carbon dioxide with the addition of 1% of CuO (Copper Oxide) nanoparticles and a small amount of distributor is approximately 140 times the viscosity of ordinary carbon dioxide; Therefore, by spraying such nanoparticles in the propellant carbon dioxide fluids, the desired mobility and high sweeping efficiency can be achieved, which leads to more oil extraction from the reservoir.

Shah Rusheet (2009), performed two experiments to investigate the effect of nanoparticles on reducing the viscosity of heavy oil. The first group uses CO_2 nanofluid consisting of carbon dioxide gas as a base fluid and nanoparticles of CuO and polydimethyl cyclohexane (PDMS) as a distributor and the second group uses VRI nanofluid consisting of viscosity reducing fluid (VRI) as a base fluid, CuO nanoparticles and polydimethyl cyclohexane (PDMS) as distributors.

Core flooding experiments performed by injecting carbon dioxide on a sample of Berea core, once alone and again with copper oxide nanoparticles, showed that injecting carbon dioxide alone resulted in 58% of oil recovery, while with the use of CuO nanoparticles this amount can be increased up to 71%. The results also show

that with the increase of PDMS and CuO nanoparticles in the carbon dioxide-based injection fluid, the density and viscosity of the injection fluid decreases, which reduces the mobility of the injection fluid and increases the sweeping efficiency, which ultimately improves oil recovery. The use of PDMS and CuO nanoparticles can also significantly reduce the viscosity of heavy oil and facilitate oil flow (Shah Rusheet, 2009).

To investigate the effect of nanoparticle size on viscosity reduction, heavy oil samples were compared with different concentrations of iron particles in micro and nano sizes at different temperatures. The results showed a greater reduction in the viscosity of nanoparticles than microparticles (Shokrlu – Babadagly, 2010). This effect can be considered due to the larger specific surface area of nanoparticles, which leads to their greater reactivity compared to microparticles; In other words, the larger the particle surface, the greater the contact of the particle surface with the oil phase, resulting in better interaction between the two phases.

2.10. Effect on the surface tension of the injected fluid

The addition of nanoparticles to the surfactant solution changes the rheological properties and increases the effect of the surfactant solution in the enhanced oil recovery operation. Munshi et al., (2008) showed that the presence of nanoparticles reduces the amount of surface tension at the oil and surfactant interface, which can be attributed to the presence of nanoparticles at the interface.

The primary purpose of using surfactants in extraction and production operations from reservoirs is to reduce surface tension and improve fluid separation operations, correct reservoir wettability, and convert it from petroleum to hydrophilic mode, which facilitates the separation of hydrocarbon fluid from the formation and also reduces the viscosity of the oil. At the same time, this causes the diameter increase and space between the layers to swell and increase using the width of the long surfactant chains, which in turn blocks the fluid filtration pathways. Also, large surfactants are absorbed due to improper structure in the initial intervals of the formation or have an inverse effect on wettability. Therefore, some properties of these materials reduce their effect in reducing capillary pressure. While the goal is to reduce capillary pressure and increase the permeability of the formation in enhanced oil recovery. Today, the use of nano surfactants due to their smaller size and the higher active surface has improved the process of using these materials.

When the dimensions of these materials are in the nanometer range, their ability to penetrate the formation cavities and their active surface area increase significantly. These materials widely affect the surface tension n of the reservoir fluid and reduce its viscosity. In this case, the fluid whose viscosity is reduced inside the reservoir and well, is lighter and flows better in the exit path of the well, and is separated from other materials in the well. Studies show that surfactants affect nanocomplexes and complex compounds in wells and alter reservoir structure. In this case, the ability of the surfactant to penetrate between the layers of the formation is very important (Tari – Alipour, 2013).

2.11. Effect on emulsions

One of the most effective methods to reduce the viscosity is emulsification, but the methods currently used for emulsification are too expensive or have poor performance for large-scale use. The use of nanoparticles can be considered as a solution to these problems. Nanoparticle-stabilized emulsions have attracted the attention of many researchers due to their many special properties and advantages over conventionally stabilized emulsions by surfactants or colloidal particles. Oil-in-water and water-in-oil emulsions stabilized with silica nanoparticles of various sizes have been investigated. Surfaces stabilized with water/oil emulsions are generally used in the oil industry. Emulsions are also produced with solid particles called stabilizers, but due to the presence of solid particles in the form of colloidal particles with micron size and easily trapped in rock cavities, they are rarely used in the oil industry. Nanoparticles have useful properties for enhanced oil recovery operations in the oil industry. Drops of emulsions stabilized with them, due to their small size, easily pass through the cavities and flow through the reservoir rock without much return. In addition, these emulsions can remain stable for several months without coagulation.

They are also able to withstand the harsh conditions of the reservoir due to the irreversible adsorption of nanoparticles on the droplet surface. In addition, the high viscosity of nanoparticle-stabilized emulsions can contribute to the degree of mobility during flooding operations, thus providing a durable way to move highly viscous oils from beneath surfaces (Zhang et al., 2010)

The results of Berea core flooding experiments indicate that oil recovery in nanofluid flooding in pure form is slightly better than nanofluid flooding followed by water flooding, which is related to the breakthrough time delay due to the formation of a viscous crude oil emulsion.

Studies on the equilibrium and stability of emulsions stabilized by colloidal particles and nanoparticles showed that the particle concentration is a key parameter in controlling the stability of emulsions so that increasing the particle concentration increases the volume and stability of the emulsion. The results also show that the average size of emulsion droplets decreases with increasing concentration, which allows more particles to be placed on the joint surface (Zhang et al., 2009)

The results of studies on supercritical CO_2 emulsions in water by Dick Son et al; and supercritical CO_2 water emulsions by Adkins et al; are of particular interest for other enhanced oil recovery processes to produce CO_2 water emulsions, they mixed water consisting of 1 to 50% by weight of silica nanoparticles with CO_2 at 25 °C and pressures varying between 34 and 700 bar. The results showed that the stability of emulsions increases with increasing nanoparticle concentration. Adkins et al., (2007) showed that water emulsions in CO_2 can be stabilized with hydrophobic silica particles with a diameter of less than 10 nm.

Water emulsions in CO2 consist of highly stable nanoparticles and form a compact layer of nanoparticles at the droplet water/CO_2 interface and have the ability to overcome many limitations such as the ability to withstand high temperature and

salinity conditions that surfactants-stabilized emulsions face. Zhang et al. (2009) studied stabilized water/oil emulsions using surface-modified silica nanoparticles. The results showed that these emulsions remained stable for weeks at room temperature and above; The reason for this was attributed to the presence of surface-modified nanoparticles by polyethylene oxide polymer.

2.12. Use of nanoemulsions

Nanoemulsion is one of the smart fluids that can recover the remaining crude oils at the bottom of the reservoir rock. Nanoemulsion, which is a family of emulsions with droplet sizes in the range of 50–500 nm, has attracted a lot of attention in recent years due to its unique properties and characteristics. The presence of very small droplets of scattered phases in them has caused the phenomenon of separation of phases in this family from materials does not occur in the short term (Nalbandi – Khalili, 2013). Nanoemulsions contain chemicals used in petroleum fields and have a wide range of applications in good operations to prevent sedimentation, acid leaching, and sediment removal. One of the important properties of nanoemulsions, which is of great interest for use in petroleum fields, is the excellent resistance of these materials against sedimentation and cream formation, which can be attributed to the lack of separation of phases in storage tanks or chemical feed lines related.

The droplet size of nanoemulsions is smaller than the pore entry pores in sandy beds and reservoir rocks, which means that the emulsion can penetrate very well without the need for fluid filtration (Nalbandi and Khalili, 2013).

Nanoemulsions, have successfully been developed in laboratories, and the upcoming challenge is to develop techniques for cost-efficient industrial-scale production techniques (Engeset, 2012). They can be designed to be compatible with reservoir fluids/rocks and be environmentally friendly (Cocuzza et al., 2012). Some newly developed nanofluids have shown extremely improved properties in applications such as drag reduction, binders for sand consolidation, gels, wettability alteration, and anticorrosive coatings (Chaudhury, 2003; Esmaeili, 2011). In heavy oil reservoirs where EOR thermal production processes are usually utilized, the application of nanotechnology yielded several breakthroughs.

2.13. Use of nanofilters

Nanotechnology has provided new insights into improved oil extraction. This technology helps to separate oil and water more efficiently. More oil can be released using nanoscale materials in oil fields. Water and petroleum products do not mix, but they can be severely contaminated and difficult to separate. There are various methods for separating water from oil, which are not cost-effective due to high operating costs, low efficiency, and large equipment. To solve this problem, a combination of carbon nanotubes and microtubules can be used.

A filter surface that has both superhydrophobic and superoleophobic properties is suitable for separating water and oil. Such a filter can be produced by stacking multi-walled carbon nanotubes on a stainless steel mesh. Carbonated materials have

oleophilic properties and therefore carbon nanotubes have high oleophilic properties due to their capillary properties. Research has also shown that increasing surface roughness causes hydrophobicity. Therefore, the fabrication of a nanotube mesh in which carbon nanotubes are placed vertically can be used to separate water from oil.

One of the advantages of this nanotube filter is that it separates water from oil and oil compounds with high efficiency. Another advantage of this filter is that it works easily using gravity and does not require a suction device. This filter is used to recycle oil spilled into the sea and separate saline water from crude oil from oil wells whose oil is mixed with saline water.

2.14. Use of nanogels and nanocomposite gels

One of the factors that reduce oil production is the production of excess water. Increased water production, along with the limited processing capacity of operating facilities, reduces production efficiency and even abandons wells. On one hand, the process of removing the produced water costs a considerable amount of money, and on the other hand, the unprincipled disposal of this water causes many problems in terms of environmental issues. One of the most common reasons for the increase in water and gas production in oil wells is the decrease in reservoir pressure due to production, resulting in a decrease in the gas-oil contact level and an increase in the water-oil level.

One of the common chemical methods to prevent the production of excess water in oil and gas wells is the use of polymer gels, which today due to low initial cost and chemical stability and low sensitivity to bacterial degradation, etc. have been considered. Gels are used to close gaps and high-permeability areas that play an important role in producing excess water.

In general, in the gel injection process, first, the gelatin solution is injected into the formation and after the formation of the gel inside the formation, the well returns to the production circuit. Today, one of the most practical types of polymer gels is polyacrylamide-chromium acetate polymer gel. The mentioned advantages, including low cost, are the reason for using these gels.

The disadvantages of these gels are low mechanical strength due to the application of mechanical stresses during the injection process through the pump and also when entering the formation. These mechanical stresses can lead to the breaking of polymer chains and a significant reduction in the molecular weight of the polymer. Therefore, the gelatin solution, which contains a polymer and a lattice agent and solvent, cannot reach significant strength inside the formation. As a result, when the well returns to the production circuit, the gel system formed with low strength is easily removed from the porous medium and practically cannot have the desired performance in reducing the permeability in the formation.

These gels are vulnerable to water formation. Because the water formation due to having a large amount of monovalent and divalent ions reduces the strength and disintegration of the gel structure. For this reason, today, by adding mineral particles

at the nanometer scale to the structure of the polymer (composites), they improve its strength and temperature properties (Bahramiyan et al., 2010).

Polymer nanocomposites are a new generation of materials that contain a matrix (polymer and a small percentage) less than 10% by weight (of a nanometer reinforcer) that are blended conveniently. The very small and very high contact surface with less load improves the desired properties and issues related to common amplifiers, such as weight gain, surface defects, and processing problems are less seen in them.

These gelling systems consist of a water-soluble polymer and one or more of the main crosslinking agents. Also, these polymers can be injected into tanks with conventional pumps due to their water-like viscosity. They transform and play their role as path reducers or blockers. In this method, due to the similarity of water viscosity and polymer gels, the cost of injection into the well is much lower than other methods. Also, the penetration depth of this type of gel is much higher than cement due to structural similarity with water; On the other hand, the strength and durability of this type of gels are more than ten times in comparison with ordinary gels and similar conditions (Tari et al., 2013).

To overcome the limitations in the use of existing polymer gels, new nanogels based on polyacrylamide clay (MMT) were developed and their properties were tested experimentally and used for polymer flooding. These nanogels showed good results in thermal, resistance, and mechanical tests compared to ordinary polymer gels. These nanogels can be classified from aqueous solution with a low concentration to an elastic solid or can be used as a crack-blocking agent or a variety of deflectors (Miyahi – Miahi 2013).

2.15. Use of nanosensors, nanorobots, and nano detectors

One of the most important operations in the operation of wells is to record accurate information about the condition of wells such as pressure, temperature, and flow at the well or the bottom of the well. Ensuring the correct operation of measuring instruments is of particular importance (Pourali – Pirmoradi, 2010).

Special types of reliable and inexpensive sensors are being developed from fiber optics to measure pressure, temperature, oil flow, and acoustic waves in wells. These sensors have received a great deal of attention due to their advantages such as small size, safety against electromagnetic interference, ability to operate at high temperatures and pressure, and harsh environments. Most importantly, it is possible to replace and exchange these sensors without interfering with the oil production process and at a reasonable cost. New sensors are very cost-effective in terms of production and take more accurate measurements (Pourali – Pirmoradi, 2010).

The technology of these sensors is expected to improve oil production by providing accurate and reliable measurements and reducing the risks associated with oil exploration and drilling. The use of nanorobots and their effect on reducing graphing error is another advantage of nanotechnology (Miyahi – Miahi 2013).

Nanorobots which are equipped with nanosensors, can be used to measure formation properties, mud properties, and the environment around the well. Nanorobots are made in such a way that they are equipped with sensors and transmit information to the surface through electromagnetic waves.Nanorobots have the ability to monitor the well at any time and can continuously measure the properties of the formation and send its information to the surface of the earth (Rostaei et al, 2010).

With the help of this technology, the environmental effects affecting the graphing operation can be reduced or minimized, which will lead to more accurate knowledge and evaluation of reservoir engineers of the static and dynamic behavior of the reservoir. It is also possible to better detect and study the movement and displacement of injected fluids in reservoirs using nano detectors (Miyahi – Miahi 2013).

2.16. Use of nanocatalysts

Improving in situ oil and converting it to lighter compounds to reduce the viscosity of the fluid in the porous medium and its ease of movement towards production wells can be used as an effective method to increase the extraction of heavy oils.

Hydrogen and colloidal catalyst can be injected simultaneously through a well. In the other method, hydrogen is injected first and after a sufficient time for the complete penetration of hydrogen into different areas of the reservoir, the catalyst mixture is injected. After the injection operation, sufficient time is given for the injected mixture to come into contact with the reservoir oil and to perform the necessary reactions to improve the heavy oil in situ through the hydrogenation process.

By successive sampling of the oil produced by the well and according to the temperature, pressure, and porosity of the formation, the suitability of the viscosity of the produced oil for its economic production will be measured. The time required for the injected mixture to come into contact with the reservoir oil, called the "catalytic wetting" time, varies from less than one day to hundreds of days, depending on the reservoir conditions and the properties of the heavy oil (Mohammadi – Ghajari, 2013).

3. RESULTS

Increasing production efficiency by modifying EOR methods while the exploration of new oil fields is declining and many oil fields are in the final stages of production is quite obvious. Because in many reservoirs of the world about two-thirds of the oil in situ cannot be extracted by conventional methods. There are many methods for increasing extraction from oil reservoirs, which are divided into two general categories of thermal and non-thermal methods.

The results of various researches indicate that the use of nanotechnology can be effective and practical in increasing oil extraction from reservoirs. Nanoparticles can increase the enhanced oil recovery by changing the wettability of the reservoir rock, affecting the viscosity, changing the surface tension of the injected fluid, and affecting the emulsions. Nanoemulsions can also recover crude oil remaining at the bottom of the reservoir rock. Nanoemulsions contain chemicals used in petroleum

fields and have a wide range of applications in good operations to prevent scale formation, acid leaching, and sediment cleaning and removal.

One of the factors that reduce oil production is the production of excess water. There are various methods for separating water from oil, which are not cost-effective due to high operating costs, low efficiency, and large equipment. To solve this problem, a combination of carbon nanotubes and microtubules can be used. It is also possible to use polymer gels, which have been considered today due to their low initial cost, chemical stability, low sensitivity to bacterial degradation, and so on. Nanocomposite gels are used to close gaps and high permeability areas that play an important role in the production of excess water.

Improving in situ oil and converting it to lighter compounds to reduce fluid viscosity in the porous medium and facilitate its movement towards production wells can be an effective way to increase the extraction of heavy oils, for which nanocatalysts can be used. Also, nanosensors, nanorobots, and nano detectors can be used to record detailed studies of the condition of wells such as pressure, temperature, and flow at the well or the bottom of the well.

4. CONCLUSION

With the review of nanotechnology, the many capabilities, and applications of using nanofluids in increasing enhanced oil recovery, increase oil efficiency between 5–35% in addition to the efficiency with the main fluid. Due to their small size, nanoparticles can pass through the cavities, they cause very little sediment in the reservoir and spread easily into the core, so the permeability decreases shortly after they cause flooding. Studies on the application of nano to increase the enhanced oil recovery of hydrocarbon reservoirs are mostly theoretical and laboratory and need to be used and developed on a field scale. The expansion and development of this research on a field scale can bring various successes to the oil and gas industry. Economic studies of the use of this technology will also reveal the possibility of doing so on a practical and field scale.

Nanofluids are obtained from the distribution of nanoscale particles in ordinary fluids, which are used as the base fluid for the dispersion of nanoparticles. In recent years, with the development of nanoscience, the use of nanoparticles in various sectors of the oil industry has been considered. With the help of nanofluids, the separation of oil and gas inside the reservoir can be facilitated and the oil extraction rate can be increased compared to current methods. By adding nanoparticles to a fluid, its properties such as density, viscosity, thermal conductivity, and specific heat can be optimally adjusted.

One of the important applications of nanoparticles is to facilitate the separation of oil and gas inside the reservoir.GP Nanotechnology Company in Hong Kong is one of the pioneers in the development of silicon carbide, a nano-sized ceramic powder. Using these powders, very hard materials can be produced. This mixture will damage the reservoir wall in the well eliminate and increase oil extraction capacity.

Some polymers have very good properties and solubility to improve injection properties in the oil reservoir. Polymers are widely used in EOR operations. Such compounds act as modifiers of properties of reservoir fluid rheology to improve continuous phase viscosity resulting in mobility ratio and flooding efficiency are taken to eventually increase the recycling rate and oil production rate. Polymer systems must have the ability to tolerate the conditions in the oil reservoir.

REFERENCES

[1] Adkins, S. S., Gohil, D., Dickson. J. L., Webber. S. E. and Johnston. K. P. (2007) Water-in-carbon dioxide emulsions stabilized with hydrophobics silica particles. *Physical Chemistry chemical physics*, Issue 48, pp. 6333–6343.

[2] Al-Manasir, Nodar, Anna-Lena Kjøniksen, and Bo Nyström. (2009). Preparation and characterization of cross-linked polymeric nanoparticles for enhanced oil recovery applications. *Journal of applied polymer science*, Vol. 113, 3, pp. 1916–1924, https://doi.org/10.1002/app.30176.

[3] Asrilhant B. (2005). A program for excellence in the management of exploration and production projects. In: *Offshore Technology Conference. Houston*, USA: Society of Petroleum Engineers. https://doi.org/10.4043/17421-ms

[4] Bahramiyan, B. Mosavi moghadam, A. Hemati, M. Vafaei safti, M. Dadvand Kohi, A. (2010). Investigation of the effect of Montmorillonite nanoparticles. On the gels of polymers used in water blocking operations in oil reservoirs. *Exploration and production*, Vol. 68, pp 52–56 (in Persian).

[5] Balshaw, D., Philbert, M., Suk, W. (2005). Research strategies for safety evaluation of nanomaterials, part III: Nanoscale technologies for assessing risk and improving public health. *Toxicological Sciences*, Vol. 88, pp 298–306, https://doi.org/10.1093/toxsci/kfi312.

[6] Borm P et al. (2006). Research strategies for safety evaluation of nanomaterials, part V: Role of dissolution Powers K et al. "Research strategies for safety evaluation of nanomaterials. part VI: Characterization of nanoscaleparticles for toxicological evaluation". *Toxicological Sciences*, Vol. 90, pp 296–303. https://doi.org/10.1093/toxsci/kfj099

[7] Chaudhury, M. K. (2003). Complex fluids: Spread the word about nanofluids. *Nature*, Vol. 423, pp 131–132. [CrossRef] [PubMed]. https://doi.org/10.1038/423131a

[8] Cocuzza, M.; Pirri, C.; Rocca, V.; Verga, F. (2012) Current and Future Nanotech Applications in the Oil Industry. *Am. J. Appl. Sci*., Vol. 9, pp 784–793 [CrossRef], https://doi.org/10.3844/ajassp.2012.784.793.

[9] Engeset, B. (2012). *The Potential of Hydrophilic Silica Nanoparticles for EOR Purposes*. Master's Thesis, Norwegian University of Science and Technology, Trondheim, Norway.

[10] Esmaeili, A. (2011). Applications of Nanotechnology in Oil and Gas Industry. *American Institute of Physics Conference Series*; Patel, R. B., Singh, B. P. (eds.). American Institute of Physics: College Park, MA, USA, Vol. 1414, pp 133–136, https://doi.org/10.1063/1.3669944.

[11] Hashemi, R. Nassar, N. N, Almao P. P. (2014). Nanoparticle technology for heavy oil in-situ upgrading and recovery enhancement: Opportunities and challenges. *Applied Energy*, Vol. 133, pp 374–387. https://doi.org/10.1016/j.apenergy.2014.07.069

[12] Hashemi, R. Nassar, N. N. Pereira-Almao, P. (2012). Transport Behavior of Multimetallic Ultradispersed Nanoparticles in an Oil-Sands-Packed Bed Column at a High Temperature and Pressure. *Energy Fuels*, Vol. 26, pp 1645–1655 [CrossRef], https://doi.org/10.1021/ef201939f.

[13] Holsapple, M. et al. (2005). Research strategies for safety evaluation of nanomaterials, part II: Toxicological and safety evaluation of nanomaterials, current challenges, and data needs. *Toxicological Sciences*, Vol. 88, pp. 12–17, https://doi.org/10.1093/toxsci/kfi293.

[14] Miyahi, N., Miahi, M. (2013). Investigation Nanotechnology applications in the upstream part of the oil industry and provide solutions to reduce the basic problems and short-term needs of Iran in This section. *Scientific-Promotional Monthly of Oil and Gas Exploration and Production*. Vol. 107, pp. 32–39 (in Persian).

[15] Mohammadi, S., Ghajari, A. (2013). Applications of nanotechnology in Oil Extraction. *Second Conference on Hydrocarbon Reservoir Engineering, Related Sciences and Industries*, Oral Presentation, published in Abstract Book, Tehran, Iran. (In Persian)

[16] Munshi, A. M., Singh, V.N., Mukesh, Kumar, Singha, J. P. (2008). Effect of nanoparticle size on sessile droplet contact angle. *J. Appl. Phys*., 103, p. 084315, https://doi.org/10.1063/1.2912464.

[17] Nalbandi, A., Khalili, A. A. (2013). Laboratory experimentFlooding of oily porous media with nanoemulsion. *Scientific-Extensive Monthly of Oil and Gas Exploration and Production*, Vol. 103, pp. 54–60 (in Persian).

[18] Nazari Moghaddam, R., Bahramian, A., Fakhroueian, Z., Karimi, A., Arya, S. (2015). Comparative study of using nanoparticles for enhanced oil recovery: wettability alteration of carbonate rocks. *Energy & Fuels*, Vol. 29, 4, pp. 2111–2119, https://doi.org/10.1021/ef5024719.

[19] Numerical Modeling of Nanotechnology-Boosted Chemical Enhanced Oil Recovery methods Chapter. http://dx.doi.org/10.5772/intechopen.89757 pp1-3.

[20] Onyekonwu, M. O., Ogolo, N. A. (2010). Investigating the Use of Nanoparticles in Enhancing Oil Recovery. *SPE*, 140744. https://doi.org/10.2118/140744-ms

[21] Owen, Ryan O. *Catalytic oil recovery*. U.S. Patent Application No. 12/685,588.

[22] Pablo D. Druetta (2019). Numerical Modeling of Nanotechnology-Boosted Chemical Enhanced Oil Recovery Methods. *Computational Fluid Dynamics Simulations*.

[23] Pourali, A., Pirmoradi, H. (2010). Review on Application of nanotechnology in oil and gas, petrochemical industries. *New process*, Vol. 18, pp 52–60.

[24] Powers K et al. (2006). Research strategies for safety evaluation of nanomaterials. part VI: Characterization of nanoscale particles for toxicological evaluation. *Toxicological Sciences*, Vol. 90, pp 296–303. https://doi.org/10.1093/toxsci/kfj099

[25] Raffa P, Druetta P. (2019). Chemical Enhanced Oil Recovery: Advances in Polymer Flooding and Nanotechnology. Berlin, Germany: De Gruyter; ISBN: 978-3-11-064024-3, https://doi.org/10.1515/9783110640250.

[26] Rostaei, A., Bahrami, A., Safarzadeh, S., Balochi, S., (2010). Nanorobots and their application in well drilling. *The first national conference of new technologies in oil and gas industries.*

[27] Saidur, R, Leong, K. Y. Mohammad, H. A. (2011). A Review on Applications and Challenges of Nanofluids. *Renewable and Sustainable Energy Reviews*, 15, pp. 1646–1668, https://doi.org/10.1016/j.rser.2010.11.035.

[28] Shah, Rusheet D, (2009). Application of nanoparticle saturated injectant gases for EOR of heavy oils. SPE-129539-STU. https://doi.org/10.2118/129539-stu

[29] Shokrlu, Y. H., Babadagly, T. (2010). Effect of Nano-Sized Metal on Viscosity Reduction of Heavy Oil/Bitumen during Thermal Applications. CSUG/SPE137540, https://doi.org/10.2118/137540-ms.

[30] Suslick, S. B., Schiozer, D., Rodriguez, M. R. (2009). Risk analysis applied to petroleum exploration and production: an overview. *Terrae*, Vol. 6, pp. 30–41, https://doi.org/10.1016/j.petrol.2004.02.001.

[31] Taghavizadeh, H. and Hashemizadeh, A. (2014). Investigating the application fields of nanotechnology in Iran's upstream oil and gas industries. *Scientific-Promotional Monthly of Oil and Gas Exploration and Production.* Vol. 111, pp. 33–39, Cross Ref. (in Persian)

[32] Tari, F., Atapour, M. (2013). Application of nanotechnology in production and extraction of oil and gas. are available in website of Nanotechnology Teaching (in Persian), http://nanoeducation.ir/article-detail/%DA%A9%D8%A7%D8%B1%D8%A8%D8%B1%D8%AF/L2Yra0N1ZUpWcUc30HVtRko2ZUIpQT09/.

[33] Towler, Brian F. et al. (2017). Spontaneous Imbibition Experiments of Enhanced Oil Recovery with Surfactants and Complex Nano-Fluids. *Journal of Surfactants and Detergents*, Vol. 20, 2, pp. 367–377. https://doi.org/10.1007/s11743-017-1924-1

[34] Tsuji, J. et al. (2006). Research strategies for safety evaluation of nanomaterials, part IV: Risk assessment of nanoparticles. *Toxicological Sciences*, Vol. 89, pp. 42–50.

[35] Zhang, T. Davidson, A. Bryantand, S. L. Huh, Ch. (2010). Nanoparticle-Stabilized Emulsions for Applications in Enhanced Oil Recovery. *SPE*, 129885, https://doi.org/10.2118/129885-ms.

[36] Zhang, T. Roberts, M. R. Bryant, S. L., Huh, Ch. (2009). Foams and Emulsions Stabilized With Nanoparticles for Potential Conformance Control Applications. *SPE*, 121744, https://doi.org/10.2118/121744-ms.

Geosciences and Engineering, Vol. 10, No. 15 (2022), pp. 202–223.
https://doi.org/10.33030/geosciences.2022.15.202

MAIN ASPECTS OF THE IMPLEMENTATION OF SEISMIC PROJECTS

BRIGITTA TURAI-VUROM

Department of Geophysics, University of Miskolc, 3515 Miskolc-Egyetemváros
brigitta.vurom@gmail.com

Abstract: The paper presents the planning and workflow of field seismic explorations. Seismic data acquisition has developed significantly over the last 15–20 years; the paper covers the most important changes and developments of this period and goes step-by-step through the process of implementing a land 3-D seismic project. In order to increase efficiency, the different cost reduction technologies appeared on the vibroseis source side in 3-D seismic, and wireless field technology is becoming more and more accepted among the forms of seismic data acquisition. The advances in seismic acquisition, including simultaneous source acquisition, wireless channel systems, and exponential growth in seismic channel count, are revolutionizing surveys. Improved receiver sampling along with high productivity are the drivers for seismic technology today, which means smaller, lighter and less power-hungry equipment, while also increasing channel counts, minimizing system-related remediation and HSE risk. A new era in land 3-D seismic surveys has arrived in Europe and in Hungary, too. The author used her experience in the implementation of many domestic and foreign 2-D and 3-D land seismic projects as an observer, shift leader, field manager, and then as a project leader in Europe. She combines these practical experiences with specific aspects of field project design and implementation. The aspects covered in this paper contribute to the professionally efficient and financially profitable implementation of field projects.

Keywords: field seismic exploration, implementation of seismic project, seismic survey, seismic data acquisition

1. INTRODUCTION

A seismic survey is a geophysical method that uses the difference in several parameters (elasticity, density, etc.) of the underground medium to infer the nature and shape of the underground strata. The seismic wave sent into the ground is artificially generated and then the return waves are registered by special sensors. Seismic exploration is the most important and effective way to solve the problem of oil and gas exploration. The assessment of oil and gas reserves is an important phase before drilling begins. During a seismic survey, we have the opportunity to form an image of the subsurface structural elements, covering a large measuring area, up to a depth of several kilometers. This method provides the right amount and quality of information cost-effectively compared to other means of gaining measurements.

Field seismic projects have played a leading role in hydrocarbon exploration since the 1950s [1]. In the first period (until 1990), these seismic surveys were made mainly in a 2-D survey system [2], which revealed the geological structures in the vertical section below the measured profile, as a function of depth. Subsequently, 3-D seismic survey technology became widespread, enabling knowledge of complete spatial geological structures [1, 3]. Today, hydrocarbon surveys use almost exclu-sively 3-D and 4-D seismic surveys [4]. Because 2-D surveys provide data in a smaller dimension, only along measurement lines, the 2-D seismic surveys are usually used only to solve local geological problems [5]. While the success rate using 2-D technology has remained constant, the success rate using 3-D seismic data has shown large-scale improvement [6]. The big oil companies have the necessary resources and expertise for the whole progress (from planning to interpreting data) in-house, while smaller oil companies rely on the experience of consultants.

The successful implementation of seismic projects is inconceivable without good advance planning. During the planning, the need for the necessary equipment (instruments, accessories, transport equipment, etc.), and the need for professional staff must be analyzed in detail. Of course, the timing of implementation and the planning of costs are also very important.

2. SEISMIC SURVEYS

A seismic survey can take place on the surface of the earth (land acquisition) or seafloor (marine acquisition) and can be realized in 2D, 3D or 4D. A source (vibrator unit, dynamite shot, air gun) generates waves into the earth that penetrate through the earth's layers with different seismic responses and reflect from different rock layers. Seismic waves generated by the source are reflected and are recorded at specified locations on the surface by receivers (geophones or hydrophones).

2.1. Marine acquisition

Marine seismic acquisition is mostly carried out using ships with one or multiple air-gun arrays for sources. Air-guns are towed behind the ship and generate a seismic signal at a given interval by forcing highly pressurized air into the water. Seismic receivers are pulled behind the ship, either individually or streamers several kilometers in length. An excellent overview of the theme is given in Dondurur [7].

2.2. Land acquisition

There are four basic components of land seismic acquisition: the location, the sour-ces, the receivers and the recorder. The location of survey determines the sources and receivers. The choices of which sources and receivers to use depend on the target of the survey along with environmental conditions and cost. A survey in a rocky desert, sandy desert, iced area, agriculturally cultivated area, forested area, densely populated area, mountainous area, flat area, or marshy area requires different conditions. This paper discusses 3-D land seismic surveying in the Pannonian Basin only.

3. PLANNING AND IMPLEMENTATION OF LAND SEISMIC PROJECTS IN EUROPE

3.1. The phase of planning

Pre-planning includes the evaluation of geophysical and non-geophysical parameters (environmental considerations, health and safety requirements, etc.) [8]. When planning reflection land seismic projects, the whole process of practical implementation must be taken into account. The implementation process of the seismic projects and the main elements of the process are shown in *Figure 1*. The main blocks of the process are described in detail in the following subsections.

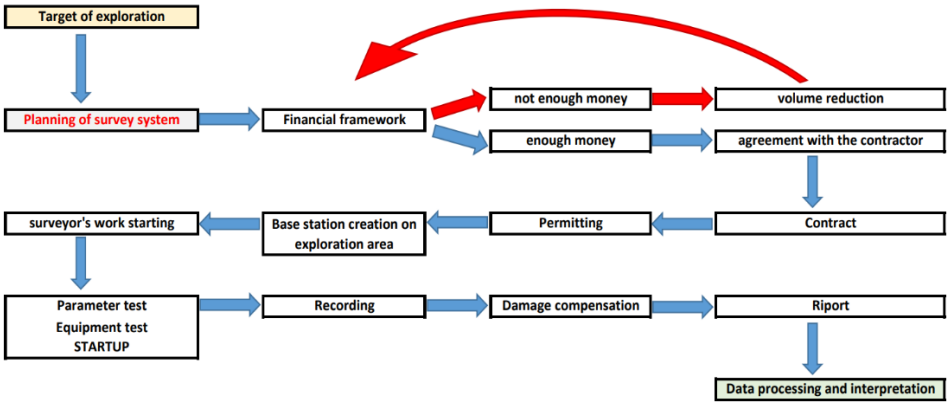

Figure 1
Flowchart of seismic project implementation

3.1.1. The target of the exploration

The pre-planning aims define the geological target of the survey with the associated geophysical parameters [8]. The target of the exploration must be clearly defined. There is usually a primary target, such as delimiting the location and shape of a reservoir rock that is already known from somewhere. There may also be secondary targets for the research, such as examining cover layers or mapping other structures. In many cases, the exploration goals conflict with each other, in which case the optimal solution must be found with careful consideration. The exploration goal should accurately describe its location, extent, depth, possible slope, and geology [6, 9]. If there is a secondary exploration goal, it is best if it is located more shallowly than the main goal, because reflections from deeper will usually be weaker [6].

The price of seismic exploration should be determined according to the benefits of the research. Not only the costs of field seismic survey but also the costs of processing and interpretation and even damage compensation must be taken into account here. The cost of seismic recording is the largest part, 70–80% of the total cost.

The survey is usually performed by a contractor (“service” company). In order to receive bids from contractors, expectations must be accurately described. When

negotiating with contractors, it is very important that we set our quality expectations. Here we not only need to describe the quality of the survey or surveying equipment we expect, but we also have to set standards for the whole crew (the accommodation of workers, quality of food, personal protective equipment, HSE [Health-Safety-Environment] guidelines, rest times, etc.). Deadlines of the sub-processes need to be clarified and the contractor must know the progress of the survey.

3.1.2. Planning of survey system

The survey system can be designed by geophysical parameters. Chaouch and Mari [8] describe the definition of the geophysical parametersthat have to be used during planning. The survey system must be defined as 2-D or 3-D. The selected target of the exploration will be determined by the shape of the network, the distances between the lines, and fold numbers [6]. The main acquisition parameters of the required 3-D survey system are presented in *Table 1*, which also shows the evolution of the geometry of 3-D surveys over the last 20 years: the space sampling and the line distances are getting denser today, the number of active channels is significantly higher and thus the CDP coverage is higher. It is worth planning at least two options; these parameters are indicative of whether the contractor has sufficient capacity to perform. A map of the designed line network should be prepared and any obstacles identified. In addition, further obstacles may occur during the survey (unexpected field object or permitting problems). Unpredictable events cause temporal and financial uncertainty that should be addressed during the planning phase.

All parameters must be determined: the source type, the recorder system, the telemetry system [10], types of cables and geophones, the navigation system, and the calculating method for static correction. The local conditions must be taken into account (weather, topography, environment, agriculture, infrastructure, culture, religion, holidays, customs, etc.).

3.1.3. Financial framework

In addition to the costs, the financial framework required for the successful implementation of the project also includes the profits of the service company. Projects should not be planned without profit because these underfunded projects will certainly not be successful and may even result in a number of future stability issues for service companies. Therefore, it is important that if there is not enough money available for the implementation of the project, then the professional goals (tasks) of the project should be narrowed down (volume reduction).

In the last 10–15 years, the prices of seismic records have been steadily declining. This is due to technical progress and its consequences. With the spread of wireless technology, the survey geometry has become much denser, surveying has become faster, and resource requirements have been reduced, eliminating the need to move tons of cables per day. Fewer people with smaller and fewer vehicles work faster, resulting in lower costs. This allows the seismic company to apply for the job at a lower seismic record price. The supply in the market has increased year by year, new

seismic companies have appeared on the European seismic market, so there is a lot of competition, which further depressed the prices. In the early 2000s, the price of a field seismic record in Central Europe was 170–240 EUR (~40 sources/km^2), around 2010 it was only 100–200 EUR (~80 sources/km^2), and today it is ~ 40–80 EUR (~100 sources/km^2). In 2011, the cost of a 530-km^2 3-D seismic survey (~46,000 source points and ~77,000 receiver points, in flat terrain, without blasting, using the pure vibroseis method, with 250 people on crew per shift) in Southeast Europe was 7.4 million euros, which did not include the amount of damage compensation, data processing, preparation phase or device mobilization costs, only the cost of field seismic acquisition.

The purchase value of the equipment used for this seismic survey is approximately 20–25 million euros, which is why the seismic survey is usually performed by a specialized service company with its own equipment and own professionals.

Table 1

A possible list of the main acquisition parameters in the 2000s and 2020s

In the early 2000s		
3D survey parameters (the data are examples only)	*Option 1*	*Option 2*
Receiver line interval (m)	500 m	300 m
Source line interval (m)	500 m	400 m
Receiver point interval (m)	50 m	50 m
Source point interval (m)	50 m	50 m
Source point in salvo	10	6
Number of channels per line	120	128
Number of active lines	14	18
Number of channels of active patch	1680	2304
Number of geophones per channel	12	12
Geophone groups length	25 m	25 m
Geophone array	linear, in-line	linear, in-line
Folds	42	72
Number of Vibrators	3 + 1 spare	4 + 1 spare
Number of Sweeps/VP	1–6 (to be tested)	1–6 (to be tested)
Sweep length	10–16 sec	10–16 sec
Sweep frequency	6–120 Hz (to be tested)	6–120 Hz (to be tested)
Max offset	4594 m	4168 m
Aspect ratio	0.92	0.80
Record length	8 sec	8 sec
Sample rate	2 ms	2 ms
Filters	Anti-alias only	Anti-alias only

In the 2020s	
3D layout (the data are examples only)	
Receiver line interval (m)	250 m
Source line interval (m)	250 m
Receiver point interval (m)	25 m
Source point interval (m)	25 m
Source point in salvo	10
Number of channels per line	280
Number of active lines	24
Number of channels of active patch	6720
Folds	168
Geometry type	orthogonal

3.2. The phase of implementing

3.2.1. Contract

The contract is an agreement with the contractor. All conditions and parameters must be fixed in the contract. It is important that all conditions and requirements are clearly set out in the contract. A field supervisor must be provided who is independent of the contractor and is able to supervise the whole process. During the survey, this person represents the client company. If it is expedient to change any of the parameters specified in the contract during the seismic survey, this can be initiated with the consent of the supervisor to the ordering company.

3.2.2. Permitting

Permitting means obtaining the necessary permits from the competent authorities and the landowners in the exploration area to carry out the project. It is important to contact the national and local authorities, obtain all necessary permits (explosion permit, environmental permit, road usage, entry into protected places, etc.). It is necessary to walk around the area in advance in order to assess the difficulties, to identify the problematic parts, to prepare for all of them or to avoid them, and to find an alternative. If the exploration is not in the desert but in a densely populated or intensively farmed area, consultation with the landowners is very important: it is essential to inform them of the exploration area and the planned time schedule in advance and get any necessary permissions from them . The lack of a single ownership consent can also cause serious problems – recording may stop for days, resulting in a significant loss of revenue. The implementation of the project can only be started with all the necessary permits because the absence of a single permit can prevent full surveying.

3.2.3. Base camp creation

The project field base station needs to be designated and constructed within or near the exploration area. It must be possible to place instruments, accessories, and means of transport on the base and ensure their proper guarding (protection of property). The site must comply with current HSE requirements. The accommodation and catering of the measuring team must be organized (this is also a very significant cost, depending on the number of employees).

3.2.4. Starting the fieldwork

3.2.4.1. Tests

We can start implementing the project fieldwork only if the planning has been done carefully, the client and the service company have concluded the contract, and all permits have been received. The parameter test and the equipment test can be done before effective work. The types of major tests are listed in *Table 2*.

Table 2
Types of main tests

PARAMETER TEST	STATUP TEST
The most suitable SWEEP parameters for the measurement must be determined:	**All equipments of the measurement must be tested:**
• Sweep frequency	• Geophone test
• Sweep length and amount	• Vibrator test
• Vibrator number and force	• Recording Instrument test • Surveyor Instrument test

The tests are performed in the presence of the field supervisor. During vibroseis measurements, can be variable vibrator and sweep parameters – included in *Table 2* –must always be selected according to the local seismic-geological conditions at the specific research site; this test process is called the parameter test. During the parameter test, we optimize the quality requirements of the signal-to-noise ratio with the costs. The appropriate sweep parameters are selected by the field supervisor according to local conditions. According to Gombár and Deák [11], the signal-to-noise ratio of seismic recordings made with a vibrator is proportional to the relation (1).

$$S/N \approx Pf \cdot Dr \cdot Nv \cdot \sqrt{Ns \cdot SL} \tag{1}$$

where
P_f – peak force of one vibrator,
D_r – drive level (20–80%),
N_v – number of vibrators,
N_s – number of sweeps at the same source point,
SL – sweep length.

The specific field recording is always preceded by a technical audit, called startup testing, where the state of the equipment is checked to see if the equipment is in accordance with the manufacturers' specifications. The entire recording cable instrument is tested simultaneously as shown in *Figure 2*, but geophones are tested separately. Using a purely wireless system has simplified this process, as fewer devices need to be tested.

Figure 2
Recording instruments test in the field before seismic acquisition

3.2.4.2. Land surveying – Surveyor staff

The location of the receiver and source lines is determined in the field by the geodetic group. Land surveying has been changing over the years because of developing technologies that have made this profession much easier and more efficient. A few years ago the only tools available to surveyors were optical levels and theodolites, but today, several kinds of surveyor work rely on GPS systems. A civilian GPS system would also provide sufficient accuracy for general orientation. DGPS systems are used to measure accurate survey coordinates. They refine the coordinates using precisely measured ground transmitters.

Important tasks of the surveyor staff are to prepare lines (clearing vegetation or forest), to provide tracks, protected areas, to set the line network, to supply input for the SPS file (this is the standard format for exchanging geophysical positioning data), and to physically mark on the field the geophone points and the source points (in recent years, the marking of source points has become less and less common, because

by coordinating the digital map with GPS placed in the vibrator, the operator can see exactly where he needs to generate the vibration). This can be done with stakes, stones in brightly coloured bags (in the desert), reflective caps, etc. Identification numbers must also be included on each marker. The job of surveyor staff is also to produce maps of geophone and source points with identification numbers for seismic acquisition workflow. Up to date, these maps inform the whole crew.

3.2.5. Recording

Seismic measurement data acquisition and recording requires appropriate source and sensor systems as well as control and digital data acquisition instruments.

3.2.5.1. Wave generation

There are two types of wave generation: pulse wave source and vibration wave source. The pulse wave source can be weight drop, exploding at the surface, exploding in a blasthole, and Air Gun. An Air Gun is mainly used for marine acquisitions [12].

The requirements for wave generation:

- good quality, high amplitude, wide frequency signal;
- easy and fast to operate;
- cost-effective;
- safe;
- minimal environmental damage.

Vibrators [13] are high-performance shaking machines that were introduced in the USA in the late 1960s; this technique has been used since 1975 in Hungary. They can create any non-pulse waveform to penetrate the ground. An important parameter of vibrators is their weight, which usually determines how much energy they are able to pump into the ground. A vibrator can also be used in urban environments. The vibrator has largely supplanted explosive technology due to its speed, safety, environmentally friendly properties, and better seismic properties:

- a better S/N ratio can be provides due to the correlation;
- adjustable parameters (force, sweep length and amount, sweep frequency);
- repeatability (important for 4D surveys).

Explosives are now used only where vibration is not possible (steep mountains, marshy areas). The peculiarity of the vibrator technique is that very strong surface noise waves are generated. To damp them, several vibrator units are used at the same time, a few meters apart (see *Figure 3*). Thus, the waves propagating on the surface are generated in phase-shift to each other. Selecting the distances properly can reduce each other. The other method is when a team of several vibrators repeats the vibration by moving a smaller distance forward. Channels registered in this way are simply added. This movement is called “move up”.

Figure 3
A vibrator group belonging to GES Ltd.

The special waveform of the vibrator is called a sweep. The commonly used sweep length is 6–20 seconds. The sweep emitted by the vibrators may have an increasing frequency or a decreasing frequency over time. The rate of frequency change can be linear, logarithmic, or exponential. Typical exploration vibroseis sweeps are in the frequency range of ~10 to 100 Hz [13]. Applying a wider frequency range results in a higher resolution, but depending on the depth, signals with a lower frequency are less absorbed [14].

Between 2000 and 2010, seismic surveys in the Pannonian Basin typically used 3–4 vibrators for source generation (see *Table 1*) at the same point, usually with sweep numbers of 2–4. Nowadays, only 1 or 2 vibrators with 1-2 sweep numbers (pushing toward low frequencies) are typical in accelerated surveys. The fuel consumption of vibrators is a significant item in the cost, so cost reduction has also appeared here. To produce low frequencies, the vibrator mass increases with the high hydraulic peak force of heavy vibrators (which can be more than 70,000 lbs).

The technologies on the vibroseis source side have improved in the last 10 years, new methods have been developed, such as “slip sweep” or “blended sweep”, which both increase efficiency and productivity. A slip sweep means that a vibrator group starts sweeping without waiting for the other vibrator group’s sweep to be completed, this method was Rozemond’s idea [15]. The slip sweep recording supplies the potential to drastically increase vibroseis production rates and to reduce the costs [16, 17]. During the slip sweep recording one vibrator begins sweeping before the previous sweep has terminated, so slip sweep data is contaminated by harmonic noise; for this problem Yongsheng et al. [16] presented a new method for eliminating harmonic distortion in slip sweep data. The slip sweep has been used effectively in the desert and other large open areas, leading to significant productivity gains, but there have also been attempts to use the slip sweep in the Pannonian Basin [17]. With slip sweep, the number of records per unit time depends primarily on the slip time, so the sweep length can be increased without loss, thus improving the signal-to-noise ratio [17]. Blended sweep acquisition allows a finer spatial source sampling and a wider range of source azimuths in a cost-effective way; for this method a good overview can be found in Berkhout et al. [18].

Figure 4
High-sensitivity 5 Hz GSG-5 (by SERCEL)

3.2.5.2. Seismic sensors

Seismic sensors (geophones and hydrophones) can be used to detect seismic waves. Geophones *(Figure 4)* are used on land and boreholes, and hydrophones are used in marshy areas, in transition zones, and for marine measurements. Groups of geophones are formed to attenuate surface disturbance waves. Thus, the geophones are connected in series or in parallel. It is important to know the transmission characteristics of the geophone group [19]. In practice, the length of the geophone group is often chosen to be the same as the distance of receiver points. This results in a continuous, non-overlapping layout, and could laid out by workers without error. Today the single sensor systems are widely spread which makes laying out workflow easier and faster. The geophone strings are heavy and take up a lot of space on cars when they are transported, and care must be taken to arrange them geometrically during layout, while the single geophone is smaller, lighter, and therefore faster to deploy, and smaller vehicles are suitable for its transport.

3.2.5.3. Recording instrument

The task of the recording instrument (in the recorder truck, also known as the "dog house", shown in *Figure 5*) with cables is to record the results of the survey with the same quality requirements. All accompanying conditions are recorded so that all data is available later during processing (it was raining, the weather was windy, a train was moving, agricultural machines were working near the layout, etc.).

Figure 5
A recorder truck in the field (left) and the inside of the recorder unit (right)

Figure 6 shows a simplified line structure of a 3-D survey with a Sercel 428XL cable syste, which is the most commonly used cable system from the 2000s. The geophone lines are connected by a line management device called LAUX. Because of the faster data transfer, optical jumper cables are used in addition to traditional cables. Through these, the 3-D data is transferred to the recorder truck, where the seismic record can be visualized for the first time. 12 V batteries are used to keep the lines alive. A battery must be connected to each LAUX and LAUL panel. It is usually necessary to insert one LAUL into the line after 40 FDUs.

One of the main problems with recording is the unreliability of the cables. All connection points are errorprone. Therefore, digitization takes place near the geophones, in the FDU ("Box"). The geophone groups are connected to the FDU. There are amplifiers and filters at the input of the FDU. These signals are fed into the recorder via cables (shown in *Figure 6*). Transmitting digital data is more secure than transmitting analog signals (these are sensitive to cable lengths, impedance changes, connections, etc.).

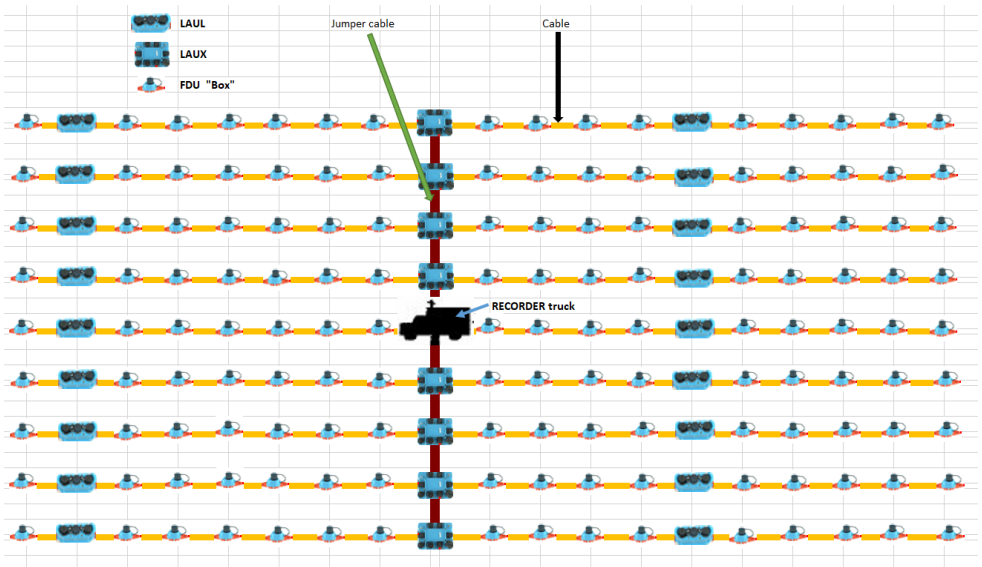

Figure 6
Elements of layout with cables in a 3-D seismic project

Reliability can be further enhanced by transmitting digital data not by cable but by radio frequency transmission [20] or by using wireless seismic technology. Today, the most advanced technology is the wireless (cable-free) field technology, which is becoming more and more accepted also in Europe. Wireless systems are recorded mostly at the sensor. Advancements in modern electronics have given an opportunity for using the completely cable-free single seismic recording unit as a "node" [21]. A node is a stand-alone acquisition unit, which contains all of the elements and technologies needed to sense, acquire, digitize, filter, and store seismic data. Every

node is comprised of internal Li-ion batteries, a processing unit, analog-to-digital converter, filters, memory, clock for timing precision, transceivers, and internal geophone sensor [21]. Wireless autonomous data recording is possible in challenging areas and this system delivers the ultimate in high fidelity data, its tools easy deployment and retrieval.

Figure 7
Quantum single-point sensor node by INOVA

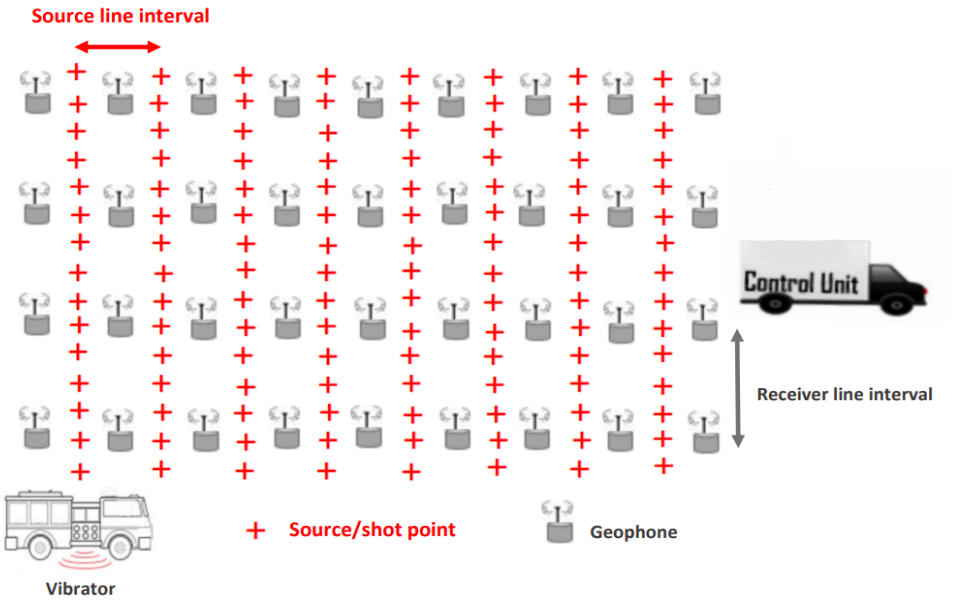

Figure 8
A wireless geophone network orthogonal 3D geometry

It is also possible to use a wired and wireless system together, but the dominance of wireless technology is becoming more common. With this newer technology, real-time quality control is not performed in the field. Shooting blind with autonomous recording systems frees the cables, which are the most vulnerable parts of the system, but it is important to mention that less logistics is needed along with this. This means fewer tools, fewer people, fewer cars, and less maintenance, that is, overall lower operational costs and less error. Wireless technology is revolutionizing seismic data acquisition together with point receivers and MEMS-based digital sensors [22, 23]. The new recording system is based on a wireless platform, providing the ability to reduce footprint and improve operational efficiencies; its single-point sensor node (see *Figure 7*) offers a large surface area and a strong geophone spike and can be buried to improve coupling and reduce environmental noise. The use of wireless geophone networks (WGN) for seismic land data acquisition *(Figure 8)* is summarized by Makama et al. [21] and cable-free land seismic acquisition is discussed in several research articles [23–26]. Need to use in the future an ultra-high channel count point receiver recording system, productivity enhancement techniques and incorporating advanced processing tools.

The big advantage of a wireless system over a wired system is that in urban seismic situation, these tools overcome hazards of traffic or yard-based operations. It is more suited for environmentally or geopolitically sensitive areas, for dense vegetation and extreme topography, and the survey flexibility provides fewer coverage gaps. It gives an easier and faster survey layout, with no need for special equipment training for field personnel or time-consuming deployment programming, and the data download is simple and fast.

3.2.5.4. Resources

The seismic channel number (the recently recorded 3-D seismic surveys now have 5,000-10,000 active recording channel) gives the number of resources as the channels are moved by people and vehicles. Hundreds of seismic channels need to be moved daily, which requires sufficient human and field vehicle capacity. The composition of the crew's human resources and vehicle resources are in *Table 3*. The number of resources required needs to be optimized, because it is not good for the number of members of the team or car-fleet to be either higher than necessary (additional cost)or lower (slower progress). The completion of the project is documented in time (day by day) by the progress map (shown in *Figure 9*).

During the surveying, the number of seismic records per day is one of the most important factors, because often payment is based on this, which means revenue, unless there is a time-based contract. By implication, the less time the crew spends in the entire research area, the less cost will be incurred and the greater the profit.

Table 3
Crew resources

THE COMPOSITION OF THE CREW'S **HUMAN & VEHICLE** RESOURCES	
Human resources	**Vehicle resources**
project manager	recorder truck
field manager	5–15 vibrators
2-3 field leaders *(who coordinate the units and assist the field manager)*	trucks and jeeps for seismic instrument *(cables, geophones, batteries, etc.)* transporting
QC (quality control of seismic records)	Field buses and jeeps for human transporting
observers *(in recording unit)*	drilling trucks
vibrator unit staff	tanker truck and water-tanker truck
drilling and explosive handling staff	
cable units staff	
surveyor staff	
support staff *(maintenance of seismic equipment and vehicles, permittmen, administration, etc.)*	

3.2.5.5. Quality control

The seismic records can first be viewed by the observers in the recording truck when a wired system is used, but the seismic data in the "dog house" are not ideal for interpretation, so these raw field recordings are pre-processed by the field QC. When using wireless technology, the observer is shooting blind with an autonomous recording system, and the common source point records are generated weeks later by the transcriber from the stand-alone receiver station. QC field processing is extraordinarily important for this technology. Continuous data quality control was already an important task 15–20 years ago but the use of new technologies has increased the importance of QC. The goal of the seismic data pre-processing is to enable the use of appropriate header information, data that are free of noise-dominated traces and flawed vertical stacking in subsequent processing steps; to create an accurate picture of the subsurface, it must remove or at least minimize artifacts in these records and noise in the data obscuring the subsurface image.

3.2.6. Damage compensation

Damage compensation means the repair and monetary compensation of damage caused during the survey (agricultural, road, and building damage). This must be done in full, as failure to do so could result in lengthy lawsuits. It is advisable to agree with the owners concerned at the permitting stage on the amounts on which

the compensation is based. Due to advances in acquisition technology, the footprint of seismic projects is getting smaller, as fewer large trucks travel, fewer people work in the fields, there is less line clearing, and the size of the sensors used is smaller, thus the reduction in costs is also reflected in the amount of damage compensation.

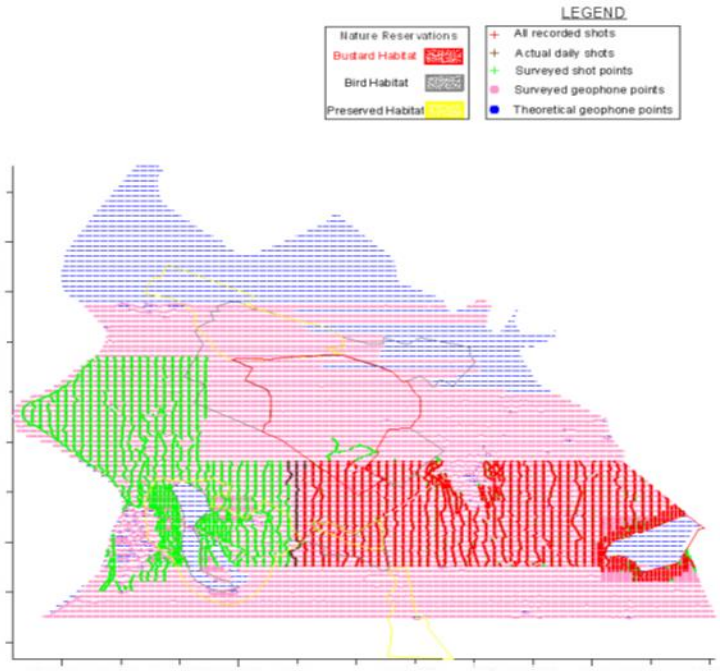

Figure 9
Progress map of a 3-D seismic project

3.2.7. Data processing and interpretation

A stack *(Figure 10)* is created from the field seismic records during different sub-processes (shown in *Figure 11*), and then the processed seismic profile is made by applying seismic migration.

Hydrocarbon exploration strives for the most detailed image of the subsurface. Global competition for hydrocarbons drives the need to expand exploration and raise recovery rates, while at the same time the full cost of the operation is very important. But no matter how much the costs dominate, seismic professionals will always play a key role in the quality of seismic data acquisition required and the proper processing/interpretation of data. The technologies and field seismic devices have been evolving and refining year after year for several decades [27]. Companies use high-technology tools to obtain data improvements. The amount of tools that can be used is now limited only by money. In the age of digitization, managing the huge amount of data generated is not impossible due to continually expanding computer capability. The continuous development of data processing should not be overlooked

either [4, 28]. The sole goal of hydrocarbon exploration is to find valuable and exploitable raw material. This requires the most accurate processing and interpretation possible. Optimization is also needed during processing to get the best possible geological image from our measurement results. The role of companies involved in the processing of seismic data has also strengthened over the past decade.

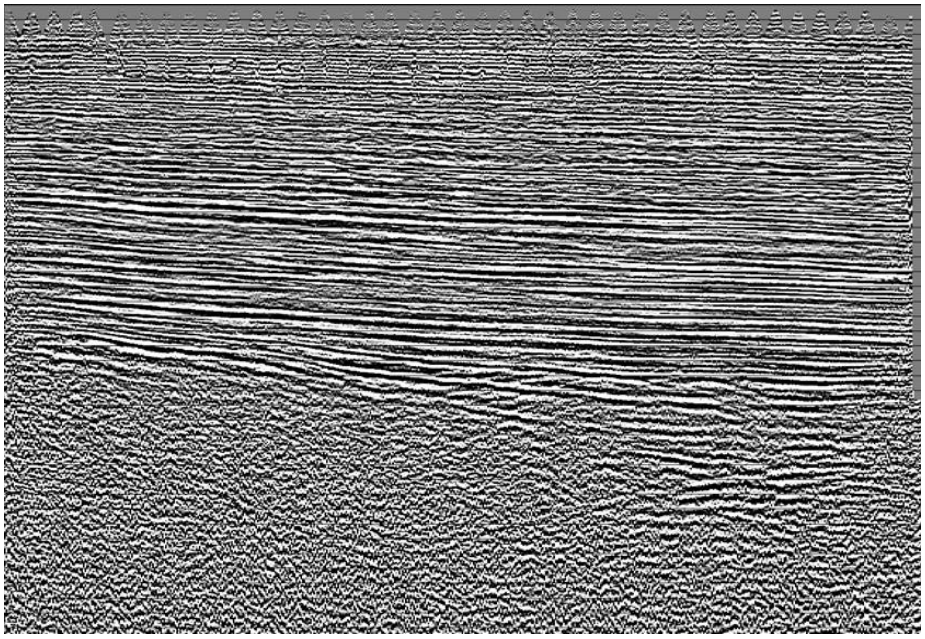

Figure 10
Stack inline

Complex processing – the combined application of several geophysical data processing methods – can greatly increase the reliability of the final result. Geophysical inversion as a tool allows the simultaneous application of several geophysical methods [29]. The accuracy of the evaluation is greatly aided by laboratory determinations of the velocities of the P and S waves performed on the core samples because this is the only way to determine the exact acoustic velocity of each rock. The advantage of ultrasonic measurements in the laboratory is that the effects of individual physical conditions (such as pressure, temperature, pore-filling) can be modeled under controlled conditions, and the disadvantage is that the core samples represent only a very small representation of subsurface formations [30]. The information obtained from laboratory tests is essential for understanding the properties of subsurface formations. All this requires the development and use of new petrophysical models that help to process and interpret field data and describe the processes that occur in nature more accurately.

After data analysis, during the interpretation, the wells are selected based on the processed seismic data.

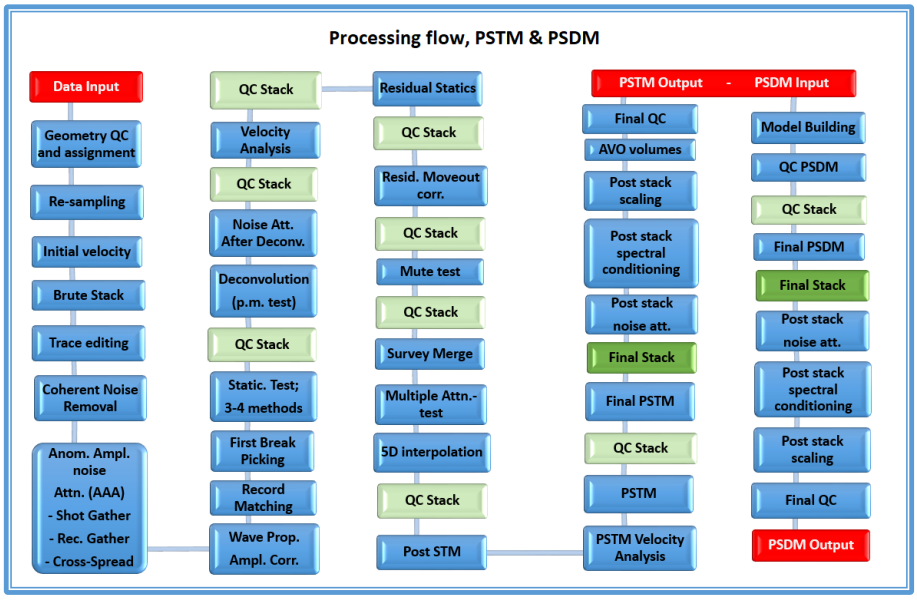

Figure 11
Main steps for seismic data processing

3.2.8. Final report of the project

The most important elements of the final report are presented in *Figure 12*. The final report of the project includes the final report of the fieldwork, the final report of the data processing and interpretation ordered in the contract, and the financial final report of the costs incurred. The final report must be presented and handed over to the customer. Financial payment for the project will be made against an invoice submitted after the final report has been accepted.

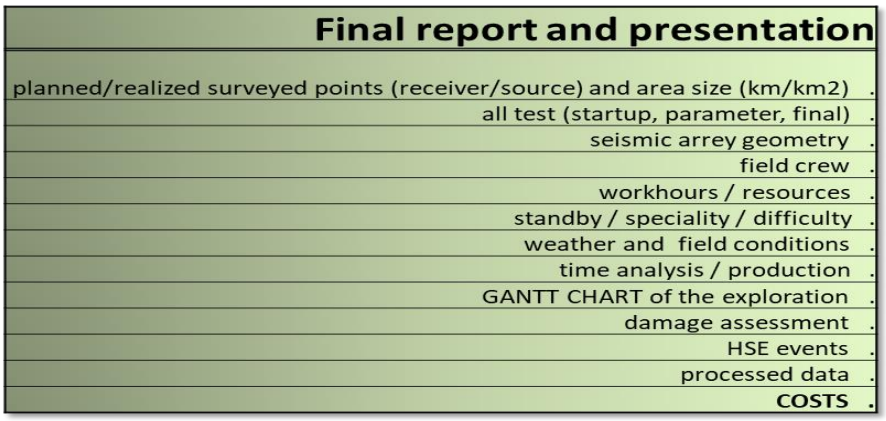

Figure 12
Main elements of the final report

4. CONCLUSION

Oil companies and their exploration crews are continually striving for a better understanding of the subsurface. Land seismic projects have changed greatly in the last two decades and have become more challenging year by year: the clients need reliable 3-D data, denser surveys at a lower cost with a reduced environmental footprint and lower HSE risk. A new era in land 3-D seismic survey has arrived in Europe and advancements in modern seismic tools have given an opportunity for completely cable-free seismic recording. Wireless technology has been used for seismic acquisition in Europe since the 2010s, in Hungary since 2014, significantly increasing productivity. Based on the author's experiences, this paper presents the main aspects and processes of 3-D land seismic projects in the Pannonian Basin, and each sub-process is detailed.

It is important to mention that each survey is unique depending on local and field conditions. To implement professionally successful and financially profitable projects, the elements outlined above must be fully taken into account. Implementing seismic projects is a task with several factors that go well beyond geophysics. All this requires complex engineering, economic and current legal knowledge as well as effective teamwork. In focus should be on collecting data as accurately as possible, interpreting seismic information in as much detail as possible, and increasing its reliability, yet in practice, cost-effectiveness is the center of all projects, so each sub-process requires careful preparation. The key to success is essentially good planning, continuous optimization, speed, and ultimately an accurate subsurface image.

ACKNOWLEDGMENTS

The author is grateful for the valuable professional assistance of Bence Kónya and dr. László Gombár, and finally, the author thanks Imre Sziráki for his technical information that has contributed to improve this paper.

REFERENCES

[1] Kovács, Zs. (editor), Babinszki, E., Bauer, M., Budai, T., Bujdosó, É., Cserkész-Nagy, Á., Gulyás, Á., Gyuricza, Gy., Herczeg Jun, A., Herczeg. A., Herczeg, Zs., Jencsel, H., Kercsmár, Zs., Kiss, J., Kovács G., Kovács Zs., Kozma, P., Lendvay, P., Maigut, V., Maros, Gy., Müller, T., Orosz, L., Ó Kovács, L., Paszera, Gy., Plank, Zs., Selmeczi, I., Szamosfalvi, Á., Takács, E., Thamó-Bozsó, E., Tiszavári, S., Veres, I., Zilahi-Sebess, L. (2018). *Hydrocarbons in Hungary, Results and opportunities*. Budapest, Hungarian Energy and Public Utility Regulatory Authority.

[2] Ádám, O. (1987). *Seismic Exploration I–II (in Hungarian)*. Budapest, Tankönyvkiadó Vállalat.

[3] Gaarenstroom, L. (1984). The Value of 3D Seismic in Field Development. *Proc. SPE Annual Technical Conference and Exhibition*, Houston, Texas, Paper No: SPE-13049-MS, pp. 1–12.

[4] Onajite, E. (2013). *Seismic Data Analysis Techniques in Hydrocarbon Exploration*. Amsterdam, Elsevier.

[5] Haldar, S. K. (2018). *Mineral Exploration, Principles and Applications*. Amsterdam, Elsevier.

[6] Cordsen, A., Galbraith, M., Peirce J. (2000). *Planning Land 3-D Seismic Surveys.* Tulsa, Society of Exploration Geophysicists, ISBN 1-56080-089-5.

[7] Dondurur, D. (2018). *Acquisition and Processing of Marine Seismic Data*. Amsterdam, Elsevier.

[8] Chaouch, A., Mari, J. L. (2006). 3-D Land Seismic Surveys: Definition of Geophysical Parameters. *Oil & Gas Science and Technology*, Vol. 61 (5), pp. 611–630, https://doi.org/10.2516/ogst:2006002.

[9] Dragoset, B. (2005). A historical reflection on reflections. *The Leading Edge*, Vol. (24), 1, pp. s1–s112, https://doi.org/10.1190/1.2112392.

[10] Dean, T., O'Connell, K., Quigley, J. (2013). A review of nodal land seismic acquisition systems. *Preview*, Vol. 164, pp. 34–39. https://doi.org/10.1071/PVv2013n164p34

[11] Gombár, L., Deák, F. (2015). Structural 3D seismic survey around the Paks Nuclear Power Plant (in Hungarian). *Magyar Geofizika*, Vol. 56 (3), pp. 139–151.

[12] Keen, K. A., Thayre, B. J., Hildebrand, J. A., Wiggins, S. M. (2018). Seismic airgun sound propagation in Arctic Ocean waveguides. *Deep Sea Research Part I: Oceanographic Research Papers*, Vol. 141, pp. 24–32. https://doi.org/10.1016/j.dsr.2018.09.003

[13] Wei, Z., Phillips, T. F., Hall, M. A. (2010). Fundamental discussions on seismic vibrators. *Geophysics*, Vol. 75 (6), pp. W13-W25.

[14] Chen, SQ., Wang, Y. (2018). Seismic resolution enhancement by frequency-dependent wavelet scaling. *IEEE Geoscience and Remote Sensing Letters*, Vol. 15 (5), pp. 654–658, https://doi.org/10.1109/LGRS.2018.2809564.

[15] Rozemond, H. J. (1996). Slip-sweep acquisition. *Society of Exploration Geophysicists, SEG Technical Program Expanded Abstracts*, pp. 64-67. https://doi.org/10.1190/1.1826730

[16] Yongsheng, S., Changhui, W., Mugang, Z., Xuefeng, Z., Zhenchun, L., Fenglei, L., Lieqian, D. (2011). A method for harmonic noise elimination in

slip sweep data. Society of Exploration Geophysicists, SEG Technical Program Expanded Abstracts, pp. 1–5. https://doi.org/10.1190/1.3627600

[17] Kónya, B. (2011). Experimental slip-sweep survey in the Pannonian Basin (in Hungarian). *Magyar Geofizika*, Vol. 52 (1), pp. 32–39.

[18] Berkhout, A. J., Verschuur, D. J., Blacquire, (2012). Illumination properties and imaging promises of blended, multiple-scattering seismic data. *Geophysical Prospecting*, Vol. 60 (4), pp. 713–732. https://doi.org/10.1111/j.1365-2478.2012.01081.x

[19] Pap, A. (1984). Criteria for the selection of geophone parameters, hookups, phone spacing, and low-Cut instrument filters. Society of Exploration Geophysicists, SEG Technical Program Expanded Abstracts, Atlanta, ISSN (print): 1052–3812, ISSN (online): 1949–4645. https://doi.org/10.1190/1.1894056

[20] Picozzi, M., Milkereit, C., Parolai, S., Jaeckel, K-H., Veit, I., Fischer, J., Zschau, J. (2010). GFZ Wireless Seismic Array (GFZ-WISE), a Wireless Mesh Network of Seismic Sensors: New Perspectives for Seismic Noise Array Investigations and Site Monitoring. *Sensors*, Vol. 10, pp. 3280–3304. https://doi.org/10.3390/s100403280

[21] Makama, A., Kuladinithi, K., Timm-Giel, A. (2021). Wireless Geophone Networks for Land Seismic Data Acquisition: A Survey, Tutorial and Performance Evaluation. *Sensors*, Vol. 21, 5171, pp. 2–22. https://doi.org/10.3390/s21155171

[22] Tellier, N., Lainé, J. (2017). Understanding MEMS-based digital seismic sensors. *First Break*, Vol. 35 (1), pp. 93–100. https://doi.org/10.3997/1365-2397.35.1.87386

[23] Dieulangard, D., Popham, M., Grant, C., O'Connell, K., Ourabah, A., Einchcomb, C. (2022). Land Seismic Recording Systems in a Changing World — a 2021 Review. *First Break*, Vol. 40 (1), pp. 59–65. https://doi.org/10.3997/1365-2397.fb2022004,

[24] Freed, D. (2011). Cable-Free land seismic data acquisition. Geoscience Technology Report. Available online: http://www.nodalseismic.com/uploads/media_items/2_cable-freeseismicdataacquisitionsept2011.original.pdf (accessed on 06 January 2022).

[25] Wilcox, S., Tellier, N. (2017). QC Practices in Wireless Land Seismic Acquisition. *Proc. of the 79th EAGE Conference and Exhibition*, Paris, France, 12–15 June 2017, pp. 1–5.

[26] Ellis, R. (2014). Current cabled and cable-free seismic acquisition systems each have their own advantages and disadvantages - Is it possible to combine the two? *First Break*, Vol. 32, pp. 91–96.

[27] Monk, D. (2014). Seismic Technology. Technological Advances Bringing New Capabilities To Seismic Data Acquisition. *The American Oil & Gas Reporter*, Editor's Choice, July 2014, https://www.aogr.com/magazine/editors-choice/technological-advances-bringing-new-capabilities-to-seismic-data-acquisitio.

[28] Yilmaz, Ö. (2001). *Seismic data analysis: Processing, inversion, and interpretation of seismic data.* Society of Exploration Geophysicists, Tulsa. https://doi.org/10.1190/1.9781560801580

[29] Dobróka, M., Szabó N. P., Szegedi H. (2014). *Geophysical Information Processing – Methods and Applications (in Hungarian).* CriticEl Monográfia sorozat 4, Miskolc, Milagrosa Kft.

[30] Kiss, A. (2018). *Petrophysical investigation of acoustic relaxation phenomena* (in Hungarian). Doctoral dissertation, University of Miskolc, Hungary.

Geosciences and Engineering, Vol. 10, No. 15 (2022), pp. 224–232.
https://doi.org/10.33030/geosciences.2022.15.224

ANALYSIS OF TOC VALUES OF MIXED SEWAGE SLUDGE FOLLOWING THE HYDRODYNAMIC TREATMENT, IN COURSE OF PILOT EXPERIMENT IN THE FRAMEWORK OF R&D GINOP ONGOING PROJECT

ÁKOS PINTÉR-MÓRICZ[2], SELLY AYU JANETASARI[3], LJUDMILLA BOKÁNYI[1]

[1]*Institute of Raw Material Preparation and Environmental Processing, Department of Bioprocessing and Reaction Techniques, University of Miskolc, Hungary*
ljudmilla.bokanyi@uni-miskolc.hu, https://orcid.gov/0000-0003-2038-6556
[2]*Institute of Applied Earth Science, University of Miskolc, Hungary*
akos.pinter-moricz@uni-miskolc.hu, https://orcid.gov/0000-0002-1174-5302
[3]*Ph.D. student, University of Miskolc, Hungary,*
Research Institute of Applied Earth Sciences
janetasari.selly.ayu@student.uni-miskolc.hu, https://orcid.gov/0009-0005-8282-6379

Abstract: The primary and secondary stages in wastewater treatment generate a large amount of sewage sludge consisting of 90% water, mineral components, nutrients and also a variety of organic and inorganic contaminants. The contaminants do not degrade completely during these processes, thus an additional degradation is needed to stabilize the sewage sludge. The innovative technology is proposed consisting of hydrodynamic cavitation process along with the addition of Bakony brown coal as adsorbent. Hydrodynamic cavitation is known as an effective tool improving sewage sludge stabilization via aerobic degradation, while adsorbent, besides the adsorption ability, has microbial cells disintegration ability as well, further enhancing the biodegradation process. The changes in total organic carbon (TOC) values of sewage sludge after hydrodynamic treatment for various retention times (0, 5, 10, 15, and 25 minutes) was traced and interpreted.

Keywords: *sewage sludge; hydrodynamic cavitation; adsorbent; aerobic degradation, total organic carbon*

1. INTRODUCTION

The removal of biodegradable compounds and organic or inorganic particulate matters in municipal wastewater treatment plants (WWTPs) by settling (primary treatment stage) and biological treatment (secondary stage) generates large amounts of sewage sludge. Sewage sludge consists of water (>90%) and solids (<10%), 50–70% of dry matter is organic, while 30–50% are mineral components (including 1 - 4% of inorganic carbon), 3.4–4.0% N, 0.5–2.5% P and other nutrients, including micronutrients [1]. Nevertheless, sewage sludge also contains a variety of contaminants, both inorganic (such as metabolic heavy metals) and organic, such as polycyclic aromatic hydrocarbons (PAHs), polychlorinated biphenyls (PCBs),

pesticides, surfactants, hormones, pharmaceuticals, and many other substances [2]. For this reason, sewage sludge needs to be treated properly prior its further utilization. The aims of sewage sludge treatment are to reduce the waste disposal amount by up to 90% and to reduce transportation costs and accompanying environmental pollution. With the stabilization of sewage sludge, it is possible to gain the new income streams from recovered resources for agriculture (fertilizer, compost) and energy production (burning, pyrolysis or gasification of RDF).

However, the pollutants containing in sewage sludge during wastewater treatment could not fully degrade, thus an additional degradation is needed to stabilize the sewage sludge. Sludge also consists of biological flocks matrices of microorganisms, nonliving organic matter, and inorganic materials. These flocks are highly hydrated colloidal structures of microbial aggregate which make sewage sludge difficult to degrade [3]. To reduce the amount of sludge, as well as to stabilize it, different technologies have been applied in the sludge treatment including physicochemical treatment by hydrodynamic cavitation.

The hydrodynamic cavitation is assumed to have a prominent role in the field of sewage sludge treatment, due to its ease of operation, low energy consumption, flexibility, and ability to vary the required intensities of cavitational conditions [4].

Cavitation is the process of creating, growing, and collapsing bubbles in a liquid because of a local pressure drop. The collapse of cavitation bubbles during the cavitation process can result in a variety of physicochemical effects [5]. Water molecules can be decomposed into a variety of species with high oxidation potential under extreme cavitation conditions, including hydroxyl radicals ($OH^{\bullet}$), $OOH^{\bullet}$, and H_2O_2, which can react with organic compounds in wastewater by enhancing the sludge biodegradability and its reuse in other biological processes [6].

The immense collapse force can break the molecular bonds of organic pollutants and destroy microorganism cell walls. Microorganism disintegration leads to the release of intercellular substances, first of all enzymes which are easily accessible to a subsequent biological degradation process and expand the biological degradation phenomenon [7]. By breaking up the filamentous structure and larger flocs, disintegrated sludge can also be used to reduce sludge bulking and foaming in sludge treatment process [8].

Given the positive role played by hydrodynamic cavitation, it has received more attention in scientific research and publications. For example, Lucia Umberto et al, 2009 [9] reviewed experimental approaches to hydrodynamic cavitation, Ilgyu Lee and Jong In Han, 2003 [10] studied the effects of pretreatment of activated sludge with hydrodynamic cavitation on methane production. In 2015, Dular Matevz et al. [11] also gave a review on the use of hydrodynamics in wastewater treatment. The same study was authored by Randhavane Shrikant, 2016 [12] which found that hydrodynamic cavitation has several positive effects on wastewater treatment. Based on the previous research data, it can be concluded that hydrodynamic cavitation as a sole treatment is an effective and efficient technique for sewage sludge treatment. Nevertheless, creation of a novel process and equipment is required. The idea of this research is to combine hydrodynamic treatment with the addition of solid adsorbent,

namely Bakony brown coal to enhance the secondary biodegradation process of sewage sludge.

2. SCIENTIFIC AND INNOVATION IDEA

The concept idea of the R&D GINOP project is to bring innovative technology based on intensive mechanical impact by cavitation and adsorption phenomena which is showed in following diagram:

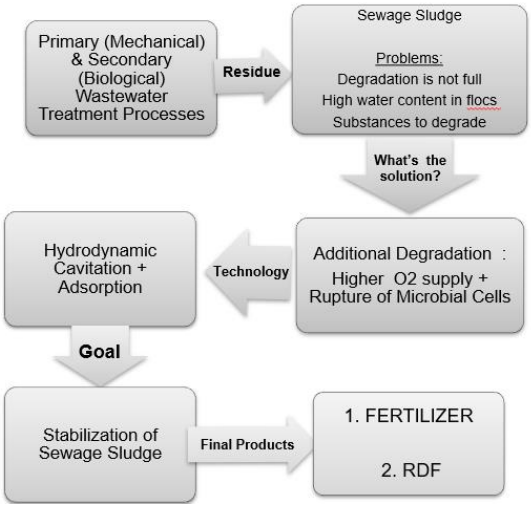

Figure 1
The Concept of Sewage Sludge Treatment in the GINOP Project

3. PILOT EXPERIMENTS IN SIÓFOK, DRV COMPANY

The pilot experiments were carried out within the framework of GINOP-2.2.1-15-2017-00069 R&D Project with the consortium consisting of Transdanubian Regional Water Works (DRV) LTD and the Institute of Raw Materials Preparation and Environmental Processing, University of Miskolc. The experimental set up, first hydrodynamic parameter measurements, preliminary laboratory work and the first industrial experiment has been done [14][15]. The experimental set up as shown in Figure 2 consisted of an open storage tank with a volume of 1.86 m^3, centrifugal pump, cavitation chamber and pipelines with different diameters. This part of the research was the second stage of the experimental program, the experiment was conducted on the site of Wastewater Treatment Plant in Siófok. The real sewage sludge was used, hydrodynamic cavitation with various retention times (0, 5, 10, 15, and 25 minutes) was conducted with adsorbent addition, namely 8% of Bakony brown coal or 8% of natural zeolite for comparison. Bakony brown coal has high porosity, high surface area and high humic acids content, as well as high adsorption potential. Natural zeolite has been chosen due to the high performance in adsorption in aqueous solution such as

ammonium and heavy metals. The effect of hydrodynamic cavitation along with adsorbent addition on sewage sludge degradation was traced and interpreted by the change of Total Organic Carbon (TOC).

Figure 2
Hydrodynamic Cavitation Set Up

4. RESULTS AND DISCUSSION

In the field of sewage sludge treatment, hydrodynamic cavitation has become widely used. HC usually used to treat aqueous effluents polluted by organic, toxic, and bio-refractory contaminants due to its oxidative capability [16]. Hydrodynamic cavitation was investigated in order to accelerate the digestion of sewage sludge, increase the degree of degradation, and thus reduce the amount of sludge to be disposed of.

To monitor the stabilization of sewage sludge, the change Total Organic Carbon (TOC) values due to the combination of hydrodynamic cavitation process along with adsorbent addition has been investigated.

Figure 3 shows the TOC values for mixed sewage sludge without addition of Bakony brown coal adsorbent at different retention times. The TOC values for mixed sewage sludge without addition of adsorbent decreased significantly from 955 mg/L to 674 mg/l already at 4 minutes retention time. At 8 minutes retention time, the TOC value increased until 1328.15 mg/L and then decreased slightly until the end of

treatment in 24 minutes of retention time. It means that the optimal retention time for hydrodynamic cavitation is below 15 min.

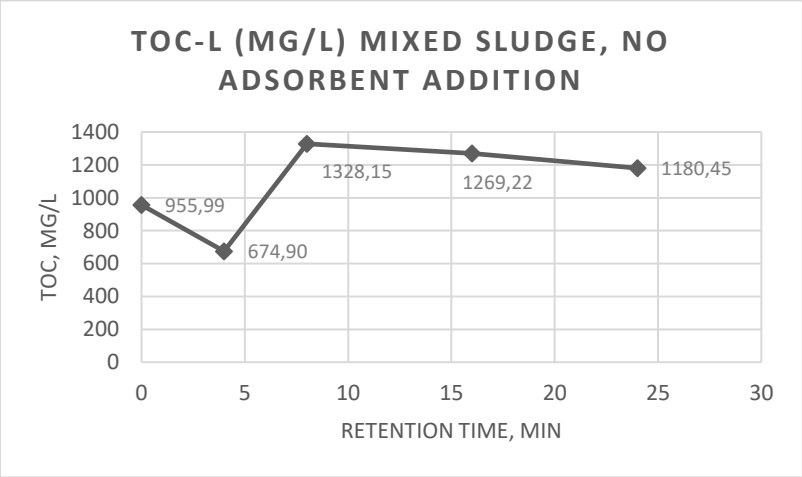

Figure 3
TOC Values due to Hydrodynamic Cavitation without Adsorbent Addition

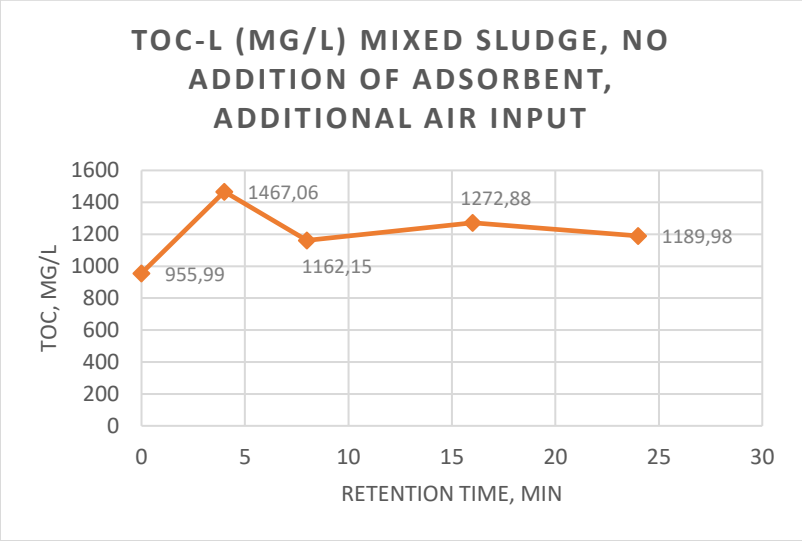

Figure 4
TOC Values Due to Hydrodynamic Cavitation with Additional Air Input

The change of TOC values also occurred in the mixed sewage sludge without adsorbent but with additional air input, as shown in *Figure 4*. TOC values increased from 955.99 mg/L to 1467.06 mg/L or 53.45% after only 4 minutes of retention time, then decreased slightly to 1162, 15 mg/L at 8 minutes of retention time [17].

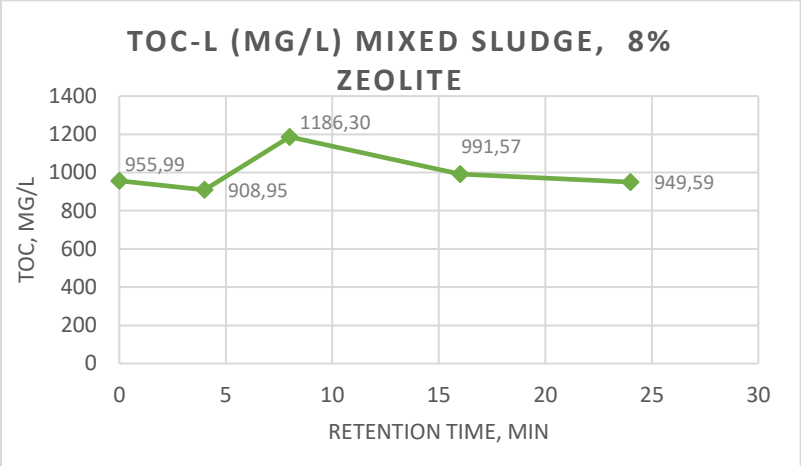

Figure 5
TOC Values Due to Hydrodynamic Cavitation with Addition of 8% Zeolite

The change in TOC value of mixed sewage sludge after hydrodynamic cavitation with adsorbents addition is shown in *Figure 5* and *Figure 6*. In the case of 8% zeolite, the TOC values of the mixed sludge with addition of 8% zeolite decreased slightly in the beginning of the treatment, then increased from 908.95 mg/L to 1186.30 mg/L at 8 minutes retention time. From that point until the end of process, the TOC values decreased continuously.

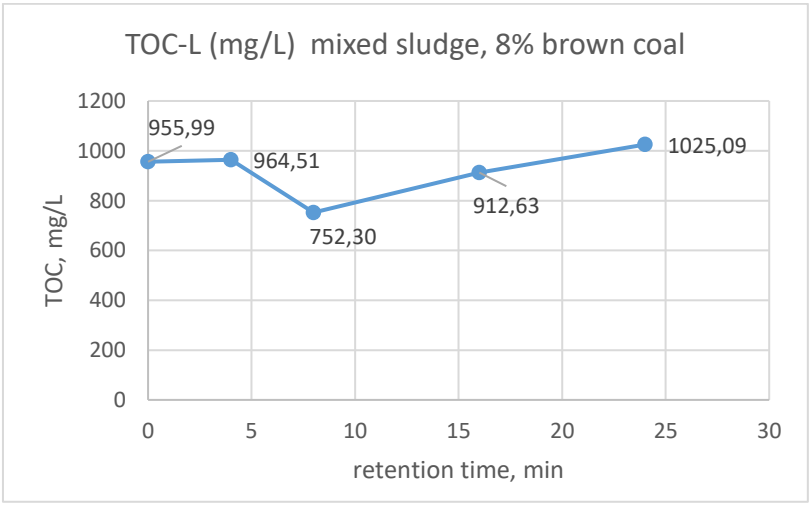

Figure 6
TOC Values Due to Hydrodynamic Cavitation with Addition of 8% Bakony Brown Coal

In contrast to zeolite, the TOC value for the 8% of Bakony brown coal addition as shown in *Figure 6*, decreased significantly at 8 minutes retention time from 964.51 mg/L to 752.30 mg/L. In the 16 minutes retention time, the TOC value then increased continuously until the end of treatment.

All the results indicate that application of hydrodynamic cavitation along with the addition of adsorbent resulted the change of TOC values. This effect could be caused due to the following phenomena: (i) liberation of water inclusions in flocks; (ii) the increase of contact surface leading to the raise of mass transfer and exposure of the free radicals; (iii) fragmentation of microbial cells, release of free enzymes into aqueous environment; (iv) achievement of a high oxygen concentration gradient, for intense additional aerobic degradation; (v) the addition of adsorbents (fossil coal and zeolite) to adsorb various species of vapour/gas and solute.

The physical effects of hydrodynamic cavitation include the production of shear forces of solid particles, dissolution of soluble compounds into fluid phase, as well as release of intracellular organic matter and enzymes present in cells' cytosol, results in the increased dissolved organic matter concentration in the liquid [19]. This phenomenon can increase the TOC values as can be seen in the treatment.

The decrease of TOC value could be caused by the intense additional aerobic degradation. When the cavitation bubble burst, there is an increase of oxygen concentration gradient, so the additional aerobic degradation takes place. Moreover, under cavitation conditions, water molecules can be decomposed into a variety of species with a high oxidation potential, including hydroxyl radicals (·OH), ·OOH, and H_2O_2, which can react with organic compounds and reduce the TOC values.

Beside the high adsorption ability towards contaminants, the addition of Bakony brown coal adsorbent may contribute to the cells rupture along with hydrodynamic cavitation, causing the TOC values increase. In the case of the mixed sludge treatment with the brown coal addition the growth in TOC is related to the coal itself as well. However, it is not easy to uncover all the reasons for the behavior, because in the system of the cell rupture due to cavitation is accompanied by an adsorption process makes the whole system very complex.

The addition of brown coal increases the added value of sewage sludge. Brown coal of Dudar is becoming a valuable fertilizer constituent because of the high content of humic acids, its calorific value is also remarkable.

5. CONCLUSIONS

Based on the experiments with mixed sewage sludge with and without addition of adsorbent, the following conclusion can be drawn:

- The hydrodynamic cavitation treatment combined with addition of adsorbent have a high potential for sewage sludge stabilization to obtain fertilizer and RDF as the final product.
- The change of TOC values due to the cavitation combined with the adsorption indicates the dissolution of colloidal solid particles into fluid phase, the

increase of dissolved oxygen consumed for fast aerobic degradation, as well as the rupture of the microbial cells.

- In general, the significant changes of TOC values occurred between 4–15 minutes of the treatment, it can be concluded that hydrodynamic cavitation needs a short retention time to work effectively.
- The addition of Bakony brown coal to hydrodynamic cavitation treatment causes the continuous increase of TOC value after 8 min retention time comparing to the addition of zeolite and the treatment without adsorbent addition.

REFERENCES

[1] Fytili, D., Zabaniotou, A. (2008). Utilization of sewage sludge in EU application of old and new methods-a review. *Renew. Sust. Energ. Rev.*, 12, pp. 116–140.

[2] Tyagi, V. K., Lo, S. L. (2013). Sludge: A waste or renewable source for energy and resources recovery? *Renew. Sustain. Energy Rev*., 25, pp. 708–728.

[3] Yin, X., Han, P., Lu, X., Wang, Y. (2004). A review on the dewaterability of bio-sludge and ultrasound pretreatment Ultrason. *Sonochem*., 11, pp. 337–348.

[4] EU, 1986. EU sludge directive 86/278/EEC (European Commission).

[5] Wu, Z., Yuste-C´ordoba, F. J., Cintas, P., Wu, Z., Boffa, L., Mantegna, S., Cravotto, G. (2018). Effects of ultrasonic and hydrodynamic cavitation on the treatment of cork wastewater by flocculation and Fenton processes. *Ultrason. Sonochem*., 40, pp. 3–8, https://doi.org/10.1016/j.ultsonch.2017.04.016.

[6] Grübel, K., Machnicka, A. (2010). Hydrodynamic disintegration of foam biomass to upgrade of wastewater. *Ecological Chemistry and Engineering S*, Selected Full Texts, 17 (2), pp. 137–148.

[7] Muller, J. (2000). Disintegration as a key-step in sewage sludge treatment *Water Sci. Technol.*, 41, pp. 123–130.

[8] Lehne, G., Moller, A., Schwedes, J. (2001). Mechanical disintegration of sewage sludge. *Water Science and Technology*, pp. 19–26.

[9] Lucia, U. Gervino, G. (2009). Hydrodynamic cavitation: From theory towards a new experimental approach *Cent. Eur. J. Phys.*, 7, pp. 638–644.

[10] Lee, I., Han, J. I. (2013). The effects of waste-activated sludge pretreatment using hydrodynamic cavitation for methane production *Ultrason. Sonochem.*, 20, pp. 1450–1455.

[11] Randhavane Shrikant, B., Khambete, A. K. (2017). Hydrodynamic Cavitation: A Novel Treatment Approach. *Mater. Today Proc.*, 4, pp. 9680–9684.

[12] Chanda, S. K. (2012). *Disintegration Of Sludge Using Ozone-Hydrodynamic*. M.Sc Thesis. The University Of British Columbia, Canada.

[13] Bokányi, L., Krizsán, G., Takács, J., Faitli, J., Abbadi, A., Mádai Üveges, V., Janetasari, S., Pintér, M. Á. (2020). Evaluation of Efficiency of Hydrodynamic Treatment on Sewage Sludge. *Proceedings Of The Miskolc Ipw - Iv. Sustainable Raw Materials International Project.*

[14] Abbadi, Alaa Imad Hasan (2020). An experimental investigation of hydrodynamic cavitation for the sake of sewage sludge treatment. M.Sc. Thesis. University of Miskolc, Supervisors: Dr. Faitli József and Dr. Bokányi Ljudmilla.

[15] Ozonek, J. (2012). *Application of hydrodynamic cavitation in environmental engineering.* CRC Press, Boca Raton. pp. 1–10, 75–76.

[16] Machnicka, A., Grubel, K., Suschka, J. (2009). The use of hydrodynamic disintegration as a means to improve anaerobic digestion of activated sludge *Water* SA, 35, pp. 129–132.

[17] Sorrels, J. L. (1998). Carbon adsorbers. *Metal Finishing*, Vol. 96, p. 76.

[18] Machnicka, A., Grubel, K., Suschka, J. (2009). The use of hydrodynamic disintegration as a means to improve anaerobic digestion of activated sludge *Water SA*, 35, pp. 129–132.

Responsible: Prof. dr. Péter Szűcs Vice-Rector
Published by the Miskolc University Press under leadership of Attila Szendi
Responsible for duplication: Erzsébet Pásztor
Technical editor: Csilla Gramantik
Proofreader: Zoltán Juhász
Number of copies printed:
Put to the press: 2023
Number of permission: MERT-2023-120-ME
HU ISSN 2063-6997